



THE  
*American Journal of*  
ANATOMY

MANAGING EDITOR  
DONALD DUNCAN  
THE UNIVERSITY OF TEXAS  
MEDICAL BRANCH  
GALVESTON TEXAS

ASSOCIATE EDITORS

BURTON L. BAKER  
UNIVERSITY OF MICHIGAN

RICHARD J. BLANDAU  
UNIVERSITY OF WASHINGTON

DON W. FAWCETT  
HARVARD UNIVERSITY

C. P. LESLOND  
McGILL UNIVERSITY

HARLAND W. MOSSMAN  
UNIVERSITY OF WISCONSIN

VOLUME 110  
JANUARY MARCH MAY 1963

PUBLISHED BY  
THE WISTAR INSTITUTE OF ANATOMY AND BIOLOGY  
PHILADELPHIA PA



# CONTENTS

## No 1 JANUARY 1962

WARREN ANDREW An Electron Microscope Study of Age Changes in the Liver of the Mouse	1
JAMES L. CONKLIN MAYNARD M. DEWEY AND RAYMOND H. LAHN Cytochemical Localization of Certain Oxidative Enzymes	19
IRA R. TELFORD CAROLINE S. WOODRUFF AND RAY H. LINFORD. Fetal Resorption in the Rat as Influenced by Certain Antioxidants	29
CAROLYN EYSTER THOMAS AND C. MURPHY CONNORS Spinal Cord Segments. A. Gross Structure in the Adult Cat	37
RUPERT P. AMANN Reproductive Capacity of Dairy Bulls. III The Effect of Ejaculation Frequency Unilateral Vasectomy and Age on Spermatogenesis	49
RUPERT P. AMANN Reproductive Capacity of Dairy Bulls. IV Spermatogenesis and Testicular Germ Cell Degeneration	69

## No 2 MARCH 1962

DONALD H. ENLOW A Study of the Post Natal Growth and Remodeling of Bone	79
JOHN M. STEIN AND HELEN A. PADYKULA. Histochemical Classification of Individual Skeletal Muscle Fibers of the Rat	103
EDWARD H. BLOCH A Quantitative Study of the Hemodynamics in the Living Microvascular System	125
DEONIS LACY AND A. B. TAYLOR. Fat Absorption by Epithelial Cells of the Small Intestine of the Rat	155
ERNESTO DE LA TORRE, OLIVER CHARLES MITCHELL AND MARTIN G. NETSEY Anatomic and Angiographic Study of the Vertebral Basilar Arterial System in the Dog	187
CHARLES E. MCCREIGHT AND NORMAN M. SULZIN Compensatory Renal Hyperplasia Following Experimental Surgical Deletions of the Kidney Complement	199

# CONTENTS

No 3 MAY 1962

K. K. HIRAKA AND C F FIRLIT The Localization of Nucleic Acids During Oögenesis in the Zebrafish	203
SAM L. CLARK, JR. The Reticulum of Lymph Nodes in Mice Studied with the Electron Microscope	217
HOMER B LATIMER AND PAUL B SAWIN Morphogenetic Studies of the Rabbit. XXXI Weights and Linear Measurements of Some of the Bones of 65 Race III Rabbits	259
DONALD H ENLOW Functions of the Haversian System	269
MALCOLM B CARPENTER AND GEORGE R. HANNA. Lesions of the Medial Longitudinal Fasciculus in the Cat	307
INDEX TO VOLUME 110	333

# An Electron Microscope Study of Age Changes in the Liver of the Mouse<sup>1</sup>

WARREN ANDREW

Department of Anatomy Indiana U University Medical Center  
Indianapolis Indiana

Since the advent of methods of adequate fixation and of ultrathin sectioning in electron microscopy a number of able investigators have directed their attention to the liver. Bernhard, Gautier and Oberling ('51) described the fibrillar elements in the hepatic cells which they felt corresponded with the ergastoplasm or basophilic material observed by light microscopists in many kinds of cells.

Dalton, Kahler Striebig and Lloyd ('50) studied the cell organelles, including the "fibrils," which they also conceived as representing the basophilic material of the hepatic cells and compared their fine structure with that of intestinal epithelial cells and cells of renal tubules.

Fawcett ('55) published a definitive paper on the electron microscopy of hepatic cells. One of the additions to knowledge presented in this paper concerned the presence of peglike projections fitting into corresponding concavities in the liver cells, apparently making for firmer adhesion of the cells as a tissue.

Cosel ('59) described Disse's space now found to be a real interval between the lining cells of the sinusoids and the hepatic cells, an interval "bridged, however by feet of the hepatic cells and occasional bundles of collagenous fibrils. This space also is continuous with intercellular spaces e.g. those between the hepatic cells.

A recent study (Porter and Brunl, '60) has shown the relationship of the endoplasmic reticulum to the processes of glycogenesis and glycogenolysis. The glycogen areas have been identified with the electron microscope by PAS staining of alternate thick sections with study of the adjacent thin sections. These areas seen in electron micrographs are filled by ill-defined masses, 0.1 to 0.2  $\mu$  in diameter

There is a center of low density surrounded by an irregular frame of greater density resembling, as the authors say, the membranous remnant of an exploded vesicle.

Upon fasting of the animal the glycogen areas become filled by profiles of vesicles and these go on to develop into a continuous lattice of tubules apparently the same in structure as the smooth form of endoplasmic reticulum. They conclude that a smooth form of the "ER" is involved in glycogen storage and release.

With the considerable amount of fine descriptive work which has been carried out on general aspects of the liver cell, and with some background which we have had in light microscope studies on age changes in the liver (Andrew Brown and Johnson, '43 Andrew '55 '56) it seemed worth while to undertake a study of age changes with the electron microscope.

## MATERIAL AND METHODS

Seventeen animals of the C57 Black strain of mice from the Roscoe B Jackson Memorial Laboratory were used in the electron microscope studies. The age in days and sex of these animals were as follows: 105  $\delta$ , 105  $\delta$ , 117  $\delta$ , 170  $\delta$ , 539  $\delta$ , 539  $\delta$ , 549  $\delta$ , 549  $\delta$ , 610  $\delta$ , 664  $\delta$ , two 664  $\delta$ , 701  $\delta$ , two 728  $\delta$ , 837  $\delta$  and 887  $\delta$ .

The animals were lightly anesthetized with ether the abdominal cavity opened by a mid-line incision and a portion of liver not more than 2 mm on any side, was removed and placed immediately into Palade's fixative, osmic acid buffered with veronal acetate. Fixation time was approximately one hour and fifteen minutes.

This study was supported by grant from the Indiana Heart Association, for which grateful acknowledgment is made.

# CONTENTS

No. 3 MAY 1962

K. K. HISAOKA AND C. F. FURLIT The Localization of Nucleic Acids During Oögenesis in the Zebrafish	203
SAM L. CLARK, JR. The Reticulum of Lymph Nodes in Mice Studied with the Electron Microscope	217
HOMER B. LAYMEYER AND PAUL B. SAWIN Morphogenetic Studies of the Rabbit. XXXI. Weights and Linear Measurements of Some of the Bones of 65 Race III Rabbits	259
DONALD H. ENLOW Functions of the Haversian System	269
MALCOLM B. CARPENTER AND GEORGE R. HANNA Lesions of the Medial Longitudinal Fasciculus in the Cat	307
INDEX TO VOLUME 110	333

whether we are looking at a megakaryocyte or at one of the enlarged and somewhat altered hepatic cells which we have found to be scattered among the more normal cells of the liver in old age.

Study of the mitochondrial preparations revealed two facts about the livers of the senile animals. First the great majority of the hepatic cells showed a cytoplasm with very many mitochondria apparently no less in number than in the younger animals. Second there are small groups of cells and in section at least individual cells, which differ markedly from the majority in showing a great diminution in number of mitochondria and a reduction in size of those present. With the light microscope the cytoplasm of such cells appears almost empty (figs. 5 and 7).

#### *Electron microscope findings*

The most prominent feature brought out in electron micrographs in the liver of senile mice is the presence in a number of the hepatic cells of nuclear invaginations (figs. 10 and 11). These vary considerably in their depth. Often, however they are deep and narrow and often pass a third or a half of the way through the nucleus. In other instances they are broad mouthed but involve a considerable part of the nuclear membrane.

The invaginations often contain large numbers of mitochondria and other cytoplasmic elements, including lipid droplets, endoplasmic reticulum and glycogen. The appearance is one of a series of steps in which such inclusions are being taken into the nucleus by a process of infolding followed by a cutting off of the infolded portion.

A second feature seen in electron microscopy of the livers of old animals is the presence of nuclei in process of degeneration (fig. 12). In such nuclei the entire karyoplasm becomes more electron dense than in ordinary nuclei and distinct clumps of very dense material, probably corresponding to the chromatin clumps of karyorrhexis as seen with the light microscope, are visible. Nucleoli seem to be lost or to become unrecognizable relatively early in the degenerative process.

The degenerating nuclei are relatively few and far between, but with the high

magnification of the electron microscope they become very conspicuous objects and are not as likely to be confused with leucocytes or other cells as in light microscopy.

Observation of small vessels seems to indicate that the focal degeneration may be due to vascular change as endothelial alteration and fibrotic change in the walls of arterioles are found in the regions where degenerating nuclei occur even though the liver as a whole may show relatively little alteration of the blood vessels.

It is interesting to note that mitotic figures are conspicuous in some of the livers in which the larger numbers of degenerating nuclei appear to be present.

The nucleoli themselves occasionally show changes even in otherwise "healthy" looking nuclei. The most common change is a clearing of the central portion giving the nucleolus the appearance of a ring in section (fig. 9).

We have made some general observations on the nucleoli or structures apparently related to them which while difficult to interpret at the present time seem to us to be worthy of recording here. The nucleoli almost always are surrounded by or enclosed in areas in which the nuclear contents appear denser than in the portion away from the nucleoli. In the electron micrographs these areas are gray (fig. 9). Many cells also show bodies in the nuclei seemingly of about the density of the material in these areas and of about the same size and shape as nucleoli. Within such a body a smaller fusiform structure frequently can be made out, although rather dimly.

Still another phenomenon seen in a number of nuclei in old animals relates again to the nuclear membrane. The great majority of the nuclei show a double membrane such as that described by various workers who have studied liver tissue with the electron microscope with the distance between the inner and outer membrane approximately 100 to 120 Å. Of this double membrane Fawcett ('35 p. 1477) said "It is not entirely clear whether both membranes should be considered as part of the karyotheca or whether only the inner membrane is to be identified with the nu-



cleus and the outer one regarded as the limiting membrane of the cytosome.

In a considerable number of cells in the liver of the old animals we see what appears to be a very much wider separation of the inner and outer membranes. In one instance, this distance is over 2,700 Å or about 27 times that described as normal! This seems to us rather remarkable in such an important cell organelle. It seems also to make more feasible the interpretation of the outer membrane as less dependent upon the nucleus as such and perhaps leads us to regard it as more likely to be an actual "limiting membrane of the cytosome."

Turning to the cytoplasm we are at first impressed in the comparison of livers of young and old mice, with the apparent lack of age change. The great majority of cells appear to have a full complement of mitochondria and the internal structure of the organelles is according to the now classical description with the peripheral double membrane invaginated to form the cristae mitochondriales.

The endoplasmic reticulum also is well formed for the most part. Its elements frequently are seen in a very intimate relationship with the mitochondria, the double membranes seeming almost to be wrapped around these structures. This is true both in young and old animals.

But in a survey over any area of a section as extensive as say one lobule of the liver areas are found where the picture is very different, both in relation to the mitochondria and the endoplasmic reticulum. In such areas, which include small groups of cells or even single cells, the mitochondria are reduced in size and in number. Also their rather uniform and smooth appearance is replaced by a varied and irregular one (fig 14). The impression is obtained that by reduction in size the mitochondria in these regions are actually wasting away and disappearing.

In such areas a rather remarkable appearance of the cytoplasm is seen with well defined trabecula-like structures forming a network (fig 15). Our observations would make it seem likely that these "trabeculae" represent the double-membrane structures of the endoplasmic reticulum

which thus would have become changed very radically.

#### DISCUSSION

The relation between observations by electron microscopy and light microscopy in this study has been a close one. The quantitative data presented in table 1 were obtained by study of hematoxylin and eosin sections with the oil immersion lens but only after the electron microscope had impressed us with the occurrence of invaginations of the nuclear membrane. This phenomenon itself is made more significant when we learn from the experimental studies of others that such inclusions actually are formed by the process of engulfment of masses of cytoplasm by invaginating portions of the nuclear membrane. This process of entrapment was first pointed out by Kleinfeld, Gelder and Frajola ('56) in studies on rats treated with thioacetamide. They observed that the composition of the inclusions is complex and that lipid, glycogen and even cell organelles may be present in them.

Leduc and Wilson ('59 a and b) studied development of intranuclear inclusions in the livers of mice fed a methionine-rich basal bentonite diet and also in mice with a transplantable hepatoma. They showed that such inclusions contain, besides glycogen and sudanophilic lipid, certain enzymes including acid and alkaline phosphatase, nonspecific esterase and  $\beta$ -glucuronidase. The abundance of these substances in the inclusions seems to vary in general with their abundance in the cytoplasm.

Their electron microscope studies showed that, in their material at least, the inclusions were formed by an invagination of the nuclear envelope.

In large liver cells (non-hepatoma) the inclusions were large and connected with the cytoplasm only by a relatively narrow duct-like opening. No normal mitochondria were present but degenerating ones were fairly

Our a	us
with th	inclusion
slows as	the
liver an	ly
interestin	the

invaginations which have been shown to bring about such inclusions.

An increasing tendency to invagination of the nuclear membrane leading to constrictions and to lobation, is a very well recognized feature of aging of the individual polymorphonuclear cells of the blood.

We have not seen descriptions of the type of change shown in figure 9 namely a type of cavitation of the nucleolus although it may represent some general type of reaction of this body to changes in other parts of the cell. It is stated (De Robertis, Nowinski, and Saenz, '60) that the less dense "lacunae of nucleoli do not really constitute a special component but represent nucleoplasm which pervades the nucleolar mass.

The bodies of nucleolar also but of an apparently lower density or degree of opaqueness to the electron beam, are rather intriguing objects and made more so by the dimly-seen fusiform structure made out in many of them. Whether they actually represent nucleoli in some stage of activity or even life-cycle is a question which further work may answer. This consideration, however does bring to mind the disappearance of nucleoli in early stages of mitosis and their reappearance upon its completion.

The only studies made on nucleoli of liver cells in relation to nutritional status concern the size of these structures. Stentam ('56) found the nucleoli to be small in starved animals (rats) and to increase in size when the animal was fed a diet with 25% casein. An increase with such a diet was seen after 8 hours while with a nonprotein diet the nucleoli did not increase in size this early but at 3, 18 and 44 days were significantly larger than those of the protein-fed animals. We have not measured nucleoli but no obvious size differences were seen in our mice of different age.

In relation to the question as to a possible role of the nucleolus in the formation of intranuclear inclusions, we are entirely in accord with Kleinfeld, Greider and Frajola ('56) who say (p. 437): "There were no indications of direct nucleolar transformation however the frequent association of nucleoli to the forming inclusions was noted.

The method of formation of intranuclear inclusions by cutting off of invaginated sacs containing cytoplasm was seen by Fischmann and Russell ('40) in cells of the fetal leptomeninges in tissue culture.

For the rest, the scattered and localized degenerative changes in the nuclei and in the mitochondrial picture make it seem probable that such changes rest upon a basis of vascular alteration.

### SUMMARY

The liver of the mouse in senility shows aggregations of ectopic lymphoid tissue and occasional lymphocytes within hepatic cells. Alterations in hepatic cells particularly the occurrence of intranuclear inclusions and of mitochondrial changes in single cells, or in small groups of cells can be seen with the light microscope.

Prominent in the electron microscopy study is the presence of invaginations of the nuclear membrane, a feature apparently often preceding formation of intranuclear inclusion. Localized areas show degeneration of nuclei and disappearance of mitochondria. It seems probable that these focal changes are dependent upon regional vascular alterations. Some histological findings relating to the nucleoli have been discussed.

### LITERATURE CITED

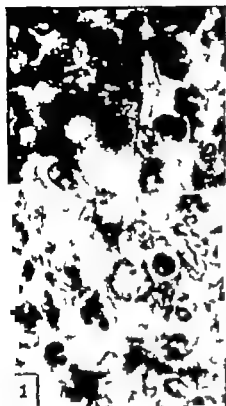
- Andrew W 1963 Autotic division in senile changes as probable means of self preservation of cells. *J Gerontol.* 18: 1-12.
- 1966 Metachromasy cell variations in various organs in old age. *Idid* 11: 47.
- Andrew W and Nancy V Andrew 1971 An age involution in the small branch of the mouse. With description of the functional process of lymphopoietic metachromasy in intestinal mucosa. *Idid.* 12: 136-151.
- Andrew W H. H. Brown and J. R. Johnson 1943 Senile changes in the liver of the mouse with special reference to the nucleus and nuclear alterations. *Am. J. Anat.* 72: 175-231.
- Andrew W and C. K. Collins 1946 Lymphocytes within the cells of intestinal epithelium in mice. *Anat. Rec.* 94: 44-47.
- Andrew W and J. M. Ross 1947 *MAKER* cells and degeneration of lymphocytes within cells of intestinal epithelium in white adult white mice. *Idid.* 9: 67-74.
- Berglund, W. A. Gendler and C. J. 1951 *Plasmalemma* and the nature of nucleolar cells. *Idid.* 10: 100-104.
- De Robertis, Nowinski and Saenz 1960 *Senile changes in the nucleus and nucleolus of the polymorphonuclear leukocyte.* *Idid.* 11: 1-12.
- Fischmann and Russell 1940 *Intranuclear inclusions in cells of the fetal leptomeninges in tissue culture.* *Idid.* 1: 1-12.
- Kleinfeld, Greider and Frajola 1956 *The role of the nucleolus in the formation of intranuclear inclusions.* *Idid.* 11: 437-447.
- Stentam 1956 *The effect of diet on the size of the nucleolus in liver cells of rats.* *Idid.* 11: 1-12.

- Coscel, L. 1959. Elektronenmikroskopische Untersuchungen zur Frage des Dissechen Raumes in der Leber. *Klin. Wochr.* 37 743-753.
- Dalton, A. J. H. Kahler M. J. Strielich and B. Lloyd 1950. Fine structure of hepatic, intestinal and renal cells of the mouse as revealed by the electron microscope. *J. Nat. Cancer Inst.*, 11 439-461.
- De Robertis, E., W. W. Nowinski and F. A. Sax 1960. *General Cytology* W. B. Saunders Company Philadelphia and London, pp. 553.
- Fawcett, D. W. 1955. Observations on the cytology and electron microscopy of hepatic cells. *J. Nat. Cancer Institute*, 15 (supplement) 1475-1504.
- Frischman, C. F. and D. S. Russell 1940. The occurrence of intranuclear inclusions in cultures of foetal leptomeninges. *J. Path. and Bact.*, 50 53-59.
- Kleinfeld R. G. M. H. Greider and W. J. Frajola 1958. Electron microscopy of intranuclear inclusion found in human and rat liver parenchymal cells. *J. Biophys. and Biochem. Cytology* 2: suppl., 435-439.
- Leduc, E. H., and J. W. Wilson 1959. A histochemical study of intranuclear inclusions in mouse liver and hepatoma. *J. Histochem. and Cytochem.*, 7 8-18.
- 1959. An electron microscope study of intranuclear inclusions in mouse liver and hepatoma. *J. Biophys. and Biochem. Cytol.*, 6 427-430.
- Porter K., and C. Bruni 1960. Fine structure changes in rat liver cells associated with glycogenesis and glycogenolysis. *Am. J. Res.*, 133, 2: 260-261.
- Stenram U. 1956. Nucleolar size in the liver of rats fed on high and non-protein diets after starvation. *Acta Anat.*, 26 359-361.

## PLATE 1

## EXPLANATION OF FIGURES

- 1 Lymphocyte within hepatic parenchymal cell in small area of ectopic lymphoid tissue, in a 213 day female mouse. This phenomenon is not common in young animals but occurs often in the livers of senile mice. Hematoxylin and eosin.  $\times 1,352$ .
- 2 A nodule of ectopic lymphoid tissue in the liver of senile mouse, a 733 day male. The central portion consists of epithelioid cells. Hematoxylin and eosin.  $\times 450$ .
- 3 Arteriole from the periportal region of 718 day male. The wall is fibrosed and hyalinized. Acid anilin fuchsin and light green.  $\times 1,210$ .
- 4 Giant nucleus of hepatic parenchymal cell of an 818 day male. An inclusion is seen in left-hand portion of the nucleus. Hematoxylin and eosin.  $\times 1,093$ .



- Cossel, L. 1959 Elektronenmikroskopische Untersuchungen zur Frage des Disseaschen Raumes in der Leber. *Klin. Wochs.*, 37 743-753.
- Dalton, A. J. H. Kahler, M. J. Striebl and B. Lloyd 1950 Fine structure of hepatic, intestinal and renal cells of the mouse as revealed by the electron microscope. *J. Nat. Cancer Inst.*, 11 439-461.
- De Robertis, E., W. W. Nowinski and F. A. Sax 1960 General Cytology W. B. Saunders Company Philadelphia and London, pp. 535.
- Fawcett, D. W. 1953 Observations on the cytology and electron microscopy of hepatic cells. *J. Nat. Cancer Institute*, 15 (supplement) 1475-1504.
- Frischman, C. F. and D. S. Russell 1940 The occurrence of intranuclear inclusions in cultures of foetal leptomeninges. *J. Path. and Bact.*, 50 53-59.
- Kleinfeld, R. G., M. H. Greider and W. J. Frajola 1956 Electron microscopy of intranuclear inclusions found in human and rat liver parenchymal cells. *J. Biophys. and Biochem. Cytology* 2: suppl. 435-439.
- Leduc, E. H., and J. W. Wilson 1959 A histochemical study of intranuclear inclusions in mouse liver and hepatoma. *J. Histochem. and Cytochem.*, 7 8-16.
- 1959 An electron microscope study of intranuclear inclusions in mouse liver and hepatoma. *J. Biophys. and Biochem. Cytol* 6 427-430.
- Porter, K., and C. Bruni 1960 Fine structure changes in rat liver cells associated with glycogenesis and glycogenolysis. *Anat. Rec.*, 136, 2: 260-261.
- Stenram, U. 1956 Nucleolar size in the liver of rats fed on high and non-protein diets after starvation. *Acta Anat.*, 25 333-361.

## PLATE 1

## EXPLANATION OF FIGURES

- 1 Lymphocyte within hepatic parenchymal cell in small area of ectopic lymphoid tissue, in 213 day female mouse. This phenomenon is not common in young animals but occurs often in the livers of senile mice. Hematoxylin and eosin.  $\times 1,352$ .
- 2 A nodule of ectopic lymphoid tissue in the liver of senile mouse, a 733 day male. The central portion consists of epithelioid cells. Hematoxylin and eosin.  $\times 450$ .
- 3 Arteriole from the periportal region of a 716 day male. The wall is fibrosed and hyalinized. Acid anilin fasten and light green.  $\times 1,210$ .
- 4 Giant nucleus of hepatic parenchymal cell of an 815 day male. An inclusion is seen in left-hand portion of the nucleus. Hematoxylin and eosin.  $\times 1,993$ .

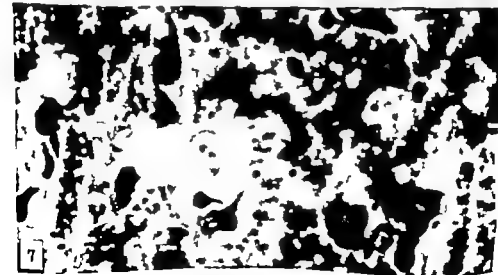


## PLATE 3

### EXPLANATION OF FIGURES

All figures are of liver tissue fixed in Regaud's fluid and stained with acid anilin fasten, to demonstrate the mitochondria, and counterstained with light green.

- 5 Liver of 716 day male. The cell near the center of the field shows degenerative changes both in nucleus and cytoplasm. Only the peripheral part of the nucleus is well stained, and the mitochondria are scanty.  $\times 1,000$ .
- 6 Liver of 716 day male. The distribution of mitochondria is irregular and they are scanty and vary in staining capacity in many cells. In the binucleate cell near the center of the field, however they are numerous.  $\times 1,000$ .
- 7 Liver of 816 day male. The cell near the center of the field is almost devoid of mitochondria.  $\times 1,000$ .







8 Portion of an hepatic parenchymal cell of senile male mouse. This cell appears essentially normal as like those of younger animals. C, lumen of capillary; D space of Disse containing cytoplasmic processes of the hepatic cell; L, lipid droplet; M mitochondrion; N nucleus  $\times 1,800$ .



9 Hepatic parenchymal cell of senile male mouse illustrating change in size of the nucleolus. The nucleolus in the upper portion of the nucleus shows large clear central area. Many hepatic cells show the appearance seen here of areas of somewhat denser appearing material surrounding the nucleoli and in some places seemingly condensed into structures of about the same size as the nucleolus. A, denser area about nucleolus B "body of nucleolar size" M mitochondrion N nucleolus.  $\times 18,500$ .

PLATE 5

EXPLANATION OF FIGURE

- 10 Hepatic cell of a senile male mouse with a very wide invagination of the nuclear membrane. It would seem probable in this case that a number of mitochondria could be enclosed by closing the sac if an intranuclear inclusion were to be formed. The structure within the nucleus is a well-formed body of nucleolar dimensions but without the density seen in definitive nucleoli. Note the smaller ovoid structure at the center of the body. Such ovoids may be seen also in figure 9. B body of nucleolar dimensions; C, cell membrane; I, lip of nuclear invagination.





- 11 Hepatic cell of senile male mouse. The nucleus has small, elongated inclusion mass and the invaginated portion appears to have been pinched off. The inclusion is similar in appearance to the cytoplasm. In this cell some lamellae of endoplasmic reticulum are especially prominent. ■ cell membrane; ER, endoplasmic reticulum; I inclusion N nucleolus.  $\times 22,300$ .



- 12 Hepatic cell with degenerating nucleus in the liver of senile mouse. The nuclear contents are uniformly more dense than in normal nuclei. Several very dense bodies are present. It is not possible to tell whether these should be described as blocks of chromatin or as altered nucleoli. The mitochondria in this cell also present some degenerative changes. The cell is binucleate. A portion of the relatively normal second nucleus is seen at the lower left.  $\times 24,000$ .



11 Hepatic cell of senile male mouse. The nucleus has a small, elongated inclusion mass and the invaginated portion appears to have been "pinched off". The inclusion is similar in appearance to the cytoplasm. In this cell some lamellae of endoplasmic reticulum are especially prominent. C cell membrane; ER, endoplasmic reticulum; I, inclusion; N nucleolus.  $\times 12,300$ .

E. M. OF AGE CHANGES IN LIVER  
WALTER ANDREW







**16** Nuclear phenomenon in liver of senile male mouse. A prominent bulging of the nuclear membrane is seen and in close relation to it series of plates of the endoplasmic reticulum. / 32,400

# Cytochemical Localization of Certain Oxidative Enzymes<sup>1</sup>

JAMES L. CONKLIN MAYNARD M. DEWEY AND RAYMOND H. KAHN  
*Department of Anatomy The University of Michigan Medical School  
Ann Arbor Michigan*

Employing the technique of cell fractionation, Schneider and Hogeboom ('56) described the localization of certain oxidative enzymes. They reported that cytochrome oxidase and succinic dehydrogenase were found only in the mitochondrial fraction while isocitric dehydrogenase was present in the supernatant and DPN and TPN cytochrome c reductases were observed to be in both fractions. More recently Thorne ('60) has reported a mitochondrial and a supernatant malic dehydrogenase.

In contrast to these reports on the localization of certain oxidative enzymes is the intracellular distribution as demonstrated by histochemical procedures. Scarpelli Hess and Pearse ('58) Hess Scarpelli and Pearse ('58) and Pearse ('60) reported that all pyridine nucleotide-linked dehydrogenases and DPN and TPN diaphorases were confined to the mitochondria. Nachlas Walker and Seligman ('58) described the intramitochondrial localization of DPN diaphorase and extramitochondrial localization of TPN diaphorase. Becker ('61) observed the mitochondrial localization of TPN diaphorase and intra and extramitochondrial distribution of DPN diaphorase. The obvious discrepancy between the evidence gained by the biochemical and histochemical methods might appear unresolvable except that the reliability of certain of the techniques employed in the previous histochemical studies are subject to question.

The current methods for the histochemical demonstration of oxidative enzyme activity depend upon the incubation of cells or tissues in a buffered medium containing the substrate, required cofactors and a tetrazolium salt. In the presence of the enzyme the substrate is oxidized and

the electrons made available by the oxidation are transferred (see below) to the tetrazolium salt reducing it to an insoluble formazan and thus indicating the site of enzyme activity. Of prime importance in these methods are the cofactors the electron transferring agents and the tetrazolium salt.

Several tetrazolium compounds have been utilized for the demonstration of oxidative enzymes. Farber Sternberg and Dunlap ('56) tested the available tetrazolium salts and reported that the best histological definition was obtained with neotetrazolium and blue tetrazolium. These compounds have subsequently been replaced by more sensitive salts. Nachlas et al. ('57) introduced the dye Nitro-BT (2,2'-di-p-nitrophenyl 5,5'-diphenyl 3,3'-(3,3'-dimethoxy-4,4' biphenylene) ditetrazolium chloride) while Pearse ('57) advocated the use of MTT (3,5-diphenyl 2-(4,5-dimethylthiazol 2-yl) tetrazolium bromide) chelated with cobaltous ions. Novikoff Shin and Drucker ('61) have reported that, of the two compounds Nitro-BT is superior for critical studies of mitochondrial morphology and oxidative enzyme activity since the deposition of MTT-Co++ is determined by physicochemical factors other than enzyme localization.

As demonstrated by Brodie and Gots ('61) the enzymatic reduction of the tetrazolium salt is dependent upon the presence of a flavoprotein a diaphorase. In actuality with the methods employed it is the diaphorase which is being localized and not the dehydrogenase (Farber Sternberg and Dunlap '56 Nachlas Walker and Seligman '58). Complications do not arise as long as the dehydrogenase and

<sup>1</sup>Research supported by USPHS Grants A-3449 and H-0-6676.

diaphorase have the same distribution. However if the dehydrogenase is located at a site which differs from the diaphorase distribution then theoretically it is impossible to demonstrate the enzyme at this site. Farber and Bueding ('56) suggested that the requirement for endogenous diaphorase could be overcome by employing another intermediate electron acceptor and utilizing phenazine methosulfate for this purpose. It has been subsequently confirmed by Dewey and Conklin ('60) and Nachlas, Margulies, Goldberg and Seligman ('60) that phenazine methosulfate can be employed as a substitute for the diaphorase in histochemical and biochemical procedures.

Another difficulty which has accompanied previous histochemical studies has been that the tissues were subjected to preparative procedures such as freezing and cryostat sectioning. The mitochondrial damage which occurs as the result of freezing could lead to leaching of the enzymes and subsequent diffusion artefact. While Pearse ('60) routinely employed mounting media made hypertonic by the addition of polyvinylpyrrolidone or suppose the necessity of using hypertonic media has been questioned by Walker and Seligman ('61) who reported that such conditions did not improve enzyme localization. These investigators and Novikoff, Shin and Drucker ('61) have advocated the use of short fixation for accurate localization of oxidative enzymes.

A final consideration in the accurate localization of enzyme activity is the interpretation of the size and distribution of the formazan deposits. It is extremely difficult to correlate formazan particles with cellular organelles unless the distribution of these organelles is confirmed by classical histological methods (Novikoff, Shin and Drucker '61).

The L strain fibroblast has been demonstrated to possess certain morphological characteristics which make it suitable material for the study of the distribution of oxidative enzymes. Under the conditions employed, the mitochondria are localized in a particular area of the cell and are clearly distinguishable from other components of the cytoplasm. (Kahn, Conklin and Dewey '62, Dewey, Kahn and Conklin,

'62.) In addition the cells may be grown as monolayers thus providing material which may be studied by phase optics and supravital staining. Furthermore oxidative enzymes may be readily demonstrated in cells which are untreated and thus adverse preparative procedures are avoided.

In the present study an attempt has been made to accurately localize several of the oxidative enzymes by employing Nitro-BT as the terminal electron acceptor and utilizing phenazine methosulfate as an intermediate electron transferring agent. The distribution of the oxidative enzymes was correlated with the distribution of cytoplasmic organelles as demonstrated by phase optics and supravital staining. In addition the effect of hypertonic media on enzyme activity and localization was evaluated.

#### MATERIALS AND METHODS

Stock NCTC 929 (L strain) fibroblasts maintained in stationary bottle cultures in medium 199 (Morgan, Morton and Parker '50) supplemented with 0.5% Bacto-peptone were subcultured on coverslips and grown for 48 hours as a monolayer. For the demonstration of enzyme activity coverslips were removed from the culture medium, rinsed in balanced salt solution, and either placed directly into the substrate or frozen at  $-70^{\circ}\text{C}$  prior to incubation. Oxidative enzyme activity was demonstrated by incubation in the following substrates:

**Glucose-6 phosphate Dehydrogenase (G6PDH)** - dipotassium glucose-6-phosphate (0.2 M), triphosphopyridine nucleotide (TPN) (0.3 mg/ml), cyanide (0.1 M), sodium fluoride (0.1 M), tris hydroxy aminomethylmethane (Tris) buffer (0.25 M, pH 7.4), phenazine methosulfate (PMS) (10  $\mu\text{g/ml}$ ), Nitro-BT (0.5 mg/ml).

**Glycerophosphate Dehydrogenase (GDH)** - sodium (DL)  $\alpha$ -glycerophosphate (0.25 M), diphosphopyridine nucleotide (DPN) (0.3 mg/ml), cyanide, PMS, Nitro-BT, Tris buffer.

**Hydroxybutyric Dehydrogenase (HDH)** -  $\beta$ -hydroxybutyrate (0.33 M), DPN, cysteine (0.01 M), nicotinamide (0.05 M), PMS, Nitro-BT, cyanide, Sorenson's phosphate buffer (0.25 M, pH 7.4).

Conservatively supplied by Dr. Donald L. Marchant.

**Lactic Dehydrogenase (LDH) Isocitric Dehydrogenase (IDH) Malic Dehydrogenase (MDH) -sodium (DL) lactate (0.1 M) disodium (DL) Isocitrate (0.25 M) and sodium (L) malate (0.25 M) respectively DPN cyanide PMS Nitro-BT phosphate buffer**

**Succinic Dehydrogenase (SDH) -sodium succinate (0.5 M) cyanide PMS Nitro-BT phosphate buffer**

**Diphosphopyridine Nucleotide Diaphorase (DPND) and Triphosphopyridine Nucleotide Diaphorase (TPND), reduced DPN (DPNH) and reduced TPV (TPNH) (0.5 mg/ml) respectively Nitro-BT phosphate buffer**

Cytochrome oxidase was localized by the method of Burstone (6) employing N-phenyl p-phenylenediamine monohydrochloride, 1-hydroxy-2-naphthol acid and cytochrome C. Cells were also incubated in substrates containing either 7.5% polyvinylpyrrolidone K-30 (PVP) 0.44 M or 0.88 M sucrose in order to determine the effect of osmolar protection on enzyme activity and localization.

Since the accurate localization of the various enzymes was the primary purpose of the study the distribution of cellular organelles was confirmed by examining viable cells with phase optics. In addition, mitochondrial morphology and distribution were revealed by supravital staining with Janus green B (0.01% in isotonic sodium chloride)

## RESULTS

The intracellular localization of oxidative enzymes in the L strain fibroblast is facilitated by the morphological characteristics of this cell. When viewed with phase optics (fig. 1) the cytoplasm of the L cell

can be divided into three distinct areas: a juxtanuclear zone a granular zone and an outer nongranular zone. The juxtanuclear zone consists of vacuoles embedded in a homogeneous cytoplasm. The granular zone surrounds both the nucleus and the juxtanuclear zone and contains numerous moderately large (ca 2  $\mu$ ) dense granules. Extending from the granular zone to the outer limits of the cells is a thin layer of nongranular cytoplasm i.e. the nongranular zone. When the cells are supravital stained with Janus green B the dye is localized only in the large dense granules of the granular zone (fig. 2) indicating that mitochondria are confined exclusively to this area. The consistent size of the mitochondria and their localization in the granular zone of the cytoplasm facilitated the interpretation of the formazan deposits produced by the various enzyme procedures. The deposits varied with the procedure employed and could be arbitrarily categorized (table 1) as to size and site of deposition and correlated with cytoplasmic structures demonstrated by other procedures. Large formazan granules corresponded in size, number and distribution to the mitochondria (figs. 4-10 and fig. 12) and were confined to the granular zone. Finer formazan granules were also observed and were present in the juxtanuclear granular and nongranular zones (figs. 5-12). These formazan granules were considerably smaller and more numerous than the mitochondria. After certain procedures the smaller formazan granules appeared to be associated with a fine reticulum which was present throughout the cytoplasm (figs. 6-12) and which was clearly separable from the larger gran-

TABLE 1  
Distribution of oxidative enzymes

Enzyme	Juxtanuclear zone	Granular zone
Cytochrome oxidase	Absent	Large granules
SDH	Absent	Large granules
IDH	Small granules, reticular	Large granules, reticular
MDH	Small granules, reticular	Large granules, reticular
HDH	Reticular	Reticular few large granules
DPND	Small granules, reticular	Large granules, reticular
LDH	Small granules, reticular	Large granules, reticular
G6PDH	Small granules, reticular	Reticular few large granules
TPND	Reticular	Reticular
GPDH	Reticular	Reticular few large granules

ular mitochondria. Cytochrome oxidase activity was present only in the large granules of the granular zone (fig. 3).

The exclusive deposition of formazan within the mitochondria after certain procedures and the presence of formazan both intra and extra mitochondrially after others, would indicate a dual localization of certain oxidative enzymes. IDH, MDH, LDH, HDH, G6DH, GDH and DPND (figs. 5-10 and fig. 12) are present within the mitochondria and also associated with extramitochondrial structures. SDH and cytochrome oxidase (figs. 3 and 4) are located only within the mitochondria while TPND (fig. 11) was observed to be exclusively extramitochondrial in localization.

The localization of the various oxidative enzymes was reproducible under all conditions of incubation. While the addition of PVP and sucrose appeared to increase the granular nature of the formazan, the distribution was identical to that obtained without the utilization of these additives. The only apparent effect of the hypertonic media was to prolong the incubation time. Likewise freezing the cells prior to incubation in the substrate did not alter the distribution of formazan. Freezing did however markedly increase the activity of all enzymes except cytochrome oxidase which was inhibited. (Activity was interpreted visually from the amount of formazan deposited in a 16 minute period and is a function of both enzyme concentration and enzyme turnover rate.) Freezing was least effective in the activation of DPND, MDH, LDH, G6DH and TPND and facilitated the demonstration of SDH, GPDH, HDH and IDH. However the latter enzymes could be demonstrated without prior freezing if the incubation period was prolonged.

When enzyme activity was demonstrated under comparable conditions a difference in the level of activity of the various enzymes was apparent. In decreasing order of relative activity the enzymes could be grouped as follows: DPND > LDH > MDH > IDH > G6DH > TPND > HDH > GPDH > SDH. The activity of cytochrome oxidase could not be directly correlated with dehydrogenase and diaphorase activity since a different cytochemical procedure was employed

In considering the relative activities of the various enzymes it was of interest that variation in enzyme activity paralleled variation in density of cell population. When grown as monolayers under the present conditions the L strain fibroblasts occur as colonies of closely grouped cells with single cells scattered between the colonies. The activity of DPND, LDH and MDH was greater in colonies of cells than in single isolated cells. This variation in activity was less evident with respect to the other enzymes studied.

#### DISCUSSION

In the present study an attempt has been made to accurately localize certain of the oxidative enzymes in the L strain fibroblast. Localization was greatly facilitated by several factors: 1. The use of viable cells which permitted study by phase optics and supravital staining. 2. The characteristic distribution of organelles in the L cell. 3. The omission of preparative procedures thus minimizing the production of artifact. 4. The use of phenazine methosulfate as an intermediate electron acceptor for the demonstration of dehydrogenase activity; and 5. The employment of Nitro-BT as the terminal electron acceptor.

The selection of the L strain fibroblast for the study of enzyme localization was most fortuitous because of the characteristic distribution of mitochondria in the granular zone of the cell (figs. 1 and 2). When oxidative enzyme activity was demonstrated in these cells it was readily apparent that some enzymes were confined to the mitochondria while others were also present extramitochondrially. An analysis of table 1 and figures 3 and 4 illustrates that only cytochrome oxidase and SDH were restricted to the mitochondria. Figures 5 through 10 and figure 12 demonstrate the dual localization of IDH, MDH, HDH, DPND, LDH, GDH and G6DH within the mitochondria as well as elsewhere in the cytoplasm. TPND activity was present only extramitochondrially (fig. 11). The inability to demonstrate the multiple localization of certain of the oxidative enzymes in previous histochemical studies may have occurred, in part, because of the failure to compare the distribution of formazan particles with the distribution of cellular

organelles. In the present study the distribution of organelles was confirmed by phase optics and supravital staining although classical techniques could have been employed. Cytoplasmic morphology should be confirmed in all histochemical studies of oxidative enzymes since the nature of the formazan deposits makes the accurate identification of organelles practically impossible. The suggestion that the DPNH technique is the best method for the demonstration of mitochondria (Scarpelli, Hess and Pearse '58) may be seriously questioned in view of the distribution of this enzyme in the L cell (figs. 1, 2 and 8). If a histochemical procedure is to be employed for the demonstration of mitochondria, the cytochrome oxidase method of Burnstone ('60) seems to be best suited (fig. 3).

Another complication introduced into previous histochemical studies of oxidative enzymes has been the failure to employ an intermediate electron acceptor. Since it is well established that electrons are transferred to tetrazolium salts at points in the electron transport chain beyond the level of the dehydrogenase (Nachlas Margulies and Seligman, '60) it is obvious that dehydrogenase activity can be demonstrated only in those sites where appropriate endogenous transferring agents are present. This dependency on endogenous agents can be overcome quite easily by employing various exogenous compounds in the substrate medium. While exogenous diaphorase may be employed, commercially available preparations are not sufficiently purified and consequently other intermediate agents are recommended. Although a variety of redox dyes have been tested histochemically (Farber and Louviers, '56) the compound of choice is phenazine methosulfate which is readily available, inexpensive and easily employed. In the present study PMS was not essential for the demonstration of the DPN-linked dehydrogenases because of the wide-spread distribution of DPN diaphorase. Phenazine methosulfate was essential for the demonstration of the TPN-linked mitochondrial G6DH since TPN diaphorase was not present within the mitochondria and therefore not available to mediate the transfer of electrons to the tetrazolium salt. Since

PMS increased the activity of the DPN linked enzymes it was routinely employed for their demonstration also. This activation effect of PMS also was noted by Walker and Seligman ('61) who reported a 6-fold increase in SDH activity in fresh-frozen tissues. In the present study PMS was found to activate cells which were either fresh or fresh-frozen. Thus in addition to improving localization PMS also increases the reaction rate and markedly facilitates the specific demonstration of dehydrogenase activity.

Although it has been claimed that osmolar additives such as PVP or sucrose are essential for the accurate localization of oxidative enzyme activity (Scarpelli and Pearse '58; Hess, Scarpelli and Pearse '58) such a requirement was not evident in the present study. The addition of these substances to the incubating medium had no effect on the localization of the various enzymes and seemed to be merely an unnecessary complication of the procedure. It also had the disadvantage of decreasing the reaction rate and prolonging the incubation time. The concept that mitochondrial integrity is maintained by employing additives is probably not justifiable especially in the case of tissues which have been frozen and subjected to cryostat sectioning. In view of the report of Ziegler and Linnane ('58) that certain substrates are not oxidized by intact mitochondria and that oxidative capacity is greatly augmented after freezing, it is probable that enzyme activity cannot be demonstrated by the usual histochemical procedure unless mitochondrial damage has occurred. The activation of certain of the enzymes after freezing, observed in the present study is assumed to be due to increased accessibility of substrate to enzyme as the result of damage to the mitochondria.

It has been suggested that mitochondrial damage can lead to the production of diffusion artefact. Presumably this artefact occurs as the result of diffusion of enzyme, reduced coenzyme or formazan. It is unlikely that any of these factors are a problem when PMS and Nitro-BT are employed. The varied and rather precise localization of the oxidative enzymes demonstrated in the present study would indicate that enzyme diffusion did not occur. Furthermore

the addition of protective compounds to the media, which should minimize such diffusion had no effect on enzyme distribution. Secondly it is also unlikely that diffusion of DPNH occurred under the conditions employed since differences in distribution were observed for the various DPN-linked dehydrogenases. In addition, in a starch gel electrophoretic study of LDH and DPND (Dewey and Conklin '60) the same substrates were employed to localize these enzymes in the starch gel and therefore reduced DPN was produced as LDH was demonstrated. If the DPNH was able to diffuse from the regions of the LDH fractions to the areas where DPND was located it could serve as substrate for the latter. Since this never occurred it is probable that the DPNH is rapidly reoxidized in the presence of PMS and Nitro-BT. Although the starch matrix is not analogous to cytoplasm it seems equally probable that in view of the redox potential and site of action of Nitro-BT (Nachlas Margulies and Seligman '60) and the activity of PMS that diffusion of DPNH does not occur. Finally although some diffusion of the formazan can occur it does not happen readily with Nitro-BT and is not a problem if the tissues are examined soon after completion of the procedure. In any event, such artefact is easily recognizable since the formazan tends to aggregate in large masses. Diffusion artefact never produces a reticular like arrangement of formazan as observed after certain procedures (figs. 4-12). While the distribution of certain of the enzymes differs from that reported in previous histochemical investigations it is felt that barring actual differences in the tissues investigated the substrates utilized in this study are better suited for the precise localization of the various enzymes. It seems very likely that the active components of the substrate solutions are of more significance to studies of localization than chemical and physical protective agents.

Although the enzymes studied were classifiable in order of relative activity very little can be deduced as to the actual metabolic state of the cells since the activity of the same enzymes in uncultured fibroblasts has not been reported. The relative activities are in general agreement

with reports of enzyme activity in various types of malignant cells (Monis, Nachlas and Seligman '59 Stolk, '60; Rees and Huggins '60). It is possible that the levels of oxidative enzyme activity of these fibroblasts will more closely resemble that of malignant cells rather than normal fibroblasts since, like other cultured cells the L strain fibroblast has undergone changes as the result of continuous culture (Earle Shelton and Schilling, '49).

The demonstration of differences in enzyme activity between the cells of the population suggests that biochemical analyses of total cell populations would be more meaningful if the metabolic state of individual cells was determined concomitantly by histochemical methods (Kahn, Conklin and Dewey '62).

#### SUMMARY

The activity of certain Kreb cycle glycolytic and pentose shunt enzymes was demonstrated histochemically in the L strain (929) fibroblast. The intracellular distribution of these enzymes was correlated with the cytoplasmic organelles demonstrable with phase optics and supravital staining. By this method of study it was possible to demonstrate that some of these enzymes were located exclusively in the mitochondria while others were located extramitochondrially as well.

The authors are deeply indebted to Mrs. Julia Ternak and Miss Denise Streibitzky for their technical assistance.

#### LITERATURE CITED

- Becker W H. 1961 The cytochemistry of anoxia and anoxo-toxic encephalopathy in rats. II. Alterations in neuronal mitochondria identified by diaphorase and triphosphopyridine nucleotide diaphorases. *Am. J. Path.* 38: 567-597.
- Brodie A. F., and J. S. Gots. 1951 Effects of an isolated dehydrogenase enzyme and flavoprotein on the reduction of triphenyltetrazolium chloride. *Science*, 114: 40-41.
- Burstone M. S. 1960 Histochemical demonstration of cytochrome oxidase with new amine reagents. *J. Histochem.* 8: 63-70.
- Dewey M. M., and J. L. Conklin. 1960 Starch gel electrophoresis of lactic dehydrogenase from rat kidney. *Proc. Soc. Exp. Biol. Med.* 105: 492-494.

- Dewey M. M., R. H. Kahn and J. L. Conklin 1962 A cytochemical and cytological analysis of the L-strain (929) fibroblast. (In preparation.)
- Earle, W. R., E. Shelton and E. L. Schilling 1949 Production of malignancy *in vitro*. I. Further results from reinjection of *in vitro* cell strains into strain C-3H mice. *J. Nat. Cancer Inst.*, 10: 1105-1113.
- Farber E., W. H. Sternberg and C. E. Dunlap 1956 Histochemical localization of specific oxidative enzymes. I. Tetrazolium stains for diphosphopyridine nucleotide diaphorase and triphosphopyridine nucleotide diaphorase. *J. Histochem.*, 4: 254-263.
- Farber E., and C. D. Louviere 1956 Histochemical localization of specific oxidative enzymes. IV Soluble oxidation-reduction dyes as aids in the histochemical localization of oxidative enzymes with tetrazolium salts. *Ibid.* 4: 347-356.
- Farber E., and E. Boedding 1956 Histochemical localization of specific oxidative enzymes. V. The dissociation of succinic dehydrogenase from carriers by lipase and the specific histochemical localization of the dehydrogenase with phenazine methosulfate and tetrazolium salts. *Ibid.*, 4: 357-362.
- Fess, R. D., G. Scarpelli and A. G. E. Pearse 1958 Cytochemical localization of pyridine nucleotide-linked dehydrogenases. *Nature*, 181: 1531-1532.
- Kahn, R. H., J. L. Conklin and M. M. Dewey 1962 Cytological and cytochemical characterization of cells grown *in vitro*. *J. Nat. Cancer Inst.*, (in press)
- Monks, B. M. M. Nachlas and A. M. Seligman 1959 Histochemical study of three dehydrogenase systems in human tumors. *Cancer* 12: 1238-1247.
- Morgan, J. F. H. J. Morton and R. C. Parker 1960 Nutrition of animal cells in tissue culture. I. Initial studies on a synthetic medium. *Proc. Soc. Exp. Biol. Med.*, 73: 1-8.
- Nachlas, M. M., K. C. Tsou, E. De Souza, C. S. Cheng and A. M. Seligman 1957 Cytochemical demonstration of succinic dehydrogenase by the use of a new p-nitrophenyl substituted diazotized. *J. Histochem.*, 5: 420-438.
- Nachlas, M. M., D. G. Walker and A. M. Seligman 1958 A histochemical method for the demonstration of diphosphopyridine nucleotide diaphorase. *J. Biophys. Biochem. Cytol.*, 4: 29-38.
- 1958 The histochemical localization of triphosphopyridine nucleotide diaphorase. *Ibid.*, 4: 467-474.
- Nachlas, M. M., R. I. Margulies and A. M. Seligman 1960 Sites of electron transfer in tetrazolium salts in the succinoxidase system. *J. Biol. Chem.*, 235: 2739-2743.
- Nachlas, M. M., S. I. Margulies, J. D. Goldberg and A. M. Seligman 1960 The determination of lactic dehydrogenase with a tetrazolium salt. *Anal. Biochem.*, 1: 317-326.
- Nevikoff, A. B., W. Y. Shin and J. Drucker 1961 Mitochondrial localization of oxidative enzymes. Staining results with two tetrazolium salts. *J. Biophys. Biochem. Cytol.*, 9: 47-61.
- Pearse, A. G. E. 1957 Intracellular localization of dehydrogenase systems using monotetrazolium salts and metal chelation of their formazans. *J. Histochem.*, 5: 515-527.
- 1960 *Histochemistry: Theoretical and Applied*. Little Brown and Co., Boston.
- Rees, E. D., and C. Haggins 1960 Steroid influences on respiration, glycolysis, and levels of pyridine nucleotide-linked dehydrogenases of experimental mammary tumors. *Cancer Res.*, 20: 963-971.
- Scarpelli, D. G., and A. G. E. Pearse 1958 Physical and chemical protection of cell constituents and the precise localization of enzymes. *J. Histochem.*, 6: 369-378.
- Scarpelli, D. G., E. Hess and A. G. E. Pearse 1958 The cytochemical localization of oxidative enzymes. I. Diphosphopyridine nucleotide diaphorase and triphosphopyridine nucleotide diaphorase. *J. Biophys. Biochem. Cytol.*, 4: 747-758.
- Schneider, W. C., and G. H. Hogeboom 1956 Biochemistry of cellular particles. *Ann. Rev. Biochem.*, 25: 201-224.
- Stolk, A. 1960 Histochemical analysis of three dehydrogenase systems in the renal adenocarcinoma of *Aplocheilichthys*. *Naturwissenschaften*, 47: 183.
- Thorne, C. J. B. 1960 Characterization of two malic dehydrogenases from rat liver. *Biochem. Biophys. Acta*, 42: 173-178.
- Walker D. G., and A. M. Seligman 1961 For malin fixation in the cytochemical demonstration of succinic dehydrogenase of mitochondria. *J. Biophys. Biochem. Cytol.*, 9: 415-427.
- Ziegler D. M., and A. W. Linnane 1958 Studies on the electron transport system. XIII. Mitochondrial structure and dehydrogenase activity in isolated mitochondria. *Biochem. Biophys. Acta*, 30: 53-62.

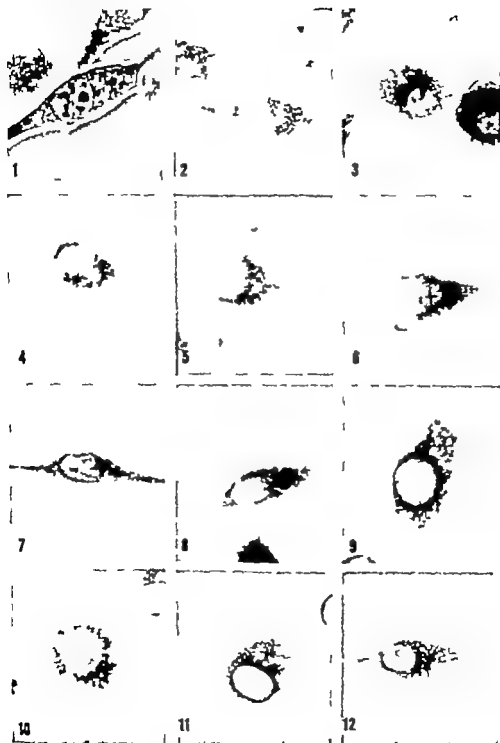


## PLATE 1

### EXPLANATION OF FIGURES

All figures are of the L strain fibroblast.  $\times 900$ .

- 1 The L strain fibroblast as viewed with phase optics. Note the juxta-nuclear zone (J) granular zone (G) and the peripheral nongranular zone (N)
- 2 Supravitality stained with Janus green B. The stain is localized in the granules (mitochondria) of the granular zone.
- 3-4 Cytochrome oxidase and succinic dehydrogenase activity respectively restricted to the mitochondria of the granular zone.
- 5-6 Lactic and malic dehydrogenase activity respectively. Note that while activity is greatest in the mitochondria of the granular zone there is reticular distribution of activity in the juxtanuclear and nongranular zones as well.
- 7-10  $\beta$ -hydroxybutyric dehydrogenase, DPN diaphorase, lactic and -glycerophosphate dehydrogenase activity respectively. Note the presence of both reticular and granular formazan deposits throughout the cytoplasm.
- 11 TPN diaphorase activity. Observe that while activity is present in all three zones of the cytoplasm, it is nongranular in nature. The vacuoles present in the region of the granular zone indicates the absence of mitochondrial activity.
- 12 Glucose-6-phosphate dehydrogenase activity. This enzyme also has a dual localization and is present throughout the cytoplasm.





# Fetal Resorption in the Rat as Influenced by Certain Antioxidants<sup>1</sup>

IRA R. TELFORD CAROLINE E. WOODRUFF AND RAY H. LINFORD  
*The George Washington University School of Medicine Department of  
Anatomy Washington, D. C.*

Some prenatal mortality is perhaps a normal phenomenon accompanying gestation in all mammals. Yet there is a paucity of definitive data on total embryonic or fetal wastage as compared with the wealth of information on the pathologic, genetic, physiologic and nutritional causes of prenatal death. Of the literature which deals with this problem in man or domesticated animals, most of it deals with fetal mortality either as stillbirths or abortions.

In the rat there are many factors that may increase fetal death and subsequent resorption as, insufficient protein (Barry '20) elevated environmental temperature (Sundstroem '27; Hsu, '48; MacFarlane Pennycook and Thrift, '57) vitamin deficiencies e.g. biotin (Kennedy and Palmer '45) pantothenic acid (Nelson and Evans '46) pyridoxine (Nelson and Evans '48) pteroylglutamic acid (Nelson Aalling and Evans '52) tocopherol (Cheng and Thomas '53) and riboflavin (Nelson et al., '56). Other causes of resorptions are ovariectomy (Harterius, '36) trypan blue injections (Wilson '54) *Lathyrus odoratus* feeding (Walker and Wirtschafter '56) and others. There is also evidence that loss due to resorption is not confined to any particular period of pregnancy but occurs throughout gestation (wild rat, Perry '46; wild rabbit, Brambell '48; mouse Holander and Strong, '50).

Because the rat resorbs rather than aborts an imperfect conceptus, a record of all implantations is retained in the uterine mucosa at the implantation sites. This record is represented by remnants of implantation ranging from resorbed fetuses to inconspicuous cicatricial plaques. A careful macroscopic examination of the incised term uterus will therefore supply data on total implantations as well as normal young.

Resorption data secured from the examination of nearly 500 pregnant rats involving approximately 5 000 fetuses and over 800 resorptions is herewith presented. In addition, we investigated the influence of certain maternally administered compounds mostly antioxidants, on the incidence of fetal loss as compared to normal animals held on normal diets. These data are the outgrowth of a larger problem concerned with the possible value of these antioxidants and related compounds in the prevention or amelioration of lesions arising from neonatal anoxia.

## MATERIALS AND METHODS

Walter Reed-Carworth Farms strain rats in their first gestation were used exclusively and weighed approximately 200 gm at time of breeding. After positive mating the females were randomly distributed into experimental and control groups and the former were given *per os* or directly into diet one of the various compounds listed in table 1. Twenty-two days after positive mating the pregnant rat was killed in 100% nitrogen and after 21 minutes the young delivered by caesarian section. Both horns of the uterus were completely incised and a careful macroscopic survey made for resorption sites. The resorptions were charted as to location in the respective region of the horns and classified as to degree of resorption. Seasonal variation in the number of resorptions were recorded.

## RESULTS

In 126 normal untreated gravid animals 40.8% had one or more resorptions and 10.6% of all recognizable implantations had terminated in resorptions. Of the 29 dietary regimens used, animals receiving

<sup>1</sup>Supported by U.S.P.H.S. research grant B-1636 and United Cerebral Palsy research grant R-117734.

TABLE I  
Effect of nitrofurant and other compounds on fetal resorption<sup>1</sup>

	Total dose	Per os or i. d. i.	Litters	Implanta- tions	Normal fetuses	Litters with resorption	Resorptions
	mg					%	%
Butyraldehyde (BUT)	0.5	D	11	11	121	18.3	2.4
d-Lipid tocopherol acetate	0.5	O	12	100	103	41.7	4.1
2,5-di-tert-butylhydroquinone	0.25	D	10	131	1.8	60.0	4.5
d-8-nitro tocopherol	0.5	O	11	137	131	45.5	4.7
D-tylated butyryl lactate (DILA)	0.5	D	13	148	137	51.7	8.5
d-8-nitro tocopherol	0.07	O	12	137	148	50.0	8.7
2,5-di-tert-butyl-4-methylphenol (DBMP)	0.5	O	11	140	131	51.5	6.4
Thiodipropionide acid	0.5	D	10	128	119	60.0	7.0
1,2-di-hydro-2,2,1-trimethyl-5-ethoxyquinoline (4 nitro im)	0.5	D	12	147	136	33.3	7.5
1,2-di-hydro-2,2,1-trimethyl-10-phenylquinoline (Santocid II)	0.25	D	11	120	1.8	54.5	7.0
Nordihydroquinazolinic acid (NDQA)	0.5	D	8	86	79	75.0	8.1
p-Tartronic acid sodium (vit B <sub>5</sub> )	0.25	D	11	138	128	27.3	8.7
Thioline hydrochloride	2.0	O	13	100	145	00.0	8.4
Ascorbic acid	2.0	O	14	146	132	71.4	9.6
Glucose	30% i. d. i.	D	5	80	251	08.0	10.3
Normal							
Thioline hydrochloride	0.5	D	128	1430	1378	40.8	10.6
2-methyl-4-tert-butyl-6-tert-butylphenol	0.25	D	8	70	67	02.5	10.7
Hydroxymethyl-2,2,1-trimethyl-10-phenylquinoline	0.25	D	8	101	00	37.5	10.9
Galactose (Thioline II)		D	17	146	136	52.9	12.1
Cytocrome C	0.05	D	8	81	73	50.0	13.1
Glutathione	0.25	D	6	65	56	66.8	13.9
d-Lipid tocopherol acetate	0.1	O	14	150	129	71.4	14.0
Ascorbic acid	0.5	D	20	235	180	70.0	15.3
N,N'-diphenyl-p-phenylene-diamine (DPPD)	0.5	D	23	375	233	00.8	16.3
Phenothiazine	0.25	D	10	80	75	70.0	15.7
2,2-methyl-4-tert-butyl-6-tert-butylphenol	0.5	D	9	111	92	66.8	17.1
p-Tartronic acid (PATA)	0.5	D	9	93	78	77.7	18.3
Hydroquinone	0.5	D	9	105	80	77.7	23.8
Methyl-4-tert-butylphenol	0.5	D	10	105	77	100.0	25.8
Methyl-4-tert-butylphenol	0.5	D	10	100	83	90.0	38.0

<sup>1</sup>For samples of nitrofurant in use, see instructions to the American Cyanamid Company for dis-alphaloc (nitrofurant) and 2,2-methyl-4-tert-butyl-6-tert-butylphenol; for dis-alphaloc (nitrofurant) and 2,2-methyl-4-tert-butyl-6-tert-butylphenol, see instructions to the American Cyanamid Company for dis-alphaloc (nitrofurant) and 2,2-methyl-4-tert-butyl-6-tert-butylphenol. For dis-alphaloc (nitrofurant) and 2,2-methyl-4-tert-butyl-6-tert-butylphenol, see instructions to the American Cyanamid Company for dis-alphaloc (nitrofurant) and 2,2-methyl-4-tert-butyl-6-tert-butylphenol.

one of 15 showed less resorptions (range 2.4-10.1%) than the controls, while rats receiving one of the other 14 diets showed an increased percentage of resorptions (10.7-38.0%) (table 1). In the dosage given none of these compounds appeared to be toxic to the mother with the possible exception of methylene blue, where poor pregnancy weight gain was noted. This compound yielded, incidentally the highest percentage of resorptions (38.0%). Of particular interest is the observation that two of the widely used commercial antioxidants, butylated hydroxytoluene (BHT) and butylated hydroxyanisole (BHA) as well as the antioxidant vitamins alpha and gamma tocopherol, at 200 mg level, and 2,5-di-tert-amylhydroquinone gave the lowest percentage of resorptions.

Data on the distribution of resorption sites in all groups revealed that 47.6% of all resorptions were located in the cranial third of the horns, 20.6% in middle third and 31.8% in the caudal third. Most of the sites seen in this cranial region were small inconspicuous cicatricial plaques suggestive of an early embryonic death.

Using the classification of Walker and Wirtschafter ('56) most of the resorptions, regardless of dietary supplement, belonged either to grade 3 representing complete resorption of the embryo but with small placenta still present, or grade 4 which are cicatrized uterine plaques marking previous placental sites. Grade 2 consisting of small macerated recognizable fetuses were seldom encountered. The number of fetuses falling into grade 1 e.g. dead, but fully formed, could not be determined since many of our fetuses were killed by anoxia treatment of the mother.

#### DISCUSSION

Since our observations dealt with the identification of placental sites *in situ* the question might be raised if identifiable plaques form at all implantation sites. That such scars do form where embryos have been resorbed is well documented by the work on rats of Davis and Emlen ('48). They reported more scars present than young born, the excess being ascribed to resorbed embryos. They also noted that scars do not occur spontaneously in non-pregnant rats. Moreover these authors

and Conaway ('55) reported that the resorption sites may remain identifiable for at least a year in the rat, and Deno ('41) made the same observation on the mouse. Therefore our use of first gestation animals avoided the possible error of counting sites of earlier pregnancies and ascribing them to the gestation under study.

The range of reported resorptions in normal rats by other investigators (11.8-6.5%) (table 2) may be due to seasonal variations in the fertility of the animals. It is generally accepted by rat breeders that fertility is lowest in winter and highest in summer (Mahn, '39). Since our data was collected throughout the year under controlled environmental conditions, we were able to separate our findings on a seasonal basis. We noted a reduction in the percentage of resorptions during the spring and summer (8.1%) and a marked increase (20.7%) during the winter and fall. Frazer ('55) using Wistar albino rats reported that 31% of all litters had some prenatal mortality on a yearly average, but that it was lowest in July-September (17%) and highest from October to December (88%). Other workers failed to present their prenatal mortality data on a seasonal basis, therefore an accurate comparison of animal groups is difficult, if not impossible.

Another variable influencing the percentage of resorptions in the rat may be the strain difference. Data on 6 different strains including the wild rat, are summarized in table 2 and with the exception of our WR-CF animals (10.6%) and Masons O.M.-Mc. rats (11.8%) the 4 remaining groups agree rather closely on resorption percentages (8.6-8.7%). Yet the strain of the animal may be important for the findings of Fekete ('47) in the mouse that fertilized ova transplanted to different strains of mice have a significantly better chance of survival in one strain than another implies that one strain provides a better environment for implantation and development of the ovum. Hollander and Strong ('50) also noted significant differences in fetal mortality among various strains of mice. It is certainly possible that in the rat also strain differences may exist which could

TABLE 2  
Prenatal mortality in mammals

Animal	Litters	Implanta- tions	Normal fetuses	Resorptions	Corpus luteum	Total prenatal mortality	Reference
Striped hamster	29	183	118	5			Fortuyn, '29
Goat	12	106	102	28.5	135	22.7	Deaneley, '31
Gray squirrel	9		27	4.6	30	10.0	Deaneley and Purdie, '33
Sheep	80	100	101	7.2	110	12.9	Hammond, '31
Pig	22	310	267	15.5	306	22.5	Hammond '31
Pig	495	3528	3485	1.2	4490	22.2	Coxner '33
Pig	102	1117	1028	8.0	1306	26.1	Crew '35
Rabbit (wild)	68	260	240	2.9	890	12.8	Hammond, '31
Rabbit (wild)	1818		8377		10574	16.0	Brambell, '48
Rabbit (wild)	2178	11383	8927	7.8	12531	9.4	Brambell and Mills, '47
Rabbit (wild)	1834	9058	291	11.3	578	32.3	Brambell and Mills, '48
Rabbit (house)	56	441	7987	10.3			Hammond, '31
Mouse	1080	500	2830	7.7	1420	30.0	Hollender and Strong, '50
Mouse <sup>a</sup>	500	3175	1136	8.3			Danforth and deAberia, '38
Rat (wild brown)	131	1238	434	11.8			Perry '45
Rat (Old-Mo)	50	493	211	6.6			Mason
Rat (Winter)	25	926	62	8.7			MacFarlane et al., '37
Rat (Winter) <sup>a</sup>	6	57					Wilson, '54
Rat (Long-Evans)	156		968		1498 (ova count)	23.4	Long and Evans '52
Rat (Long Evans) <sup>a</sup>	42	447	410	8.3			Nelson et al., '53
Rat (Holzman)	111	371	347	6.5			Cheng and Thomas, '53
Rat (WR-Cp) <sup>a</sup>	1 <sup>a</sup>	1430	1278	10.8			Telford, Woodruff, Linford

<sup>a</sup>Quoted from this data were 11 litters with all implanted embryos resorbing.

<sup>b</sup>From data on 500 pregnancies during last third of gestation as compared to 800 litters 1-5 days old.

Old-Mo designates mixed strain derived from Osborne-Mendel and McCollum inbred strains (data from personal communication).

Winter designates mixed strain derived from Old-Mo-Mendel and McCollum inbred strains (data from personal communication).

WR-Cp indicates original Carworth Farms stock but inbred at Walter Reed Army Research Center.

account for the fairly wide range of prenatal death rates.

Our analysis of the location of resorption sites in the various regions of the uterine horn revealed that 47.6% of all resorptions were found in the cranial third of the horn, with 20.7% in middle third and 31.8% in caudal third confirming our impression that the cephalic tapered extremity of the horn was, perhaps, an unfavorable location for the developing embryo. This concept is supported by the observation of Fawcett, Wislocki and Waldo (47) that the overcrowding by the developing mouse ovum in the anterior chamber of the eye inhibited the growth of adjacent implanted ova. However, Frazer's (55) data on the rat does not favor this idea, for he demonstrated that the percentage resorption was the same in both horns even though different number of ova were implanted in the different horns. Furthermore the overcrowding of a mouse uterine horn with an unusually larger number of implanted ova did not influence adversely the resorption rate, as shown by Hollander and Strong (50).

Another variable influencing fetal loss is the maternal age or weight. Frazer (55) noted in two strains of rats that the heavier the mother the higher resorption rate. Similar findings had been reported earlier by Hollander and Strong (50). All of our animals were standardized at approximately 200 gm giving us uniform test animals thus eliminating the possible discrepancies due to age or weight.

Combining the data in table 2 for all groups of the same species reveals that the same rat values fall roughly in the middle of the other mammalian data. For example the same rat data show that 9.2% of all implantations end in resorptions. Those mammals with a lower percentage of resorptions are pig (3.7%), stoat (4.6%), sheep (7.2%), wild rabbit (7.3%) and wild rat (8.3%). Those animals suffering on the average greater fetal loss than the rat are tame rabbit (11.3%), mouse (15.9%) and wild hamster (38.3%). While fetal wastage is probably common to all mammals considerable species variation does exist.

Basic to our study of the value of anti-oxidants in the reduction of fetal mortality

is the question of their mode of action and whether the site of action of the compound is on the fetal or maternal side of the placenta or both. Most of the agents reported here have been previously used in animal experimentation (Bunnell et al. '55 Schwarz, '58 Mertz and Schwarz, '58 Dam et al., 48 '51). From the results of these workers we assumed that the compound could be assimilated into the blood stream and may exert some influence on the developing placenta and might affect fetal growth. Evidence of placental transfer however is available only on a limited number of the tested agents, such as glucose (Huggett '54)  $\alpha$ -tocopherol (Neuwessler 49) thiamine chloride (Slobody Willner and Mestern, 49) ascorbic acid (Hamil et al. 47) and phenothiazine (Behn, Frahm and Fretwurst, '56). The rate of placental transfer of fat and water soluble vitamins is quite different with the lipid soluble vitamins being much slower. In fact in the rat the transfer may be so slow that the cord blood content of vitamin A (Lund and Kimble 43) or E (Straumfjord and Qualle 46) may under certain circumstances be less than in maternal blood. In the rat Mason and Bryan (40) reported only limited placental transfer of vitamin E derived from a wheat germ oil concentrate. Yet if 250 mg tocopherol is administered to women 4-8 hours before term the vitamin E level in the cord is raised significantly (Varangot Chaffley and Rieux, 44). By contrast the water soluble vitamins thiamine chloride (Slobody Benson and Mestern, 46) and ascorbic acid (Manahan and Eastman '38 Chow and Okuda, '60) showed consistently higher concentrations in cord than maternal blood suggesting even perhaps a concentration of the vitamins by the placenta.

There is a great deal of evidence that in the rat vitamin E is essential for normal fetal development for example Cheng Chang and Bairnson (57) showed that in vitamin E deficiency 100% resorption of embryos occurred, while no resorption occurred in pregnant rats receiving daily 2 mg d,l- $\alpha$ -tocopherol acetate. Our data showed only 4.1% resorption in rats receiving 10 mg per  $\alpha$  for 20 days during gestation as compared to 10.6% for all



normal untreated controls. Daily 5 mg dosages of  $\alpha$ -tocopherol administered to another group of pregnant animals had no beneficial effect on resorption rate in fact some negative response was noted (14% resorptions).

In addition to high dosages of  $\alpha$ - and  $\gamma$ -tocopherol our data suggest some beneficial effects on resorption rate were obtained from 2,5-di-tert-amylhydroquinone, butylated hydroxytoluene (BHT) butylated hydroxyanisole (BHA) 2,6-di-tert-butyl-4-methylphenol (DBMP) thiodipropionic acid, 1,2-di-hydro-2,2,4-trimethyl-6-ethoxyquinoline (Santoquin) 6-phenyl 1,2-di-hydro-2,2,4-trimethylquinoline (Santoflex B) nordihydroguaiaretic acid (NDGA); while methylene blue, hydroquinone paraaminobenzoic acid (PABA) n-propyl galate 2,2-methylene bis (4-ethyl-6-tertiary butyl phenol) phenothiazine and N,N-diphenyl-p-phenylenediamine (DPPD) all substantially increase resorption rates.

One is impressed from the data summarized in table 2 that the total prenatal mortality in mammals is much higher than might be suspected from the resorption data alone. Brambell (48) contends in the rabbit, that the loss between ovulation and full term is not less than 43% of ova ovulated and may be and indeed probably is substantially heavier. Data on total wastage in the rat is scanty limited to the early work of Long and Evans (22) and later Perry (45) on the wild rat. These workers reported respectively 33.4% and 20.0% total prenatal mortality while resorption rate was 8.3% for the two strains of rats.

Other mammals follow a similar trend ranging from an elevenfold increase in total mortality over resorptions in pig (Corner '23) to less than a twofold increase in sheep (Hammond, '21). Such observations certainly provide a challenge to animal research workers to seek out the causative factors for such an enormous wastage. These factors are legion but include such environmental disturbances as abnormalities of blood supply of placenta, an unfavorable implantation site faulty development of the decidua abnormal environmental temperature and others. Maternal influences may adversely affect normal implantation and development such

as, inanition avitaminoses blood dyscrasias, endocrine disorders, infections and the presence of unphysiologic compounds in the blood such as some of the antioxidants herein reported.

#### SUMMARY AND CONCLUSIONS

1 In 126 untreated normal pregnant rats 40.8% had one or more resorptions and 10.6% of all implantations terminated in resorptions.

2. The cranial third of the uterine horn contained 47.6% of all resorptions while the middle third held only 20.8% of the total resorptions.

3. The percentage resorptions in the tame rat falls intermediate among the other mammalian groups.

4 Of the maternally administered compounds, the tocopherols ( $\alpha$  and  $\gamma$ ) BHT BHA, amyhydroquinone and DBMP appear to have definite prophylactic value in reducing the frequency of resorptions in the rat, while methylene blue hydroquinone and paraaminobenzoic acid markedly increase resorption rates.

5 Possible extrinsic and intrinsic factors that may influence prenatal mortality in the rat are discussed.

#### LITERATURE CITED

- Barry L. W. 1920 The effects of inanition in the pregnant albino rat, with special reference to the change in the relative weights of various parts, systems and organs of the offspring. *Contr. Embryol. Carnegie Inst.*, 11 91-136.
- Behn, W. M. Frahm and E. Freiwurst 1936 Ueber den diaplacentaren Uebergang von Phenothiazin Derivaten. *Klin. Wchnschr.* 34 871.
- Brambell, F. W. R., and J. H. Mills 1947 Studies on sterility and prenatal mortality in wild rabbits. III. Loss of ova before implantation. *J. Exp. Biol.*, 34 199-210.
- 1948 Studies on sterility and prenatal mortality in wild rabbits. IV. The loss of embryos after implantation. *Ibid.*, 35 241-269.
- Brambell, F. W. R. 1948 Prenatal mortality in mammals. *Biol. Rev.* 23 370-407.
- Bunnell, R. H. L. D. Matterson, E. P. Fingersh, L. M. Potter and A. Kozoff 1935 Studies on encephalomalacia in the chick. 3 The influence of feeding or injecting various tocopherols and other antioxidants on the incidence of encephalomalacia. *Poultry Sci.*, 34 1068-1075.
- Cheng, D. W. and B. H. Thomas 1933 Relationship of time of therapy to teratogen in maternal avitaminosis E. *Proc. Iowa Acad. Sci.* 60 290-299.
- Cheng, D. W. L. F. Chang and T. A. Ralston 1937 Gross observations on developing bac-

- mal embryos induced by maternal vitamin E deficiency. *Anat. Rec.*, 129: 167-186.
- Chow B F., and K. Okuda 1960 Transfer of vitamins from mother to fetus. *J.A.M.A.*, 172: 423-425.
- Conaway C. H. 1935 Embryo resorption and placental scar formation in the rat. *J. Mammal.*, 36: 516-532.
- Corner G. W. 1923 The problem of embryonic pathology in mammals, with observations upon intra-uterine mortality in the pig. *Am. J. Anat.*, 31: 523-545.
- Crow F. A. Z. 1925 Prenatal death in the pig and its effect upon sex ratio. *Proc. Royal Soc. Edin.*, 46: 9-14.
- Dam, H., L. Kruse, L. Prange and E. Sondergaard 1948 Influence of dietary ascorbic acid, nordihydroguaricetic acid, and cystine on vitamin E deficiency symptoms in chicks. *Biochemica et Biophysica*, 2: 501-513.
- 1951 Substances affording a partial protection against vitamin E deficiency symptoms. *Acta Physiol. scand.*, 22: 309-310.
- Danforth, C. H., and S. B. de Abrie 1928 The functional interrelation of the ovaries as indicated by the distribution of fetuses in mouse uteri. *Am. J. Anat.*, 41: 65-74.
- Davis, D. E., and J. T. Emken 1948 The placental scar as a measure of fertility in rats. *J. Wildlife Mgt.*, 12: 162-166.
- Deansley R., and A. S. Parkes 1933 The oestrous cycle of the grey squirrel (*Sciurus carolinensis*). *Phil. Trans. Royal Soc. B.*, 223: 47-96.
- Deansley R. 1935 Growth and reproduction in the stoat (*Mustela erminea*) *Ibid.*, 225: 459-492.
- Deno, R. A. 1941 A criterion for distinguishing between virgin and parous animals. *Pharm. Arch.* 12: 19-16.
- F. wett, D. W. G. E. Wislocki and C. M. Waldo 1947 The development of mouse ova in the anterior chamber of the eye and in the abdominal cavity. *Am. J. Anat.*, 81: 413-443.
- F. kete E. 1917 Differences in the effect of uterine environment upon development in DBA and C57 strains of mice. *Anat. Rec.*, 98: 409-415.
- Fertuyn, A. B. D. 1929 Prenatal death in the striped hamster (*Cricetulus griseus*) *Arch. de Biol.*, 39: 583-606.
- Fraser J. F. D. 1935 Foetal death in the rat. *J. Embryol. and Exp. Morph.*, 5: 13-29.
- Haral, R. M., B. Munks, E. Z. Moyer M. Knecher and H. H. Williams 1947 Vitamin C in the blood and urine of the newborn and in the cord and maternal blood. *Am. J. Dis. Child.*, 74: 417-433.
- Hammond, J. 1921 Further observations on the factors controlling fertility and foetal atrophy. *J. Agric. Sci.*, 11: 337-366.
- Harteris, H. O. 1938 Reduction in litter size and maintenance of pregnancy in the oophorectomized rat: evidence concerning the endocrine role of the placenta. *Am. J. Physiol.*, 114: 399-406.
- Hollander W. F. and L. C. Strong 1950 Intra-uterine mortality and placental fusion in the mouse. *J. Exp. Zool.*, 115: 131-147.
- Hsu, Chin-Yun 1948 Influence of temperature on development of rat embryos. *Anat. Rec.*, 100: 79-90.
- Juggett, A. St. G. 1954 The transport of lipids and carbohydrates across the placenta. *Cold Spring Harbor Symposia Quant. Biol.*, 19: 82-92.
- Kennedy C., and L. S. Palmer 1945 Biotin deficiency in relation to reproduction and lactation. *Arch. Biochem.*, 7: 9-13.
- Long, J. A., and H. M. Evans 1922 The oestrous cycle in the rat and its associated phenomena. *Mem. Univ. Calif.* 6: 1-148.
- Lund, C. J. and M. S. Kimble 1943 Plasma vitamin A and carotene of newborn infant, with consideration of fetal-maternal relationships. *Am. J. Obst. and Gynec.*, 46: 207-221.
- MacFarlane, W. V. P. R. Pennycook and E. Thrift 1957 Resorption and loss of fetuses in rats living at 35 C. *J. Physiol.*, 125: 451-459.
- Main, R. J. 1939 The care of small rat colony. C. V. Mosby Company St. Louis.
- Manahan, C. F. and N. J. Eastman 1938 Cavitic acid content of fetal blood. *Bull. Johns Hopkins Hosp.*, 63: 478-481.
- Mason, K. E., and W. L. Bryan 1940 Placental and mammary transfer of vitamin E in the rat. *J. Nutrition*, 30: 501-517.
- Mertz, W. and K. Schwarz 1958 Reversal of respiratory decline in necrotic liver degeneration by interspecific antioxidants. *Proc. Soc. Exp. Biol. and Med.*, 99: 808-812.
- Nelson, M. M., and H. M. Evans 1946 Pantothenic acid deficiency and reproduction in rat. *J. Nutrition*, 31: 497-507.
- 1948 Effect of deoxyhypoxanthine on reproduction in the rat. *Proc. Soc. Exp. Biol. and Med.*, 69: 274-276.
- Nelson, M. M., C. W. Ailing and H. M. Evans 1953 Production of multiple congenital abnormalities in young by maternal pteroylglutamic acid deficiency during gestation. *J. Nutrition*, 48: 61-80.
- Nelson, M. M., C. D. E. Baird, H. V. Wright and H. M. Evans 1956 Multiple congenital abnormalities in the rat resulting from riboflavin deficiency induced by antimetabolite galactosarin. *Ibid.*, 58: 123-134.
- Neuweller W. 1949 Vitamin E — Uebertritt von Mutter of Kind. *Internat. Ztschr. Vitaminforsch.*, 21: 83-87.
- Perry J. S. 1945 The reproduction of the wild brown rat (*Rattus norvegicus* Erxleben) *Proc. Zool. Soc. London*, 115: 19-48.
- Schwarz, K. 1953 Effects of antioxidants on dietary necrotic liver degeneration. *Proc. Soc. Exp. Biol. and Med.*, 89: 20-24.
- Slobody L. B., R. A. Benson and J. Mestern 1946 A comparison of the vitamin C in mothers and their newborn infants. *J. Pediatrics*, 29: 41-44.
- Slobody L. B. M. M. Willner and J. Mestern 1949 Comparison of vitamin B<sub>12</sub> levels in mothers and their newborn infants. *Am. J. Dis. Child.*, 77: 735-739.
- Straussford, J. V. and M. L. Quail 1946 Vitamin E levels in maternal and fetal blood plasma. *Proc. Soc. Exp. Biol. and Med.* 61: 360-371.

Sundstroem, E. G. 1927 Physiological aspects of tropical climates. *Physiol. Rev.* 7 320-362.  
 Varangot, J. H. Chailley and N. Rieux 1944 Sur la teneur du sang du cordon en vitamine E et sur le passage du tocophérol de la mère au fœtus. *Compt. rend. Soc. de biol.*, 138 24-25.

Walker D. G., and Z. T. Wirtschafter 1936 Resorption of embryos in rats on *Lathyrus odoratus* diet. *J. Nutrition*, 58 147-159.  
 Wilson, J. G. 1954 Withdrawal of claim that are blue causes congenital malformations. *Proc. Soc. Exp. Biol. and Med.*, 87 1

# Spinal Cord Segments

## A. GROSS STRUCTURE IN THE ADULT CAT

CAROLYN EYSTER THOMAS AND C. MURPHY COMBS<sup>1</sup>

Department of Anatomy Northwestern University Medical School  
Chicago Illinois

Süßling (1859) Luderitz (1881) Donaldson and Davis ('03) and Hovelacque ('27) described in varying degrees of detail the manner in which the rootlets comprising each pair of spinal nerves are attached to the spinal cord. Comparison of these studies is hampered by the differing ways in which the investigators have handled the rootless or interroot, distances which exist in certain cord regions, and by the differing ways in which they have defined a spinal cord segment. In addition it appears that some of these studies were made exclusively with dorsal measurements; the assumption being that the ventral would be identical. All of these authors were primarily interested in human cords but Süßling (1859) made some observations in the calf and Luderitz (1881) included some findings in the rabbit.

There appears to be no precise study of spinal cord segment structure using the cat or monkey. Since these animals are so commonly used in the research laboratory such descriptions are needed. In addition some of the fundamental conclusions concerning cord structure and development that were reached by the above investigators, should be tested in other species. The present study is limited to the adult cat.

### MATERIALS AND METHODS

Complete bilateral, dorsal and ventral root dissections were done in 12 adult cats, each weighing about 2.5 kg. Immediately after the animal's death the entire vertebral column with intact spinal cord and associated structures was removed and placed in 10% formalin where it was kept for several weeks. For better differentiation between small arteries and roots two of the animals were injected through the

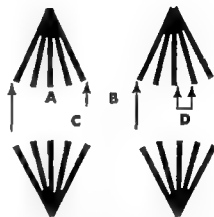


Fig. 1. Diagram of rostrocaudal measurements taken from the spinal cord. A, root attachment length; B, interroot length; C, segment length; D, interrootlet space.

heart with colored latex at the time of death.

All dissections were performed under a 10 $\times$  or 20 $\times$  dissecting microscope. Because of their greater fragility the ventral roots were exposed first. The vertebral bodies were removed from about one fourth of the vertebral column and the corresponding section of dura mater was slit along the ventromedian sulcus. The arachnoid was either lifted off or gently pushed back from the roots.

Figure 1 is a diagram of the cord attachments of 2 pairs of spinal nerve roots with arrows to indicate the rostrocaudal measurements determined. A, root attachment length, the length of the cord surface to which the rootlets of each root were attached; B, interroot length, the length of the cord surface devoid of rootlets lying between the attachments of adjacent roots.

<sup>1</sup>Senior Research Fellow (87-347-C), Division of General Medical Sciences, U. S. Public Health Service.



*Segment lengths.* In the present study the rostrocaudal distance between the uppermost attachments of successive nerve roots will be defined as the segment length. This measurement was obtained by adding the length of cord occupied by each set

of rootlets to the length of whatever caudally adjacent space devoid of rootlets was present.

Figure 2 depicts graphically the results obtained from the ventral cord surface. The upper and lower steplike lines repre-

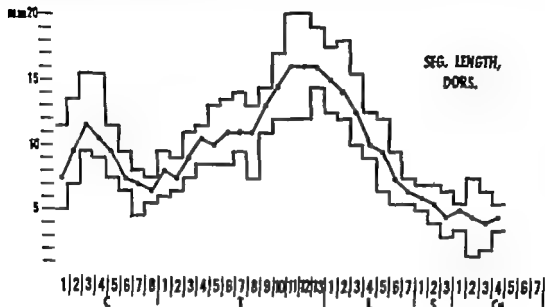


Fig. 3 Dorsal segment lengths.

#### VENTRAL

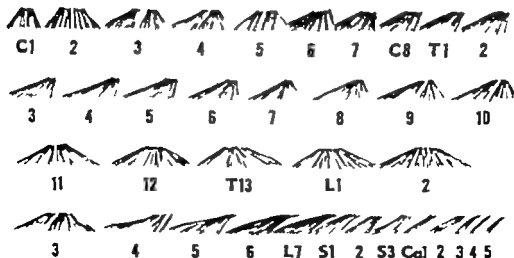


Fig. 4 Pattern of ventral root attachments.

sent the upper and lower limits in millimeters of the 24 measurements taken, 12 on the left and 12 on the right. The single middle line shows the average of the lengths of each segment at the various levels. Since the desired data can be derived from the graph only certain points require comment. Segments T11 through L1 are definitely the longest averaging 16 to 17 mm in length. Cephalically the shortest segments are C1 and those from C6 through T3 all of which show an average length of about 7 mm. Caudally beginning at L3 the segment lengths become progressively less until the sacral and caudal measurements range between 4 and 5 mm.

Figure 3 comprises similar data obtained from the dorsal cord surface. Since both the ranges and the averages are essentially the same as those measurements taken on the ventral surface of the cord either graph can be used to represent a composite of the characteristic lengths of the segments.

*General characteristics of rootlets* Fig. 4 and 5 are drawings of the typical arrangements found for ventral and dorsal root attachments. As the rootlets of each root attach to the cord, they comprise 8 to 30 subdivisions. These rootlets or

filaments show much variation from one cord level to another in such characteristics as: the number of rootlets per root at the point of attachment to the cord, the diameters of individual rootlets; susceptibility to being accidentally pulled off; the rostrocaudal length of the site of root attachment; the extent to which the rootlets of a given root are spread out or separated from one another the degree of regularity of rootlet distribution along the line of attachment and the rostrocaudal angle of attachment.

Generally ventral rootlets exit irregularly from the ventrolateral sulcus whereas dorsal rootlets exit evenly from the dorsolateral sulcus. At the cord, the ventral roots consist of many relatively small rootlets while the dorsal roots usually have a small number of large coarse rootlets. The ventral rootlets usually have significantly less tensile strength than the dorsal ones. This factor combined with a more widespread attachment makes the ventral dissection much more tedious particularly in the lower thoracic and upper lumbar levels. Ventrally in some regions blood vessels lying in an interrootlet position make accurate measurement difficult. Dorsally the vessels lie ventral to the rootlets and are of no concern. Upon reaching the

# DORSAL

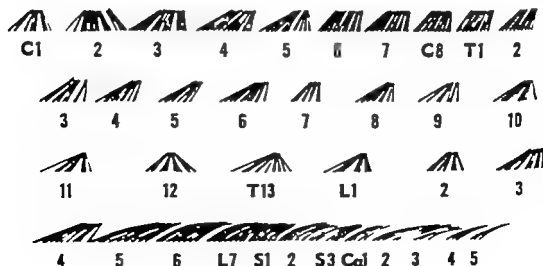


Fig. 5 Pattern of dorsal root attachments.

cord the ventral rootlets tend to branch out much more than do the dorsal ones particularly in the lower thoracic and upper lumbar regions.

**Root attachment lengths** Figures 4 and 5 show that, due to the variability of the spaces in between the sites of root attachment, measuring the distances between the uppermost rootlets of successive nerves would not give a true indication of the actual length of the line of attachment for

each set of roots. Consequently measurements were made between the uppermost and lowermost fila within each root. The ranges and averages for the lengths of ventral root attachments are shown in figure 6. Although there is a slight lowering of the whole curve its contour is essentially like that for the segment lengths (fig. 2). On the other hand the corresponding graph of dorsal root measurements (fig. 7) shows a striking reduction

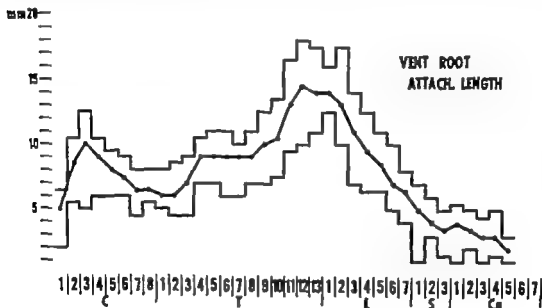


Fig. 6 Ventral root attachment lengths



Fig. 7 Dorsal root attachment lengths.



in the lengths for levels T10 through L2. The segment lengths (fig. 3) at these levels average 16 mm per segment, but the distances for the root attachments average only 9 mm. Otherwise the two curves are essentially alike. Since the

graphs for lengths of root attachments dorsally and ventrally differ from the graphs for lengths of segments determined dorsally and ventrally then the dorsal and ventral interroot distances, must bear an equally dissimilar relationship.



Fig. 8 Ventral interroot lengths.



Fig. 9 Dorsal interroot lengths.



Fig. 10 Ventral interrootlet spaces.

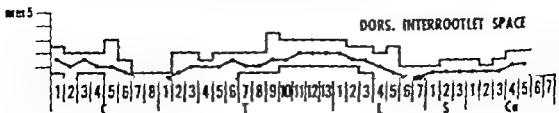


Fig. 11 Dorsal interrootlet spaces.

**Interroot lengths.** The measurements for the interroot lengths are graphed in figures 8 and 9. Ventrally the averages vary from zero to three mm, with an individual range up to 7 mm. Dorsally they vary from 0.5 mm to 7.5 mm with an individual range up to 10 mm. Ventrally the interroot distances make up a minor part of the segment lengths, whereas dorsally at levels T10 to L1 they make up almost half of the segment lengths.

**Interrootlet spaces.** The spaces between individual rootlets within each set of root attachments that is, interrootlet spaces, vary from one level to another. Since it was possible that the greater interroot lengths found dorsally between individual sets of roots might be compensated for by a much closer grouping of rootlets than would be found ventrally these interrootlet spaces were compared. However the smallness of these spaces makes their quantitative evaluation difficult. A fairly accurate measure of the degree of change from one level to another can be obtained by calculating the length of the greatest distance found within each set of rootlets, since this varies proportionately with the smaller spaces at the same level. The find-

ings for the ventral (fig. 10) and dorsal (fig. 11) surfaces are essentially the same and show that the interrootlet lengths are generally longest where the sites of root attachments and the rootless areas are longest, and shortest where these are shortest.

Thus all three measurements, both dorsally and ventrally essentially increased or decreased together — all contributing in varying degrees to the segment lengths.

The data obtained from the right and the left sides were tabulated separately and compared. Generally the sides were similar except that dorsally between levels T3 and L4 differences of two to three mm were common.

Conceivably the averages and ranges of the measurements taken might not represent the actual characteristics of any one cord. To test this possibility individual graphs of root attachment lengths and interroot distances were made for each cord and compared to the group graphs. In every instance the individual graph showed a general contour which was like that of the average. However from one segment to another the individual graphs did show much fluctuation above and be-

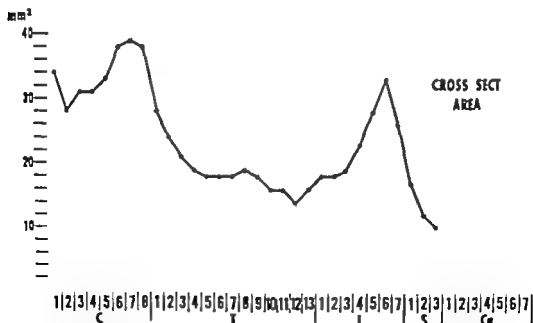


Fig. 12. Cross-sectional Areas. See text for explanation.

low the average. Although the longest cords had more distances above the average they also had rather evenly dispersed ones well below the average. Thus it follows that graphs of the averages would suffice for predicting the overall pattern of measurements which could be expected in any one cord, but would fail to foretell the findings at a specific level.

For comparison among different animals graphs were made for segment lengths expressed as percentages of the total cord length in each specimen. No significant differences existed between these and the previously drawn graphs.

**Cross-sectional areas** The averages of the results obtained in the 6 cords measured are presented in figure 12. The cord enlargements are obvious at C6 through

C8 and L5 through L7 where the greatest areas are respectively 39 mm<sup>2</sup> and 33 mm<sup>2</sup>. The smallest nonsacral area is 14 mm<sup>2</sup> found at level T12. Measurements within segments but taken above and below the midlevel used for these data showed no significant deviations from the ones used.

Graphs of the areas for individual cords were made and compared to the average. Four of the 6 curves were essentially identical to the average. In one nonconforming specimen the values found at C1 through C5 were about 6 mm<sup>2</sup> greater than the average. However below C5 this cord showed areas which matched the average. In the other specimen the cervical segments were generally small, especially at C3 and C4 where the areas measured only 20 mm<sup>2</sup>. In all cords the greatest cross-

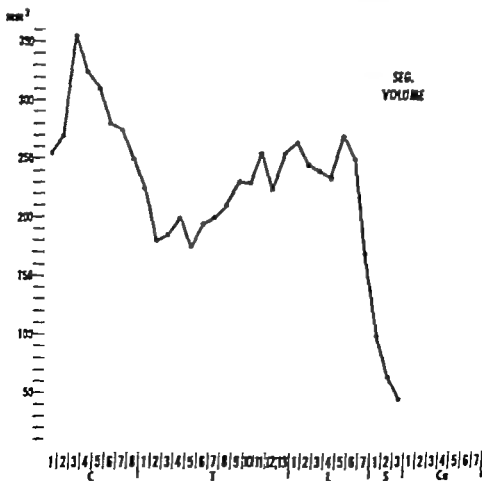


Fig. 13 Segment volume. See text for explanation

sectional area was found in the cervical region at C7.

**Segment volume** The data for this were obtained by multiplying the averages for cross-sectional areas by the averages for segment lengths. The results are given in figure 13. The largest value occurs at C3 where the volume is 385 mm<sup>3</sup>. Caudally from this level, the curve declines sharply to T2. The volume then gradually increases until it reaches 270 mm<sup>3</sup> at L5 and then tapers off rapidly into sacral levels.

Individual graphs of segment volumes were made for each of the 6 specimens studied. Although much variation was found, the validity of the average curve was established. In 5 of the individual determinations the contour of the curve was identical to that of the average. The variation that existed was in the overall

height of the curve. This probably reflects variation in the sizes of the animals used. In the one specimen that differed significantly from the average the high volume peak was absent in the cervical region. In this animal the volume at C1 was about 350 mm<sup>3</sup> as was the average, but no increase occurred through the other cervical levels as it did in the remaining specimens. However the measurements for the remainder of the cord did match the average. This specimen was the same as the one which showed cervical cross-sectional areas much below the average.

In figure 14 the graphs for segment length, cross-sectional area and volume are superimposed in order to show how strikingly they differ from each other. This comparison emphasizes the necessity of using all three measures when thinking of segment size.

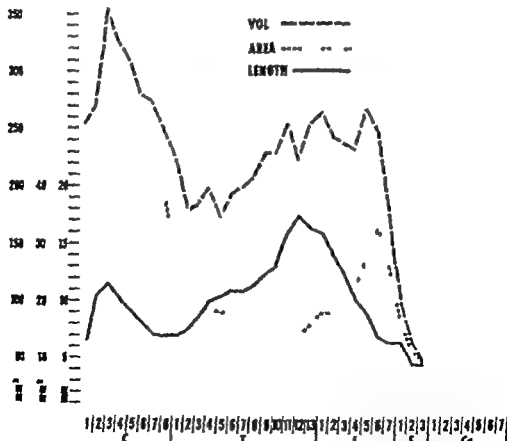


Fig. 14 Comparison of segment length, area and volume. See text for explanation.

Grossly the cervical and lumbar enlargements can be seen at cord levels C6 through C8 and L5 through L7

### DISCUSSION

Luderitz (1881) measured segment lengths in 5 human cords of various ages. The cervical segments within each cord showed similar lengths except in three of the specimens where C5 was somewhat the longest. In all of the cords the lengths increased from T1 to T7 which was usually the longest of all the cord segments. Caudally the lengths gradually became shorter.

Donaldson and Davis ('03) reported segment lengths on 4 human cords. The data for three of these were obtained from photographs in the publications of other investigators. Their findings confirmed and supplemented those of Luderitz (1881).

The results of the present study in the cat have shown segment length variations like those in the human except that the longest segments are the lower thoracic and upper lumbar instead of the mid thoracic as in the human.

Luderitz (1881) and Donaldson and Davis ('03) were aware of variation in interroot lengths, but they reported no measurements on them. These spaces were included as part of their segment lengths. Stilling (1859) however excluded interroot lengths from his measurements on the calf and human by taking the distance between the uppermost and lowermost fila of each root. The variations in the calf were much like those described in the present study for dorsal root attachments except that C3 was remarkably long. In the human the proportions resembled those described for segment lengths by Luderitz (1881). Donaldson and Davis ('03) and the present study. If human cords show the same differences between dorsal and ventral root attachments as have been demonstrated in the cat it is probable that Stilling measured ventral root attachments rather than dorsal ones in the human.

This interpretation is supported by the results obtained by Hovelacque ('27) who measured root attachment lengths and interroot lengths on the dorsal surfaces of 20 human cords. He obtained averages of

the root attachment lengths which varied from 10 to 12 mm in cervical regions from 8 to 12 mm in upper thoracic levels from 17 to 12 mm in lower thoracic levels; and from 8 to 10 mm in lumbar levels. For interroot lengths Hovelacque ('27) reported a 2 to 5 mm range at upper cervical levels; no measurable spaces at lower cervical levels; averages from 5 to 12 mm through thoracic levels and no measurable separation at lumbosacral levels.

In the cat, as apparently in the human, the dorsal and ventral segment length patterns are essentially alike. However significant differences are found in the cat between the dorsal and ventral patterns for lengths of root attachments and interroot lengths. Dorsally from T3 through L3 each interroot length occupies a significant part of the segment length. At several levels this length almost equals that of the adjacent root attachments. Ventrally the interroot lengths are greater in this region than elsewhere but they are not usually a significant part of the segment length.

The cross-sectional cord areas in the cat have been found to agree with the proportions described in the human by Sulling (1859). In both studies the greatest areas were at lower cervical and lower lumbar segments with the former being the greater of the two.

Other investigators have not calculated segment volume as has been done here for the cat. Although this adds no new information it is a convenient way to visualize the overall sizes of the various segments. The fact that C3 has the greatest volume and that T11 T13 L1 and L5 have greater volumes than L6 emphasize the major role played by segmental length in determining segmental volume.

### SUMMARY

Dorsal and ventral roots were bilaterally dissected on the spinal cords of 18 adult cats. Three rostrocaudal measurements were made: the length of cord surface to which the rootlets of each root were attached (root attachment length); the length of cord surface devoid of rootlets lying between the attachments of adjacent roots (interroot length); and the greatest distance between adjacent rootlets within

the region of each root's attachment (interrootlet space). The segment length was derived by adding the length of cord occupied by each set of rootlets to the length of whatever caudally adjacent space devoid of rootlets was present. In 6 cats typical cross-sectional areas at the various cord levels were determined with a planimeter. Also segment volume was obtained by multiplying the averages for cross-sectional areas by the averages for segment length. All results were graphed.

Segments T11 through L1 are significantly the longest, averaging 16 to 17 mm in length. Cephalically the shortest segments are C1 and those from C6 through T3 all of which show an average length of about 7 mm. Caudally beginning at L3 the segment lengths become progressively less until the sacral and caudal measurements range between 4 and 5 mm. Ventral and dorsal surfaces are essentially alike.

Compared to segment lengths, the root attachment lengths ventrally are generally somewhat shorter. Dorsally however root attachment lengths show a striking reduction in lengths for levels T11 through L2.

Ventrally the interroot lengths make up a minor part of the segment lengths averaging from zero to 3 mm. Dorsally however they make up almost half the segment length at levels T10 to L1.

The interrootlet spaces are essentially the same dorsally and ventrally. They are small, but are generally longest where the site of root attachments and the interroot lengths are longest, and shortest where these are shortest.

Dorsally and ventrally all three measurements increase or decrease together contributing in varying degrees to the segment length.

The greatest cross-sectional areas are at C8 through C8 and L5 through L7. The smallest non-sacral area is at T12.

The greatest segment volume is at C3. From this level the volume decreases sharply to T2, then increases until L5 is reached and finally tapers off rapidly into sacral levels.

#### LITERATURE CITED

- Donaldson, H. H., and D. J. Davis. 1903. A description of charts showing areas of the cross sections of the human spinal cord at the level of each spinal nerve. *J. Comp. Neur.* 12, 19-46.
- Horselacque, A. 1927. *Anatomie des Nerfs Crâniens et Rachidiens et du Système Grand Sympathique chez l'Homme*. 2 vols., Gaston Doin et Cie. Paris. Vol. 1 288-297.
- Lödewitz, C. 1881. Ueber das Rückenmarksgewicht. Ein Beitrag zur Morphologie und Histologie des Rückenmarks. *Archiv f. Anat. u. Entwickl. Anat. Abtheil.* pp. 421-495.
- Stilling, B. 1859. Neue Untersuchungen ueber den Bau des Rückenmarks. Cassel. pp. 1900.



# Reproductive Capacity of Dairy Bulls

## III. THE EFFECT OF EJACULATION FREQUENCY UNILATERAL VASECTOMY AND AGE ON SPERMATOGENESIS<sup>1,2</sup>

RUPERT P. AMANN

Dairy Breeding Research Center Department of Dairy Science  
The Pennsylvania State University University Park

Despite much speculation, the effect of ejaculation frequency and spermatozoan output on spermatogenesis apparently has not been investigated. Dairy bulls are ideal for such studies because large amounts of semen can be collected by artificial vagina. Since detailed criteria from quantitative investigations of bovine testicular histology were lacking, these had to be established before determining the effect of ejaculation frequency and sperm output on spermatogenesis. This paper also considers effects of age on testicular histology; spermatogonia renewal and testicular germ cell degeneration are discussed elsewhere (Amann, '81b).

As early as 1871 von Ebner had recognized that spermatogenesis could be classified into a series of stages based on the general appearance of seminiferous tubule cross sections. Von Ebner (1871-1888) Schoenfeld ('00-'01) and Regaud ('01a, '01b) described the morphological changes during bovine spermatogenesis. However their suggestion that spermatogenesis could be quantified frequently has been ignored. An extensive series of reports by Roosen-Runge ('51-'52, '53-'56) Roosen-Runge and Barlow ('53) Clermont and Leblond ('53-'55-'59) Oakberg ('56a, '56b) and Ortavant ('58) has provided quantitative data on cyclic testicular changes in laboratory rodents, monkeys, sheep, and humans. Use of the periodic acid-Schiff stain enabled Leblond and Clermont ('52a) to define 14 stages in the seminiferous epithelial cycle of the rat based on spermatid morphology. However for simplicity Cupps and Laben ('60) and Ortavant ('58, '59) have continued to use 8 stages similar to those described by Curtis ('18) and Roosen-Runge and Giesel ('30). Systems used for classifying the

seminiferous epithelial cycle in stages have been reviewed by Leblond and Clermont ('62b) and Ortavant ('58, '59).

Between '02 and '55 there were only a few pertinent reports on the bovine testis (Bascom and Osterud, '25; Haq, '48; Knudsen, '54). These were concerned primarily with diameters of seminiferous tubules and germ cells. Spermiogenesis in bulls was described in detail by Cavazos and Melampy ('54) Ortavant ('56) and Cupps and Laben ('60) presented limited data on the relative duration of the stages of the seminiferous epithelial cycle but the only detailed investigations of bovine spermatogenesis were summarized in a brief report by Ortavant ('59) and in a thesis by Kramer ('60).

### EXPERIMENTAL PROCEDURE

#### Preslaughter treatment

Two groups of bulls were used in the investigation. Group A consisted of nine 29-month-old Holstein bulls which were ejaculated 8 times weekly for 5 weeks and then unilaterally vasectomized. Following a three-week recuperation period at sexual rest, they were assigned to one of three treatment groups on the basis of preoperative semen characteristics and sexual behavior. The three postoperative treatment groups, of three bulls each, were sexual rest (SR) two ejaculates per week (2X) and 8 ejaculates per week (8X). Each group had a similar average daily sperm output during the preoperative period.

Authorized for publication on May 2, 1961 as Paper No. 2326 in the journal series of The Pennsylvania Agricultural Experiment Station.

The data contained in this paper are part of a thesis submitted by the author to the Graduate School of The Pennsylvania State University in partial fulfillment of the requirements for the degree of Doctor of Philosophy.



(about 4.5 billion) but the 8X group was selected to include those bulls with the highest level of sexual activity. During the 20-week postoperative period the SR bulls were not ejaculated, the 2X bulls were ejaculated once on Monday and Friday and the 8X bulls were ejaculated twice on Monday Wednesday and Friday and once on Tuesday and Thursday. To increase sperm output, intensive sexual preparation (one false mount, two-minute restraint, and two additional false mounts) was used prior to each ejaculation. Unilaterally vasectomized bulls were utilized to give greater precision in the histological data since then each bull could serve as his own control.

Group II consisted of one mature Guernsey and 4 mature Holstein bulls. Prior to slaughter two of these bulls were sexually rested (SR) and three were ejaculated 6 to 8 times weekly (6-8X). These bulls were included to provide data on normal, intact bulls and to investigate the effect of age on testis histology. The experimental treatments duration of preslaughter treatment, preslaughter daily sperm output, and age at slaughter for all 14 bulls are included in table 2. Detailed data on semen characteristics gonadal and extra gonadal sperm reserves testicular daily sperm production and sperm resorption for these bulls will be presented elsewhere.

#### HISTOLOGICAL METHODS

On the day of slaughter the bulls were trucked 30 miles to an abattoir and killed at approximately 10:00 A.M. Tissue samples were taken at three loci from each testis, sliced into smaller pieces (about  $7 \times 7 \times 4$  mm) and placed into Bouin's and Orth's fixatives. The three testicular loci sampled were:

- Locus 1    dorso-anterior    immediately below the apex of the caput epididymis
- Locus 2    posteromedial-central    adjacent to the ductus deferens about one-half way between the poles of the testis.
- Locus 3    anteriolateral-ventral    adjacent to the cauda epididymis near the junction with the corpus epididymis.

About 20 minutes elapsed between the stunning shot and placement of the last tissue sample in fixative.

After fixation the tissues were dehydrated, embedded in Tissuemat and serially sectioned at  $7 \mu$  in a plane parallel to the tunica albuginea. Slides were prepared so that each contained 8 sections separated from the adjacent sections by a minimum of  $120 \mu$ . These coded slides were stained using combinations of Harris hematoxylin and eosin-Y for Bouin's fixed tissues and Feulgen azure A-Schiff and periodic acid-Schiff for Orth's fixed tissues.

#### *The cycle of the seminiferous epithelium*

After study of bovine testicular tissue stained by the Feulgen azure-A-Schiff periodic acid-Schiff technique it was found that the cycle of the seminiferous epithelium could be classified into 8 stages similar to those used by Roosen-Runge and Giesel ('30) for rats and Ortavant ('58) for rams. The criteria used for scoring the tubule cross sections were as follows:

- Stage I    From the complete disappearance of spermatozoa from the luminal surface of the germinal epithelium to onset of elongation and increased stainability of the young spermatid nuclei.
- Stage II    From the start of elongation until the onset of grouping of young spermatids into distinct bundles.
- Stage III    From the formation of spermatid bundles until the first maturation division of primary spermatocytes.
- Stage IV    From the first maturation division to the end of the second maturation division. If three or four spermatocytes were in metaphase anaphase or telophase of either maturation division or if secondary

- spermatocytes were present, the tubule was scored as Stage IV
- Stage V** From the second maturation division until the young spermatid nuclei appeared dusty. At this stage young spermatids contained a light staining chromatin network.
- Stage VI** From end of Stage V to the start of acrosome development in the nuclei of young spermatids. At the end of Stage VI the old generation of spermatids had started to separate from the Sertoli cell nuclei.
- Stage VII** From the end of Stage VI until all the old spermatids lined the luminal surface of the germinal epithelium.
- Stage VIII** From when old spermatids were at the luminal surface of the germinal epithelium until all spermatozoa were released into the tubule lumen.

Figure 1 summarizes the cellular relationships during the 8 stages of the cycle of the seminiferous epithelium. In conjunction with photomicrographs of typical tubule cross sections (figs. 2 to 9) the chart shows that in any seminiferous tubule cross section (vertical axis on chart) there are 4 or 5 germ cell type generations. In Stages I to IV there are two generations of spermatocytes while in Stages V to VIII there are two generations of spermatids. Only in Stage II is one type of spermatogonium found. Although it requires approximately 45 cycles of the seminiferous epithelium to form 64 spermatozoa from a stem A-spermatogonium (Amann, '61b) during each cycle spermatozoa are released from any given point in a seminiferous tubule at the end of Stage VIII.

#### Quantitative histological evaluation

The volumetric ratio between seminiferous tubules and interstitial tissue was determined (X125) by Chalkley's (43) technique using slides prepared from Bouin's fixed tissue. Objects recorded as hits were seminiferous tubules (including basement membrane) Leydig cells, other interstitial tissue and space or artifacts

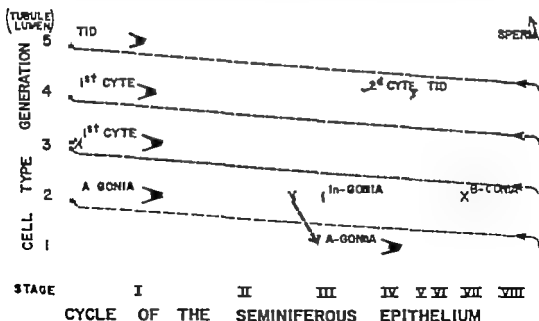


Fig. 1 The cycle of the seminiferous epithelium in the bull.

outside of the seminiferous tubules. Statistical analysis of duplicate determinations on 10 slides showed that differentiation between Leydig cells and other interstitial tissue was unreliable. Therefore, only the percentage of seminiferous tubules was calculated for each locus (800 minus the artifact hits divided into the hits on seminiferous tubules).

The relative frequencies of the 8 stages of the cycle of the seminiferous epithelium were determined (X500) by scoring 500 randomly selected, round seminiferous tubule cross sections per testis locus using Orth's fixed tissue. The repeatability of such determinations was established by calculating the coefficient of repeatability from triplicate evaluations of 10 randomly selected slides, it was +0.82.

The cellular content of 10 Stage I seminiferous tubules in each testis locus was determined by counting (X1,250) the nu-

clei present in round tubule cross sections in which all B-spermatogonia had divided into young primary spermatocytes (Orth's fixed tissue). The cells counted included Sertoli cells, A-spermatogonia, young or preleptotene primary spermatocytes, old or pachytene primary spermatocytes, and spermatids. Abnormal primary spermatocytes, abnormal spermatids, and cells of the various types found free in the tubule lumen were recorded separately. In each tubule cross section, the diameter of a typical cell nucleus of each type was measured. Major and minor diameters were recorded for the oval spermatogonia as well as for each seminiferous tubule and tubule lumen. Nuclei were measured to the nearest 0.7  $\mu$  and seminiferous tubules to the nearest 2.2  $\mu$ .

The following formula based on those of Abercrombie (46) and Ortavant (38) was used to correct cell counts for variations in nuclear diameter

$$\text{True count} = \left[ \frac{\text{Observed count}}{\text{Section thickness}} \right] \left[ \frac{\text{Section thickness}}{1 + \sqrt{(\Delta v \cdot \text{dia.}/2)^2 - (\Delta v \cdot \text{dia.}/4)^2}} \right]$$

Abercrombie's formula assumes that cell nuclei of infinitely small size can be counted. The present formula assumes that cells sectioned so that their nuclear diameter is less than one-half that of the true nuclear diameter will not be visualized. Major and minor diameters of spermatogonia were averaged for calculation of the correction term. The numbers of Sertoli cells and abnormal germ cells were not corrected.

At each stage of the cycle of the seminiferous epithelium the diameters of 10 seminiferous tubules and tubule lumens were measured for each testis. Since counts and measurements on Stage I seminiferous tubules were not affected by testis locus, unilateral vasectomy or ejaculation frequency only slides for the posteromedial-central locus from the testis on the intact side of Group A bulls and both testes of normal Group B bulls were evaluated.

To correct linear measurements for tissue shrinkage resulting from histological processing, the magnitude of shrinkage was estimated using 4 nonexperimental

bull testes. Blocks of tissue were fixed and routinely processed while adjacent tissue blocks were placed in small vials in crushed ice. Within three hours after slaughter the latter samples were sectioned at 25  $\mu$  on a freezing microtome without fixation. The minor diameter of 100 round seminiferous tubule cross sections was measured for each unfixed testis sample using phase contrast microscopy. After embedding and staining, 100 tubules in each fixed testis sample were measured. Linear shrinkage (table 1) averaged 19.5% which represents a volumetric shrinkage of 48%. These values are simi-

TABLE 1  
Linear shrinkage of testicular tissue fixed in Orth's fluid, dehydrated, and embedded in Tissuemat

Testis	Minor tubular diameter ( $\mu$ )		% Net shrinkage
	Frozen sections	Paraffin sections	
A	249 $\pm$ 3	204 $\pm$ 2	18.0
B	265 $\pm$ 4	199 $\pm$ 2	24.5
C	266 $\pm$ 4	223 $\pm$ 2	16.2
D	277 $\pm$ 4	224 $\pm$ 2	19.0

Mean  $\pm$  standard error.

lar to those reported by Frontera (39) for monkey brains fixed in Orth's fluid. The various measurements were corrected for linear shrinkage by multiplying the observed diameters by a factor of 1.242. Thus, the diameters in tables 5, 7 and 8 should approximate the values in living bulls.

### RESULTS

In Group A, the average daily sperm output prior to slaughter (table 2) of 2.17 billion for 8X bulls was 52% greater than that of 1.43 billion for 2X bulls. Combined with the increased precision obtained from unilateral vasectomy the differences in daily sperm output among the SR, 2X, and 8X subgroups should have been sufficient to permit detection of differences in testis

histology associated with levels of sperm output. The daily sperm output for the 6-8X bulls in Group B averaged 5.75 billion.

The data in table 2 suggest that testis weight was not affected by unilateral vasectomy or ejaculation frequency. With the exception of bulls 160 and 168 there was very little intra-bull variation in testicular weight although among the 14 bulls testicular weight ranged from 250 to 496 gm. The difference between the average testis weight of 293 gm for the young Group A bulls and 402 gm for the mature Group B bulls was highly significant ( $p < 0.01$ ).

The differences among the three testis loci were not statistically significant ( $p >$

TABLE 3

Characteristics of the experimental bulls: testicular weight, and percentage of semiferrous tubules in the testis excluding the testis atrophy and mediastinum

Pre-slaughter treatment	Bull	Duration of pre-slaughter treatment weeks	Pre-slaughter daily sperm output $10^6$	Age at slaughter weeks	Testis weight gm		Volume of seminiferous tubules in testis cc	
					Intact side	V. sect. side	Intact side	V. sect. side
Group A bulls								
SR	158	11	none	30	304	307	78	80
	160	23	none	36	356	303	80	76
	162	33	none	38	280	279	73	74
	A				307	296	77	76
2X	163	20	1.02	36	321	316	78	80
	165	20	1.14	36	253	231	78	76
	172	20	1.61	32	285	290	76	78
	Av		1.43		287	286	77	78
8X	166	20	2.73	36	346	318	79	77
	169	20	2.18	36	296	269	75	77
	170	20	1.57	36	231	250	78	77
	A		2.17		294	286	77	77
A Group A				25	306	229	77	77
Group B bulls								
SR	Brill	8	none	29	406	478	72	71
	Regal	20	none	104	343	327	76	76
8X	137	26	6.20	63	422	405	73	70
7X	Wayne	19	6.78	104	437	478	68	73
4X	135	17	4.29	77	302	312	74	73
A Group B				88	404	400	72	73
SR	NH-10	18	none	216	333	364	28	50

Daily sperm output is the total number of sperm collected per week divided by 7. Group A bulls were unilaterally vasectomized and, therefore, the values are for output of one testis only. Was collected at frequency of 4 ejaculations or more per week for 40 weeks immediately prior to slaughter.

outside of the seminiferous tubules. Statistical analysis of duplicate determinations on 10 slides showed that differentiation between Leydig cells and other interstitial tissue was unreliable. Therefore, only the percentage of seminiferous tubules was calculated for each locus (800 minus the artifact hits divided into the hits on seminiferous tubules).

The relative frequencies of the 8 stages of the cycle of the seminiferous epithelium were determined (X500) by scoring 500 randomly selected round seminiferous tubule cross sections per testis locus using Orth's fixed tissue. The repeatability of such determinations was established by calculating the coefficient of repeatability from triplicate evaluations of 10 randomly selected slides. It was + 0.92.

The cellular content of 10 Stage I seminiferous tubules in each testis locus was determined by counting (X1,250) the nu-

clei present in round tubule cross sections in which all B-spermatogonia had divided into young primary spermatocytes (Orth's fixed tissue). The cells counted included Sertoli cells, A-spermatogonia, young or preleptotene primary spermatocytes, old or pachytene primary spermatocytes and spermatids. Abnormal primary spermatocytes, abnormal spermatids and cells of the various types found free in the tubule lumen were recorded separately. In each tubule cross section the diameter of a typical cell nucleus of each type was measured. Major and minor diameters were recorded for the oval spermatogonia as well as for each seminiferous tubule and tubule lumen. Nuclei were measured to the nearest 0.7  $\mu$  and seminiferous tubules to the nearest 2.2  $\mu$ .

The following formula based on those of Abercrombie (46) and Ortavant (58) was used to correct cell counts for variations in nuclear diameter

$$\text{True count} = \left[ \frac{\text{Observed count}}{\text{Section thickness}} \right] \left[ \frac{\text{Section thickness}}{\text{Section thickness} + \sqrt{(\Delta v) \left( \frac{d_{\text{obs}}}{2} \right)^2 - (\Delta v \cdot d_{\text{obs}}/4)}} \right]$$

Abercrombie's formula assumes that cell nuclei of infinitely small size can be counted. The present formula assumes that cells sectioned so that their nuclear diameter is less than one-half that of the true nuclear diameter will not be visualized. Major and minor diameters of spermatogonia were averaged for calculation of the correction term. The numbers of Sertoli cells and abnormal germ cells were not corrected.

At each stage of the cycle of the seminiferous epithelium the diameters of 10 seminiferous tubules and tubule lumens were measured for each testis. Since counts and measurements on Stage I seminiferous tubules were not affected by testis locus unilateral vasectomy or ejaculation frequency only slides for the posteromedial-central locus from the testis on the intact side of Group A bulls and both testes of normal Group B bulls were evaluated.

To correct linear measurements for tissue shrinkage resulting from histological processing the magnitude of shrinkage was estimated using 4 nonexperimental

bull testes. Blocks of tissue were fixed and routinely processed while adjacent tissue blocks were placed in small vials in crushed ice. Within three hours after slaughter the latter samples were sectioned at 25  $\mu$  on a freezing microtome without fixation. The minor diameter of 100 round seminiferous tubule cross sections was measured for each unfixed testis sample using phase contrast microscopy. After embedding and staining 100 tubules in each fixed testis sample were measured. Linear shrinkage (table 1) averaged 19.5% which represents a volumetric shrinkage of 48%. These values are simi-

TABLE 1  
Linear shrinkage of testicular tissue fixed in Orth fluid, dehydrated, and embedded in Tissuemat

Testis	Minor tubular diameter ( $\mu$ )		% linear shrinkage
	Frozen sections	Paraffin sections	
A	249 $\pm$ 3	204 $\pm$ 2	19.0
B	263 $\pm$ 4	189 $\pm$ 2	24.8
C	266 $\pm$ 4	223 $\pm$ 2	16.3
D	277 $\pm$ 4	224 $\pm$ 3	19.0

Mean  $\pm$  standard error



TABLE 5

Diameters of germ cell nuclei in Stage I seminiferous tubules (microns)

Cell type	Corrected diam.			Uncorrected diam.			Correction term <sup>a</sup>
	Major	Minor	A	Major	Minor	A	
Group A testes							
A-spermatogonia	10.8	9.8	10.2	8.7	7.8	8.2	0.683
Young primary spermatocytes			7.0			5.7	0.740
Old primary spermatocytes			8.5			6.8	0.703
Young spermatids			7.0			5.6	0.742
Group B testes							
A-spermatogonia	11.0	10.0	10.5	8.8	8.0	8.4	0.637
Young primary spermatocytes			6.7			5.4	0.751
Old primary spermatocytes			8.4			6.7	0.708
Young spermatids			6.8			5.3	0.753

Correction derived from data in table 1.

Correction term used to correct germ cell counts for variations in nuclear diameter.

$$\text{Correction term} = \frac{\text{section thickness}}{7.0} \left[ \sqrt{(\pi \text{ dia.}/2)^2} - (\text{A dia.}/4) \right]$$

$$= \frac{7.0}{7.0} \text{ Av dia.} \sqrt{3/16} = 7.0 (\text{A dia.})(0.433)$$

The nuclear diameters of germ cells (table 5) were very consistent although there appeared to be small differences between the two groups of bulls. Since the measurements were only to 0.7  $\mu$  these differences probably are meaningless. The average diameters, uncorrected for histological shrinkage were used to calculate the required correction terms.

Table 6 shows the corrected numbers of germ cells per seminiferous tubule cross section. In most cases intra-bull variation was small and the differences between the two testes averaged, for example, 0.4 spermatogonia and 9.4 spermatids for Group A bulls. For all 28 testes the spermatid numbers per tubule cross section ranged from 168 to 254. The differences in germ cell

TABLE 6

Average corrected number of germ cells in 7- $\mu$  cross sections of Stage I seminiferous tubules

Pre-treatment	A-spermatogonia	Young primary spermatocytes	Old primary spermatocytes	Lumen and primary spermatocytes	Spermatids	Lumen spermatids
Group A testes						
SR intact	2.8	53	54	0.2	215	4.0
SR vasect.	2.7	58	55	0.2	216	6.0
EX intact	2.4	53	51	0.2	187	3.6
EX vasect.	2.2	56	54	0.2	185	3.8
IX intact	2.9	54	50	0.2	193	4.2
IX vasect.	2.8	51	49	0.2	184	3.5
Av intact	3.1	54	52	0.2	187	4.0
A vasect.	2.9	54	52	0.2	195	4.4
A Group A	2.8	54	52	0.2	196	4.2
Group B testes						
SR	2.9	55	52	0.2	189	1.6
6-SX	3.7	64	62	0.1	226	3.0
A Group B	3.4	60	58	0.2	211	2.5
A all testes	3.1	56	54	0.2	202	2.6
$\pm$ S. E. (N = 28)	0.1	1	1	0.03	5	0.3

numbers between the Group A and Group B testes were not significant and probably reflect the difference in tubular diameter. Germ cell degeneration also was greater in Group B testes (Aman, '61b). The differences between the 4 SR and the six 6-8X testes in Group B were significant except for spermatogonia and spermatids free in the tubule lumen. This may be a bull rather than a treatment difference. In Group A each bull served as his own control through comparison of the intact and vasectomized sides; intra-bull differences were negligible. Thus, in Group A there was no effect of ejaculation frequency on testis histology. If the differences between SR and 6-8X bulls in Group B actually represent a true treatment effect, then testes of young and mature bulls respond differently to ejaculation frequency. Further investigations are needed to clarify this point.

The fate of morphologically normal primary spermatocytes and spermatids found in the tubule lumen is unknown; possibly they were artifacts. The occurrence of normal germ cells in the tubule lumen was not related to ejaculation frequency or vasectomy but Group A testes appeared

to have more spermatids in the lumen than Group B testes. On the basis of these data, it would appear that a small amount of sloughing of the germinal epithelium is normal and thus, it was surprising that mature spermatozoa seldom were seen free in the lumen of Stage I seminiferous tubules. Even in Stage VIII, mature sperm were either attached to the germinal epithelium or had been eliminated from the tubule lumen.

Based on the Group A testes it was concluded that neither ejaculation frequency nor vasectomy affected the numbers of germ cells in Stage I seminiferous tubules. Although not apparent from these data for 3- to 9-year-old bulls it is possible that in 10- to 15-year-old bulls there may be a decline in germ cell numbers.

#### *Seminiferous tubule diameter*

Major and minor tubule and lumen diameters (corrected for histological shrinkage) of Stage I seminiferous tubules are summarized in table 7. The minor diameter more closely represents the true diameter of the tubule, but the major diameter indicates the degree of ovalness of the cross sections examined and is essential

TABLE 7  
Average corrected major and minor diameters of Stage I seminiferous tubules and tubule lumen<sup>a</sup> (microns)

Precastration treatment	Tubule diam.		Lumen diam.	
	Major	Minor	Major	Minor
Group A testes				
SR intact	287	238	64	50
SR vasect.	288	258	89	47
6X intact	283	253	61	64
6X vasect.	282	257	83	67
8X intact	271	249	70	53
8X vasect.	270	248	88	54
Av intact	280	254	73	58
Av vasect.	278	254	70	58
Av Group A ± S.E. (N = 10)	280 3	254 2	71 3	56 3
Group B testes				
SR	294	268	83	60
6-8X	286	270	70	57
A Group B ± S.E. (N = 10)	285 3	269 2	76 6	58 6

<sup>a</sup>Correction derived from data in table 1.



for quantifying germ cell numbers in a testis. In Group A, the average seminiferous tubule diameter for 8X bulls was less ( $p < 0.05$ ) than that for SR and 2X bulls. Intra-bull differences were very small. In Group B bulls no effect of ejaculation frequency on tubular diameter was evident. The differences between Groups A and B were highly significant. It was concluded therefore, that ejaculation frequency and associated daily sperm output as well as vasectomy did not affect the diameter of Stage I seminiferous tubules.

The Stage I lumen diameters were inconsistent and did not fall into any pattern either within or among testes. The average lumen diameter for the 28 testes was  $58 \pm 3 \mu$ .

The average minor diameters of seminiferous tubules and their lumens at various stages of the cycle of the seminiferous epithelium are shown in table 8. Tubular diameter was much greater in Group B testes than in Group A testes. However variation among stages within the two groups was not significant. The lumen diameters gradually increased to a maximum at Stage VII. Thus the diameter of seminiferous tubules was independent of the cycle of the seminiferous epithelium but luminal diameter showed significant cyclic variations.

TABLE 8

*A stage corrected minor diameters of seminiferous tubules and tubule lumens at various stages of the cycle of the seminiferous epithelium (microns)*

Stage of cycle	T. tube diam.		Lumen diam.	
	Group A	Group B	Group A	Group B
I	255	271	66	76
II	255	272	64	75
III	258	268	74	75
IV	255	269	76	80
VI	248	270	81	85
VII	254	276	87	91
VIII	252	270	81	87
A	254	271	76	81

Correction derived from data in table 1.

#### DISCUSSION

These studies show that testis histology and the pattern of spermatogenesis are not affected by ejaculation frequency or rate of sperm removal by collection. The possibility that the absolute duration of the cycle of the seminiferous epithelium might

be altered by variations in collection frequency appears remote. Koefoed-Johnsen ('58 '60) found that when the time required for epididymal transit was considered, the interval between administration of phosphorus-32 to bulls and the appearance of radioactive sperm in semen was not influenced by ejaculation frequency. These and other data (Amann, '61a) suggest that sperm pass into the epididymis at a relatively constant rate and that changes in daily sperm output are compensated for by reciprocal changes in the rate of sperm resorption in the excurrent ducts.

The finding of no differences among the testicular loci is essentially in agreement with reports by Kennelly ('60) for boars and Roosen-Runge ('56) for humans. They found that the amount of interstitial tissue was similar in peripheral areas while there was a slight increase in the percentage of interstitial tissue near the mediastinum. In the present study the three loci were from peripheral areas.

The volume percentage of seminiferous tubules in the testis (77% for young bulls and 73% for mature bulls) agrees with the range of 76 to 84% reported by Bascom and Osterud ('25) for 4 testes from 4 young bulls. Determinations on 6 non-experimental bull testes indicated that the tunica albuginea comprised  $8.7 \pm 0.2\%$  of the testicular weight (Amann, '61a) which also agreed with Bascom and Osterud's ('25) data. However this value and that for shrinkage during histological processing should be confirmed by more extensive studies. Since the mediastinum occupies about 1% of the testis volume and testicular weight and volume are similar (density 1.04 gm/cm<sup>3</sup>) a value of 9.7% was used to correct testis volume for these nonproductive areas. The total length of the seminiferous tubules was estimated from testis volume (minus 9.7%) percentage of the testis which was seminiferous tubules, and the corrected major and minor tubule diameters. Total tubule length was  $3,518 \pm 87$  meters in Group A testes and  $4,050 \pm 197$  meters in Group B testes a significant difference. Both values are less than that of 4,496 calculated by Bascom and Osterud ('25) for 4 testes from young bulls. This difference

probably results from their failure to consider tissue shrinkage during histological processing.

As contrasted to the report by Roosen-Runge ('55) for rats in the present study the diameter of the seminiferous tubules did not differ among the various stages of the cycle of the seminiferous epithelium; however in both species tubular lumen diameter increased during the later stages of the cycle. Since the number of spermatogonia per tubule cross section is greater in the later stages of the cycle of the seminiferous epithelium and these stages contain 5 rather than 4 germ cell generations (see fig. 1) it appears that the increase in lumen diameter results from a marked reduction in spermatid volume during the last half of spermiogenesis. The degeneration of spermatids also may contribute to this apparent reduction in germ cell volume.

The uncorrected diameters of germ cell nuclei are similar to those reported for bulls by Haq (48) but with the exception of spermatogonia, are somewhat smaller than values reported by Krudsen ('54). The uncorrected counts of germ cells in Stage I seminiferous tubules are slightly greater than those in the brief report by Ortavant ('59).

Species variations in testicular histology are summarized in table 9. The relative frequencies of the 8 stages of the cycle of the seminiferous epithelium in the present study were almost identical with values reported for bulls by Ortavant ('59) but differ from those of Cupps and Laben ('60) for normal bulls. All three investigations utilized essentially the same classification scheme. Because different classification systems were used by Clermont and Leblond ('59) for monkeys and Oakberg ('56) for mice, values for 8 stages were calculated from their data. Nevertheless, comparisons should be relatively accurate since correlation between the 12 and 8 stage systems is quite precise at Stages I, IV and VIII. With the exception of rats the duration of Stage IV is relatively uniform among the various species. However there is a distinct shift in the proportion of the cycle of the seminiferous epithelium comprising the last 4 stages from a low value of 26% for bulls to "2" for rats. The physiological

significance of these differences remains obscure. However it is possible that this shift in the relative duration of the stages of the cycle of the seminiferous epithelium is associated with the differences in spermatocytogenesis which apparently exist among species. Ortavant ('59) noted that an increase in the relative duration of Stages V to VIII appeared to be associated with a decrease in the retention of fertilizing capacity of spermatozoa stored *in vitro*.

From the limited data of Bascom and Osterud ('25) and others for the percent age of seminiferous tubules in the testis and seminiferous tubule diameter it appears that these characteristics vary less among species than do the quantitative aspects of spermatogenesis, e.g. relative frequency of the stages of the cycle of the seminiferous epithelium and the duration of spermatogenesis. Unfortunately many of the values summarized in table 8 represent observations on only a few testes for a particular species. Sufficient numbers of animals with a known reproductive history seldom have been thoroughly examined. In addition to showing the necessity for a comparative approach to quantitative studies of testicular physiology the data in table 9 emphasize the dangers in extrapolating from one species to another.

The present data suggest that neither ejaculation frequency and sperm output nor vasectomy affect bovine testicular histology and spermatogenesis. However as a bull increases in age from three years to 8 years there appears to be an increase in testicular weight, seminiferous tubule diameter, total seminiferous tubule length, the percentage of Leydig cells and other interstitial tissue and the incidence of intra-testicular germ cell degeneration.

#### SUMMARY

Testicular histology was quantitatively evaluated in nine 3-year-old unilaterally vasectomized bulls and 5 mature intact bulls. To investigate the effects of ejaculation frequency and daily sperm output on testicular histology and spermatogenesis bulls were either sexually rested or collected at various ejaculation frequencies for approximately 20 weeks prior to slaughter. Average daily sperm output

TABLE 8  
Species variations in quantitative testicular histology and spermatogenesis

Stage	Boal	Rees	Menckey	Rees	Mat
	Relative frequency of the stages of the cycle of the seminiferous epithelium (%)				
I	20	24	19	11	4
II	14	18	29	27	8
III	31	23	18	2	14
IV	15	8	7	14	8
V	8	—	4	11	31
VI	6	11	13	21	8
VII	8	13	13	13	34
VIII	7	11	13	13	13
I to III	10	10	8	14	28
IV	22	21	48	30	23
V to VIII	12	8	7	14	8
Reference <sup>a</sup>	26	31	42	57	78
	(11)	(8)	(4)	(11)	(13)
	Approximate duration of spermatogenesis (days)				
Reference	60	48	unk.	unk.	48
	(2)	(10)		(8)	(5)
	Volume of seminiferous tubules in testis (%)				
Reference	77 and 75	83	unk.	70	80
	(1)	(3)		(7)	(12)
	Uncorrected diameter of seminiferous tubules ( $\mu$ )				
Reference	204 and 218	210	unk.	223 to 225	181 to 201
	(1)	(3)		(2)	(3)

Values for the monkey and mouse are approximations and were calculated from the original data.

References: (1) Amann, '51; (2) Amann, '51; (3) Amann and Odendaal, '51; (4) Clarnson and Odendaal, '58; (5) Clarnson, Odendaal and Menckey, '58; (6) Clarnson and Odendaal, '58; (7) Kennedy, '50; (8) Odendaal, '58; (9) Odendaal, '58; (10) Odendaal, '58; (11) Odendaal, '58; (12) Odendaal, '58; (13) Odendaal, '58.

after unilateral vasectomy for three young bulls ejaculated 8 times weekly was 2.17 billion or 62% greater than that of 1.43 billion for three similar bulls ejaculated twice weekly. Three mature bulls ejaculated 6 to 8 times weekly had an average daily sperm output of 5.75 billion.

No differences were detected as a result of unilateral vasectomy or frequency of ejaculation and sperm output. Likewise differences among three testicular loci were not significant.

Seminiferous tubules comprised 77% and 73% of the testis volume in young and mature bulls. The cycle of the seminiferous epithelium was described. The relative frequencies for Stages I through VIII of the cycle of the seminiferous epithelium were not affected by age and averaged 30.3 16.1 17.0 10.4 1.6 6.3 7.5 and 10.8% for 28 testes respectively. In 7- $\mu$  cross sections of Stage I seminiferous tubules the corrected numbers of A-spermatogonia young primary spermatocytes old primary spermatocytes, and spermatids averaged 3.1 56 14 and 202 respectively; differences associated with age were not significant. Minor seminiferous tubule diameter (corrected for histological shrinkage) averaged 271  $\mu$  for mature bulls and 254  $\mu$  for young bulls. Although the diameter of seminiferous tubules did not fluctuate during the 8 stages of the cycle of the seminiferous epithelium, the diameter of the seminiferous tubule lumen increased significantly from Stage II to Stage VII. The histology of the bovine testis was compared with data for other species.

Although certain age effects were evident, it was concluded that testis histology and spermatogenesis are not affected by ejaculation frequency rate of sperm removal by collection, or closure of the excurrent duct by vasectomy. There may be a difference in the response of testes of young and mature bulls to ejaculation frequency.

#### ACKNOWLEDGMENT

The author wishes to express his appreciation to Drs. J. D. Almqvist and Adam Anthony for assistance in preparation of the manuscript.

#### LITERATURE CITED

- Abercrombie M. 1946 Estimation of nuclear populations from microtome sections. *Anat. Rec.*, 94 238-248.
- Amann R. P. 1961 Reproductive physiology of the male bovine. Ph.D. Thesis, The Penn. State Univ. University Park.
- 1962b Reproductive capacity of dairy bulls. IV Spermatogenesis and testicular germ cell degeneration. *Am. J. Anat.*, 110 69-78.
- Bascom, K. F. and H. L. Osterud 1925 Quantitative studies of the testicle. II. P. term and total tubule length in the testicles of certain common mammals. *Anat. Rec.*, 31 159-169.
- Cavazos, L., and R. J. Malampy 1954 A comparative study of periodic acid-reactive carbohydrates in vertebrate testes. *Am. J. Anat.*, 95 467-496.
- Chalkley H. W. 1943 Method for the quantitative morphologic analysis of tissues. *J. Nat. Cancer Inst.*, 4 47-53.
- Clermont, Y. and C. P. Leblond 1953 Renewal of spermatogenesis in the rat. *Am. J. Anat.*, 63 473-502.
- 1955 Spermiogenesis of man, monkey, ram and other mammals as shown by the periodic acid-Schiff technique. *Ibid.*, 66 229-234.
- 1959 Differentiation and renewal of spermatogonia in the monkey *Macaca rhesus*. *Ibid.*, 104 237-274.
- Clermont, Y. C. P. Leblond and B. Mesaulier 1959 Durée du cycle de l'épithélium séminal du rat. *Arch. Anat. Microscop.* 48 37-58.
- Crype, P. T., and R. C. Leben 1960 Spermatogenesis in relation to spermatozoa concentration in bovine semen. *J. Dairy Sci.*, 43 73-76.
- Curtis, G. M. 1918 The morphology of the mammalian seminiferous tubule. *Am. J. Anat.*, 24 339-394.
- Ebner V. von 1871 U tersuchungen über den B der Samenkanälchen und die Entwicklung der Spermatozoen. *Arch. mikr. Anat.*, 7 (cited by V. von Ebner *Arch. mikr. Anat.*, 31 306, 1886).
- 1888 Zur Spermatogenese bei den Säugthieren. *Ibid.*, 31 238-291.
- Fronters, J. G. 1939 The effects of some dehydrating techniques on the measurements of the brain of Macaques. *Anat. Rec.*, 135 83-92.
- Hag I 1948 Some morphological characteristics of the epithelial cells lining the genital tract of the bull. *Vet. J. (Lond.)* 104 5-22.
- Kennelly J. J. 1960 Spermatogenesis in boars. I. The testicular and epididymal spermatozoan reserves. II. Estimated potential daily production of spermatozoa. M. S. Thesis, Cornell Univ. Ithaca.
- Kradsen, O. 1954 Cytomorphological investigation into the spermiocytogenesis of bull with normal fertility and bull with acquired disturbances in spermiogenesis. *Acta path. microbiol. Scand. Suppl.* 101 1-79.

- Koeford-Johnsen, H. H. 1936 Undersøgelser over sæddannelsen (Investigations on sperm formation) Den kongelige Veterinær-og Landbohøjskole Institut for Sterilitetsforskning Aarsberetning, p. 18.
- 1960 Influence of ejaculation frequency on the time required for sperm formation and epididymal passage in the bull. *Nature* 185 49-50.
- Kramer M. F. 1960 Spermatogenesis bij de stier. Doctor's Thesis Rijksuniversiteit te Utrecht, Utrecht. Citation in Excerpta Med., Section I, 14 672. 1960.
- Leblond, C. P., and Y. Clermont 1952a Spermatogenesis of rat, mouse, hamster and guinea pig revealed by the periodic acid-fuchsin sulfurous acid technique. *Am. J. Anat.*, 90 167-215.
- 1952b Definition of the stages of the cycle of the seminiferous epithelium in the rat. *Ann. N. Y. Acad. Sci.* 55 545-573.
- Oakberg, E. F. 1956a A description of spermatogenesis in the mouse and its use in analysis of the cycle of the seminiferous epithelium and germ cell renewal. *Am. J. Anat.*, 99 391-413.
- 1956b Duration of spermatogenesis in the mouse and timing of stages of the cycle of the seminiferous epithelium. *Ibid.*, 99 507-515.
- 1957 Duration of spermatogenesis in the mouse. *Nature* 180 1137-1138.
- Octaviani, R. 1956 Spermatogénèse et réserves / Spermatiques chez le Taureau et le Bœuf III Intern Congr. Animal Reprod. (Cambridge) 1 44
- 1958 Le Cycle spermatogénétique chez le Bœuf D. Sc. Thèse Univ. of Paris Paris.
- 1959 Spermatogenesis and Morphology of the Spermatozoon. *Reproduction & Domestic A. Dual* Vol. II H. H. Cole and P. T. Cupps, ed. Academic Press, New York, Ch. p. 1.
- Regaud, C. 1901 Etudes sur la structure des tubes séminifères et sur la spermatogénèse chez les mammifères. *Arch. Anat. Microscop.* 4 101-155.
- 1901b Etudes sur la structure des tubes séminifères et sur la spermatogénèse chez les mammifères. *Ibid.*, 4 231-360.
- Rosen-Runge E. C. 1931 Quantitative studies on spermatogenesis in the albino rat. II. The duration of spermatogenesis and some effects of colchicine. *Am. J. Anat.*, 88 163-176.
- 1932 Kinetics of spermatogenesis in mammals. *Ann. N. Y. Acad. Sci.* 55 574-584.
- 1933 Quantitative studies on spermatogenesis in the albino rat. III Volume changes in the cells of the seminiferous tubules. *Anat. Rec.*, 123 385-398.
- 1936 Quantitative investigations on human testicular biopsies. I. Normal testis. *Fertil. and Steril.*, 7 251-261.
- Rosen-Runge, E. C., and F. D. Barlow 1933 Quantitative studies on human spermatogenesis. I. Spermatogenesis. *Am. J. Anat.*, 93 143-170.
- Rosen-Runge, E. C., and L. O. Giesel J. 1930 Quantitative studies on spermatogenesis in the albino rat. *Ibid.*, 87 1-30.
- Schoenfeld H. 1900 La Spermatogénèse chez le Taureau. *Biblog. Anat.* 8 74-98.
- 1901 La Spermatogénèse chez le Taureau et chez les mammifères en général. *Arch. Biol. (Liege)* 16 1-72.

## PLATE I

## EXPLANATION OF FIGURES

All figures in this and the following plates are photomicrograph of Orth fixed tissue stained with Feulgen Azure-A Schiff and periodic acid-Schiff stains. Figures 2 to 9 are 1 magnification / 385 and figures 10 to 13 are 1 magnification / 97

- 2 Stage I seminiferous tubule showing both B-spermatogonia (B) and young primary spermatocytes (C) as well as old primary spermatocytes (CC) and spermatid (T). The dark staining acrosome covers the anterior portion of the spermatid.
- 3 Stage II seminiferous tubule. The spermatid have long tails and their acrosomes have distinct pex anterior to the nucleolar material.
- 4 Stage III seminiferous tubule. The spermatids are grouped into distinct bundles.
- 5 Stage IV seminiferous tubule showing young primary spermatocytes (C) old primary spermatocytes in the first reduction division and secondary spermatocytes (2C) as well as spermatogonia and spermatids.

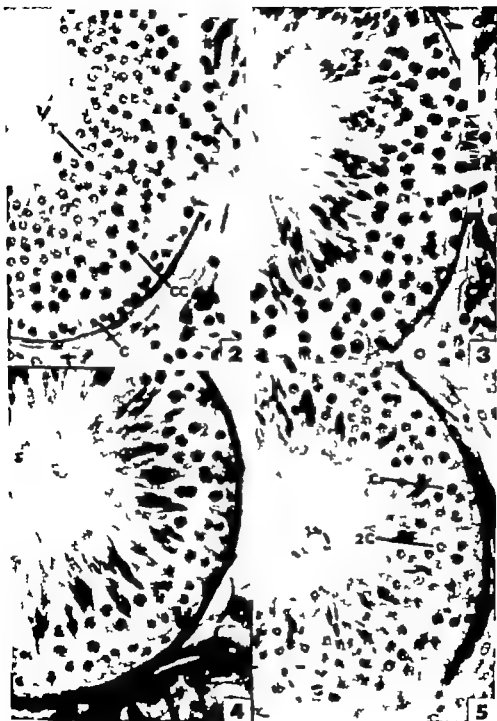


## PLATE 2

### EXPLANATION OF FIGURES

- 6 Stage V seminiferous tubule (the upper one-fourth of the tubule is Stage IV) comparing the morphology of the secondary spermatocytes (SC) of Stage IV with the young spermatids (T) of Stage V. Also indicated are Sertoli cell (S) and A-spermatogonium (A) and old spermatids (TT).
- 7 Stages VI seminiferous tubule showing the two generations of spermatids and one generation of primary spermatocytes. The old spermatids deeply penetrate toward the basement membrane.
- 8 Stage VII seminiferous tubule. The old spermatids have moved toward the tubule lumen. Although not distinctly shown, the acrosome of the spermatid is starting to form.
- 9 Stage VIII seminiferous tubule. Spermatozoa line the tubule lumen just prior to release.





### PLATE 3

#### EXPLANATION OF FIGURES

- 10 Testis from intact side of bull 168 (8 ejaculates per week) with the stage of each seminiferous tubule numbered.
- 11 Testis from the vasectomized side of bull 168. Comparison with the testis from the intact side (fig. 10) revealed no histological differences. The preponderance of Stage I seminiferous tubule cross sections in this small area as compared with the numerous Stage III tubules in figure 10 emphasizes the importance of recognizing the various stages of the cycle of the seminiferous epithelium when evaluating the effects of treatment on testis histology.
- 12 Ventral pole of the left testis of an 18-year-old bull (NH 16) showing the marked infiltration of connective tissue (64%) and high incidence of atretic seminiferous tubules. A few essentially normal seminiferous tubules also were in the same histological section. The dorsal two-thirds of the testis appeared to be similar to figure 13.
- 13 Ventral pole of the right testis from bull NH 16. Although there was an obvious increase in interstitial tissue (50%) and the occurrence of atretic tubules, essentially normal seminiferous tubules predominated.





# Reproductive Capacity of Dairy Bulls

## IV SPERMATOGENESIS AND TESTICULAR GERM CELL DEGENERATION<sup>1,2</sup>

RUPERT P. AMANN

Dairy Breeding Research Center Department of Dairy Science  
The Pennsylvania State University University Park,  
Pennsylvania

The earliest descriptions of bovine spermatogenesis were by von Ebner (1871, 1888), Schoenfeld ('00 '01) and Regaud ('01a, '01b) but the exact mode of spermatogonia renewal and multiplication still has not been clearly delineated in this species. These workers distinguished two types of spermatogonia, the indifferent cells which are now called A-spermatogonia and the spermatogonia which probably represent both In- and B-spermatogonia. Schoenfeld ('01) suggested that in bulls an indifferent cell divided to form two indifferent cells, one of which subsequently divided to form two spermatogonia. The two spermatogonia were believed to divide twice and produce 8 primary spermatocytes while the remaining indifferent cell was thought to serve as a stem cell for the next generation. Ortavant ('39) described a similar scheme by which 16 primary spermatocytes were formed from a stem A-spermatogonium. However, Kramer ('60) reported that in bovine testes there is variation in the multiplying pattern of a stem spermatogonium to form primary spermatocytes. He found a mean of 12 primary spermatocytes per stem spermatogonium, but the values for 8 testes ranged from 8 to 20 spermatocytes. Failure of some cells to divide rather than cellular degeneration was thought to account for this variability.

For rats, Roosen-Runge and Giesel ('30) suggested that an A-spermatogonium divides two or three times to form B-spermatogonia which in turn divide twice and form primary spermatocytes. They concluded that spermatogonia renewal was accomplished through the failure of a few A-spermatogonia to transform into B-sper-

matogonia. Rolshoven (41) however suggested that each division of a rat spermatogonium produced a new spermatogonium and a primary spermatocyte.

Most of these reports agree in general with the stem cell renewal theory proposed by Clermont and Leblond ('33 '34 '39). They suggested a rigid pattern in which at a particular division, one of the A-spermatogonia did not divide but rather remained as a new stem A-spermatogonium. The exact location of this division (which results in two daughter cells with a different potential) as well as the number of divisions between formation of a stem A-spermatogonium and its daughter primary spermatocytes appear to vary among species. However, the general principle is similar in the rat (Clermont and Leblond '33), mouse (Oakberg, '36), hamster (Clermont, '34), monkey (Clermont and Leblond '39) and ram (Ortavant, '38). Since the method of spermatogonia renewal in the bovine testis has not been completely elucidated, the problem of spermatogenesis and accompanying germ cell degeneration has been reinvestigated.

### EXPERIMENTAL PROCEDURE

Tissue samples were taken from the testis on the intact side of 9 unilaterally vasectomized 36-month-old Holstein bulls and from both testes of one normal mature Guernsey and three normal mature Holstein bulls. Detailed information on

Authorized for publication on May 12, 1961 as Paper No. 2350 in the Journal series of The Pennsylvania Agricultural Experiment Station.

The data contained in this paper are part of those submitted by the author to the Graduate School of The Pennsylvania State University in partial fulfillment of the requirements for the degree of Doctor of Philosophy.

the prelaugher treatment and quantitative testicular histology for these 13 bulls has been presented (Amann '61). All tissue samples were taken from a postero-medial-central area adjacent to the ductus deferens and about one-half way between the poles of the testis. Following Orth's fluid fixation 7  $\mu$  sections were stained by a combination of the Feulgen azure-A-Schiff and periodic acid-Schiff techniques. For each testis spermatogonia nuclei in 10 round seminiferous tubule cross sections at each stage of the cycle of the seminiferous epithelium, except Stage V were classified and counted (X1,250). Spermatogonia were classified as either type A or B in Stage I, as type A in Stage II, as either type A or In in Stages III-IV and VI and as either type A or B in Stages VII and VIII. In sections from the 8 testes of mature bulls the number of young primary spermatocytes in the Stage I tubule cross sections also was recorded. Values for primary spermatocytes and spermatids in Stage I were similarly obtained from other tubules in which all B-spermatogonia had divided into young primary spermatocytes. The correction of spermatogonia counts for variations in nuclear diameter and other details of the procedure have been described (Amann '61).

## RESULTS

Average corrected spermatogonia counts for 9 young bull testes (Group A) and for 8 mature bull testes (Group B) are presented in table 1. In general, numbers of spermatogonia per tubule cross section were significantly greater in Group B testes but the pattern or ratio of cell numbers was similar in both groups. The data suggested that A-spermatogonia were at their basal value in Stages I-VI, VII, and VIII and the number of A-spermatogonia per tubule cross section in these 4 stages averaged  $3.39 \pm 0.19$  for Group A and  $4.36 \pm 0.34$  for Group B. In Group B testes counts of A-spermatogonia also appeared to be at their basal value in Stage IV.

Certain spermatogonia which had a homogeneous finely granular nucleus without a nucleolus and which were about the same size as A-spermatogonia were present in Stages I to VII. These cells were considered to be either A-spermatogonia sectioned so that the nucleolus was excluded or A-spermatogonia in prophase, but they may have been abnormal or degenerating cells. They were most prevalent in Stages I-II and III and although counted separately are included as A-spermatogonia in table 1.

Average  $\pm$  standard error

TABLE 1

Corrected number of germ cell nuclei in 7  $\mu$  cross sections of seminiferous tubules at various stages of the cycle of the seminiferous epithelium  
(Average  $\pm$  standard error)

Stage of cycle	A-spermatogonia	In- and B-spermatogonia	Spermatogonia in div	Young primary spermatocytes	Old primary spermatocytes	Young spermatozoa
Nine Group A testes						
I	$3.4 \pm 0.3$	$7.5 \pm 0.9$	0.70			
II	$6.4 \pm 0.2$		0.10			
III	$5.6 \pm 0.3$	$5.2 \pm 0.5$	0.30			
IV	$3.9 \pm 0.3$	$8.9 \pm 0.3$	0.10			
VI	$3.4 \pm 0.2$	$10.9 \pm 0.5$	0.10			
VII	$3.4 \pm 0.3$	$17.4 \pm 0.5$	0.20			
VIII	$3.4 \pm 0.2$	$22.0 \pm 0.8$	0.30			
I				$54.9 \pm 2.0$	$53.0 \pm 2.5$	$203.9 \pm 10.8$
Eight Group B testes						
I	$4.7 \pm 0.6$	$10.2 \pm 1.1$	1.30	$33.0 \pm 1.7$		
II	$9.5 \pm 0.4$		0.03			
III	$5.0 \pm 0.4$	$7.6 \pm 0.4$	0.22			
IV	$4.5 \pm 0.4$	$9.6 \pm 0.6$	0.04			
VI	$4.3 \pm 0.4$	$12.6 \pm 1.0$	0.15			
VII	$4.0 \pm 0.3$	$19.4 \pm 0.8$	0.20			
VIII	$4.4 \pm 0.2$	$25.5 \pm 0.8$	0.40			
I				$63.1 \pm 2.2$	$58.1 \pm 2.3$	$220.2 \pm 11.2$

The number of spermatogonia in division is uncorrected.

Since classification of spermatogonia as In- or B-spermatogonia was somewhat arbitrary certain of the cells classified as B-spermatogonia in Stages VII and VIII may have been In-spermatogonia. It was not difficult to distinguish In- from B-spermatogonia, but it was impossible to distinguish between B-spermatogonia in Stages VII and VIII either by size or morphology. The average major and minor nuclear diameters of A In- and B-spermatogonia were  $8.4 \times 7.5$   $7.4 \times 6.6$  and  $6.6 \times 6.1$   $\mu$ , respectively.

Mitosis of spermatogonia was observed in all stages of the cycle of the seminiferous epithelium but peaks appeared to occur in Stages I, III, VII, and VIII (table 1). Many of the divisions in Stage I were those of B-spermatogonia into young primary spermatocytes although some were A-spermatogonia dividing to form new A-spermatogonia. This was evidenced by the doubling of the number of A-spermatogonia in Stage II as compared to Stage I. The peak in Stage III apparently represented division of A-spermatogonia into A and In-spermatogonia. In Stage VI and especially Stages VII and VIII the more diffuse peaks of division probably were those of In-spermatogonia forming B-spermatogonia. Aramer ('60) found spermatogonia in mitosis in all 10 of the stages in which he divided the cycle of the semi-

niferous epithelium. Peaks of division appeared to occur at stages equivalent to those of high mitotic activity in this study. Ortavant ('59) however suggested that spermatogonia division occurs in Stages I, III, IV and VIII.

## INTERPRETATION

### Spermatogonia renewal

Using the average number of A-spermatogonia in Stages I, VI, VII, and VIII as a base the ratios of different types of spermatogonia for each testis at each stage of the cycle of the seminiferous epithelium were calculated. These individual testis ratios as well as those for primary spermatocytes and spermatids in late Stage I were averaged for presentation in table 2. Also shown in table 2 are ratios calculated from the preliminary data of Ortavant ('59). A series of t-tests demonstrated that the ratios of A-spermatogonia in Stages II and III and In-spermatogonia in Stage IV differed significantly between Group A and Group B testes. The values for primary spermatocytes and spermatids also were significantly different. These data suggest that theoretically each A-spermatogonium produces 16 primary spermatocytes and 64 spermatids. However since there appeared to be a loss of germ cells in mature Group B bulls the

TABLE 2  
Ratios of germ cell nuclei : various stages of the cycle of the seminiferous epithelium

Cell type	CrII 1979	Stage of cycle of the seminiferous epithelium								I
		I	II	III	IV	V	VI	VII	VIII	
Group A testes										
A-spermatogonia	1.0	1.9	1.7	1.2	—	1.0	1.0	1.0		
In- and B-spermatogonia	2.2	0.0	1.3	2.7	—	3.3	3.2	6.6		
Young primary spermatocytes										16.6
Old primary spermatocytes										15.7
Sperm tids										61.4
Group B testes										
A-spermatogonia	1.1	2.2	1.2	1.0	—	1.0	0.9	1.0		
In- and B-spermatogonia	2.4	0.0	1.3	2.2	—	2.9	4.6	5.9		
Young primary spermatocytes	7.3									14.9
Old primary spermatocytes										13.8
Spermatids										51.7
Octavant										
A-spermatogonia	1.0	0	2.9	—	—	—	—	1.0		
In- and B-spermatogonia				—	—	4.3	4.3	8.8		
Young primary spermatocytes										16.2

Calculated from the corrected counts.

Ratios calculated from the uncorrected counts in table VII of Ortavant ('59).

remainder of the interpretation will be based on testes from Group A bulls.

Oakberg ('58) emphasized the difficulty in determining the exact pattern of spermatogonia renewal because of germ cell degeneration. However unless degeneration during the proliferation of spermatogonia in bull testes amounts to 33% so that 24 primary spermatocytes theoretically are formed rather than 18 degeneration appears to be unimportant during this phase of spermatogenesis. In the rat (Clermont and Leblond '53, Roosen-Runge '52) and mouse (Oakberg, '58) stem A-spermatogonia are formed as a result of the second division of spermatogonia but a total of 24 primary spermatocytes are formed rather than 18 as in bulls and rams (Ortavant, '58). This results from an extra division whereby one of the A-spermatogonia present in Stage II produces 4 In-spermatogonia while the other produces two In-spermatogonia and a stem A-spermatogonium (fig. 1). As evident from table 2 neither the present data nor those of Ortavant ('59) indicate that this occurs in bulls since only 18 primary spermatocytes are formed from each stem A-spermatogonium. A rapid degeneration of A-spermatogonia in Stages I, II and III could result in a low count for A-spermatogonia and hence erroneous cell ratios but there was no evidence for cell loss at this point in spermatogenesis. Kramer ('60) concluded that few A-spermatogonia degenerated but that degeneration of B-spermatogonia occurred during the last

half of the cycle of the seminiferous epithelium. This would not result in erroneous cell ratios through underestimation of the basal number of A-spermatogonia. Although attributed by Kramer to variations in the multiplication pattern rather than germ cell degeneration an average of only 12 primary spermatocytes per stem A spermatogonium was found.

Although the exact pattern of spermatogonia renewal was not clear cut, the present data suggest the probable pattern of spermatogenesis in bulls. The relative time sequence of various events was established from the relative frequency of the 8 stages of the cycle of the seminiferous epithelium which was 30.3 16.1 17.0 10.4 16 6.3 7.5 and 10.8% respectively (Amann '61). On the basis that 18 primary spermatocytes are formed from each stem A-spermatogonium three possible patterns for spermatogonia renewal in bulls have been developed. Figure 2A is based on the description presented by Ortavant ('59) while the patterns in figures 2B and 2C were developed from the present study.

Both sets of data (Group A and Ortavant's) show that there were twice as many A-spermatogonia in Stage I as in Stage II. Thus the stem A-spermatogonium (present in Stages IV through I) divides late in Stage I or early in Stage II. In Stage III (Group A) there was a total of three spermatogonia with approximately equal numbers of A and In-spermatogonia. Ortavant ('59) however suggested that one of these spermatogonia was the new stem A-spermatogonium while the other two divided again in Stage IV (see fig. 2A). Of the three proposed patterns only that in figure 2C meets the requirement of having both A and In-spermatogonia in Stage III.

Ortavant did not present data for Stage IV but apparently he assumed that 4 In-spermatogonia were formed during Stage IV since in Stages VI and VII he found 4 In-spermatogonia. The present study indicates that 4 In-spermatogonia are not present in Stage IV. The differences among the values for In and B-spermatogonia in Stages III through VIII were highly significant and there was a low frequency of cell division in Stage IV. It was

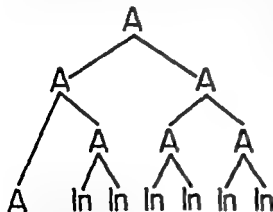


Fig. 1. Renewal of spermatogonia. 13.  
Adapted from Roosen-Runge ('52) and Clermont and Leblond ('53)

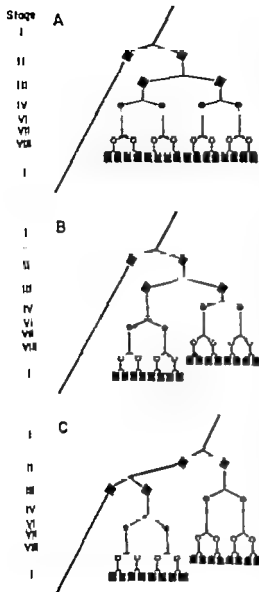


Fig. 2 Three possible patterns for spermatogonia renewal in bulls. Spermatogonia types are diamond, A-spermatogonia; solid circle In-spermatogonia; open circle B-spermatogonia; square young primary spermatocytes. Mitosis occurs between the point where vertical line branches and the next cell symbol.

Patterns A and B differ in the timing of the divisions forming In- and B-spermatogonia and primary spermatocytes. Pattern C differs from Pattern A both in the time of formation of the stem A-spermatogonium and in the formation of In-spermatogonia and subsequent cell types. The major difference between Patterns B and C is in the time of formation of the stem A-spermatogonium.

concluded that in Stage IV there are two In-spermatogonia which were formed late in Stage III, a stem A-spermatogonium and an A-spermatogonium which was formed early in Stage III and starts to divide into two additional In-spermatogonia late in Stage IV. Although Kramer ('60) did not propose a pattern for spermatogenesis this interpretation is not contrary to his data. Stage V is of extremely short duration and counts were not made.

In Stages VI, VII, and VIII the patterns for spermatogonia renewal in figures 2B and 2C are similar and agree with the observed values. However Ortavant ('59) found identical numbers of In-spermatogonia in Stages VI and VII and concluded that spermatogonia did not divide in these stages but that the B-spermatogonia were all formed in Stage VIII. His values were based on counts of only 13 to 27 seminiferous tubule cross sections at each stage of the cycle of the seminiferous epithelium. Kramer ('60) mentioned the presence of both In- and B-spermatogonia, but in presenting his data did not differentiate between these two cell types. He found that the combined number of In- and B-spermatogonia per tubule cross section increased from less than one at the start of Stage IV to 11 in Stage VI, 16 in Stage VII, 17 in Stage VIII, and 19 in early Stage I (Stages 13, 15, 16, and 5 in Kramer's classification). These data and the significant differences in the present study among values for Stages IV, VI, VII, and VIII do not support figure 2A.

The data in tables 1 and 2 and the reports by Ortavant ('59) and Kramer ('60) suggest that at least some B-spermatogonia are present early in Stage I. The value of 2.2 for Group A testes represents an average for B-spermatogonia throughout Stage I. Since Stage I is rather long (30.3% of the cycle) it is impossible to tell exactly where the division of B-spermatogonia into young primary spermatocytes occurs. In 90 Stage I tubules scored for Group A, 60 contained at least one B-spermatogonium while the other 30 were devoid of B-spermatogonia. More detailed examinations for Group II showed that 5 tubules contained only B-spermatogonia, 49 contained both B-spermatogonia and young primary spermatocytes and 26 contained



only young primary spermatocytes. These data suggest a pattern in Stages VIII and I such as shown in figures 2B and 2C. This hypothesis is supported by the observed value of 16.6 young primary spermatocytes for late Stage I tubules. Although all portions of a tubule cross section may not be in the same sub-stage of development, the present study suggests that the divisions of B-spermatogonia to young primary spermatocytes do not occur simultaneously.

Figure 3 shows the theoretical total number of spermatogonia (A and B-spermatogonia combined) in Stages I to VIII and the theoretical number of spermatogonia and young primary spermatocytes early in Stage I (Ia) and late in

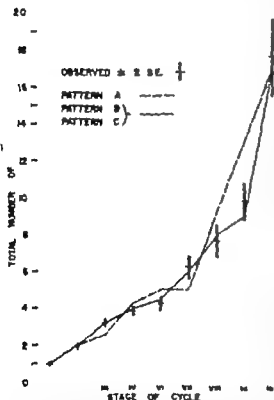


Fig. 3. A comparison of the total number of spermatogonia at each stage of the cycle of the seminiferous epithelium according to each of three proposed patterns (Fig. 2) with the average value ( $\pm$  2 S.E.) recorded for 8 testes from Group A bulls. The values for Stage I represent spermatogonia only in Stage I while those for Stage Ib represent the A-spermatogonia and young primary spermatocytes late in Stage I. According to postulated Pattern A 17 cells should be present in both Stages I and Ib.

Stage I (Ib). Also shown are the totals of the observed ratios. It is obvious that Pattern A for spermatogonia renewal does not agree with the data. Patterns B and C have essentially the same total numbers of cells at any given stage of the cycle of the seminiferous epithelium and both agree with the observed values for total cells. However when cell types are considered Pattern B does not appear to fit the observations as well as Pattern C. The scheme presented in figure 2C is thought to be the best approximation of spermatogonia renewal in bulls. Data for Group B testes also support this hypothesis.

Reconstruction of seminiferous tubules as utilized by Clermont and Leblond ('39) or a more exact classification of the stages of the cycle of the seminiferous epithelium based on spermatid morphology may give a more critical evaluation of spermatogonia renewal. However based on testicular analysis using these two methods Kramer ('60) was unable to determine the pattern of spermatogenesis in bulls. In fact, he concluded that the sequence of spermatogonia divisions was variable and did not follow a rigid pattern. This conclusion is inconsistent with the work on mice, rats, hamsters, monkeys, pigs and sheep. In all these species rigid patterns for spermatogenesis have been reported. It is unlikely that bovine spermatogenesis does not follow a consistent pattern.

The method of spermatid formation from primary spermatocytes is less complex. From examination of many tubule cross sections, it was obvious that in Stage IV the old primary spermatocytes divided into secondary spermatocytes which in turn divided to form spermatids. These meiotic divisions appear to be well synchronized. Figure 4 shows the postulated pattern of spermatogenesis in bulls. Since stem A-spermatogonia are formed in Stage III it requires about 4.5 cycles of the seminiferous epithelium for the complete spermatogenic process although spermatozoa are released into the tubule lumen at the end of each Stage VIII. Figure 4 represents the spermatogenic potential of the species but as observed in testes from mature Group B bulls degeneration of germ cells may reduce actual production to less than 84 spermatids per stem A-spermatogonium.

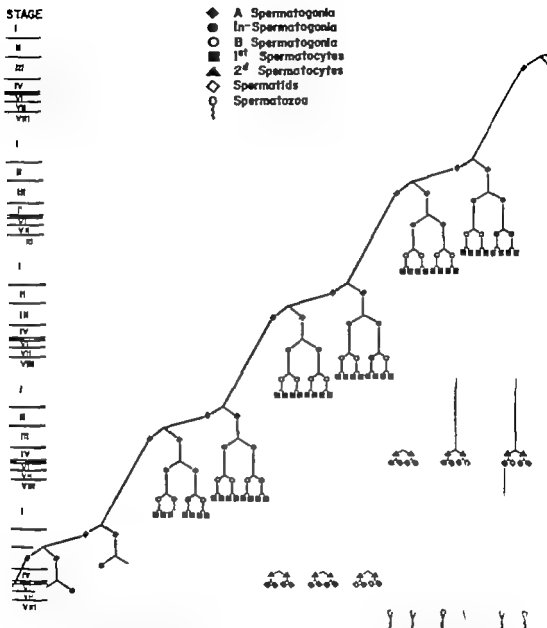


Fig. 4 The tentative pattern of spermatogenesis in bulls. Spermatogenesis starts with the formation of stem A-spermatogonium in Stage III and terminates approximately 4.5 cycles of the seminiferous epithelium later with the release of 64 spermatozoa at the end of Stage VII.

gonium. However this loss of potential germ cells is not related to ejaculation frequency or rate of sperm output (Amann '61)

### *Testicular germ cell degeneration*

The loss of potential spermatozoa for ejaculation apparently occurs at two loci: the testis and the epididymis. This discussion will be confined to testicular losses. In rats, Roosen-Runge ('55) found that the ratio between B-spermatogonia present in Stage VIII and young spermatozoa in Stage VI was not 1:4 but rather 1:3.18. The 22% loss of potential spermatozoa was distributed as follows: 10% degenerated as young primary spermatocytes near the basement membrane; 2% during the first maturation division; and 10% as young spermatozoa. Roosen-Runge ('55) emphasized that germ cell degeneration occurred in obviously normal seminiferous tubules with the same regularity as cell division and differentiation.

Oakberg ('56) considered that the degenerating cells stated by Roosen-Runge ('55) to be spermatocytes were in reality A-spermatogonia which had not completed division in Stages I to III. Contrary to the present study with bulls, Oakberg observed degenerating spermatogonia in mouse testes at all stages of the cycle. Although they amounted to less than 2.5% of the spermatogonia in any given stage depending upon the method of calculation, these degenerating spermatogonia resulted in a loss of 14 to 25% of the potential germ cells. There was no evidence of degeneration during the long prophase of the primary spermatocytes but there was a loss of about 13% during the two meiotic divisions. Oakberg ('56) found an overall loss of about 27% which is in good agreement with that of 22% reported by Roosen-Runge ('55) for rats; however the exact stages of degeneration appear to differ in the two species.

Ortavant ('58) has presented the most striking demonstration of testicular germ cell degeneration. He found an inverse relation between the length of daily illumination of rams and germ cell formation. Long illumination (16 hours) resulted in an 11% reduction in the basal number of A-spermatogonia. A different interpreta-

tion of his data suggests that this loss may have been as great as 30% with subsequent losses during spermatocytogenesis amounting to 43% with long illumination as contrasted to 20% in testes from rams with short illumination (8 hours). Ortavant's ('58) histological data suggest a total decrease of from 40 to 50% in the number of spermatozoa for 16 hours of illumination.

The data on spermatogenesis in tables 1 and 2 suggest that there is very little testicular germ cell degeneration in 36-month-old bulls but that it becomes of greater importance with advancing age. The ratios of the basal number of A-spermatogonia to young primary spermatocytes, old primary spermatocytes and young spermatozoa were 10 : 166 : 157 : 614 for testes from young Group A bulls as compared with 10 : 14.9 : 13.8 : 517 for testes from mature Group B bulls. Thus, there was no germ cell degeneration during the first 2.5 cycles of spermatogenesis in Group A testes but apparently 4% of the potential spermatozoa were not formed from old primary spermatocytes. If this small difference from the theoretical value (4 times the value for old primary spermatocytes) represents a true loss ( $p < 0.05$ ) it could be attributed to failure of a few primary spermatocytes to complete the meiotic divisions. This is supported by the occasional observation of degenerate PAS positive old primary spermatocytes late in Stage III and in Stage IV. For mice, Oakberg ('56) also concluded that degeneration of primary spermatocytes during the long prophase was negligible, but that losses occurred during the meiotic divisions. Data for the occurrence of abnormal germ cells in Stage I seminiferous tubule cross sections also indicate that the loss of germ cells was negligible in Group A testes (Amann '61). The incidence of abnormal primary spermatocytes was 0.05% and of abnormal spermatozoa 0.80%. Occasionally pyknotic spermatozoa were observed in Stage II but they probably represented less than 1% of all spermatozoa present. Kramer ('60) also observed abnormal and degenerating spermatozoa in Stage II.

The germ cell ratio for Group B of 10 : 14.9 : 13.8 : 517 indicates that degeneration was more prevalent in these 63-month

104-month-old bulls although the ratios for the 4 bulls were similar. About 7% of the potential young primary spermatocytes degenerated during spermatogonia multiplication and an additional 7% of the young primary spermatocytes degenerated during the cycle of the seminiferous epithelium when they are in prophase. From the report by Kramer ('60) it can be concluded that the cell loss during spermatogonia multiplication occurred during divisions of the In- and B-spermatogonia. During the two meiotic divisions there was a 5% loss of potential spermatids; a value similar to that for Group A. Kramer ('60) found a 7% loss of germ cells during meiosis. The loss of potential spermatids during the first 3.5 of the 4.5 cycles of the seminiferous epithelium required for spermatogenesis totaled 19% in mature bulls. This value approaches those of 22% for mature rats (Roosen-Runge '55) and 27% for mice (Oakberg '56). Kramer ('60) found an average of 42 spermatids per stem A-spermatogonium in one testis from a one-year-old bull. This represents a degeneration of 34% of the potential spermatids if 64 are theoretically formed from each stem A-spermatogonium. Although not directly investigated, it appeared that losses during the last cycle of spermatogenesis were slight. It is impossible to state conclusively that the basal number of A-spermatogonia was not reduced through degeneration. However when the larger seminiferous tubule diameter of Group II bulls was considered, the number of A-spermatogonia per 100  $\mu$  of tubular circumference was similar for Group A and II testes.

#### SUMMARY

Corrected counts of spermatogonia nuclei in 10 seminiferous tubule cross sections at each stage of the cycle of the seminiferous epithelium for 17 testes were used to evaluate spermatogenesis and testicular germ cell degeneration in bulls. The numbers of spermatogonia at each stage were significantly greater in 8 testes from 65- to 104-month-old bulls than in 9 testes from 36-month-old bulls. A-spermatogonia were at their basal value in Stages VI VII VIII and I. In Stage II there was twice the basal number of A-spermatogonia.

In Stage III one-half of the A-spermatogonia divided into In-spermatogonia while the remaining A-spermatogonia divided to produce two new A-spermatogonia; one stem A-spermatogonium and a second which divided in Stages V and VI into two In-spermatogonia. The In-spermatogonia formed in Stage III apparently divided into B-spermatogonia in Stage VII while the In-spermatogonia formed in Stages V and VI did not divide into B-spermatogonia until late Stage VIII or early Stage I. Division of B-spermatogonia into young primary spermatocytes in Stage I also appeared to be asynchronous, but divisions of all primary spermatocytes and all secondary spermatocytes were synchronized. Thus, it appears that divisions for the formation of In-spermatogonia, B-spermatogonia, and primary spermatocytes each occur in two separate peaks. Since stem A-spermatogonia were formed in Stage III, it requires about 4.5 cycles of the seminiferous epithelium to complete spermatogenesis.

In testes of young bulls the degeneration of potential germ cells during the first three quarters of spermatogenesis was only 4% but in mature bulls it amounted to 19%. The latter losses were distributed as follows: 7% during spermatogonial multiplication, 7% during the first cycle of the seminiferous epithelium in which the primary spermatocytes are in prophase and 5% during the cycle of the seminiferous epithelium containing the two meiotic divisions. There did not appear to be an appreciable loss of spermatids during spermiogenesis.

#### ACKNOWLEDGMENT

The author gratefully acknowledges the assistance of Drs J. O. Almquist and Adam Anthony during the preparation of the manuscript.

#### LITERATURE CITED

- Amann R. W. 1962 Reproductive capacity of dairy bull III. The effect of ejaculation frequency unilateral section and reanastomosis on spermatogenesis. *Am. J. Anat.* 110: 49-63.  
 Clermont, Y. 1954 Cycle de l'épithélium séminal et mode de renouvellement des spermatogonies chez le Hamster. *Rev. Canad. Biol.* 13: 708-15.  
 Clermont, Y. and C. F. Leblond. 1953 Renewal of spermatogonia in the rat. *Am. J. Anat.* 63: 475-502.

- 1959 Differentiation and renewal of spermatogonia in the monkey *Macacus rhesus*. *Ibid.*, 104: 237-274.
- Ebner V von 1871 Untersuchungen über den Bau der Samenkanälchen und die Entwicklung der Spermatozoiden. *Arch. mikr Anat.*, 7: 236. 1888.
- 1898 Zur Spermatogenese bei den Säugthieren. *Arch. mikr Anat.*, 31: 236-292.
- Kramer M. F. 1960 Spermatogenesis bij de stier. Doctor's Thesis, Rijksuniversiteit te Utrecht, Utrecht. (English summary)
- Oakberg, E. F. 1936 A description of spermiogenesis in the mouse and its use in analysis of the cycle of the seminiferous epithelium and germ cell renewal. *Am. J. Anat.*, 99: 391-413.
- Ortavant, R. 1958 Le Cycle spermatogénétique chez le Bâlier D.Sc. Thesis, Univ. of Paris, Paris.
- 1959 Spermatogenesis and Morphology of the Spermatozoen. *Reproduction in Domestic Animals* Vol. II H. H. Cole and P. T. Cupps, ed. Academic Press, New York, Chap. 1.
- Regaud, C. 1901a Etudes sur la structure des tubes séminifères et sur la spermatogénèse chez les mammifères. *Arch. Anat. Microscop.*, 4: 101-153.
- 1901b Etudes sur la structure des tubes séminifères et sur la spermatogénèse chez les mammifères. *Ibid.*, 4: 231-380.
- Rolshoven, E. 1941 Zur Frage des Alterns der generativen Elemente in den Hodenkanälchen. *Anat. Anz.*, 91: 1-8.
- Roosen-Runge, E. C. 1933 Kinetics of spermatogenesis in mammals. *Ann. N. Y. Acad. Sci.*, 55: 574-584.
- 1938 Untersuchungen über die Degeneration Samenbildender Zellen in der Normalen Spermatogenese der Ratte. *Z. Zellforsch.*, 41: 231-233.
- Roosen-Runge E. C., and L. O. Giesel, Jr. 1950 Quantitative studies on spermatogenesis in the albino rat. *Am. J. Anat.*, 67: 1-30.
- Schoenfeld, H. 1900 La Spermatogénèse chez le Taureau. *Biblioth. Anat.*, 8: 74-98.
- 1901 La Spermatogénèse chez le Tureau et chez les mammifères en général. *Arch. Biol. (Liege)* 18: 1-72.

# A Study of the Post Natal Growth and Remodeling of Bone<sup>1</sup>

DONALD H. ENLOW

Department of Anatomy The University of Michigan,  
Ann Arbor Michigan

Skeletal growth involves a variety of modeling processes which result in the rearrangement and recombination of histological components. Compact bone is formed as a composite of structural zones produced by the progressive accumulation of architectural changes. The purpose of this study is (a) to trace the sequence of specific remodeling changes during growth, and (b) to relate remodeling processes with corresponding patterns of microscopic structure.

## History

Plato said that "God formed bone in this way. Sifting earth until it was pure and smooth, he kneaded it and moistened it with marrow then he placed this mass in the fire and next cast it into water and again into the fire and again into water and so changing it from one into the other in turn, he made it of such a kind that it can not be dissolved by anything. Arnobius reported that a goddess is mentioned in ancient writings who hardens and solidifies the bones in young infants. Riolan commented that the ancients invented a certain goddess to care for the bones since the shape of the body depends on the skeleton. Hippocrates said that bones are produced by the burning and drying of fat (in the marrow). Both Aristotle and Galen believed that bone substance represents the "less noble component of seminal residue which is not utilized elsewhere during the formation of the body from the seed. In the book of Ecclesiastes (11:5) it is said that as thou knowest not what is the way of the spirit, nor how the bones do grow in the womb of her that is with child: even so thou knowest not the works of God who maketh all.

Vesalius realized the cartilaginous nature of early fetal bones, and his pupil Fallopius first recognized and described the

epiphyseal plate of cartilage (Portal 1770). Caspar Bartholin (1676) said that bones in the embryo are at first a fluid which is later filled with sinew becomes cartilaginous and then slowly acquires the hardness of bone. During the late 1600's and through the middle of the 1700's standard textbook descriptions of bone growth maintained that a secretion of thin bone juice from the blood congeals first into transparent cartilage which is then transformed into soft bone and which finally becomes hardened by deposits of saline-like nutrients ("succus nutritivus"). This latter element was drawn from the blood either by heat, reduced diameter of vessels by evaporation, or by rotational forces in the blood itself (Havers, 1661; Malpighi, 1743; Cheesden 1733; Monro 1763). An interesting prelude to our modern understanding of bone growth was made as early as 1631 by Adrianus Spigelius. He was apparently the first to suggest that the periosteum itself can produce new bone and that bone increases in mass by a process of apposition. He also noticed the formative difference between skull bones (intramembranous) and long bones (endochondral). This latter observation was to be independently rediscovered at least three times in subsequent history (Neublit, 1736; Meckel 1832, gives credit to Howship; Huxley 1859, gives credit to Sharpey). Grew (1681), Leeuwenhoek (1693) and Malpighi (1743) compared the functional role of the periosteum in bone growth with that of the cambium in bark. Duhamel (1739-43) made the same analogy and he termed the osteogenic component of the periosteum as the cambium layer. Havers did not recognize the osteogenic function of the

Supported by U.S.P.H.S. Grant D-1123.

The foregoing accounts have been taken from translations into the Latin by Aldine (1737).

- 1939 Differentiation and renewal of spermatogonia in the monkey *Macacus rhesus* *Ibid.*, 104 237-274
- Eboer V von 1871 Untersuchungen über den B der Samenkanälchen und die Entwicklung der Spermatozoen. *Arch. mikr. Anat.*, 7 Cited by V von Eboer *Arch. mikr. Anat.*, 31 236. 1888.
- 1888 Zur Spermatogenese bei den Säugethieren. *Arch. mikr. Anat.*, 31 238-292.
- Kramer M. F. 1960 Spermatogenesis bij de stier Doctor's Thesis, Rijksuniversiteit te Utrecht, Utrecht. (English summary)
- Oakberg E. F. 1938 A description of spermatogenesis in the mouse and its use in analysis of the cycle of the seminiferous epithelium and germ cell renewal. *Am. J. Anat.*, 99 391-413.
- Ortavant, R. 1933 Le Cycle spermatogénétique chez le Bœuf D.Sc. Thesis, Uni. of Paris, Paris.
- 1939 Spermatogenesis and Morphology of the Spermatozoon. *Reproduction in Domestic Animals* Vol. II H. H. Cole and F. T. Cupps ed. Academic Press, New York, Chap. 1
- Regaud, C. 1901 Etudes sur la structure des tubes séminifères et sur la spermatogénèse chez les mammifères. *Arch. Anat. Microscop.*, 4 101-153.
- 1901b Etudes sur la structure des tubes séminifères et sur la spermatogénèse chez les mammifères. *Ibid.*, 4 231-340.
- Rolshoven, E. 1941 Zur Frage des Alterns der generativen Elemente in den Hodenkanälchen. *Anat. Anz.*, 91/ 1-8.
- Roosen-Runge E. C. 1953 Kinetics of spermatogenesis in mammals. *Ann. N. Y. Acad. Sci.*, 65: 574-684
- 1955 Untersuchungen über die Degeneration Samenbildender Zellen in der Normalen Spermatogenese der Ratte. *Z. Zellforsch.*, 41 231-235.
- Roosen-Runge, E. C., and L. O. Giesel, J. 1950 Quantitative studies on spermatogenesis in the albino rat. *Am. J. Anat.*, 87 1-30.
- Schoenfeld, H. 1900 La Spermatogenèse chez le Taureau. *Bibliog. Anat.*, 8 74-88.
- 1901 La Spermatogenèse chez le Taureau et chez les mammifères en général. *Arch. Biol. (Liège)* 18 1-72.

preparation and examination of large numbers of samples without the need for embedding and sectioning with a microtome (Enlow '61). In all bone specimens from 108 monkeys and 83 rats were examined. Monkeys were grouped into relative age levels according to dental formulae. Bone tissues in the femur were studied in all of the animals and bone from the tibia, radius, humerus and mandible were examined in many of the individuals. Multiple, semi-serial sections were prepared throughout the length of each bone. Entire longitudinal sections of rat bones were made with the aid of the Gilling-Bronwill apparatus. One-per cent alizarin was administered to some of the white rats to establish reference marks in the growing bone. This procedure was used in order to trace the sequence and specific regional location of tissue changes involved in remodeling. Alizarin markers were also used to confirm the periosteal or endosteal nature of bone deposits.

Specific varieties of basic bone tissues were identified in different representative areas of each bone. The structural and developmental relationships of each bone type were determined. Combinations and progressive recombinations in the arrangement, pattern, and structure of these tissue types were then mapped according to sequential formation and particular regional location.

#### OBSERVATIONS

The developmental and structural interpretations of the observations described below are based on the classic scheme of progressive bone remodeling used by Kolliker (1853) Brash ('34) Weinmann and Sieber ('47) Leblond ('50) and Tomelin ('53). This generalized plan is illustrated in plate 1. Note that the metaphysis is progressively reduced in diameter as the bone increases in length and that metaphyseal bone is relocated in relative position to become part of the diaphysis. This process of metaphyseal remodeling involves resorption of periosteal surfaces in combination with apposition on the endosteal margin.

**Cortical stratification.** In all species examined the compact bone substance of the cortex becomes stratified during growth and remodeling. This stratification is the

result of (1) successive reversals in the direction of outward (periosteal) and inward (endosteal) growth and (2) the formation of various kinds of bone tissues which are associated with different local growth circumstances. Growth reversals are produced by the increase-decrease-increase in diameter involved in metaphyseal to diaphyseal relocation following growth in length (Figs. 1-3). Specific bone tissue types are characteristically located in particular and specific layers. The structural result is a compacta which is composed of conspicuous "zones" each of which can be interpreted in terms of developmental origin and specific location. While the overall shape and surface outlines of the growing bone remain constant the substance of the compact bone itself becomes a structural conglomerate of reorganized growth levels (figs. 14-19-27).

During remodeling and reconstruction pre-existing bone is not entirely removed or destroyed. Some more or less remains. This bone of older generations becomes enclosed or incorporated into the revised form as zones, layers, islands or as a vestige of interstitial bone. Since new osseous deposits can form only on some surface exposure of a bone (endosteal, periosteal, cancellous or the inner surface of a canal) the surface configuration of pre-existing bone determines the minute architectural patterns formed by subsequent deposits. The significance of these concepts to a developmental interpretation of structural arrangement will be seen in the following observations.

#### *Lamellar compaction of coarse cancellous bone*

This structural conversion produces a distinctive and characteristic type of compact bone tissue which is clearly recognizable in routine section preparations. If inward or endosteal growth, during metaphyseal reduction in diameter proceeds into areas already occupied by coarse cancellous bone the compaction of these cancellous trabeculae results in a cortex which is composed of coarse irregular whorls or convolutions of compact bone (figs. 21-26). Or depending on the density and



ized rapid accumulation of new periosteal bone. During fast diametrical growth just following birth stratified layers of primary osteones together with interstitial non-lamellar tissue are formed (figs 24-25). Following later remodeling incomplete zones of this tissue remain in the compacta (fig. 19). In addition this type of bone tissue is often present in processes to which tendons attach (fig. 20) or in any former areas of such attachment which have since been relocated through remodeling shifts. Primary osteones located selectively in tubercles seem to result from the formation of original fine cancellous deposits resulting from disproportionately rapid growth in this area. They are apparently not implicated in a direct cause and effect relationship with stress forces associated with muscle or tendon insertion. This observation is in contradiction to the hypothesis that "osteones" represent a response to tension (Murray '38).

Internal reconstruction within the compacta itself results in the formation of bone tissues which are composed largely of secondary osteones. Secondary Haversian bone is not involved in the bone tissue of many mammalian species including the white rat (Enlow and Brown, '38).

Primary and secondary osteones like any other bone tissue type occur regularly in distinct zones within the compacta. The sequential developmental history of these zones can be traced and interpreted on the basis of preceding descriptions. Primary osteones are found in growing bone of both the rat and monkey but distribution is noticeably sparse in the rat. This can be explained on the basis of comparative differential growth and the relative quantities of bone which are deposited in a given period since the primary osteone is a structural result of larger volumes of bone formation in less time.

*Structural variations in different bones.* The relative proliferative activity of the proximal and distal epiphyseal cartilages is an important factor contributing to architectural arrangement within the cortex of the shaft. Inequalities in growth rate produce a characteristic distribution of endosteal and periosteal bone tissues which is identified with specific bones. The proximal and distal epiphyseal plates of the

tibia are approximately equal in their contribution to the overall length of the whole bone. Periosteal deposition in the tibia, as evidenced by alizarin lines or by the identification of zones and associated tissues, occupies a considerable area extending well toward both epiphyses. In the femur (fig. 8) however the proximal epiphyseal plates are subordinate to the growth activity of the distal plate and they provide linear growth which is restricted largely to the neck and to the greater or lesser trochanters. As a result bone formed by endosteal apposition following proliferation of the distal plate represents the predominant cortical volume in the growing shaft (fig. 9).

The diameter of the femoral neck, following the proliferation of its own epiphyseal plate becomes reduced by periosteal resorption together with endosteal compaction of underlying cancellous bone (fig. 8). Sub-periosteal lamellar apposition appears as the neck grades into the adjacent shaft. The contact zone between this endosteal bone and the periosteal bone of the shaft is evident in microscopic sections.

#### DISCUSSION

The traditional textbook pattern of compact bone tissue structure is a combination of outer and inner circumferential lamellae enclosing a middle core of Haversian bone (fig. 23). This is one example of the multi-layering of zones produced by inward and outward reversals in growth. Such an arrangement is rarely so simple, however. If the formation and structural arrangement of compact bone is considered with respect to the various remodeling agencies including metaphyseal-diaphyseal transition changes in shape zone formation shifts in axis osseous drift the formation and reformation of bony processes and the development of various bone tissue types it is apparent that a considerable variety of structural patterns are likely to be encountered. A mid-diaphyseal transverse section will differ from one prepared near the end of the diaphysis and this in turn differs noticeably in structural arrangement from sections made through the metaphysis and so on up and down levels of the bone (plate 7). Correspondingly the various sections differ with age

with the specific skeletal unit studied and with the particular species considered.

If a transverse section is prepared through the approximate level of 7b in figure 6 three or 4 clearly identifiable zones would be expected. These actual zones are observed in figure 19 a cross section through such an area. The original endochondral trabeculae of the metaphyseal medulla containing spicules of calcified cartilage matrix, can be identified. These trabeculae have been compacted and subsequently were incorporated as a zone within the cortex during inward growth. External to this layer sub-periosteal, fine cancellous non-lamellar bone has been filled with lamellae to form another distinct zone. The results of inward growth by endosteal lamellar apposition, and outward growth by periosteal lamellar deposition following reversal, can both be recognized as inner and outer circumferential zones or layers. The results of drift, following a shift in axis are seen as the zones arch to the periosteal margin (fig. 19) and there become exposed as an active surface of erosion. The middle two zones in figure 19 appear abruptly sheared at the outer cortical margin. Periosteal and endosteal lamellar deposition have followed in the direction of the shift.

In view of the various factors just described it is evident that any section of bone must be interpreted as an individual and local situation which has been produced by the cumulative effects of gross remodeling in that particular region.

**Species variation** Widespread differences exist in the structure of bone between vertebrate groups (Foote, '36; Petersen, '30; Amprino and Godina, '47; Enlow and Brown '36 '37 '38). The basis for many of these structural differences can be resolved by a comparative interpretation of developmental processes. The results of this study suggest that differential rates of growth between different species is an important factor. This was first proposed and supported by Amprino ('47). The rate of deposition determines the volume of bone laid down in a given period of time and this strongly influences the particular type of bone tissue which is to be deposited. The widespread distribution in a skeleton of fine cancellous non-lamellar bone primary Haversian bone or plexiform bone

(Enlow and Brown, '38) represents a developmental response to relatively rapid skeletal growth or to the production of large quantities of bone tissue in a short period of time as in bovines larger carnivores, and proboscideans. Relatively slow skeletal growth on the other hand results in the formation of typical circumferential lamellar bone either with or without the inclusion of primary non-Haversian canals. Certain vertebrate groups including most reptiles have this particular bone variety as a predominant and characteristic component of structure. A great many forms possess bone types which are associated with more rapid accretion, but subsequent to periods of active skeletal growth other bone tissue varieties characteristic of slower growth are produced. This may be either a local or a widespread situation in any individual bone. Mixed combinations of bone tissue types thus, are frequently present. Related to differential rate of growth is the life span of the form and the size, specific shape, and the proportions of individual bones considered. These factors determine the regional distribution of various tissue types and represent individual structural results produced by remodeling processes. Marked differences are found for example in the bone structure between the laboratory rat and human or monkey bones. This can be explained on the basis of the endosteal and periosteal distribution of bone which determines the nature and orientation of component structures and which is in direct relation to differences in growth rate and size of the forms. Small rodents as well as other mammals of similar size and with a similar rate of skeletal growth, possess mid-diaphyseal bone which has a predictable "radial" orientation of vascular canals in the compacta (Enlow and Brown, '38). Since much of the cortex in the mid-diaphysis of a rat long bone is composed of endosteal, circumferential lamellar bone (fig. 9) the radial arrangement of Volkmann canals is explicable (see previous descriptions of endosteal lamellar bone). In mammalian forms of larger body size however the progressively increased diameter of the diaphyseal cortex following reversals of growth results in the addition of relatively greater amounts of periosteal bone with a proportionate removal of endosteal bone

The distribution of endosteal radial canals while present, is thus minimal except in local areas where the diameter of the shaft is undergoing active reduction during gross remodeling.

### *Generalized sequence of growth*

Based on the structural observations previously described and discussed the traditional plan of superimposed growth stages (figs 1 ■ 3) has been expanded (figs. 4 5 6). The purpose of this more detailed scheme is to illustrate the developmental sequence in (a) the regional formation of cortical zones (b) the formation and arrangement of different tissue types, and (c) the progressive rearrangement and relocation of structural components during remodeling processes.

*Stage one (fig 4).* Specific areas and zones are identified by code numbers

Alizarin deposits are scattered beneath the epiphyseal plate from 10a to 11a and from 10b to 11b as linear growth proceeds by endochondral ossification. Metaphyseal diameter has increased from 9b to 11b by the sub-periosteal apposition of fine cancellous non-lamellar bone tissue forming an intramembranous sheath of bone around the endochondral medulla (fig. 15). Note that the diameter of the metaphysis in this same region on opposite side (10a to 11a) has undergone reduction. A sheath of sub-periosteal bone is not present, and the endochondral trabeculae have been abruptly and directly invaded by inward resorption (fig. 16). This arrangement in an actual bone section is seen in figure 11. Metaphyseal reduction in diameter by periosteal resorption has also occurred from 3a to 11a and from 3b to 9b. Compaction of coarse cancellous bone during inward growth is seen from 6a to 11a and from 6b to 9b. With continued elongation of the entire bone following epiphyseal activity this area will become partially interred between more recently formed endosteal and periosteal layers produced by subsequent inward and outward reversals (see Stages two and three). Endosteal deposition of internal circumferential lamellae during metaphyseal reduction is seen from 3a to 6a and from 2b to 6b. Cancellous compaction is not involved in these areas. The diameter of the mid-diaphysis has increased by sub-periosteal growth from 1a to 3a and from

1b to 2b following outward reversal in direction of growth. This periosteal bone tissue may be in the form of circumferential lamellae (figs. 22 23) or fine cancellous non-lamellar bone (fig. 24) depending on relative rates of growth. Deposits of fine cancellous bone when formed received subsequent lamellar compaction.

*Stage two (fig 5).* Cancellous bone in the metaphysis has been omitted for clarity of illustration but the arrangement in this region would be a repetition of Stage one. Areas of bone remaining from Stage one (solid black) are embedded within the new bone of this generation and the distribution of alizarin lines partially describe the contours of the old bone.

Increase in diameter by sub-periosteal deposition of fine cancellous non-lamellar bone has occurred from 14b to the end of the metaphysis. Periosteal resorption during metaphyseal reduction, following inward reversal in direction of growth can be seen from 4b to 13b and 6a to 15a. Compact bone produced by cancellous compaction during endosteal growth is present from 7a to 11a and from 6b to 11b. Irregular contours of old alizarin lines are seen. This zone represents levels 6a to 10a and 6b to 10b in Stage one following compaction and relocation. Endosteal deposition of circumferential lamellae during reduction in diameter has occurred from 5a to 7a and from 3b to 7b and endosteal growth by the compaction of cancellous trabeculae has proceeded from 11a to 15a and from 11b to 14b. Increase in diameter by the sub-periosteal apposition of either circumferential lamellar or fine cancellous non-lamellar bone is seen from 1a to 6a and from 1b to 4b. The eroded surfaces of Stage one are present on the outer margin of the bone from 6a to 11a and from 4b to 11b. In this region the external surfaces are composed of older bone which was originally endosteal in its formation and which was located on the inner surface. This bone tissue has been relocated from the inner to the outer side where it now occupies a resorptive surface during metaphyseal reduction in diameter.

*Stage three (fig 6).* The old contours of Stage one (black) and Stage two (lined) can be observed within the present growth stage (stippled). Deeply enclosed alizarin lines formed during Stage one are still ap-

parent. Note that the contours of the bone as a whole are maintained as symmetrical, even surfaces although the substance of the compact bone itself is a composite of irregular zones. Periosteal resorption has taken place from 7b to 18b and from 7a to 20a. Endosteal deposition by cancellous compaction (in the metaphysis) or by the apposition of inner circumferential lamellae (toward the diaphysis) has proceeded from 5a to 20a and from 4b to 18b. Earlier zones of compacted cancellous bone from 7a to 12a and from 6b to 10b are now partially or completely enclosed by subsequently formed zones of other tissue types produced during growth reversals. Outward sub-periosteal deposition has taken place from 1a to 7a and from 1b to 7b. The inner surface of the mid-diaphysis now undergoes resorption (not shown in diagram) as the diameter of the shaft increases.

#### SUMMARY AND CONCLUSIONS

The cortex is composed of stratified compact bone. Each stratum represents a distinct growth zone and the composite of zones represents the cumulative result of various remodeling processes outlined below.

Repeated endosteal and periosteal reversals in direction of lateral growth contribute to the formation and stratification of cortical zones. Growth reversals follow the increase-decrease-increase of diameter involved in metaphyseal to diaphyseal relocation of compact bone during linear growth.

Regional progressive changes in sectional shape involved in metaphyseal-diaphyseal relocation are produced by a process termed osseous drift.

Zone formation involves a variety of basic osseous tissues. Specific bone tissue types are characteristically associated with particular zones.

Fine cancellous non-lamellar bone tissue is widely distributed in the neo-natal cortex. In post natal long bones this bone type has been observed to develop largely by sub-periosteal rather than by sub-endosteal apposition. Compacted fine cancellous bone occupies distinct zones in the cortex following the formation of other zones and tissue types during subsequent growth reversals.

Since the contour of existing bone surfaces at any stage of developmental reorganization determines the architecture and configuration of subsequent bone deposits inward growth by endosteal deposition produces several distinctive bone tissue varieties. Cortical bone resulting from the lamellar compaction of fine cancellous endochondral trabeculae is identifiable by the presence of calcified cartilage spicules. Endosteal growth into areas occupied by coarse cancellous trabeculae produces whorls of irregular compacted cancellous bone. This is a common tissue type in the proximal and distal thirds of the shaft. Inward endosteal growth uncomplicated by the presence of cancellous bone results in the formation of inner circumferential lamellae. These various tissue types are routinely seen as distinct zones in the compacts following growth reversals. Different tissue types represent a response not only to local direction of growth but also to differential rate of local growth.

Marked variation exists in the structure of bone between different ages, different bones and between different sections at various levels of the same bone. These structural variations can be explained on the basis of regional developmental and remodeling processes.

Species variations in the microscopic structure of bone can be largely explained by a comparative interpretation of the specific growth processes described in this study.

#### ACKNOWLEDGMENTS

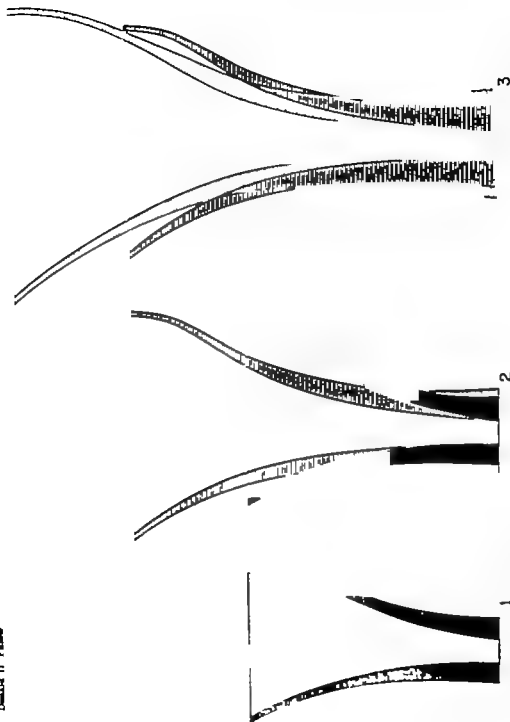
The author is indebted to Miss Harriet Jameson, Rare Book Librarian at the University of Michigan, for her assistance in the translation of difficult passages from early Latin works.

Large numbers of healthy normal embalmed specimens of young growing monkeys were made available through the courtesy of Dr. Paul Ayres Parke Davis and Co., Rochester, Michigan. Rare bone materials from older monkeys of known age were provided by Dr. G. van Wageningen, Department of Obstetrics and Gynecology, Yale University. Bones from neo-natal Rhesus monkeys were provided by Dr. William F. Windle, Director, National Institute of Neurological Diseases and Blindness, National Institute of Health. Numerous bone specimens were made available by

Dr James Gavin, Medical College of South Carolina. Rats were provided by the Upjohn Co.

## LITERATURE CITED

- Albinus, B. S. 1737 *Accademicorum anastomosis*. 7 45-49.
- Amprino R. 1947 La structure d'osseux envisagée comme expression de différences dans la vitesse de l'accroissement. *Arch. de Biol. LVIII*, 4 315-330.
- Amprino R., and A. Bistrati 1936 Processi di ricostruzione di riassorbimenti nella sostanza compatta della ossa dell'uomo. *Zachr Zellforsch.* 24 439-511.
- Amprino, R., and G. Godina 1947 La struttura delle ossa nei vertebrati. *Comment. Pont. Acad. Sci.*, 11 329-467.
- Bartholin C. 1676 *Diaphragmatis structure nova*. *Acta med. et phil.*, Hafn., 4 14-16.
- Beichert J. 1736 An account of the bones of animals being changed to red colour by all ment only. *Phil. Trans.*, 34 287-289.
- Brash, J. C. 1934 Some problems in the growth and developmental mechanics of bone. *Edinb. Med. J.* 41 305-318 363-367.
- Brulle and H. guery 1845 Experiences sur le développement des os mammifères et les osseux. *Ann. des Sci. Nat.*, IV 283-357.
- Cbeselden, W. 1733 *Orthographie*. London.
- Dubamel H. L. 1739 Sur une racine qui a la faculté de teindre en rouge les os des animaux vivants. *Mém. Acad. R. Sci. Paris*, 1-13.
- 1742 Sur le développement et la croissance des os des animaux. *Mém. de l'Acad. Roy des Sci.*
- 1743 Cinquième mémoire sur les os. *Ibid.*
- Enlow D. H. 1954 A plastic-seal method for reuniting sections of ground bone. *Stain Tech.*, 29 21-22.
- 1961 Preparation of decalcified and stained section of bone by thin-section grinding. *Ibid.* July 36 4 250-251.
- 1961 Sequence of microscopic structural changes involved in the gross remodeling of bone. *Abstract, Anat. Rec.*, 139 226.
- Enlow D. H., and E. O. Brown 1956 A comparative histological study of fossil and recent bone tissues. Part I. *Tex. J. Sci.*, VII, No. 4 405-443.
- 1957 A comparative histological study of fossil and recent bone tissues. Part II. *Ibid.*, IX, No. 2 185-214.
- 1958 A comparative histological study of fossil and recent bone tissues. Part III. *Ibid.*, X, No. 2 187-230.
- Flourens M. 1845 Experiences sur la resorption et la reproduction successive des têtes des os. *Ann. d. Sci. N. L.*, IV 358-363.
- Foots J. S. 1916 A contribution to the comparative histology of the femur. *Smithsonian Contr.* XXXV 3.
- Frost, H. M. 1960 Observations on fibrous and lamellar bone. *Henry Ford Hosp. Med. Bull.* 8 199-207.
- Grew N. 1681 *Natural and artificial rarities*. London, G.
- Hales, S. 1727 *Vegetable statics*.
- Haller A. V. 1786 *Elements physiologiae corporis humani*.
- Flavers, C. 1691 *Osteologia nova*. London.
- Hoyle D. A. N. 1960 Alizarin as an indicator of bone growth. *J. of Anat.*, 94 432-440.
- Hunter J. 1796 Experiments and observations on the growth of bones. *Hunter's works*. Palmer's Ed. 1837 p 315.
- Huxley T. 1853 Edited translation of *Manual of Human Histology* by A. Kölliker.
- Kölliker A. 1853 *Manual of human histology*. Trans. by George Bush and Thomas Huxley. London J. 363.
- Lacroix, P. 1845 Remarques sur le mécanisme de l'allongement des os. *Arch. de Biol.* 16: 185-197.
- Leblond, C. P. & W. Wilkinson, L. F. Branger and J. Robichon 1950 Radio-autographic visualization of bone formation in the rat. *Am. J. Anat.*, 60 289-341.
- Leuwenhoek, A. 1693 Observations on the texture of the bones of animals compared with that of wood. *Phil. Trans. Roy Soc. London*, 17 561-562.
- Lemnius 1567 *De miraculis occultis naturae*. Colonia.
- Loven, C. 1863 *Studier och undersökningar öfver Benväfaden, förhållningst med afseende på dess utveckling*. Stockholm.
- Malpighi, M. 1743 *De ossium structura*. Ex. Op. Posth., Venice.
- Meckel, J. F. 1833 *Manual of anatomy*. Translated by Jourdan and Brauchet, Philadelphia, 1 200.
- Mizakides 1866 *Memorabilia utilium et iocundorum centurie*. Lotisiae.
- Monro, A. 1763 *The anatomy of the human bones*. Edinburgh.
- Murray P. D. F. 1936 *Bones*. Cambridge University Press. P 167-171.
- Neubitt, R. 1736 *Human osteogeny*. London.
- Orban B. J. 1957 *Oral histology and embryology*. C. V. Mosby Co. p. 206-216.
- Payton, C. G. 1931 The growth in length of the long bones in the madder fed pig. *J. Anat.* 66 414-425.
- Petersen, H. 1930 *Die Organe des Skeletsystems*. H. ndbuch der Mikroskopischen Anatomie des Menschen. V. Moellendorf Berlin p. 521-670.
- Portal, A. 1770 *Histoire de l'anatomie et de la chirurgie*. Paris. W. F. Didot le jeune 53.
- Pritchard J. J. 1956 *General anatomy and histology of bone*. Biochemical and Physiology of Bone ed. by G. H. Bourne. Acad. Press N. Y. p. 1-23.
- Schäffer Josef 1888 *Die Verknöcherung des Uterklefers und die Metaplasiefrage*. *Arch. Mik. Anat.*, 32 300.
- Spigelius, A. 1631 *De formato foetus*. Opus posthumum p. 61.
- Smith J. W. 1961 Cell and fibre patterns in mammalian bone. *J. of Anat.* 94 329-344.
- Tomelin D. H. K. M. Henry and S. K. Koon 1953 Autoradiographic study of growth and calcium metabolism in the long bones of the rat. *Brit. J. N. tit.*, 7 235-251.
- Weinmann J. P. and H. Eicher 1953 *Bone and bones*. 2nd Ed. C. V. Mosby Co.



1-3 Successive growth stages of schematic long bone. Stage one is superimposed over two, and Stage two is then superimposed over three. This plan is used in plate 2 in order to map the detailed distribution of zones, areas, and tissue types resulting from progressive remodeling changes.

## PLATE 2

### EXPLANATION OF FIGURES

- 4 *Stage One* represented in black. Remnants of this growth level, following subsequent remodeling can be traced in figures 5 and 6. Alizarin markers are indicated by red lines. Detailed explanation in text.
- 5 *Stage Two*, represented by horizontal-lined pattern. Metaphyseal cancellous bone, as found in *Stage one*, is omitted for simplicity of illustration. The alizarin markers of *Stage one* have been enclosed by subsequent endosteal or periosteal deposits. Detailed explanation in text.
- 6 *Stage Three* represented by a stippled-pattern. Endosteal and periosteal deposition has enclosed vestiges of *Stages two* and *three* following remodeling. Detailed explanation in text.

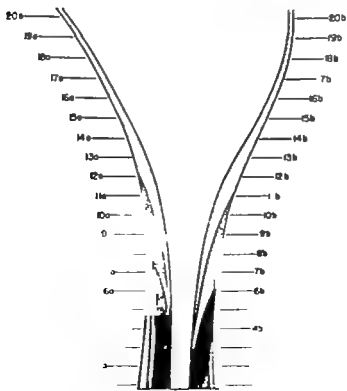
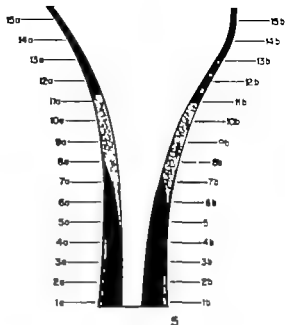
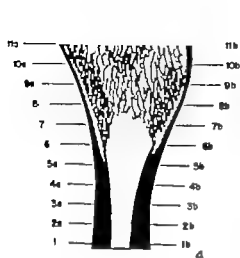
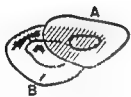




### PLATE 3

#### EXPLANATION OF FIGURES

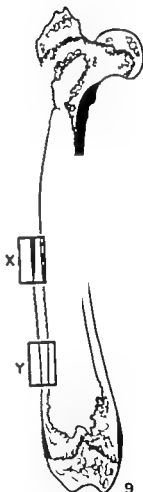
- 7 A lateral shift in axis during metaphyseal-diaphyseal transition is involved in changes of shape and size, as well as in the curvature formation of the bone. This process is termed osseous drift. The structural results of lateral drift, as level A is superimposed over level B can be seen in figure 12.
- 8 Longitudinal section of growing post-natal rat femur. Alizarin markers are indicated by black lines. Cancellous composition, recognizable by the convoluted nature of the tissue can be seen in the distal metaphysis and in the neck. Extensive endosteal growth, as indicated by alizarin markers, has formed in the distal half of the bone. Subperiosteal deposition has occurred in the proximal "basin" of the shaft adjacent to the neck.
- 9 Periosteal bone is represented by solid black and endosteal bone is white. Note the widespread distribution of the growing rat femur of endosteal bone. Enlargement of areas X and Y are found in plate 4 figures 13 and 14.



7



8



9

## PLATE 4

### EXPLANATION OF FIGURES

- 10 Longitudinal section of a growing rat femur.  $\times 3$ . The information presented in figures 8 and 9 and the enlargements in figures 13 and 14 were made from this section.
- 11 Longitudinal section of a growing rat tibia.  $\times 1.5$ . Compare opposite sides of the proximal metaphysis. One side (B) shows sub-periosteal apposition adjacent to the epiphyseal plate while the other side (A) has received immediate reduction by process of periosteal resorption in combination with endosteal deposition. See figures 15 and 16 below for comparable sections under higher magnification.
- 12 This transverse section of growing monkey humerus illustrates the structural result of osseous drift. Periosteal lamellar apposition (A) is combined with endosteal resorption (B) on one of the sections, and endosteal lamellar apposition (C) and periosteal resorption (D) is seen on the opposite side. Drift has proceeded in a direction toward the top of the illustration. This common situation is found in routine bone sections of all species and at all age levels.  $\times 6$ .
- 13 Enlarged transverse section of Area Y figure 9.  $\times 60$ . This area of compact bone is composed entirely of endosteal bone tissue. Growth has proceeded from left to right by process of endosteal apposition and periosteal resorption. The metaphysis is undergoing reduction in diameter. Note the characteristic perpendicular arrangement of canals in this endosteal bone. Compare this pattern with the periosteal canals seen in figure 22.
- 14 Enlarged transverse section of Area X, figure 9.  $\times 60$ . The arrow indicates the contact between endosteal bone toward the right, and periosteal bone on the left. The middle zone is composed of endosteal bone which was formerly located in the metaphysis. Three zones are thus seen representing the structural product of growth reversals involved in metaphyseal to diaphyseal remodeling.
- 15 Longitudinal section of developing human long bone adjacent to the epiphyseal plate.  $\times 30$ . Note the increase in diameter by sub-periosteal apposition of non-lamellar bone in the area indicated by the arrow. Compare with level 10b, figure 4.
- 16 This is the opposite side of the same section seen in figure 15.  $\times 30$ . Here the diameter of the bone is undergoing reduction (arrow) by the periosteal invasion of recently formed endochondral trabeculae. Note the total absence of sub-periosteal bone. Compare with area 10a figure 4. Although the epiphysis and immediately adjacent metaphyseal area are increasing in diameter the metaphysis itself is being reduced in dimension in direction toward the diaphysis. Progressive endosteal growth will later result in cortical compact bone which embodies remnant of older endochondral trabeculae. Such remnant following repeated growth reversals, can be seen in figure 19.

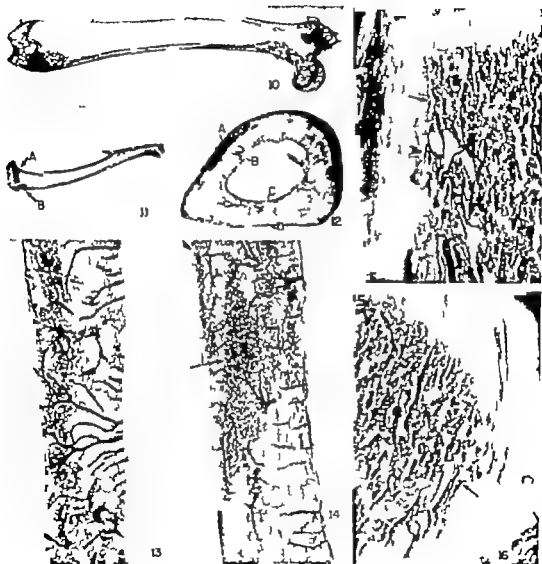


## PLATE 5

### EXPLANATION OF FIGURES

- 17 Endosteal lamellar growth in the long bone of post-natal rodent (*Cavia*)  $\times 100$ . A cancellous trabecula (arrow) is being progressively enclosed within the cortex during inward growth. Such pattern is frequently observed in compact bone located in or near the metaphysis.
- 18 Non-lamellar fine cancellous bone in the mid-diaphysis of neo-natal rat tibia.  $\times 60$ . Subsequent compaction of this bone together with the formation of additional layers following reversals in direction of growth will produce stratified cortex composed of distinctive zones as illustrated in figure 19.
- 19 Transverse section of growing post-natal rat femur through level represented by 7b, figure 6.  $\times 60$ . Four zones are evident. Sub-periosteal lamellar deposition (A) is seen on the outer margin of the bone at the top of the illustration. Beneath this circumferential yet is zone (B) of compacted, fine cancellous bone composed of primary osteons with non-lamellar interstitial tissue. This specific zone is structural derivative of the bone tissue type either neo-natal or post-natal, seen in figure 18 (above) or in figure 20. A zone of compacted endochondral bone (C) is present in the mid-compacta. Vertices of calcified cartilage spicules have been retained. This is result of endosteal growth into an re of older metaphyseal fine-cancellous trabeculae produced by the epiphyseal plate. A layer of circumferential lamellae (D) following continued endosteal growth found on the inner margin. The results of osseous drift are evidenced by the eccentric orientation of the partially removed component zones.
- 20 Transverse mid-diaphyseal section through the femur of young, growing rat.  $\times 50$ . Observe the formation of fine-cancellous non-lamellar bone by sub-periosteal deposition (B). Lamellar filling of the enclosed primary spaces will later produce primary osteons separated by non-lamellar interstitial bone seen in figure 19 B. The characteristic occurrence of primary osteons in bony processes is frequent observation. Note the presence of chondroid tissue (A) at the apex of the enlarging process.



## PLATE 5

### EXPLANATION OF FIGURES

- 17 Endosteal lamellar growth in the long bone of post-natal rodent (*Cavia*)  $\times 100$ . A cancellous trabecula (arrow) is being progressively enclosed within the cortex during inward growth. Such pattern is frequently observed in compact bone located in or near the metaphysis.
- 18 Non-lamellar fine cancellous bone in the mid-diaphysis of a neo-natal rat tibia.  $\times 60$ . Subsequent compaction of this bone together with the formation of additional layers following reversals in direction of growth, will produce stratified cortex composed of distinctive zones, as illustrated in figure 19.
- 19 Transverse section of growing post-natal rat femur through level represented by "b" figure 6  $\times 60$ . Four zones are evident. Sub-periosteal lamellar deposition (A) is seen on the outer margin of the bone at the top of the illustration. Beneath this circumferential layer is zone (B) of compacted, fine cancellous bone composed of primary osteones with non-lamellar interstitial tissue. This specific zone is structural derivative of the bone tissue type (fiber neo-natal or post-natal, seen in figure 18 (above) or in figure 20. A zone of compacted endochondral bone (C) is present in the mid-compacta. Vestiges of calcified cartilage spicules have been retained. This is a result of endosteal growth in an area of older metaphyseal fine-cancellous trabeculae produced by the epiphyseal plate. A layer of circumferential lamellae (D) following continued endosteal growth, is found on the inner margin. The results of osseous drift are evidenced by the eccentric orientation of the partially removed component zones.
- 20 Transverse mid-diaphyseal section through the femur of young growing rat.  $\times 50$ . Observe the formation of fine-cancellous, non-lamellar bone by sub-periosteal deposition (B). Lamellar filling of the enclosed primary spaces will later produce primary osteones separated by non-lamellar interstitial bone as seen in figure 19. The characteristic occurrence of primary osteones in bony processes is frequent observation. Note the presence of bondroid tissue (A) at the apex of the enlarging process.

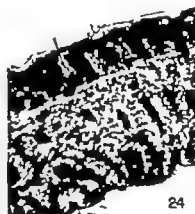
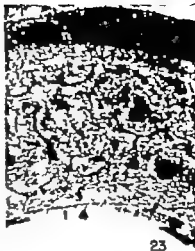
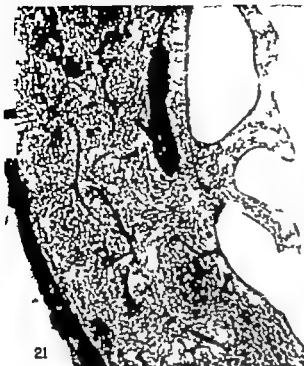
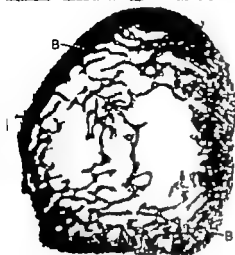




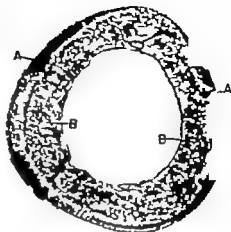
## PLATE 7

### EXPLANATION OF FIGURES

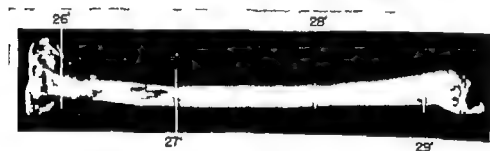
- 26 Tibia, Rhesus monkey  $\times 11.5$ . The cortex is composed entirely of compacted coarse cancellous bone (B) produced by endosteal deposition during reduction in diameter.
- 27 A layer of circumferential lamellae produced by outward growth (A) encloses zone of compacted coarse cancellous bone (B) produced during endosteal growth. An inner zone of endosteal circumferential lamellae (C) has formed in an area lacking cancellous trabeculae. Note that the bone has "drifted" laterally to the right.
- 28 Periosteal circumferential bone (A) encloses an inner zone of endosteal bone produced by compaction of coarse cancellous trabeculae. Note the irregular orientation of canals and the "whorled" arrangement of lamellae in the endosteal bone.
- 29 Cortical bone composed entirely of endosteal compacted coarse cancellous bone.



26

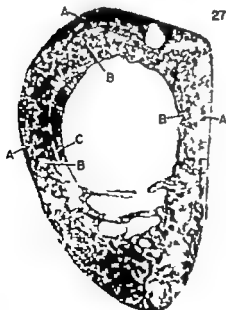


28



27

29



27



29



# Histochemical Classification of Individual Skeletal Muscle Fibers of the Rat<sup>1</sup>

JOHN M. STEIN<sup>2,3</sup> AND HELEN A. PADYKULA

Department of Anatomy Harvard Medical School, Boston, Massachusetts

The striking differences among the fiber types which compose vertebrate skeletal muscles are receiving increasing recognition. Recent electron microscopic studies have revealed differences between red and white muscles with regard to the amount and distribution of mitochondria and sarcoplasmic reticulum (Bennett and Porter '53; Porter and Palade, '57; Peachey and Porter '59; Bennett, '60; Huxley and Hanson, '60). Some biochemical comparisons also indicate muscular heterogeneity (Lawrie '52; Paul and Sperling, '52; Stentz Gjorgyi, '53; Tomzetic and Kure '60; Hazzard and Leonard, '61) and physiological measurements confirm this and suggest that differentiation of muscles into pale fast ones and red, slow ones is under neural control (Kuffler '53; Buller et al. '60a and b). The marked heterogeneity of the fibers that compose vertebrate skeletal muscles is demonstrated most readily by the histochemical approach which permits characterization of individual fibers (Semenoff, '35; Padykula, '52; Wachstein and Meisel '55; George et al. '57-'58-'59; Nachmias and Padykula '58; Dubowitz and Pearce '60; Drews and Engel '61). Recent histochemical evidence suggests that in mammalian muscles there are more fiber types than merely red and white.

In an effort to define this heterogeneity more precisely a histochemical classification of individual skeletal muscle fibers of the rat gastrocnemius and soleus was undertaken. Histochemical methods for the demonstration of glycogen and the enzymes, succinic dehydrogenase, adenosine triphosphatase and non-specific esterase were used to examine several aspects of this heterogeneity in these two muscles of the hind limb. With several histochemical methods serial sections were used so that individual muscle fibers could be compared

in the various preparations. Three fiber types (types A, B and C) were defined on the basis of the cytochemical distribution of succinic dehydrogenase activity in the rat gastrocnemius. From serial sections, the other histochemical properties were collated to prepare a "histochemical profile" for each of the three fiber types.

In the medial head of the gastrocnemius an inverse general relationship between succinic dehydrogenase activity and glycogen content is described. An attempt was made to correlate the quantity of glycogen present in an individual fiber with its enzymatic activities. Three fiber types occur in the medial head of the gastrocnemius but the rat soleus has only two (types B and C). The evidence suggests that the type A fiber represents the classical "white" fiber whereas types B and C fibers represent two types of "red" fibers.

## MATERIALS AND METHODS

### A. Preparation of muscle sections

Muscles were obtained from 46 male and female albino rats weighing between 175 and 200 gm. Preanesthetic medication was pentobarbital 3 mg and atropine 15 mg per 100 gm body weight. Ether anesthesia was used, and the sciatic nerve was infiltrated with procaine in the popliteal space to prevent agonial twitching of the gastrocnemius. The skin was stripped from thigh to foot and the gastrocnemius, plantaris and soleus were undetermined and separated from the rest of the leg with a piece of aluminum foil, leaving the origins and insertions of the muscles attached to the limb. The neurovascular supply to the

<sup>1</sup>Supported by U.S.P.H.S. Grant R12-2236 (C7).  
<sup>2</sup>Jeffrey Wyman Scholar 1958-60.

<sup>3</sup>Present address: New York Hospital, N. Y. 100  
N. Y. London Research Fellow of the U. S. Public Health Service

muscles was isolated and left intact until the limb was detached from the animal at mid femoral level. The detached leg was quickly fastened to a dowel with both knee and ankle joints in a neutral position half way between extension and flexion. The entire limb was then immediately immersed in a bath of 95% ethanol and solid carbon dioxide ( $-75^{\circ}\text{C}$ ) for 10 to 15 minutes. Upon removal from the bath, the specimen was rapidly wiped dry and placed into a cryostat at  $-15^{\circ}\text{C}$ . There the origins and insertions of the gastrocnemius soleus and plantaris were severed and the isolated muscles were stored in a deep freeze at  $-25^{\circ}\text{C}$  for not more than one week.

Serial cross sections (10  $\mu$ ) were cut in the cryostat at  $-15^{\circ}\text{C}$ . Red muscle fibers were generally better preserved in these sections than white. All sections were rapidly thawed by placing a warm finger under the slide.

#### B Histochemical and staining methods

Sections to be used for the succinic dehydrogenase (SDH) reaction were then dried at room temperature in front of an electric fan for two minutes and immediately placed into an incubating medium at  $33-35^{\circ}\text{C}$ . Earlier incubations had been carried out at  $36-38^{\circ}\text{C}$  but at this temperature large needle-like crystals of diformazan resulted which were avoided at the lower temperature. Except for the variation in temperature the method for demonstration of SDH followed that of Nachlas et al. (37).

Sections destined for all other reactions (i.e. for adenosine triphosphatase esterase periodic acid Schiff and hematoxylin and eosin) were mounted on clean glass slides thawed rapidly and air dried for 30 minutes under an electric fan. They were placed in boxes and stored in a refrigerator at about  $10^{\circ}\text{C}$  until the reactions were carried out. The maximum storage was 10 days and no loss of intensity of reactions was noted during that interval.

Two types of adenosine triphosphatase reactions were performed using "fixed" and "unfixed" section. Chemical fixation was accomplished by immersion in Novikoff's (38) formal-calcium solution for 15 min-

utes at  $10^{\circ}\text{C}$ . Fixed sections were washed in two rinses of distilled water and incubated for one hour in the medium described by Padykula and Herman (35a and b). Unfixed sections were immersed directly in the medium and incubated for only 10 minutes.

Pearse's alpha-naphthyl acetate method was used for demonstration of esterase activity (Pearse '60). Sections were fixed in 10% buffered formalin and washed in distilled water before incubation. Incubation was carried out at room temperature for 20 minutes. The sections were then washed in distilled water and mounted in glycerogel.

Sections to be used for the demonstration of glycogen were fixed for 10 minutes in Rossman's fluid at  $5-10^{\circ}\text{C}$ . They were then hydrated through 100% 95% and 50% ethanol and brought to distilled water. Controls were digested with 0.5% malt diastase in a 0.1 M phosphate buffer at pH 6.8. Both controls and test sections were then subjected to the McManus periodic acid-Schiff (PAS) technique (Pearse '60).

Dried cryostat sections were also stained with hematoxylin and eosin. They were fixed in cold ( $5-10^{\circ}\text{C}$ ) Rossman's fluid for 10 minutes and hydrated through ethanol to distilled water. Sections were stained for two minutes in freshly filtered Harris hematoxylin in routine fashion. They were then transferred to 95% ethanol and subsequently to an alcoholic eosin solution for about two minutes. Three rinses of 100% ethanol followed and the total time in this bath did not exceed two minutes. It was found that the eosin did not stain the sections properly unless (1) the correct fixative was used (2) staining in eosin continued for two or three minutes and (3) the total time in 100% ethanol did not exceed two minutes. Serra's fluid or 10% buffered formalin prevented the development of adequate eosinophilia. Sections were cleared and mounted in the routine manner.

The abbreviations used in this paper are: ATPase adenosine triphosphatase; DPN diphosphopyridine nucleotide; H&E, hematoxylin and eosin; PAS, periodic acid Schiff; SDH, succinic dehydrogenase.

### C. Evaluation of sections

Comparison was made by photomicrography of corresponding fields from sets of 6 serial cross sections.

A standard field was chosen for study. This field was located in the medial head of the gastrocnemius in a cross section  $\frac{1}{4}$  cm from its origin. The field was selected because it contained a sample of fibers that varied in size as well as in intensity of reaction in all histochemical preparations. It was easily identified by the consistent presence of a muscle spindle in the region (fig 1).

The homogeneity of muscle fiber staining in the H&E preparation allowed selection of individual fibers without regard to the histochemical properties of the selected fibers. The specific fibers to be studied were designated by numbering them on the photomicrograph of the H&E preparation. The numbered muscle fibers were then correspondingly numbered on the photomicrographs of the histochemical sections.

The intensity of reaction was then graded by eye by two investigators independently in the photographs of the unfixed ATPase, fixed ATPase, PAS, and esterase reactions. The SDH sections were classified by the cytological distribution of the diformazan at oil immersion magnification rather than by intensity of reaction.

Since sharp boundaries of individual fibers are discernible in the H&E preparation, these were used for determination of the cross-sectional areas of fibers by use of a Keuffel and Esser Compensation Planimeter. The average of two readings was used for each fiber.

### D. Summary of methods

Fresh frozen serial cross sections of rat gastrocnemius were made. These were stained with H&E and reacted for SDH, fixed ATPase, unfixed ATPase, non-specific esterase, and glycogen. A region of the medial head of the gastrocnemius near a constant spindle fiber that could be used as a landmark was selected for fiber-to-fiber analysis. The method for classifying individual muscle fibers was outlined, and

the cross-sectional area of each fiber was determined.

## RESULTS

### A. The degree of succinic dehydrogenase activity in relation to the glycogen content of muscle fibers

At low magnification, comparison of succinic dehydrogenase activity and glycogen content in serial sections of the medial head of the rat gastrocnemius suggests that regions highest in glycogen content are low in succinic dehydrogenase activity (figs. 1 and 2). The superficial portion of the medial head is high in succinic dehydrogenase activity whereas the deeper parts are of low activity (inset fig. 1). Although the area of high enzymatic activity is red to the eye in fresh and frozen cross-section and the less active zone is white, each of these two general regions is actually heterogeneous in terms of the activities of individual fibers. A neighboring section shown in figure 2, indicates the distribution of glycogen in the medial head. The superficial region, which is composed principally of fibers of high succinic dehydrogenase activity, is very heterogeneous in terms of the glycogen content of the fibers. Also many fibers in this region lack glycogen. Conversely the region composed principally of fibers of low succinic dehydrogenase activity is high in glycogen content and lacks glycogen-free fibers. George and Naik ('67 '68 '69) have reported a similar complementary relationship in flight muscles of birds and bats.

### B. Three types of distribution patterns of succinic dehydrogenase (SDH) activity

To explore the above relationship further, fiber-to-fiber comparisons in the medial head of the rat gastrocnemius are presented here. Under high power the relative succinic dehydrogenase activity of the fibers cannot be established by the amount of diformazan deposition alone because three different patterns of diformazan distribution are seen in cross-sections of muscle fibers. These three patterns of succinic dehydrogenase activity are demonstrated in figure 3 and most likely reflect the number and distribution of mitochondria.

dria in various parts of the sarcoplasm. The possibility that the differences in pattern merely reflect differences in plane of section has been considered. It is thought, however, to be an unlikely explanation in view of the distinct "histochemical profile" which will be presented below for each type of pattern. Since the length of mammalian sarcomeres is 2-3  $\mu$  (Huxley and Hanson '60) it is also unlikely that obtaining cross sections through different parts of the sarcomere accounts for the general pattern differences. Furthermore when a section from both the beginning and the end of a series of 13 serial 10  $\mu$  sections are reacted for succinic dehydrogenase activity both sections show individual fibers to remain constant in the pattern of diformazan distribution.

The three fiber types in SDH reaction are depicted in figure 3 at oil immersion magnification. The type A fiber which is presumed to be the classical white or light fiber is characterized by

1. A network of small diformazan particles which vary in size but are similar in size to those seen in the B type fiber and are consistently smaller in size than those which distinguish the type C fiber.

2. Particles arranged in an open network suggesting a relative sparsity of mitochondria and a high concentration of myofibrillar material. Particles form long streaks which are frequently parallel to one another but in places the streaks meet at angles with a somewhat larger particle forming the center of a stellate configuration.

3. A lack of distinct subsarcolemmal SDH activity thus having an indistinct margin.

The type B fiber has the following characteristics

1. A network of particles of similar size as those of the type A fiber.

2. Particles arranged in small polygons presumably surrounding myofibrils or groups of myofibrils. On changing to a different plane of focus concentric rings appear as depicted in figures 10 and 11.

3. A lack of strong subsarcolemmal SDH activity thus having an indistinct margin similar to the A type fiber.

The type C fiber is characterized by:

1. Large spherical particles which are preferentially distributed toward the periphery of the fibers.

2. Particles which are lined up in short parallel streaks in the interior of the fiber.

3. A clearly defined although discontinuous rim of heavy subsarcolemmal SDH activity marked by large elongated masses of diformazan.

Further distinction among the A, B and C type fibers can be made by a study of their cross-sectional areas. The cross-sectional area was greatest in the A fiber, intermediate in the B fiber and smallest in the C fiber as measured in a single sample of 71 fibers of the medial head of the gastrocnemius.

#### C. "Histochemical profiles of individual muscle fibers of the gastrocnemius and soleus"

**Gastrocnemius (medial head)** Seventy three individual muscle fibers were selected from hematoxylin and eosin preparation and then classified as type A, B or C on the basis of the succinic dehydrogenase reaction. These same fibers were then graded in photomicrographs of the serial cross-sections which demonstrated the presence of unfixed ATPase, fixed ATPase, esterase and glycogen. The grading was accomplished by estimating the intensity of reaction as dark, intermediate or light. The intensity level presumably reflects relative enzymatic activity or the glycogen content. Unclassified fibers were usually poorly preserved ones.

The characteristics of 27 type A fibers in the 4 other histochemical preparations are presented in table 1. The predominant

The areas of single sample of fibers were used in arbitrary unit of area with Krafft and Lauer compensating planimeter. The sample consisted of the 71 fibers (of the same 73 fibers which were studied histochemically) which were well preserved in the H&E preparation. The data is presented with the note that the sample is taken from selected area in single cross section of single muscle.

After the fibers are had been measured, they were divided into A, B, and C fibers by the previously described criteria in the SDH reaction. The mean and standard error of the areas of A fibers is  $451 \pm 18$  and of B fibers is  $378 \pm 13$  and of C fibers is  $219 \pm 13$ . Student's "t" test indicates that the difference between the means of A and C fibers and the difference between the means of A and B fibers is significant. Similar confidence limits on the difference between the means of B and C fibers have probability falling between 93 and 99%.

intensity (i.e. the intensity displayed by a majority of the fibers) in a given reaction is indicated in the last line of the table. The series of predominant intensities that accompanies the fiber type is called the fiber profile. This fiber type has high ATPase activity which is usually inhibited after fixation in formal-calcium. The activity of esterase was predominantly low. The glycogen content of the type A fiber is usually high. These histochemical characteristics can be followed visually in the two fibers marked A in the serial cross sections illustrated in figures 4-8. Despite the obvious predominant intensities, it is evident from table 1 that the type A fibers may display a wide spectrum of activity for fixed ATPase, esterase and even glycogen content.

The characteristics of 23 type B fibers are presented in table 2. The predominant intensities indicate that this fiber has low ATPase activity in unfixed and fixed sections. The esterase activity is uniformly high and this fiber stores variable amounts of glycogen. These histochemical char-

acteristics can be observed in the fibers marked B as illustrated in figures 4-8. In addition to a striking variation in glycogen content, this fiber shows some variation in ATPase activity.

Table 3 reports the characteristics of 23 type C fibers. ATPase activity remains high after fixation. Esterase activity is uniformly high and glycogen storage is clearly variable. These properties can be observed in fibers labeled C as illustrated in figures 4-8. Except for glycogen content, this fiber type shows the least variation in its histochemical properties.

Some outstanding histochemical characteristics of these three fiber types are:

- (1) the sensitivity of ATPase in the type A fiber to chemical fixation
- (2) a parallelism between esterase and succinic dehydrogenase activities both being low in the A fiber and high in B and C fibers, and
- (3) the striking variation in the glycogen content of types B and C which may reflect various phases in a cycle of glycogen storage and release.

Comparison of tables 1, 2 and 3 reveals that the type A fibers as designated in the succinic dehydrogenase preparation, show the greatest variation in other enzymatic activities. It is unknown whether this variability reflects the limitations of this scheme of classification or whether in the frozen section variations in physiological activity have been preserved. This fiber should correspond to the classical white (or light) fiber whereas the other two types fit into the general category of red (or dark) fibers.

TABLE 1  
Characteristics of type A fibers

Intensity of staining reactions	Unfixed ATPase	Fixed ATPase	Esterase	Glycogen
Dark	27	6	2	23
Intermediate	0	0	2	3
Light	0	15	19	1
Unclassified	0	0	4	0
Predominant intensity	Dark	Light	Light	Dark

Twenty-seven fibers, classified as Type A in the succinic dehydrogenase reaction, show low or high ATPase activity depending on chemical fixation. Possess low esterase activity and store much glycogen.

TABLE 2  
Characteristics of type B fibers

Intensity of staining reactions	Unfixed ATPase	Fixed ATPase	Esterase	Glycogen
Dark	4	3	20	5
Intermediate	0	0	1	10
Light	19	20	0	8
Unclassified	0	0	2	0
Predominant intensity	Light	Light	Dark	Variable

Twenty-three fibers, classified as Type B in the succinic dehydrogenase reaction, have predominantly low ATPase activity, high esterase activity and store variable amounts of glycogen.

TABLE 3  
Characteristics of type C fibers

Intensity of staining reactions	Unfixed ATPase	Fixed ATPase	Esterase	Glycogen
Dark	23	21	20	12
Intermediate	0	2	1	4
Light	0	0	0	7
Unclassified	0	0	2	0
Predominant intensity	Dark	Dark	Dark	Variable

Twenty-three fibers classified as Type C in the succinic dehydrogenase reaction, have high ATPase and esterase activities and contain variable amounts of glycogen.



TABLE 4  
Histochemical profiles  
Summary of predominant intensity of the  
three main fiber types

SDH	Unfixed ATPase	Fixed ATPase	Esterase	PAS
A	Dark	Light	Light	Dark
B	Light	Light	Dark	Variable
C	Dark	Dark	Dark	Variable

The histochemical profiles presented in table 4 are derived from a group of fibers and not from any individual one. Therefore it is necessary to see how well the profiles serve to classify individual fibers. Of the 73 fibers originally considered 66 are well preserved in all 5 histochemical preparations and thus complete histochemical profiles are available for them. Seventy per cent of these fibers show compatibility between their classification in the SDH preparation and their profiles as determined by the 4 other histochemical reactions. Of the 66 fibers 43% classified as type A in the SDH preparation have the A fiber profile; 81% of the type B fibers have the type B profile; and 88% of the C fibers have the C type profile. Twenty-six per cent of the 66 fibers are associated with a series of histochemical reactions that fail to conform to any of the three standard profiles. In only 4% is there an incompatibility such that the SDH preparation designates one type of fiber whereas the remaining 4 histochemical reactions (i.e. the histochemical profiles) are characteristic of another type.

The fiber types studied in longitudinal sections are homogeneous in all these reactions throughout their lengths. The possibility that differences in intensity in cross sections of fibers may be caused by sections through different levels of the sarcomere (1-2  $\mu$  long) seems unlikely since 10  $\mu$  cross sections were used in this study.

**Soleus.** This hind limb muscle has been viewed as a homogeneous red muscle. No large regions of generally high and low SDH activity and glycogen storage were noted in the soleus as they had been in the gastrocnemius. Some variation in the SDH activity of its fibers was observed by Nachmias and Padykula ('58). Investigation of this muscle in the present study has further defined its heterogeneity. Ac-

cording to the criteria described above for the fibers of the gastrocnemius only types B and C fibers are found in the SDH preparations of the soleus (fig. 12). No regions predominant in either of the two fiber types are found, i.e. B and C type fibers are evenly distributed throughout cross sections of the soleus. Fiber-to-fiber comparisons further reveal that all the type B fibers have low unfixed ATPase activity whereas all the C fibers have high activity (fig. 13). The esterase activity is uniformly high while the glycogen content is variable. Thus these 2 fiber types of the soleus show striking conformity to the histochemical profiles of fiber types B and C of the gastrocnemius. The only observed difference between the fibers of the soleus and the B and C fibers of the gastrocnemius is that those of the soleus are of greater cross-sectional area.

#### DISCUSSION

*The heterogeneity of mammalian skeletal muscles.* Differences among various muscles of the same species and among muscles of different species have long been noted (Schwann 1839, Kölliker 1857, Holmgren '10). The characterization of muscles as red or white, slow or fast, and as containing large or small motor units is also well known. However the differences in the fiber content within separate vertebrate muscles are relatively unknown. Heterogeneity in fiber content which is readily recognized in histochemical preparations characterized all mammalian skeletal muscles which have been examined histochemically to date. Further more there is a characteristic arrangement or zonation of fiber types within many muscles.

This heterogeneity is closely related to the nerve supply of the muscle. In 1929 Denny Brown showed that differentiation into fast and slow muscles occurs postnatally in kittens. All muscles are slow in contraction time in kittens two weeks old but some weeks later there is differentiation into the adult patterns of fast pale and slow red muscle. The muscles used for phasic contraction (e.g. gastrocnemius) developed fast contraction whereas the tonic muscles (e.g. soleus) remained slow. Buller et al. ('60a and b) have defined

the role of innervation on differentiation into slow and fast muscle. In kittens the normally slow soleus can be made fast by anastomosing its nerve to the nerve that originally served the fast peroneal muscles. Conversely the normally fast and light colored gracilis is made slow and red by cross-innervation with the normally slow and red crureus muscle.

Interesting differences among muscles are also evident from study of neuromuscular disorders. Denny-Brown ('53) stated that the rate of atrophy in different muscles is quite variable. For example after denervation the laryngeal muscles atrophy quickly while the *vastus medialis* may last for years. Dubowitz and Pearse ('60) speculate that the degree of dystrophic involvement of a particular muscle may be related to the types of fibers which compose that muscle. In the lateral head of the gastrocnemius from both normal patients and those with pseudohypertrophic muscular dystrophy fibers high in oxidative enzymes (lactic dehydrogenase and DPN diaphorase) are low in phosphorylase and the converse is also true. Furthermore the largest fibers in pseudohypertrophic muscular dystrophy are the ones with high glycogen content and phosphorylase activity. Dubowitz and Pearse consider the possibility that one type of fiber is preferentially involved in muscular dystrophy. If different proportions of the several fiber types compose the various somatic muscles this may account for the clinically observed lack of uniformity of dystrophic involvement of different muscles.

The present histochemical study has revealed that the fiber types in the medial head of the rat gastrocnemius follow a characteristic course through the muscle. As has been illustrated in figures 1 and 2 the medial head of the rat gastrocnemius near its origin is easily divided into 2 regions: a white region which has high glycogen content and low SDH activity and a red region which has low glycogen content and high SDH activity. As sections are taken in a progression from the origin toward the insertion, the clear separation of the two regions becomes obscured as bundles of red fibers apparently interdigitate with white fascicles to form suc-

cessively different morphological relationships. These changing relationships are easily brought out in histochemical preparations of cross sections of muscle. Denny Brown ('29) analyzed the medial head of the cat gastrocnemius using gross dissections and alkaline Sudan III preparations. He found two fiber types with separate courses through that muscle. Although the significance of the characteristic non-parallel course of fiber types through this muscle is unknown it is a fact which ultimately must be considered in determining the coordinated activity of the whole muscle.

*Cytologically fast mammalian muscles* have been characterized by a sparse mitochondrial content while the slow muscles are rich in mitochondria. There is considerable current interest in the structural variations in the sarcoplasmic reticulum which is viewed as the intra-fiber conduction system (Porter and Palade, '57; Bennett, '60). Peachey and Porter ('59) in reviewing the existing literature on the ultrastructure of smooth cardiac and skeletal muscle of a variety of animals hypothesize that the sarcoplasmic reticulum is most extensive in muscle fibers with fast contractility. Evidence supporting this has been presented in recent studies on a fast-acting muscle (Revel, '61). The structural pattern of the sarcoplasmic reticulum which varies in different species and also within muscles of a single species, may be different in the various fibers within a single muscle (Bennett, '60).

It is thus seen that the differences among various types of muscle fibers are established on several grounds. Differentiation into fast and slow fibers apparently takes place in the immediate post-natal period and innervation may play an important role in the process. The fact that differentiation has taken place is borne out by physiological, histochemical and morphological studies of healthy and diseased muscle. The present study describes further aspects of muscle heterogeneity which are evident in histochemical preparations and suggests that significant qualitative and quantitative metabolic differences exist among mammalian muscle fibers.

It is speculated that many of the physiological and biochemical differences noted among various muscles are due to the presence of different proportions of the several types of muscle fibers as well as the gross arrangement of the various fiber components.

### Mitochondria

A point of considerable concern raised by this paper relates to the location of mitochondria within muscle fibers. The concentration of granules around the nuclei and in the sarcoplasm between myofibrils was first noted by Schwann (1839). These granules were intensively studied by Höllicker (1857-1888) who reconfirmed their extrafibrillar and perinuclear arrangement and demonstrated their swelling in hypotonic solutions. Holmgren (10) characterized the granules of J or Q fibers (I or A granules) depending on their relationship to the sarcomere. A lack of clear definition of the differences in the localization of mitochondria within various types of muscle fibers still exists. Electron microscopic studies of skeletal muscles are beginning to offer precise localizations (Bennett and Porter '53; Palade '56; Porter and Palade '57; Andersson-Cedergren '59). Four specific locations of mitochondrial concentration are frequently mentioned: (1) the nuclear poles, (2) the subsarcolemmal region, (3) the myoneurial junction, and (4) between the myofibrils with or without relationship to the cross-striations. In general the mitochondria are distributed in longitudinal rows among myofibrils but they may also encircle the myofibrils. Porter and Palade ('57) defined two fiber types in the rat sartorius and obliqui on the basis of mitochondrial number, structure and arrangement. One type of fiber is usually of small diameter and is rich in mitochondria which have many cristae; the mitochondria branch and encircle almost every I band. The other fiber type is larger in diameter and is poor in mitochondria; these mitochondria are small, have few cristae and are usually not related to the I band.

Another method for determining the location of mitochondria is the histochemical procedure for the mitochondrial en-

zyme succinic dehydrogenase. This enzyme is tightly bound to the mitochondrial membrane (Skegsvik and Watson '56). Although cytochemical efforts to localize the enzyme within mitochondria with the electron microscope have been made (Bennett and Palade '57; Yaeger '61), the methods employed (potassium tellurite and nitro BT) have not permitted convincing localizations. Despite this cytochemical limitation, the specificity of the histochemical tetrazolium method for SDH (Seligman and Rutenburg, '51) is well established and the reaction product is known to form at the mitochondrial surface. Its particular usefulness in this study has been to offer a better three-dimensional concept of mitochondrial arrangement within three types of fibers in the medial head of the gastrocnemius (see especially figures 10 and 11). Earlier histochemical studies localizing SDH in muscle emphasized the validity of this reaction in reflecting mitochondrial number and thus differentiating between "red" and "white" fibers (Padykula, '52). Wachstein ('55) reported a concentration of SDH activity at the I band in some but not all human rat and rabbit muscles. Nachmias and Padykula ('58) correlated high subsarcolemmal and perinuclear SDH activity with aggregations of mitochondria at these sites. There are some cytochemical claims for a myofibrillar localization of SDH activity (Bergman and Walker '59; Cogan and Kuwabara '60) despite the strong evidence from differential centrifugation which indicates that SDH is exclusively a mitochondrial enzyme (Paul and Sperling '52; Hoogeboom et al. '57).

In the present study three fiber types are demonstrated in the medial head of the gastrocnemius while the soleus has but two. One type of fiber has heavy subsarcolemmal SDH activity and the other two have much less. The high subsarcolemmal activity correlates well with the abundance of mitochondria in subsarcolemmal and perinuclear stations. The position of the mitochondria in the three fiber types in the medial head of the rat gastrocnemius is reflected by the localization of SDH. The A fiber is presumed to be the classical white fiber with few mitochondria per unit

volume and a relative lack of mitochondrial aggregation in the perinuclear position. Preliminary electron micrographs demonstrate a mitochondria-poor fiber in the medial head of the gastrocnemius and also a fiber type with strong I band and subsarcolemmal mitochondrial concentration, similar to the distribution of sarcosomes in the rat diaphragm as described by Palade ('56). This latter pattern correlates well with the ultrastructure that would be expected for the type C fiber. The ultrastructure of the type B fiber would be expected to reveal a somewhat lower sarcoplasm to myofibril ratio than that seen in the type C fiber. The subsarcolemmal concentration of mitochondria would not be as heavy. Concentric laminations of SDH activity are observed in the type B fiber (fig. 11) and would be expected in electron micrographs of this fiber in the rat gastrocnemius.

The category of red fibers may be further divided into at least two subcategories (types B and C fibers). The evidence for this division rests on several bases: (1) the difference in the distribution of succinic dehydrogenase activity within the cells; (2) the concentric laminations seen only in the type B fiber in SDH preparations; and (3) differences in the ATPase reaction of the two fiber types. All these differences except those demonstrated by the two ATPase preparations could possibly be explained by differences in plane or location of section. It is thought, however, that the evidence presented thus far tends to favor the individuality of the B and C fiber. Further support for the existence of two red fibers is gained by the histochemical heterogeneity of the soleus. It is hoped that electron microscopic study of the rat soleus (which contains only B and C fibers) will permit conclusive differentiation of the two types by their ultrastructure.

#### *Glycogen*

The deep portion of the medial head of the gastrocnemius is rich in glycogen (fig. 2) and is composed predominantly of A or white fibers. In the superficial part where fibers are heterogeneous in terms of glycogen content, there is a mixture of all three fiber types. Regional seg-

regation of fibers with high glycogen content has also been found in the pectoralis muscle of several species of birds (George and Nalk, '58, '59a and b). In the rat gastrocnemius the glycogen content of the A fibers is generally high, but it is quite variable in the B and C fibers. Furthermore although the classification of the intensity of the PAS reaction is arbitrarily limited to three categories (light, intermediate and dark, cf. tables 1 to 4) there are actually many more gradations in the intensity of the reaction. This variation in the glycogen content of the muscle fibers may reflect different phases of a cycle of glycogen storage and utilization which were "caught" in the frozen section. The consistently high glycogen content of the A fiber may be interpreted as evidence that these fibers are the most avid synthesizers or that they are the least avid users of glycogen. These histochemical variations may be tangible reflections of the dynamic state of glycogen which has been shown to have a half life of 4 days in rat muscle (Stetten and Stetten, '60). The existence of a spectrum of different glycogen structures is proposed by Stetten and Stetten ('60). They view the difference between the free (TCA extractable) and fixed (hot KOH extractable) glycogens as indicating differences in the structure of the glycogen polymers. Furthermore they suggest different metabolic roles for the various glycogens, because great quantitative fluctuations of free glycogen are seen under various metabolic states while fixed glycogen remains quantitatively more constant in a given tissue regardless of its metabolic state. On the other hand Hanson et al. ('60) think that the constancy of fixed glycogen speaks for it representing glycogen trapped in the precipitates which are formed during quantitative determinations of glycogen. Although the histochemical results reported here cannot be directly related to the various types of glycogen molecules which have been proposed it would be worthwhile to follow glycogen depletion in muscle in a correlated biochemical-histochemical study to determine whether glycogen depletion occurs preferentially in one or more of the fiber types described here.

Although histochemical descriptions reflect the inequality in glycogen storage of skeletal muscle fibers (Dempsey et al. '48; George and Naik '58; Nachmias and Padykula, '58) no differences in the cytological pattern of glycogen storage of various fibers have been noted. The problem is complicated by the fact that the position of glycogen may be easily shifted during fixation and thus accurate localization is difficult to achieve. There is general agreement that glycogen occurs as particles or aggregates in the sarcoplasm of striated muscle fibers (Dempsey et al., '48; Beck et al. and Bourne, '58; Bergman and Walker '59; Bergman, '60; Engel, '61; Revel et al. '61). Several cytochemical studies demonstrate the sarcoplasmic glycogen to be concentrated adjacent to one of the myofibrillar bands creating a striated appearance. Although the area near the Z band is frequently mentioned, there is lack of agreement as to the site of storage (Mancini '48; Bergman and Walker '61; Engel '61). There are some claims for storage of glycogen within the myofibrils as well as within the sarcoplasm (Dempsey et al. '48; Bergman '60).

Epinephrine, insulin and steroids as well as exercise and denervation, are known to influence the glycogen levels of muscle (Lazere et al. '43; Krahil, '51; Sutherland '51; Nachmias and Padykula, '58; Larner et al. '60; Todd '60). In this study the rats were undoubtedly stressed to some extent by the anesthesia and handling. However in view of the standard conditions under which the animals were kept and the reproducibility of the results these preparations most likely reflect the glycogen content of the normal caged rat.

#### *Adenosine triphosphatase*

Although the histochemical ATPase reaction has been useful in this study for differentiating several types of muscle fibers the nature of this enzymatic reaction has not yet been fully elucidated. The reaction employed here was performed at pH 9.4 and undoubtedly involves myosin-ATPase activity (Padykula and Herman '55b; Freiman and Kaplan, '60; Wachstein, Meisel and Niedzwiedz, '60). According to Wachstein et al. ('60) fixation in cold

neutral formalin inhibits the myofibrillar ATPase activity at pH 7.2.

The multiplicity of the ATPase reaction at pH 9.4 in the biceps femoris of the rat was noted by Nachmias and Padykula ('58) in relation to the action of cysteine and sulfhydryl inhibitors. Our results here at pH 9.4 show a general inhibition of ATPase activity by calcium-formol fixation. However upon extended incubation (one hour) of fixed sections the characteristic activity of B and C fibers as seen in unfixed preparations is demonstrable. That of the A fibers however remains completely inhibited. Thus there is a differential effect of calcium-formol fixation on the ATPase activity of the A fiber. The confusion surrounding the histochemical localization of ATPase activity originates most likely in the multiplicity of the ATP splitting enzymes as well as in the heterogeneity of skeletal muscle fibers.

#### SUMMARY

Individual fibers of the rat gastrocnemius and soleus were classified histochemically by comparing their various characteristics in serial cryostat sections. The serial sections were prepared to demonstrate the following constituents: glycogen, succinic dehydrogenase (two kinds of adenosine triphosphatase and esterase).

At low magnification a histochemical zonation is evident in the medial head of the gastrocnemius near its origin. The deep part of the medial head has low overall succinic dehydrogenase activity and abundant glycogen. Conversely the superficial region has high overall succinic dehydrogenase activity and contains little glycogen. However the individual fibers in both regions show distinct heterogeneity for both constituents. Cytochemical examination reveals three different fiber types which are distributed throughout the medial head in varying proportions.

These three fiber types (A, B and C) of the gastrocnemius can be recognized by their characteristic patterns of distribution of succinic dehydrogenase activity. The diformazan particles which localize this activity vary in size and position within the three fiber types and are arranged in distinctive networks which reflect the dis-

tribution of mitochondria. For example the type C fiber is distinguished by heavy subsarcolemmal activity which is absent in the other two. One of the fibers (type A) is usually rich in glycogen, whereas the other two fibers (types B and C) show striking variability in glycogen content. The deep region which has high glycogen content is composed principally of type A fibers which are presumed to be the classical white fibers. In fiber types B and C the evidence suggests that individual fibers were observed at various phases in a cycle of glycogen deposition and release. The distinctiveness of type A, B and C fibers is confirmed by differences in their esterase and adenosine triphosphatase activities.

The rat soleus, which has been considered to be a homogeneous red muscle is actually heterogeneous histochemically. It is composed entirely of B and C fibers which are distributed throughout the muscle without the conspicuous segregation which is evident in the gastrocnemius.

This histochemical evidence is interpreted as indicating that the type A fiber represents the classical "white fiber" whereas types B and C represent two types of "red" fibers.

#### ACKNOWLEDGMENT

We wish to acknowledge the technical assistance of Miss Eileen Hall in the histochemical methodology and the photographic work of Mr Leo Talbert.

#### LITERATURE CITED

- Anderson-Cedergren, E. 1956 Ultrastructure of motor end plate and sarcoplasmic components of mouse skeletal muscle fiber. *J Ultrastructure Res.*, 1 Suppl., 1-181.
- Barnett, R. J. and G. E. Palade 1957 Histochemical demonstration of the sites of activity of dehydrogenase systems with the electron microscope. *J Biophys. Biochem. Cytol.*, 3: 577-584.
- Beckett, E. B., and G. H. Bourne 1938 Some studies on the glycogen of normal and diseased human skeletal muscle using lead tetra-acetate-Schiff and periodic acid-Schiff techniques. *Acta Anat.*, 34: 233-248.
- Bennett, H. S., and K. R. Porter 1953 An electron microscope study of sectioned breast muscle of the domestic fowl. *Am. J. Anat.*, 63: 61-103.
- Bennett, H. S. 1960 The structure of striated muscle as seen by the electron microscope. In *The Structure and Function of Muscle* Vol. I, G. H. Bourne, ed., Acad. Press, Inc., N. Y. pp. 137-181.
- Bergman, R. A., and D. G. Walker 1959 The cytochemical localization of oxidative enzymatic activity and glycogen in frog striated muscle. *Bull. Johns Hopkins Hosp.*, 104: 179-196.
- Bergman, R. 1960 Further observations on the localization of glycogen in frog striated muscle. *Bull. Johns Hopkins Hosp.*, 107: 307-319.
- Buller, A. J. J. C. Eccles and R. M. Eccles 1960a Differentiation of fast and slow muscles in the cat hind limb. *J. Physiol.*, 150: 309-416.
- 1960b Interactions between motoneurons and muscles in respect of the characteristic speeds of their responses. *J. Physiol.*, 150: 417-439.
- Cogan, D. G., and T. Kuwabara 1960 Tetrazolium studies on the retina. IV. Distribution of reductase in ocular tissue. *J. Histochem. Cytochem.*, 8: 380-384.
- Dempsey, E. W. G. B. Wlodek and M. Singer 1946 Some observations on the chemical cytology of striated muscle. *Anat. Rec.*, 96: 231-247.
- Denny-Brown, D. E. 1929 The histological features of striped muscle in relation to its functional activity. *Proc. Roy. Soc.*, B104: 371-411.
- 1953 Clinical problems in neuromuscular physiology. *Am. J. Med.*, 15: 368-390.
- Dreus, G. A., and W. K. Engel 1961 An attempt at histochemical localization of myoglobin in skeletal muscle by the benididine-peroxidase reaction. *J. Histochem. Cytochem.*, 9: 204-207.
- Dubowitz, V. and A. G. E. Pearce 1960 Reciprocal relationship of phosphorylase and oxidative enzymes in skeletal muscle. *Nature*, 183: 701-702.
- Engel, W. K. 1961 Cytological localization of glycogen in cultured skeletal muscle. *J. Histochem. Cytochem.*, 9: 39-43.
- Fretwell, D. G., and M. Kaplan 1960 Studies on the histochemical differentiation of enzymes hydrolyzing adenosine triphosphate. *Ibid.*, 8: 159-170.
- George, J. C., and D. Jyot 1957 Studies on the structure and physiology of the flight muscles of birds. 2. The relative reduction of fat and glycogen in the pectoralis major muscle during sustained activity. *J. Animal Morph. and Physiol.*, 4: 119-122.
- 1958 Studies on the structure and physiology of the flight muscles of the bat. 2. The relative reduction of fat and glycogen in the pectoralis major muscle during sustained activity. *Ibid.*, 5: 67-69.
- George, J. C., and R. M. Nalk 1955 Studies on the structure and physiology of the flight muscles of birds. 1. The variations in the structure of the pectoralis major muscle of few representative types and their significance in the respective modes of flight. *Ibid.*, 4: 23-32.
- 1957b Studies on the structure and physiology of the flight muscles of bats. 1. The occurrence of two types of fibers in the pectoralis major muscle of the bat (*Hippobosca spearia*) their relative distribution, nature of the fuel store and mitochondrial content. *Ibid.*, 4: 95-101.

- 1953 Relative distribution and chemical nature of the fuel store of the two types of fibers in the pectoralis major muscle of the pigeon. *Nature* 181 709-711.
- 1959a Study of the structure and physiology of the flight muscles of birds. 4. Observations on the fiber architecture of the pectoralis major muscle of the pigeon. *Biol. Bull.*, 116 239-247.
- 1959b Studies on the structure and physiology of the flight muscles of birds. 5. Some histochemical and cytochemical observations on the structure of the pectoralis. *J. Animal Morph. and Physiol.*, 6 16-23.
- George J. C., and K. B. Scaris 1959 Histochemistry of muscle lipase. *Ibid.*, 5 43-48.
- George J. C., A. K. Sushela and K. B. Scaris 1958 A quantitative and histochemical study of lipase activity in the pectoralis major muscle of the bat. *Die Naturwissenschaften*, 45 93.
- Hanson, R. W. H. S. Schwartz and S. B. Barker 1960 "Free" and "fixed" glycogen as physiological entities. *Am. J. Physiol.*, 198 800-808.
- Hazzard, W. R., and S. L. Leonard 1961 Phosphoglucomutase activity in skeletal muscles of vitamin E-deficient chicks. *Proc. Soc. Exp. Biol. Med.*, 106 838-841.
- Hoggeboom, G. H. E. L. Kuff and W. C. Schneider 1957 Recent approaches to the cytochemical study of mammalian tissues. *Intern. J. Rev. Cytol.*, 6 425-467.
- Holmgren, E. 1910 Untersuchungen über die morphologischen nachweisbaren stofflichen Umsetzungen der quergestreiften Muskelfaser. *Archiv für Mikros. Anat.*, 75 240-236.
- Huxley H. E., and J. Hanson 1960 The molecular basis of contraction. In *The Structure and Function of Muscle*, Vol. 1 G. H. Bourne, ed. Acad. Press Inc., N. Y. pp. 183-227.
- Kauffer A. 1857 Einige Bemerkungen über die Endigungen der Nerven und den Bau der Muskeln. *Zell. f. wiss. Zool.*, 6 311-325.
- 1868 Zur Kenntnis der quergestreiften Muskelfaser. *Ibid.*, 47 689-710.
- Krahl, M. E. 1951 The effect of insulin and pituitary hormones on glucose uptake in muscle. *Ann. N. Y. Acad. Sci.*, 54 649-670.
- Kuffer S. W. 1953 The two lateral nerve-muscle systems in frog. *Arch. Exp. Path. and Pharmacol.*, 270 116-135.
- Larner J. C. Villar Palasi and D. J. Richman 1960 Insulin-stimulated glycogen formation in rat diaphragm. Levels of tissue intermediates in short-time experiments. *Arch. Biochem. Biophys.*, 86 50-60.
- Lawrie R. A. 1952 Biochemical differences in red and white muscle. *Nature* 170 122-123.
- Lazere B. J. D. Thompson and H. M. Illies 1943 Studies on the glycogen metabolism of trophic and regenerating muscle. *Am. J. Physiol.*, 133 357-363.
- Mandini, R. E. 1948 Histochemical study of glycogen in tissues. *Anat. Rec.* 101 149-159.
- Nachlas, M. M. K. C. Tsou E. DeSouza, C. S. Cheng and A. M. Seligman 1957 Cytochemical demonstration of succinate dehydrogenase by the use of a new  $\beta$ -nitrophenyl substituted dihydrozole. *J. Histochem. Cytochem.* 5 420-436.
- Nachlas, V. T., and H. A. Padykula 1958 A histochemical study of normal and denervated red and white muscles of the rat. *J. Biophys. Biochem. Cytol.*, 4 47-64.
- Novikoff A. B. and B. Masck 1958 Survival of lactic dehydrogenase and DPNH diaphorase activities after formal-calcium fixation. *J. Histochem. Cytochem.*, 6 317.
- Padykula, H. A. 1953 The localization of succinate dehydrogenase in tissue sections of the rat. *Am. J. Anat.*, 91 107-132.
- Padykula, H. A., and E. Herman 1955a Factors affecting the activity of adenosine triphosphatase and other phosphatases as measured by histochemical techniques. *J. Histochem. Cytochem.*, 3: 161-169.
- 1955b The specificity of the histochemical method for adenosine triphosphatase. *Ibid.* 3 170-195.
- Palade, G. E. 1956 Electron microscopy of mitochondria and other cytoplasmic structures. In *Enzymes. Units of Biological Structure and Function*. O. H. Gaebler ed., Acad. Press, Inc., N. Y. pp. 185-215.
- Paul, M. H., and E. Sperrling 1953 Cyclophorase system XXIII Correlation of cyclophorase activity and mitochondrial density in striated muscle. *Proc. Soc. Exp. Biol. Med.*, 78 352-354.
- Peaschey L. D. and K. R. Porter 1959 Intracellular impulse conduction in muscle cells. *Science* 129 721-723.
- Pearse A. G. E. 1960 Histochemistry Theoretical and Applied, 2nd Edition. Little, Brown & Co., Boston.
- Porter K. R., and G. E. Palade 1957 Studies on the endoplasmic reticulum III. Its form and distribution in striated muscle cells. *J. Biophys. Biochem. Cytol.*, 3 289-300.
- Ravel J. P. L. Napolitano and D. W. Fawcett 1960 Identification of glycogen in electron micrographs of thin tissue sections. *Ibid.* 8 575-589.
- Ravel J. P. 1961 Electron microscopic study of the bat cricothyroid muscle. *Anat. Rec.* 129: 267.
- Schwann, Th. *Mikroskopical researches into the accordance in the structure and growth of animals and plants*, translated for Sydenham Soc. 1847 from Schwann book of 1839.
- Seligman, A. M., and A. M. Huttenberg 1951 The histochemical demonstration of succinate dehydrogenase. *Science* 113 317-320.
- Sennoff W. E. 1935 Mikrochemische Bestimmung der Aktivität der Succinat-Dehydrogenase in den Organen des Rana temporaria. *Zell. f. Zellforsch. u. Mikro. Anat.*, 22 305-309.
- Siekevitz, P. and M. L. W. Ison 1956 Cytochemical studies of mitochondria II. Enzymes associated with mitochondrial membrane fraction. *J. Biophys. Biochem. Cytol.*, 2 633-670.
- Steinen, De Witt, J. and M. R. Steinen 1960 Glycogen metabolism. *Physiol. Rev.* 40 505-537.
- Szent-Gyorgyi, A. 1953 Chemical Physiology of Contraction in Body and Heart Muscle. Acad. Press N. Y.

- Todd, W. R., and M. Allen 1960 Tissue glycogen synthesis in adrenalectomized rats fed glycine-containing diets and given hydrocortisone. United States Air Force Arctic Aeromedical Laboratory Technical Report, Vol. 58-23 pp. 1-5.
- Touretich J. and M. R. Kare 1960 Adenosine triphosphatase in red and white muscle. Arch. Biochem. Biophys., 89 195-200.
- Wachstein, M., and E. Meisel 1955 The distribution of histochemically demonstrable succinic dehydrogenase and of mitochondria in tongue and skeletal muscle. J. Biophys. Biochem. Cytol., 1 483-488.
- Wachstein, M., E. Meisel and A. Niedzwiedz 1960 Histochemical demonstration of mitochondrial adenosine triphosphatase with the lead-adenosine triphosphatase technique. J. Histochem. Cytochem., 8 387-388.
- Yarger J. A. 1961 Microscopic and submicroscopic localization of succinic dehydrogenase activity in the muscle cells of mouse diaphragm. Exp. Cell. Res., 22: 483-502.



# PLATE I

## EXPLANATION OF FIGURES

The general topography of the cross section of the *gastrocnemius* muscle of the rat taken 5 mm from its origin is diagrammed. The striped portion represents the superficial region of the medial head which contains predominantly red fibers. The remainder of the box encloses most of the rest of the medial head and contains an area whose fibers appear grossly white. The box encloses an area similar to that seen in the photomicrographs of figures 1 and 2. A = Anterior (deep); L = Lateral; M = Medial; P = Posterior (superficial)

- 1 Succinic dehydrogenase activity (SDH) Cross section 5 mm from the origin of the medial head of the rat gastrocnemius muscle. The area shown in this figure is enclosed by the box in the inset. It shows the superficial region (cf inset) has high overall SDH activity whereas the deeper fibers (which appear at the lower margin of the photomicrograph) have lower overall SDH activity. Note also that some less active fibers are present in the area of generally high activity and some more active ones are present in the area generally low in activity. Observe the muscle spindle (arrow) which is constant finding in the dark superficial portion of the medial head near the origin. Compare this figure with figure 2 which is a serial section of the same field demonstrating glycogen by PAS technique ( $\times 50$ ).
- 2 Glycogen PAS technique. This serial section depicts the same field as figure 1. Note the orienting muscle spindle designated with an arrow. Observe that the regions which are richest in glycogen (i.e. the right and lower margins) are poorest in SDH as seen by comparison with figure 1. It is pointed out that the superficial red muscle (striped area in inset of fig. 1) has high overall SDH activity and low overall glycogen content, but that some individual fibers in this region have high glycogen concentration. Control sections previously digested by malt diastase show no PAS positive material in the cell interiors and only slight reactivity at the cell borders ( $\times 50$ ).

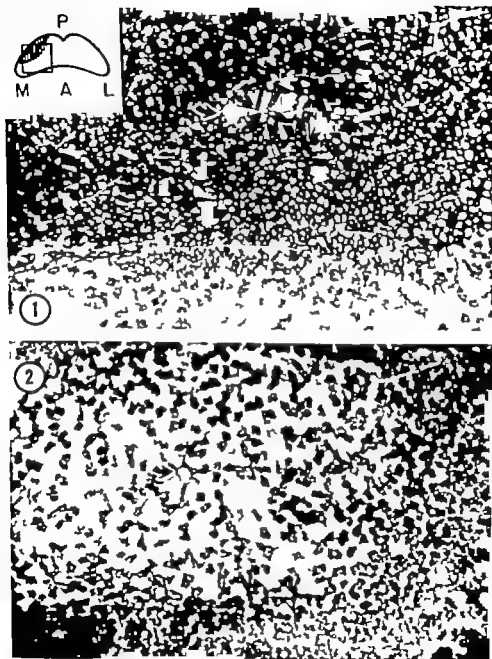


## PLATE 2

### EXPLANATION OF FIGURE

- 3 Succinic dehydrogenase activity (SDH); this montage is composed of three separate photographs made at oil immersion magnification. The cytological patterns characteristic of the A, B and C type fibers from the medial head of the rat gastrocnemius are demonstrated (A, B, and C indicate types A, B and C fibers.) ( $\times 1,220$ .)

Type A is characterized by

1. Lack of distinct subsarcolemmal activity
2. Particles arranged in an open network
3. Particles arranged in streaks which are sometimes parallel and at other times meet at junctions marked by larger particles thus creating stellate configuration.

Type B characterized by

1. Lack of strong subsarcolemmal activity
2. Particles arranged mostly in the form of small polygons.

Type C is characterized by

1. Very strong subsarcolemmal SDH activity with elongated masses of diformazan.
2. Large spherical particles preferentially arranged toward the fiber periphery
3. Particles aligned in short palisaded streaks.



# PLATE 3

## EXPLANATION OF PICTURES

Figures 4-9 represent serial cryostat sections of the same field from the medial head of the rat gastrocnemius.  $\times 230$

Two fibers of each type are labeled with the letter designating its fiber type (A, B and C). An individual fiber may be followed through all 6 reactions to obtain its "histochemical profile." The two fibers bearing identical letters in a given figure can be separated by their spatial relationships which remain constant in all figures throughout this plate. These 6 figures illustrate the predominant histochemical characteristics of the three main fiber types.

### 4 Hematoxylin and eosin.

The relative positions of the selected A, B and C fibers are indicated here. In this histological preparation, the three fiber types are homogeneous.

### 5 Succinic dehydrogenase

Type A — light      Type B — intermediate      Type C — dark

The distribution of diformazan particles is shown at higher magnification in figure 3.

### 6 Unfixed ATPase

Type A — dark      Type B — light      Type C — dark

### Fixed ATPase

Compare this reaction with that in the soleus shown in figure 13.

Type A — light      Type B — light      Type C — dark

### 8 Esterase (non-specific)

Type A — light      Type B — dark      Type C — dark

### Glycogen (PAS)

Type A — dark      Type B — variable      Type C — variable

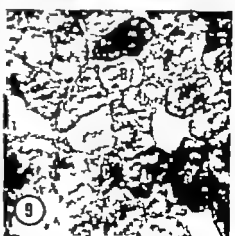
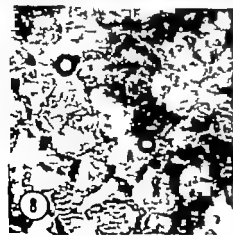
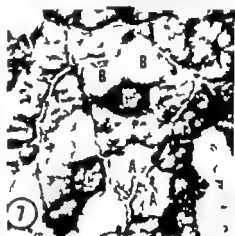
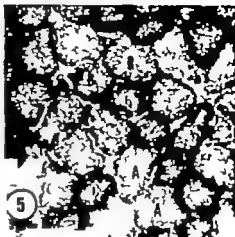
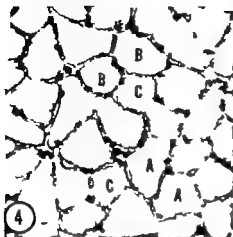
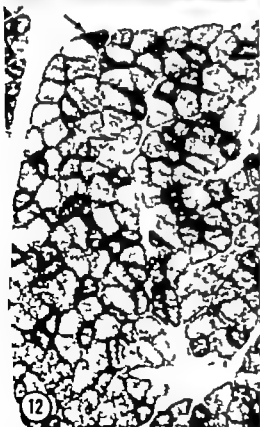


## PLATE 4

### EXPLANATION OF FIGURES

- 10-11 The same type B fiber is presented in 2 different planes of focus in an SDH preparation of the medial head of the rat *ps. trochanterius*. Note that the fine polygonal arrangement of the diformazan in figure 10 yields to pattern of concentric lamellae in figure 11 ( $\times 1100$ .)
- 12 Succinic dehydrogenase activity; rat soleus. Two types of muscle fibers are evident. The lighter fibers fulfill the cytochemical criteria for B fibers while the darker ones conform to the criteria for C fibers. One arrow points to lighter B fiber and two arrows point to darker C fibers. Compare with figure 13. ( $\times 125$ .)
- 13 Fixed ATPase reaction rat soleus. Two types of fibers are again evident. Note the parallelism in intensity between ATPase and SDH activity. Three corresponding fibers can be compared by following those indicated by arrows in figures 12 and 13. ( $\times 125$ .)







# A Quantitative Study of the Hemodynamics in the Living Microvascular System<sup>1</sup>

EDWARD H. BLOCH

Department of Anatomy Western Reserve University Cleveland, Ohio

The purpose of this paper is to describe the results of a quantitative study of blood flow in the microvascular system. This study has differed from others wherein the rheology of blood flow was examined, by employing several methods simultaneously to examine blood flow in living microscopical vessels (Bayliss '32 Bloch '36 Harding and Knisely '58 Jäger '35 Lutz et al '30 McDonald '60 Taylor '35 Thoma '27). These procedures have permitted an evaluation of the advantages, limitations and a statement of what is required of the methods which may lead to a more complete characterization of the rheology of blood.

These goals were achieved by magnifying the contents of the vessel and recording the blood flow at motion picture framing speeds (fps) up to 1000 per sec, so that when the film was projected at 16 fps cellular movement was slow enough to trace the pathways of individual cells. Such data were compared with that obtained from vessels by direct visualization with the microscope, television microscopy and ciner recordings taken at 16 to 64 fps.

In spite of numerous studies of cells in flowing blood their behavior had been incompletely analyzed and quantitative data for the peripheral plasma layer and axial stream were sparse (Bayliss, '32; Bloch, '36; Clark and Clark, '35; Jäger '35; Knisely et al '44 '47; Krogh '29; Lutz, Fulton and Akers '30; Nicoll and Webb '48; McDonald '60; Thoma '27; Vierordt '1867). The methods in general which had been used were inadequate for discriminating individual cells. Occasionally the recording rates were adequate but data for sequential analyses of cellular movement were not reported (Bayliss '32; Bloch '36; Brookes and Monro '37; Clark and

Clark, '35; McDonald and Potter '49; McDonald '52a, '60; Monro '60; Thoma '27).

The goal of all studies was to obtain data which would assist in understanding the mechanics of the cardiovascular system in regard to: the distribution of blood cells within the vascular system, the influence of cellular movement on the mixing of plasma, the production of murmurs and the energy required to move blood cells through vascular channels (Bayliss '32a; Bloch, '33; Fahraeus, '52; Fahraeus and Lindquist, '31; Hale et al, '35; Hamilton, 1884; Hess, '17; Harding and Knisely '58; Jäger '35; Knisely et al, '47 '60; Madow and Bloch '36; McDonald '52b; Ralston and Taylor '45; Poiseuille 1842; Thoma, '27).

## METHOD

### Animals

Frogs, mice, rats and rabbits were used.

### Anesthesia

Frogs weighing 25-50 grams were anesthetized with 0.6 to 0.7 ml of a 2.5% solution of ethyl carbamate which was injected subcutaneously and mammals were anesthetized intravenously by injecting 20 mgms of sodium pentobarbital per kilo body weight.

### Surgery

The intestine in frogs was exposed by incising the thoracoabdominal wall with an electrocautery and in mammals by a midline incision using scissors and maintaining hemostasis with clamps and ligatures. To maintain the mesentery flat and maneuverable for microscopic study it was

<sup>1</sup> This work was supported by The Life Insurance Company of North America, The American Heart Association, and the United States Public Health Service.

spread against an optically flat quartz plate by suturing the small intestine to the frame of the plate with 5-0 silk (fig. 10).

The method used to expose the lung of mammals was as follows: a cannula (which was to deliver O<sub>2</sub> to the lung) was inserted into a tracheostomy so that it occupied about three quarters of the opening. (The opening external to the cannula permitted excess gas to escape thereby helping to prevent hyperdistention of the lung.) The right lung was then exposed by making an incision between the fifth and sixth ribs which extended approximately from the parasternal to the mid-axillary line. To achieve hemostasis ligatures were placed around each rib distal to ends of the anticipated incision.

The liver was exposed by a midline incision of the skin and abdominal muscles extending from the tip of the xiphoid process to the umbilicus.

#### METHODS OF TRANSLUMINATION

The quartz-rod method of translumination was used for studying the circulation of the liver, lung, skeletal muscle and mesentery. Also in the study of the mesentery by translumination standard microscopy was used.

Due to the intense light required for high speed cinerecording it was necessary to modify the standard quartz rod method of translumination. The modifications involved the light source, the temperature control system and the addition of a temperature recording system. A 1,200 watt tungsten filament lamp replaced the 750 watt lamp and was maintained at its optimal light output of 120 volts with an auto-transformer. The light was transmitted to the tissue via a modified quartz rod (fig. 8). Information about the maintenance of thermal hemostasis of the intensely transluminated area was essential. This was achieved by replacing the standard method of temperature control for the irrigating solutions by a servocontrolled proportional feedback system which has been described in detail (Bloch and Haas 1960b). Briefly in this system of control the temperature of the irrigating solutions issuing from the tip of the quartz rod and auxiliary irrigating units were maintained at a constant predetermined level through

the use of thermocouples which detected the thermal fluctuations produced by variations in light intensity or flow rate of the irrigating solutions. Such temperature fluctuations acted on the thermocouples to produce small voltages which were amplified and this current activated the heat exchangers of the temperature controlling equipment.

For observing or recording the circulation of the mesentery with monochromatic light the animal was placed on a tray attached to the mechanical stage of a standard microscope. The quality of the images improved not only because it was possible to use a substage condenser but by placing the microscope on an optical bench it was possible to obtain critical alignment with the light source (fig. 9). Monochromatic light was obtained with a 250 mm grating monochromator (Bausch and Lomb) which was used to transmit the desired wave length of 407 414 435 550 and 620 mμ. The light source was a 100 watt high pressure mercury lamp (Osram) in conjunction with a power supply which delivered a stable current to the lamp. This light was focussed on the tissue by moving the substage condenser until the edges of the exit slit of the monochromator and the image of the tissue were in focus. The image of the vessel was studied or recorded directly or focussed on the camera of an image orthicon or vidicon television system and the resultant image observed or recorded from a monitor (fig. 9).

#### Optics

Dry or water immersion lenses were used. For the study of quartz rod transluminated tissues both a stereobinocular microscope (4 × 6 × 8 × and 1 × objectives and 12.5 × oculars) and a monocular monoobjective microscope (10 × 20 × and 50 × water immersion objectives and 10 × or 12.5 × oculars) were used. On the optical bench a monocular microscope was used. When cinerecording the oculars were either removed or photographic oculars inserted.

#### Cinerecording

Two high speed cameras were used and Eastman Kodak Type III and a Wol

lensak Fastex WF3. The latter camera was similar to the Eastman camera except that the shutter was a glass cube and its maximum recording speed was 8 000 fps — twice that of the Eastman camera.

The 16 mm Eastman Kodak High Speed camera was used to record the circulation at framing speeds of 420 to 3,800 per second (figs. 5-7). One hundred feet of film (4 000 frames) were exposed at one time which resulted in the recording of approximately 3,500 sequential images. The film was accelerated slowly by a rheostat mechanically coupled to a 1/5 HP motor which moved the film and the shutter. Approximately 25 feet of film were needed to reach 80% of the desired framing speed while the remaining 20% was reached gradually. For example to obtain a framing rate of 3 000 per second, 65 to 70 feet of film were required. In contrast to a standard motion picture camera in this camera, the film moved continuously. The image which reached the film passed through a shutter which consisted of a rotating optically flat glass plate (fig. 1). The ends of the glass plate were capped with metal to act as framers blocking the light to the film until the angle of rotation of the plate to the film plane was such as to reduce the optical distortion to a minimum. Light passed through this shutter during approximately 1/5 of the rotation of the plate. (At 3,000 fps the exposure was 1/15,000 second.) The frame fre-

quency was calculated by measuring the length of exposed streaks on the edge of the film. (This exposure was produced by the flashing of an argon lamp mounted in the camera which flashed 120 times per second for a 60 cycle current.)

A 16 mm Kodak Cine Special camera was used to photograph the circulation at 16 or 24 frames per second.

Color and monochromatic film were used in both cameras. Kodachrome Type A, Eastman Ektachrome ER (Kodak SO 270 Type B color reversal film) and Kodak TRI X negative films were used.

#### *Analysis of the high speed film*

The film which was taken at framing rates of 480 to 7 600 per second was projected with a Bell and Howell "Time and Motion" projector either by stopping each frame to study it using the hand crank for slow motion, or the motor to view them at 16 or 24 frames per second.

The images were projected on graph paper sketched through sequential frames counted (by a counter attached to the shaft of the projector) and the magnification of the projected image and rate of movement calculated. Magnification of the projected image was calculated from the initial optical magnification and the projection distance while the rate of cellular movement was calculated from the frame speed which was indicated on the edge of the film and the distance that cells moved between sequential images. These data were inserted into the formula

$$V = \frac{D}{M} \cdot \frac{T}{C}$$

where V was the velocity in mm/sec. D the distance in mm that the cell moved when projected; M the magnification of the projected image; C the number of frames that the cell had been traced and T the average frame speed attained during the total number of frames that the cell's pathway was traced.

#### *Methods used in determining the peripheral plasma layer and axial stream*

These components were analyzed by direct visualization through the microscope from motion picture film which had re-

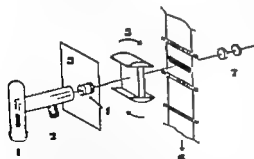


Fig. 1 Diagram of the optical path used for high speed cinematography. 1. Light source. 2. Light conducting unit (quartz rod with side opening for irrigating solution). 3. Object plane. 4. Microscope optics. 5. Shutter of high speed camera. 6. Motion picture film. Vertical bar indicates object in focus which is brought into focus by viewing it through the back of the film with the viewing telescope.

TABLE 1  
The degree of taper of mesenteric vessels in the frog<sup>1</sup>

Arterioles				Venules			
P	D	L	T	P	D	L	T
85	78	650	-1 06'	88	70	1050	+0 59'
107	108	1080	-0 93'	88	108	1575	-0° 37'
105	105	1313	0	114	105	2450	+0 13'
105	123	1923	-0° 33'	123	123	2100	0°
117	117	650	0	140	175	963	-2 05'
135	135	1350	0°	140	158	1750	-0° 35'
135	108	1080	+1 32'	158	175	1313	+0 41'
140	150	3300	-1 50'	158	210	1050	-2 50'
162	162	2700	0	189	169	891	0°
193	175	1488	+0° 41'	193	175	1488	+0 42'
193	193	1050	0°	193	228	1839	-1 05'
216	162	2700	+1 06'	193	175	1050	+0° 59'
216	189	2430	+0 36'	193	245	1750	-1 45'
245	228	1750	+0° 34'	263	210	1138	+3 40'
245	245	2500	0	263	263	1238	0°
263	263	3500	0°	280	245	1750	+1 00'
263	253	2925	+0° 19'	280	263	1760	+0 35'

(P internal diameter of the vessel in micra toward the heart; D internal diameter of the vessel in micra toward the capillary system; L length in micra between P and D; T degree of taper (sin P D/L).)

TABLE 2  
A comparison of the internal diameters of mesenteric vessels in the rat which were parallel to each other with their tapers

Vessel	Proximal (P)	Distal (D)	Length between proximal and distal measurement (L)	Angle of taper (d P D/L)
Arteriole	210	210	122	0
Venule	350	350	122	0
Arteriole	228	210	675	+1 11'
Venule	438	419	675	+1 14'
Arteriole	105	105	875	0
Venule	175	210	875	-1 18'
Arteriole	175	175	1575	0°
Venule	262	227	1575	+1 16'
Arteriole	88	70	1050	+0 59'
Venule	175	123	1050	+2 52'
Arteriole	123	158	1050	-1 09'
Venule	263	175	1050	+4 0'
Arteriole	210	210	1050	0
Venule	385	350	1050	+1 49'
Arteriole	123	140	700	-1 23'
Venule	263	263	700	0
Arteriole	189	169	2700	0
Venule	270	297	2700	-0 31'
Arteriole	213	216	2700	+0 31'
Venule	378	405	2700	-0 31'
Arteriole	140	123	1750	+0 25'
Venule	280	263	1750	+0 33'

TABLE 3

The peripheral plasma layer axial stream and linear velocity of blood flow in mesenteric arterioles

Internal diameter (ID)	Peripheral plasma layer (PPL)			Linear velocity blood flow <sup>1</sup>	Axial stream	Ratio TTPL:ID
	A	B	Total PPL			
$\mu$	$\mu$	$\mu$	$\mu$		$\mu$	
FROG (Selected from 1,148 measurements)						
28	2.2	2.2	4.4	4+	23.6	1.84
28	4.4	6.5	10.9	3+	17.1	1.25
32	4.1	3.5	7.6	1+	24.4	1.43
36	2.6	5.2	7.8	4+	29.3	1.46
65	6.0	6.0	12.0	4+	83	1.54
65	13.0	0	13	1+	82	1.5
74	3.6	3.6	7.2	3+	66.6	1.18
75	3.6	3.6	7.2	3+	67.3	1.10
90	2.7	1.4	4.1	1+	64.9	1.22
90	6.3	4.5	11.8	3+	78.5	1.79
90	11.7	9.9	21.6	4+	63.4	1.43
102	4.1	9.0	13.1	4+	86.9	1.77
105	4.1	9.0	13.1	4+	91.9	1.8
118	3.0	3.6	6.6	4+	109.5	1.18
117	2.7	2.5	5.2	4+	111.6	1.22
137	3.6	0	3.6	4+	123.4	1.38
137	8.1	10.8	18.9	4+	116.1	1.73
145	4.5	0	4.5	4+	140.5	1.32
147	7.8	8	15.8	4+	131.3	1.93
180	5.4	3.6	9	4+	171	1.20
180	2.7	0	2.7	4+	177.3	1.67
201	9	5.4	14.4	4+	166.6	1.14
202	4.5	2.7	7.2	4+	197.6	1.28
232	4.5	7.2	11.7	4+	40.3	1.21
232	9	8.1	17.1	4+	234.9	1.15
270	5.3	6.3	11.6	4+	256.4	1.23
270	2	7.2	14.4	4+	235.6	1.19
RAT (Selected from 338 measurements)						
5	1.0	1.0	2.0	4+	3	1.25
8	1.1	0.8	2.0	4+	3	1.23
10	1.5	1.2	2.7	4+	7.5	1.37
10	1.5	1.3	2.8	4+	2	1.26
15	3.1	2.4	5.7	4+	9.3	1.26
18	2.5	1.6	4.3	4+	10.7	1.35
20	2.3	2.3	4.6	4+	10.7	1.44
20	1.3	1.7	3.0	4+	17	1.67
23	1.3	1.7	3.0	4+	20	1.77
23	2.0	0	2.0	4+	21	1.115
33	0	2.0	2.0	4+	31	1.165
33	2.8	1.1	6.0	4+	28	1.66
35	6.0	6.0	12.0	4+	23	1.3
35	6.3	5.9	12.2	3+	22.6	1.23
47	6.9	7.0	13.9	3+	33.1	1.34
47	7.0	7.2	14.2	4+	36.6	1.33
93	11	2.2	3	4+	90.6	1.42
100	3.0	2.5	4.5	1+	93.3	1.22
108	2.5	3.0	5.5	1+	102.5	1.19
130	3.0	3.5	6.5	4+	123.5	1.22
135	3.0	3.0	6.0	4+	129	1.22
135	3.0	3.5	6.5	4+	128.5	1.21

<sup>1</sup> Linear velocity of blood flow, 4- blood flow so rapid that no cellular discrimination was possible  
 3 cells barely discriminated, 2 cells readily discriminated, 1 cell flows slowly, 0, no flow

TABLE 4

*The peripheral plasma layer axial stream and linear velocity of blood flow in mesenteric venules*

Internal diameter (ID)	Peripheral plasma layer (PPL)			Linear velocity blood flow	Axial stream	Ratio TPPL:ID
	A	B	Total PPL			
A	A	B	A	FROG		
				(Selected from 806 measurements)		
37	8.1	7.2	15.3	4+	21.7	1.24
61	5.4	9.0	14.4	3+	48.6	1.43
100	12.6	17.1	30.7	4+	70.3	1.33
104	1.0	1.7	2.7	3+	101.3	1.38
110	6.3	8.4	14.7	3+	66.5	1.94
123	6.5	1.0	1.5	3+	121.5	1.62
134	4.5	3.0	7.5	3+	123.5	1.18
137	6.3	8.4	14.7	3+	125.3	1.18
151	6.3	9.7	9.0	3+	143.0	1.17
180	4.5	0	4.5	3+	175.5	1.40
180	4.5	4.5	9.0	3+	171.0	1.20
230	5.4	9.0	14.4	3+	225.6	1.16
230	8.1	9.0	17.1	3+	212.9	1.14
250	7.2	8.4	12.6	4+	237.4	1.20
273	0	9.0	9.0	4+	254	1.13
275	5.4	7.2	12.6	1+	262.4	1.23
286	9.0	13	22	4+	204.0	1.18
290	11.7	11.7	23.4	4+	265.6	1.13
325	6.0	6.0	12	4+	313	1.22
328	4.5	7.2	11.7	4+	316.3	1.28
380	7.2	8.4	12.6	4+	347.4	1.29
380	5.4	3.6	9.0	4+	351.6	1.40
377	6.0	4.0	10	4+	367.0	1.38
416	13.0	13.0	26	4+	390.0	1.16
				RAT		
				(Selected from 496 measurements)		
8	0.9	1.1	2.0	3+	8.0	1.29
9	0.9	1.3	2.1	3+	8.9	1.39
10	1.2	1.0	2.2	4+	7.8	1.43
10	1.0	1.1	2.1	4+	7.9	1.47
13	1.5	1.5	3.0	4+	10.0	1.43
13	1.4	1.5	2.9	4+	10.1	1.45
14	1.5	1.5	3.0	4+	11.0	1.46
14	1.4	2.0	3.4	4+	10.8	1.41
16	2.1	1.7	3.8	4+	12.2	1.42
16	3.6	4.0	7.6	4+	8.4	1.21
18	1.7	2.5	4.0	4+	14.0	1.43
18	1.6	2.1	3.7	4+	14.5	1.48
20	1.9	1.7	3.6	3+	16.4	1.53
20	1.6	2.0	3.6	4+	16.4	1.53
23	3.6	4.5	7.5	4+	15.8	1.3
23	1.4	2.0	3.4	4+	19.6	1.68
25	3.3	4.0	7.3	4+	17.7	1.33
25.1	3.3	3.8	7.1	4+	18.0	1.36
30	3.3	3.5	6.8	4+	25.8	1.44
30	2.0	3.0	5.0	4+	23.0	1.6
34	2.3	1.6	4.9	4+	22.0	1.7
35	3.2	1.5	4.7	1+	30.3	1.73
40	8.8	8.0	10.3	4+	29.7	1.39
40	5.7	6.0	11.7	3+	28.3	1.24
50	11.0	16.5	27.5	3+	22.5	1.18
110	5.7	3.8	6.3	4+	104.5	1.17
110	3.7	4.4	7.1	4+	102.9	1.16

Linear velocity of blood flow 4 blood flow so rapid that no cellular discrimination is possible  
 3 cell barely discriminated 2 cells readily discriminated 1 cell flowing slowly 0. no flow

TABLE 5

A comparison of the average ratios of the internal diameter (ID) of mesenteric arterioles and the peripheral plasma layer (PPL)<sup>a</sup>

FROG			RAT		
Internal diameter	PPL ID		Internal diameter	PPL ID	
	Arterioles	Venules		Arterioles	Venules
60-70	1.0	1.7	5-10	1.4	1.4
80-90	1.18	1.15	11-15	1.4	1.5
91-100	1.18	1.18	16-20	1.4	1.5
101-130	1.17	1.19	21-25	1.9	1.4
131-140	1.16	1.19	26-30	1.7	1.6
141-180	1.16	1.34	31-35	1.7	1.6
181-170	1.17	1.28	36-40	—	1.5
171-180	1.24	1.26	41-45	—	1.7
181-190	1.34	1.20	46-50	—	1.7
191-220	1.23	1.24	100-135	1.21	1.13
221-240	1.23	1.26			
241-270	1.21	1.26			
271-300	1.22	1.24			

<sup>a</sup>Total peripheral plasma layer.

the vessel increased the ratio decreased. Or as the peripheral plasma layer increased the diameter of the vessel decreased. Exceptions occurred.

A study was made of the peripheral plasma layer as it was effected by altering the intravascular pressure locally and by changes in the linear velocity of flow. Linear velocity of flow was influenced by altering the depth of anesthesia or by the local application of epinephrine which increased the local intravascular pressure. A wide variety of responses occurred. The peripheral plasma layer decreased did not change, or increased as the linear velocity of flow decreased (tables 3-4). In general as the linear velocity of flow decreased so did the peripheral plasma layer. However when the linear velocity became sufficiently slow so that the gravitational forces became greater than the propulsive forces engendered by the heart and great vessels sedimentation occurred and the peripheral plasma layer became increasingly larger toward the top of the vessel. When the intravascular pressure increased and the linear velocity of flow decreased due to peripheral constriction occurring after the application of epinephrine locally (the pressure being measured by an indwelling rigid microcannula connected to a transducer) the peripheral plasma layer decreased. In those instances where the layer increased cellular sedimentation was occurring.

### The axial stream

In the transilluminated blood vessel of the arterial and venous systems the flowing cells appear as a red column, the axial stream, usually surrounded at the periphery by a colorless margin the peripheral plasma layer. (An axial stream exists essentially only in vessels whose diameters are greater than three to five times the smallest diameter of the species erythrocyte. Frequently in the center of the stream a more transparent central stream or core is observed.) While the axial stream exists in all vessels but capillaries difficulties were encountered in detecting and measuring the more transparent core in the microvascular system of the rat. In 798 measurements of the peripheral plasma layer and axial stream in these animals only 10 measurements of the core were possible. Therefore the results which pertain to this core were data derived from the frog where 208 measurements were made in the arterial and 189 in the venous circulations. The greatest sources of error in measuring this axial core were that it was difficult to establish the peripheral boundary of this core and to determine the velocity of linear flow. These parameters had to be measured almost simultaneously and no entirely satisfactory method was found. The minimum error existed when the linear velocity was rapid and maximal. When this occurred



maximum contrast existed between this portion of the axial stream and the peripheral portions of the axial stream. But as rapid flow was defined as the lack of visual perception of any cellular detail in the stream, there was a rather wide latitude between this and the actual maximal linear rate of flow.

The ratio of the core of the axial stream and the diameter of arterioles was relatively constant for any linear velocity of flow. The ratio was 1:4 for arterioles whose diameters measured 20 to 160  $\mu$  and 1:4.4 for those measuring 160 to 300  $\mu$  when the linear velocity of flow was rapid. When there was a perceptible slight reduction in linear velocity the ratio decreased to 1:2.4 in arterioles measuring 20 to 160  $\mu$  but was unchanged for the larger arterioles.

The ratio was 1:1 to 1:1.2 for arterioles up to 300  $\mu$  for the axial stream (ID AS) when the linear velocity of flow was so rapid that cellular detail could not be observed or when occasional cellular detail was visible. A similar relationship was found for venules.

In general as the linear velocity of flow increased the diameter of the axial stream decreased. Conversely as the flow rate decreased, the diameter of the axial stream increased, reaching its maximum diameter when flow stopped but before sedimentation of the cells occurred.

#### *Microspectrophotometric study of the peripheral plasma layer and axial stream*

In these studies the mesentery was supported vertically and transilluminated at wave lengths of 355 407 414 435 519 625 m $\mu$  and in white light. Maximum contrast between the blood and vessel wall was obtained when the tissue was transilluminated at 414 m $\mu$  because at this wave length the hemoglobin absorbed intensively turning the column of blood black against a light purple background (figs. 14 16 20 25 26 28). When such an image was projected onto the face plate of an image orthicon television camera tube and the image displayed on a monitor there was further control of brightness and contrast of the blood and the vessel wall (fig. 14). These factors helped by

sharply delineating the erythrocytes and the vessel wall thereby increasing the accuracy in measuring the peripheral plasma layer and axial stream. The more transparent core of the axial stream was not visible at 414 m $\mu$  because the blood stream was opaque. Another advantage of studying the blood stream at this wave length was that the leucocytes appeared as colorless globules among the black erythrocytes. They were found to be randomly distributed throughout the blood stream by all methods used in this study. Preponderance of leucocytes at the periphery of the stream occurred only when pathology was present.

#### *The analysis of blood flow with high speed cinephotomicrography*

About 800 experiments were made during the past 7 years where the blood flow in the vessels of the microvascular system were recorded with high speed photography. In more than 650 of these experiments blood flow was recorded from the mesentery while about 50 recordings were made from the liver lung and skeletal muscle of frogs (*Rana pipiens*). Approximately 75 recordings were made from the mesentery of rats and 25 from the lungs of rabbits. Each recording consisted of 100 feet of film.

In the description of the experiments which follow the data from the mesenteric circulation were selected as examples due to the greater number of experiments which were made in this tissue. Similar data were obtained from the circulation in the vessels of the lung and skeletal muscles. No satisfactory data however were obtained from the liver.

#### *The peripheral plasma layer*

When the film of blood flow in mesenteric arterioles which had been taken at framing speeds of 480 to 7 600 per second was analyzed and compared with film of the same vessels which had been taken at 16 or 24 fps there was considerable difference in the appearance of the peripheral plasma layer. In the control film 16 or 24 fps the peripheral plasma layer was a sharply defined clear zone but when the high speed motion picture film was studied the layer extended in an irregular

manner toward the center of the vessel. Its complex configuration was unstable changing every few msec. Such spaces or "layers" were interspersed by erythrocytes which slid against the wall and a few msec thereafter another irregular "peripheral plasma layer" recurred (figs. 18-20). For example a peripheral plasma layer in an 80  $\mu$  arteriole (frog) extended as much as 30 to 40  $\mu$  toward the center of the vessel and was maintained for a distance of approximately 100  $\mu$  before changing its configuration. In such instances the cellular components were stable in regard to their position for approximately 100  $\mu$  or 5 msec.

In venules whose diameters ranged between 50 and 500  $\mu$  the pattern of the peripheral plasma layer was similar to that of the arterial system (fig. 28). The principal difference was that in venules the rate at which the cells changed their position was slower.

#### Axial stream

The diameter of the axial stream was not measured *per se* from the high speed motion picture film because of the irregularity in its configuration which has been described in the section on the peripheral plasma layer.

#### The behavior of erythrocytes in flowing blood

Movement of the amphibian and mammalian erythrocytes was decreased sufficiently in the arterial and venous circulations to trace the pathway of these cells through contiguous frames of the motion picture film when the recording rates were greater than 2,800 frames per second, in frogs under light anesthesia and in rats under deep anesthesia. Under these conditions cellular movement was never stopped entirely even in terminal arterioles at framing rates up to 4,000 fps for the amphibian and 7,600 fps in the mammal when the cells were magnified  $\times 200$  to  $\times 500$ . The best cellular discrimination was obtained by using a  $\times 50$  water immersion objective with a  $\times 10$  ocular. The determining factor in the study of the movement of the cells was the diameter of the vessel. For the frog the limiting internal diameter was approximately 100 to

150  $\mu$  and for the rat 30 to 40  $\mu$ . The ideal condition was one in which not more than one or two cells were interposed in the optical path, conditions found only at a distance extending 5 to 40  $\mu$  from the internal wall of vessels.

The total length that any cell could be followed was a distance of 100 to 150  $\mu$  when an initial magnification of 500 $\times$  was used. Not infrequently the cell moved out of focus in about half this distance. Both in the rat and frog the forward movement of the erythrocyte was complex in the arterial and venous circulations. In arterioles (*Rana pipiens*) with internal diameters ranging between 150  $\mu$  and 35  $\mu$  the cells described a helical pathway. The forward movement consisted of an apparent attempt of alignment of the long axis of the cell in the direction of flow. To achieve this a rotational movement of the cell occurred about its short and long axis. During its movement toward the capillary a complex path of motion was described which consisted of a decreasing helical spiral, decreasing as the cell moved toward the center of the moving column of blood. In traversing this pathway the cell produced a sphere of disturbance in the plasma and affected other cells by striking them, thereby modifying their flow pattern.

In vessels greater than 150  $\mu$  in diameter it was possible to trace cells for short distances and their pathway if anything was more complex than in vessels with smaller diameters. At bifurcations (arterioles) erythrocytes not infrequently first moved 45 to 90 across the width of the tributary vessel before describing the spiral pathway described above.

Adequate analysis of the cellular flow pattern in the arterial system of the rat has been limited to vessels to about 20  $\mu$  and then only under deep anesthesia. Most of the analyses have been made from film which recorded the circulation at 3,600 fps. The pilot experiments which were made with the Wollensak Fastex WF3 camera at 7,600-8,000 fps did not stop the movement of cells in arterioles and the quality of the images were inadequate for tracing the pathway of cells therefore the Eastman Camera was used and the

linear velocity of flow reduced approximately to that of the frog's circulation.

The size of the rat's red-cells precluded the analysis of cellular movement in vessels whose internal diameter exceeded 20 to 30  $\mu$  due to the overlaying of too many cells in the optical path. (Rat erythrocytes in the circulation measured 3-3.5  $\mu \times 7 \mu$ )

Critical analysis has been possible of the flow of rat erythrocytes in 9  $\mu$  to 15  $\mu$  mesenteric arterioles when recorded at 3,600 fps. The complexity of the cellular behavior was not appreciated from observing the film at projection rates of 16 fps. At these projection rates the position of erythrocytes was noted to be at various angles in regard to the direction of flow varying from a right angle to being parallel to the wall (figs. 29-30). Frequently cells adjacent to each other were oriented differently. In general, the cells had different rates and degrees of orientation from each other. Some red-cells changed their orientation 360° within a distance of 15  $\mu$  to 40  $\mu$ , equivalent to 2-10 msec (figs. 2-4). Other cells did not appear to change their position for a distance equal to width of the motion picture frame approximately 100  $\mu$ . It was found that this was not so when the pathway of such cells were traced through sequential frames. Such cells had a corkscrew helical pattern of motion similar to that described for the frog.

The distortions of the rat erythrocytes and their alterations in position in the stream are illustrated in figures 2 to 4. Like the amphibian red-cell that of the rat had a helical forward motion turning on its long and short axes but doing so much more frequently. Furthermore considerable cellular distortion occurred and

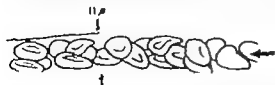


Fig. 2. A cine tracing of a single motion picture frame to 11 frames showing the orientation of erythrocytes in 11  $\mu$  mesenteric arteriole of the rat photographed at 1/15,000 second (3,600 fps). (All cells in the vessel were traced.) Compare with figures 3, 4, 29 and 30.

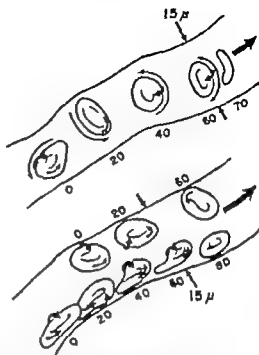


Fig. 3. Cine tracings through sequential frames of the flow pattern of 3 erythrocytes in a mesenteric arteriole of the rat (each exposure 1/15,000 sec or 3,600 fps). The number along the vessel indicates the number of frames between tracings and the arrows (thin) the direction in which the cell were spinning. The broad arrows indicate the direction of blood flow. Note the cellular distortion.

this in vessels which were three to five times wider than the greatest dimension of the cell. Red-cells were compressed, lengthened, folded, or twisted. Undistorted forms existed only a few msec. In other words the undistorted form occurred no more frequently than the multitude of intermediate forms. Cells were lengthened to 10 or 10.5  $\mu$  being about 50% longer than the normal. Such alterations in shape occurred through distances as short as 15  $\mu$  equivalent to 7 msec in straight or curved arterioles where bifurcations were either proximal or distal.

In venules a similar complexity in the cellular flow pattern existed. Sometimes cells remained in a lamina for a long period of time and their rotational changes were slower (figs. 27-28). The movement of cells in the lamina adjacent to the plasma stream in confluent streams has not been studied.

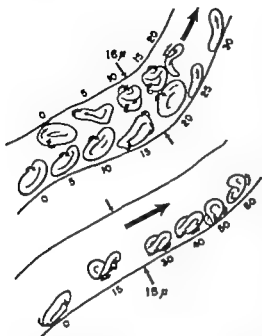


Fig. 4 The same arteriole as in figure 3. Cine tracing of three other erythrocytes. Photographic data as in figure 3. Shading denotes the opposite side of the cell. Note lengthening, compression, and folding of cells, occurring within 1/180 to 1/360 sec.

*The movement of erythrocytes in vessels whose diameters were approximately that of the cell*

The vessels which were of the same magnitude as the cell, or less, were the terminal segments of the arterial system and capillaries.

The orientation of cells in terminal arterioles was also different from what had been expected either from direct visualization or from recordings of this circulation by cinephotomicrography at 16-64 fps. With the standard methods of recording streamlines were seen (fig 21). Since the vessels were just slightly wider than the longest dimension of the erythrocyte the cells were presumed to be flowing parallel to each other with their shortest diameter oriented in the direction of flow. There was present also a small but constant peripheral plasma layer. When this circulation was analyzed from motion picture film taken at framing speeds of 2,200 to 3,800 per second an entirely different

picture was revealed. The erythrocytes were randomly oriented. Many erythrocytes were oriented with their largest dimension at right angles to the direction of flow (figs. 22 and 23). Other cells had their shortest diameter oriented to the direction of flow or were oriented between these two extremes.

Deformation of the erythrocytes was common (figs. 22-24). Cells which were flowing at right angle to the wall were distorted so that they were either convex or concave.

The number of cells per unit volume of blood varied in terminal arterioles. Per millisecond, the cellular concentration of erythrocytes varied (in 50  $\mu$  segments of arterioles) from zero to nearly all cells. In these arterioles plasma skimming had not been observed in the control film nor during direct visualization.

In capillaries whose internal diameters were greater than the largest diameter of the erythrocyte the red cells were oriented similarly to those in arterioles. When the diameter of the vessel was less than that of the erythrocyte the cells were elongated and folded (compare fig. 25 with fig. 26).

A statement of the behavior and distribution of leucocytes as analyzed from high speed cinephotomicrography was not possible because too few of these cells were encountered. When such cells were observed they were randomly distributed in respect to their position in the vessels of the arterial, venous and capillary systems.

#### *Cellular velocity*

The linear velocity was calculated for 51 erythrocytes in arterioles of the frog and 37 in the rat from the high speed film. The velocity of cellular flow in the frog was as follows: in 25  $\mu$  arterioles from 3.0 to 10.2 mm/sec with an average of 5.9 mm/sec; in 35  $\mu$  arterioles from 2.6 to 9.0 mm/sec with an average velocity of 6.6 mm/sec; and in 150  $\mu$  arterioles from 2.4 to 13.2 mm/sec with an average of 6.4 mm/sec. In the rat the velocity of erythrocytes in 9  $\mu$  arterioles averaged 2.23 mm/sec, varying from 1.98 to 2.41 mm/sec; in 13  $\mu$  arterioles the average rate was 1.32 mm/sec with a range of 0.74 to 2.16 mm/sec; and in 16  $\mu$  arterioles the

average rate was 2.13 mm/sec with minimum rate of 1.67 and a maximum of 4.5 mm/sec.

Using the above data, calculations were made to determine how long it would require 100 000 frog erythrocytes to flow through arterioles which were approximately the diameter of the cells. For a flow rate of 2 mm/sec it would require 14 minutes for these cells to flow through a 27  $\mu$  arteriole and 7.5 minutes if the rate was 4.5 mm/sec in a 26  $\mu$  arteriole.

#### *The dimension of amphibian erythrocytes in the arterial circulation*

It was possible to measure the dimensions of frog erythrocytes in arterioles from the high speed film. While many thousands of cells were sketched 201 were oriented at an angle which permitted measuring one of their three dimensions.

The length of 128 erythrocytes was measured. The average cell's length was 25.1  $\mu$  with a maximum of 34  $\mu$  and a minimum of 22  $\mu$ .

The width was measurable in 24 cells whose average was 16.1  $\mu$  with a minimum of 13  $\mu$  and a maximum of 19  $\mu$ .

In 49 cells the average thickness was 5.8  $\mu$  and it varied between 3  $\mu$  and 9  $\mu$ .

#### *Film*

Adequate exposure for analysis of blood flow was obtained with Kodachrome Type A, Eastman Ektachrome ER and TriX negative films at framing rates to 3 600 per second using white light from the mercury (Osram) or tungsten light sources at microscopic magnification to  $\times 550$ . TriX film has been overexposed at 8 000 fps with the Osram mercury light source at a magnification of  $\times 500$ . In general when monochromatic light was used TriX film was most satisfactory. Kodachrome Type A film gave the best definition although normal color balance was not achieved due to the mercury light source and the underexposure which usually occurred at the maximum recording rates.

#### *DISCUSSION*

To bring the data of this study into perspective with those of others (Bayliss '52, Bloch '56; Brookes and Monro '37, Harding and Knisely '38, Jager '35, Jeffords

and Knisely '56; Knisely et al. '47, '60, Lutz et al., '50; McDonald and Potter '49, McDonald '52b, Ralston and Taylor '45, Taylor '55, Thoma, '27) the discussion is divided into: instrumentation, the peripheral plasma layer and axial stream as observed with standard recording methods, and then these data are compared with data derived from high speed cinerocording.

This study has differed from others wherein the rheology of blood was studied by using several methods to examine blood flow in living microscopic vessels. The procedures have permitted an evaluation of the advantages, limitations and a statement of the requirements of the methods which may lead to a more complete characterization of the rheology of blood *in situ*. To achieve such a goal it is necessary to measure in the living microvascular system the volume of blood in a segment of vessel, the rate of flow and the pressure. The present status of the ability to measure these components is as follows:

Blood volume may be calculated in any arbitrarily selected segment of a vessel providing that the vessel is small enough at least to discriminate all of the erythrocytes. Static volume can be determined from the cinephotomicrographic image of the vessel which is projected simultaneously with a calibrated scale whereby the numerical magnitudes are obtained. These values are then inserted into standard formulas for determining the volume of a cone or cylinder. Dynamic cellular (erythrocyte) volumes may be calculated by inserting the values of the dimensions of properly oriented cells in the circulation into formulas which describe the volume of biconcave discs or ellipsoids. (The dimensions of width and length of the frog erythrocytes which were measured in the living circulation, av.  $25.1 \times 16.1 \mu$  were in agreement with the av.  $25.0 \times 17.0 \mu$  which were obtained of similar cells *in vitro* suspended in physiological solutions and with the literature (Knisely et al. '60).) Only an average cellular volume can be obtained due to the variation in size of erythrocytes and the probability that platelets or leucocytes may be missed because of superimposed erythrocytes.

While this error will occur probably its magnitude is small because the number of leucocytes and platelets in such a volume is small and frequently these cells are absent. Thus the total cellular volume is realistically the total red-cell volume.

The linear velocity of cellular flow in the arterial and venous systems can be determined from high speed cinerecording in vessels whose diameters do not exceed 100  $\mu$  for the amphibian and 30  $\mu$  for the mammalian circulation. In this study the cellular velocities which were calculated were average velocities because the framing rate was determined by measuring the number of frames between the exposed strips of film from the beginning of one strip to the beginning of the next one (25 frames for a frame speed of 3 000 per sec.) It is possible that the rate of film travel may vary during this distance without altering the total length of the strip. While this may be infrequent in occurrence it is a possible source of error which can be eliminated and was, in a few experiments by photographing a time signal on each motion picture frame. A more serious criticism of the method is that the analysis is sharply limited by the focal depth of the optical system which will only permit the resolution of cells at the periphery of the moving column of blood in vessels whose internal diameters exceed the species erythrocytes 5 to 10 times.

Historically the linear velocity of blood cells in the microvascular system was first determined by Leeuwenhoek (1798) and since that time many investigators have studied this problem by measuring either cellular flow or whole blood flow in either the gross or microvascular systems (Vierordt, 1862; Tigerstedt, '05; Basler '27; Brookes and Monro '57; McDonald '52a). Of all the methods which have been devised to date the one that apparently produces the least derangement of vascular physiology and can be used in the unanesthetized and unrestrained animal is the electromagnetic flow meter (Kolin '36; Kolin et al. '57; Olmstead '60). Until a similar method can be developed for the microvascular system the high speed cinephotomicrographic method

holds the most promise for measuring cellular flow rates.

The linear velocities of red-cell flow in arterioles obtained in this study represent but special instances of physiology and cannot be considered representative for the species. Considerable more data are needed before representative values can be established.

In this study only one of the many high speed cameras was used to any extent. A variety of high speed cameras were available (Garvin, '51 Industrial Photography '59). Many of the high speed cameras were not applicable to the study of biological events because of the light intensities required. For example, the light which would be required to expose film at framing rates of  $10^3$ – $10^4$  per second, would preclude any degree of homeostasis. It would, however be desirable to utilize cameras with framing rates of 15 to 30 000/sec. Such framing rates will probably be required to study the detail of cellular flow in the microcirculation in small mammals under minimum anesthesia and with adequate magnification. (In the present study the Eastman camera gave superior images to the Fastax instrument.)

Other methods exist which may be applicable for measuring cellular velocity in the arterial and venous circulations. P. A. G. Monro ('60) and Brookes and Monro ('57) described a method which employed a pulsed cathode ray beam transilluminating the tissue (rabbit ear chamber). The microscopic image of blood flow was transilluminated first at a rate of one msec and the frequency was reduced until there was no apparent movement of the cells when the frequency was reduced further the apparent direction of cellular motion was reversed. Quantitative data of cellular flow rates were not reported. This method indicates that it is possible to determine the linear velocity of flow in mammals by obtaining cellular discrimination at frequencies below 1 000 sec. In the present study no reversal of flow was seen when the flow was recorded continuously from 480 to 7 600 fps. It would appear that a frequency of 1 000 per sec or less which was used by Monro is an untrustworthy value to use for calculating the linear velocity of cells.

It would be desirable to determine the velocity of plasma flow but at present no methods are available for determining this value in the microvascular system simultaneously with the other parameters.

The other parameter which is required for determining the rheology of blood is the pressure at two points within the microscopic vessel. Since blood flow varies during the cardiac cycle dynamic pressures must be obtained. Progress is being made to achieve such measurements. Dynamic pressuregrams can be obtained in vessels whose internal diameters are as small as  $80 \mu$  (Rappaport et al., '59). At present the smallest useful internal orifice of the cannula is  $35 \mu$  whereby an adequate frequency response is obtained.

From this brief review of methods it is suggested that sufficient advances have been made in instrumentation that an approximation of the rheologic characteristics of blood can be made at the microscopic level *in situ* which is anticipated to be more meaningful than determinations made *in vitro*. And these data, when they are inserted into meaningful equations, will characterize the rheology of blood in the living system the goal since the time of Poiseuille (1842).

One other method the image converter system (Wachtel et al. '58) is perhaps worth mentioning for the study of the dynamic morphology of cells in circulating blood. This system has unique advantages for the study of dynamic biologic events because it is a light amplifier has good resolution and is relatively simple. With this system it is possible to transilluminate a tissue with light intensities which are equal to or less than those which are used for direct visualization. In this method the image from the microscope is projected on to the face plate of the converter. Within this tube the intensity of the image is amplified and projected on to the distal part of the tube which contains a fluorescent screen. There is a wide range in the frequency at which this image can be displayed. For example an image can be displayed at a frequency of  $1 \times 10^4$  sec ( $1 \mu$  sec) and be repeated at such a frequency or repeated at msec sec or minute intervals. The intensity available on the fluorescent screen how-

ever for recording such images on motion picture film is probably of the order of magnitude equivalent to standard recording rates.

No new data were obtained in this study in regard to blood flow in vessels of the microvascular system by standard microscopy using white light. The data were in agreement with other reports (Bloch '56 Clark and Clark, '55; Knisely '47; Lutz et al. '50 Nicoll and Webb '48). Again it was found that the images of cellular blood flow in the microvascular system appear to be so rapid that cellular discrimination is absent in all vessels but capillaries, that visible aggregates are absent, and that the peripheral plasma layer is cell free.

Detailed reports do not exist of blood flow analyzed with television microscopy although investigators have used the vidicon and image orthicon systems in monochrome and color have indicated some of the advantages gained from the use of television, and have made cine-recordings to illustrate these points (Bloch et al. '58 Warner and Brown, '60). Detailed analysis was not attempted in this study. When white light was used with the monochrome television system, the only gain was the ability to have some control of contrast most of which resided in the vessel wall and in the tissue. (This discussion is limited to those factors pertaining to information of structure and reaction not to other factors inherent in these systems such as light and size amplification which do not necessarily increase resolution and thereby information.)

This study is also in essential agreement with those who state that arteries and veins of all sizes are cone shaped with the taper of the cone in the direction of the capillary system. (Capillaries are considered to be cylinders.) The only quantitative data to support this concept is the report of Jeffers and Knisely ('56) although the photographs of many investigators support the concept qualitatively. In this study considerable variation was found in the degree and direction of the taper. Some of the data were in agreement with Jeffers and Knisely and others were not. The discrepancy in the data was not due to animals or tissue since

they were similar in both studies and in both the mesentery had to be spread to visualize the vessels. In this study as many as 6 different observers reported similar results with regard to the variation in the direction of the "normal" taper although there was some difference in the magnitude of the measurements made by these observers. Perhaps the data reported by Jeffers and Knisely were selected deliberately to illustrate the general principle of taper with which this report concurs. The important point is that in the characterization of blood flow its rheology the direction of the taper of the vessel cannot be taken for granted but must be determined.

It is surprising that published quantitative data were absent on the magnitude of the peripheral plasma layer and axial stream in the living-microvascular system although every time the system is observed these parameters are seen. The relation of peripheral plasma layer and axial stream to the internal diameter of vessel are important factors in the study of the rheology of blood because the ratio of cells to plasma would affect the viscosity of the fluid. It has been repeatedly demonstrated *in vitro* that the viscosity of blood decreases as the diameter of the tubes decrease especially in those which are comparable in size to those in the living microvascular system (Bayliss '52, '59; Fahræus and Lindqvist '31; Hagenbach 1860; Haynes '60; Poiseuille 1842; Taylor '55). Such a decrease in viscosity is presumably due to a decrease in the number of cells per unit volume of blood. This was indicated by the change in ratio of the peripheral plasma layer and the diameter of the vessel. The ratio of the peripheral plasma layer was found to decrease as the vessel decreased in size with a ratio of 1:4 in the smaller vessels to a ratio of 1:20 or more for the larger vessels of the microvascular system.

The question of the ability to measure the peripheral plasma layer accurately has been questioned recently (Bayliss '59). In the past this layer has been noted with such ease that at one time it was suggested that a membrane existed between the peripheral plasma layer and the axial stream because they were so sharply

demarcated (Thoma '27). Recently Taylor ('55) and Bayliss ('59) have applied absorption microscopy to the study of blood (human dog) flow through narrow glass tubes. Bayliss ('59) has found that in no experiment was the transmittance of a magnitude which would indicate that all of the erythrocytes had left the peripheral plasma layer. Furthermore, the increase in transmittance was not correlated with the reduction in apparent viscosity nor was it possible to determine to what degree the erythrocytes were oriented in the direction of flow. Corroborative evidence of the presence of erythrocytes in the peripheral plasma layer was also obtained in the present study when blood flow was examined with monochromatic light at a wave length at which intense absorption of hemoglobin occurred and the stream observed with either standard or television microscopy. And like Bayliss found it was not possible to state to what extent the cells were oriented in the direction of flow as the flow rates increased except when the flow became pulsatile at which time the erythrocytes were randomly oriented during the time of zero flow. (Zero flow however has never been demonstrated during the normal cardiac cycle in the arterial vessels of the mesentery the lung or in skeletal muscles. Pulsatile flow with a zero flow component, was produced artificially by the local application of epinephrine.) Also, when dynamic pressures were determined in the vessel simultaneously with flow and the peripheral plasma layer wide variations occurred in flow and pressure without a significant alteration in the peripheral plasma layer. One consistent finding was that as the diameter of vessels decreased the peripheral plasma layer increased the smaller the vessel the larger the peripheral plasma layer capillaries excepted.

What was learned of blood flow that had not been known when the data of blood flow determined by standard methods were compared with data derived from the high speed cinerecording method?

Perhaps one of the most unexpected results of the analysis was the finding that streamlines were no indicator of either cellular orientation or position. This fact was most significantly demonstrated in



the smaller branches of the arterial system. When the flow of blood was observed either with the microscope directly or from film which recorded this flow at normal framing speeds, obvious streamlines were present suggesting that the cells were flowing parallel to each other. This was emphatically not the case when this flow was studied from the high speed film. There was found to be a random orientation of the cells. Then why did the flow appear streamlined? Probably because the edges of groups of randomly oriented cells were fused in the visual integrating system of the observer as well as by the film (standard recording frequencies) to give the appearance of streamlines. Therefore neither the eye nor the standard photographic procedures were capable of resolving the true position or orientation of the cells.

The rate of reorientation of the cells especially in the mammalian (rat) arterial circulation was surprisingly rapid. Such changes could occur within a few msec. This fact was not determined even from study of the high speed film at normal projection speeds but only by tracing single cells through sequential fields. There does not appear to be any indirect evidence that this could occur.

The concept and fact is common knowledge that capillaries can contain primarily plasma when ingress to the vessel has been partially occluded (Krogh '29). This phenomenon of plasma skimming, however had not been observed in the arterial or venous system when the diameter of the vessel was greater than the largest dimension of the erythrocyte. In this study it was demonstrated by analysis of the high speed film, that the cellular concentration per unit volume could vary and therefore plasma skimming could occur in these vessels. This was found in both the amphibian and mammalian circulations and is suggestive that it may be a common pattern of cellular flow.

The question has been raised by the *in vitro* studies of Bayliss ('39) that the peripheral plasma layer is not free of erythrocytes and by the present study where standard methods of visualization were combined with monochromatic light whereby occasional erythrocytes were found in

this layer. The presence of cells in this layer was elucidated further from the analysis of blood flow with high speed cinerecording. Erythrocytes were found frequently in very close proximity to the wall apparently touching the wall or 1-2  $\mu$  from it sometimes in nearly every frame of the film. Also in nearly every frame the "peripheral" plasma layer extended varying distances from the wall to the center of the vessel (in arterioles measuring 10 to 100  $\mu$  often to the center of the vessel or  $\frac{1}{2}$  to  $\frac{3}{4}$  of this distance). So far the largest volume of data has been obtained from the amphibian circulation and the results have been corroborated in the mammalian (rat) circulation. An explanation must exist to account for the apparent discrepancy between the appearance of the peripheral plasma layer as observed by direct microscopic observation in contrast to the appearance of this layer in the high speed film. It is suggested that this discrepancy is due to a lack of contrast of the erythrocytes adjacent to the wall of the vessel, a decrease in their number because of volume and shallowness of the optical path at the sides of the vessel, coupled with bands of plasma which extend for various distances toward the center of the vessel. The summation of these factors produces the classical peripheral plasma layer. While the absorption studies and television microscopy indicate the presence of erythrocytes in the peripheral plasma layer the true state of affairs could not be appreciated until this zone was analyzed with a method which produced cellular discrimination.

It has been frequently demonstrated that erythrocytes deform readily but this has been seen invariably only in vessels whose diameter were less than the erythrocyte (Krogh '29; Nicoll and Webb '48). That considerable deformation could occur of the erythrocyte especially the mammalian erythrocyte in vessels which were larger than such cells has not been reported. High speed recording has shown that not only are the cells deformed as they flow through vessels which are considerably larger than they are but they can alter their spatial position in the vessel at rates which can be of the order of msec. Because of these activities there

must be considerable agitation of the plasma and therefore it is questionable that a still layer of plasma exists of any appreciable magnitude adjacent to the wall of the vessel (Bayliss, '52).

The *in vitro* studies of Veffens ('38), Müller (48) and Taylor ('55) and *in vivo* studies of McDonald ('52, '60) and Prec et al. (49) have indicated that the parabolic velocity profile of blood flow was not consonant with the classical concept of lamellar flow but more akin to that of turbulent flow (Bateman, '56; Reiner 49 Reynolds, 1883). This study extends these concepts to the living microvascular system by the presentation of data of the behavior of erythrocytes in the arterial and venous systems.

Finally one may well ask what name should be given to describe normal blood flow in the arterial and venous systems — laminar mixed or turbulent flow. According to the majority of students of blood flow it is laminar in the peripheral circulation while it may be turbulent in short segments of the central circulation (Bayliss '52; Burton, '60; Hale et al. '35; Hess '17; Potter and McDonald, '52; McDonald '52a; Prec et al. 49; Ralston and Taylor 45; Thoma, '37). They have derived their opinion from the study of blood flow in the vessels of the macrovascular system by a variety of methods (In a few instances from high speed cinerecording, up to 1 500 fps) and from the study of blood flow in narrow glass tubes. Recently Taylor ('55) has questioned this concept of laminar flow and has presented evidence that it is neither laminar nor turbulent and he suggests that it be called mixed. In this study the flow was found to consist of a complex pattern where erythrocytes spin about their long and short axes deform readily and travel across the lamina in an irregular helical spiral. So far no length of vessel has been found in which a stable pattern was established although an attempt is made to orient the cell with its smallest dimension in the direction of flow. Such a pattern does not conform to the classical description of laminar flow. Therefore the least accurate name to describe the normal flow of blood in the microvascular system is "laminar." Perhaps before applying an-

other name to replace the well established name of "laminar" to normal blood flow it would be more useful to continue repeat and extend the study of blood flow with high speed cinephotomicrography and other methods which can produce cellular discrimination so that a thorough description of normal flow can be made, and then consider replacing the current name with a more appropriate one.

#### SUMMARY

Quantitative aspects of the rheology of blood, its dynamic morphology were determined in the living microvascular system of the mesentery lung and skeletal muscles.

Blood was analyzed with the following methods: direct visualization with the microscope; television microscopy; absorption microspectroscopy; dynamic pressuregrams; standard and high speed cine photomicrography where recording rates to 7 600 fps were used.

Quantitative data were presented for the peripheral plasma layer and axial stream as determined by standard methods.

The current status of the methodology was examined for obtaining data from the living microvascular system which could be inserted into formulas to characterize the rheology of blood in the living rather than to withdraw the blood, as is done now and then determine its flow characteristics.

Blood flow was described as determined by direct microscopic visualization; television microscopy; absorption spectroscopy and standard cinephotomicroscopy and then contrasted with data obtained from high speed cinephotomicrography.

High speed cinephotomicrography of cellular blood flow revealed that the standard methods gave an imperfect understanding of cellular flow. Cellular flow was found to be complex and could not be designated as laminar.

The major features of cellular blood flow elucidated in this study from high speed cinephotomicrography were as follows: The forward motion of erythrocytes was a complex pattern which could be roughly described as an irregular helical path which decreased in diameter in the direction of flow. Erythrocytes spun

around their short and long axes. Erythrocytes deformed compressed elongated twisted and folded rapidly within vessels in all vessels of the microvascular system. Streamlines were no indication of cellular orientation.

The data were discussed in relation to current concepts of blood flow

#### LITERATURE CITED

- Berman, H. 1956 Turbulent flow. In Hydrodynamics. H. L. Dryden, F. D. Murnaghan and H. Bateman. Dover Publications, Inc., pp. 235-492.
- Bayliss, L. E. 1932 Rheology of blood and lymph. In Deformation and flow in biological systems. Ed. by A. Frey Wyssling. Interscience Publishers Inc., New York, pp. 355-418.
- 1959 The axial drift of the red cell when blood flows in a narrow tube. *J Physiol.*, 149 583-613.
- Basler, A. 1927 Eine Methode zur Untersuchung der Strömungsgeschwindigkeit in den Blutkapillaren. *Handbuch der Biologischen Arbeitsmethoden*, Abt. V Teil 4 2 Hälfte. Ed. by E. Abderhalden. Urban und Schwarzenberg, Berlin.
- Bloch, E. H. 1953 In vivo high speed cinephotomicrography technique and applications (motion picture). *Anat. Rec.*, 115 383.
- 1956 Microscopic observation of the circulating blood in the bulbar conjunctiva in man in health and disease. *Ergebnisse d. Anatomie u. Entwicklungsgeschichte* 35 1-98.
- 1960 High speed cinephotomicrography of hemodynamics (motion picture). *Fed. Proc.* 19 89.
- 1961 Principles of hemodynamics in the microvascular system (motion picture). *Anat. Rec.* 139 340.
- Bloch, E. H. and A. Nordstrom 1953 A camera stand for cinephotomicrography. *Photographic Science and Technique* 198 47-49.
- Bloch, E. H., L. Warner, M. C. Brown and J. W. Christensen 1956 Color circulation of microcirculation (motion picture). *Anat. Rec.* 124 478.
- Bloch, E. H. and R. H. Hays 1960 The thermal control of tissue temperatures and red transillumination. *Ibid* 138 261-267.
- Brooks, A. M. F. and P. A. G. Monro 1957 Application of flash photo ray tube to the study of the circulation in live tissue. In *Proceedings of the Third International Congress on High-Speed Photography*. Ed. by R. B. Collins. London, Butterworth Scientific Publications, pp. 142-143.
- Burton, A. C. 1960 Hemodynamics and the physics of the circulation. In *Medical physiology and biophysics*. Ed. by T. S. Ruth and J. F. Fulton. W. B. Saunders Company Philadelphia. Chapt. 27 pp. 643-666.
- Clark, E. R. and E. L. Clark 1933 Observation on changes in blood vascular endothelium in the living animal. *Amer. J. Anat.*, 57 385-438.
- Fahraeus, R. 1933 The viscosity of normal and pathological blood. In *Deformation and flow in biological systems*. Ed. by A. Frey Wyssling. Interscience Publishers, New York, pp. 489-499.
- Fahraeus, R., and T. Lindquist 1931 Viscosity of blood in narrow capillary tubes. *Am. J. Physiol.*, 98 563-568.
- Garvin, E. L. 1951 Bibliography on high-speed photography. *SIAPTE*, 56 80-111.
- Hagenbach 1890 Ueber die Bestimmung der Zähigkeit einer Flüssigkeit durch den Ausfluss aus Röhren. *Ann. Phys. (Lpzg)* 19 385-436.
- Hale, J. F. D. A. McDonald and J. R. Womersley 1955 Velocity profiles of oscillating arterial flow with calculations of viscous drag and the Reynold's number. *J. Physiol.*, 124 626-640.
- Hamilton, M. B. 1854 On the circulation of the blood-capsules considered from a physical basis. *Ibid* 6 66-90.
- Harding, F. M. H. Knisely 1958 Settling of Sludge in human patients. *Angiology* 9 317-361.
- Haynes, R. H. 1960 Physical basis of the dependence of blood viscosity on tube radius. *Am. J. Physiol.*, 198 1183-1200.
- Hess, W. R. 1917 Über periphere Regulation der Blutzirkulation. *Pflügers Arch.*, 188 439-460.
- Industrial photography 1959 A directory of high speed cine cameras. *Industrial Photography* 8 33-38.
- Jäger, A. 1935 Die Anordnung und Stellung der roten Blutkörperchen im strömenden Blut. *Pflügers Arch.*, 215 703-722.
- Jeffords, J. V. and M. H. Knisely 1956 Concerning the geometric shapes of arteries and arterioles. *Angiology* 7 125-126.
- Knisely, M. H. W. K. Sistrman-Thomas, T. S. Elliot and E. H. Bloch 1944 Microscopic pathological circulatory physiology of rhesus monkeys during acute Plasmodium knowlesi malaria (motion picture). M. H. Knisely The Medical College of the State of South Carolina, Charleston South Carolina.
- Knisely, M. H., E. H. Bloch, T. S. Elliot and L. Warner 1947 Sludged blood. *Science* 106 431-442.
- Knisely, M. H., L. Warner and F. Harding 1960 Ante mortem settling. *Angiology* 11 535-543.
- Kolli, A. 1936 An electromagnetic flow meter. *Proc. Soc. Exper. Biol. and Med.*, 35 83-86.
- Kolli, A., N. A. Tall, G. Herrold and R. Jensen 1957 Electromagnetic determination of regional blood flow in unanesthetized animals. *Proc. N. A. Acad. Sci.*, 43 527-540.
- Krogh, A. 1929 The anatomy and physiology of capillaries. Yale University Press, New Haven pp. 5 7-12.
- Leuwenhoek, A. van 1708 Certain positions laid down by the author respecting the circulation of the blood in a human body with his opinion respecting the manner of exhibiting the circulation by the injection of quicksilver in The selected works of Anthony van Leeuwenhoek.

- wenhoek. Samuel Hooke. Henry Frey London. Part the first, 231-330.
- Lutz, R. R., G. P. Fulton and R. P. Akers 1930 The neuromotor mechanism of the small blood vessels in membranes of the frog (*Rana pipiens*) and the hamster (*Mesocricetus auratus*) with reference to the normal and pathological conditions of blood flow *Exper. Med. and Surg.* 8: 256-287.
- Lutz, R. R., and G. P. Fulton 1934 Living microscopic blood vessels. Normal and pathological conditions (motion picture). G. P. Fulton, Boston University Department of Biology Boston, Mass.
- Madow N., and E. H. Bloch 1936 The effect of erythrocyte aggregation on the rheology of blood. *Angiology* 7: 1-15.
- McDonald, D. A. 1952a The velocity of blood flow in the rabbit aorta studied with high speed cinematography *J. Physiol.* 110: 323-325.
- 1952b The occurrence of turbulent flow in the rabbit aorta. *Ibid.* 116: 340-347.
- 1960 Blood flow in arteries. Williams and Williams, Baltimore.
- McDonald, D. A., J. M. Potter 1949 Blood streams in the hamster artery (motion picture). American Medical Association, 535 N. Dearborn Street, Chicago, Illinois.
- Monro, P. A. G. 1960 Measurement of corpuscular velocity in small blood vessels. *Anat. Rec.* 136: 357-358.
- Müller A. 1948 Über das Druckgefälle im Blutgefäßsystem, insbesondere in den Kapillaren. *Helv. Physiol. Acta.* 6: 161-195.
- Nicoll, P. A., and R. L. Webb 1948 Subcutaneous blood flow in the bat's wing (motion picture). Audio-Visual Center Indiana University Bloomington, Indiana.
- Olmstead, F. 1960 Measurement of cardiac output in unanesthetized dogs by an implanted electromagnetic meter. In *Medical Electronics*, Ed. by C. N. Sanyal Hiffe and Sons Ltd., London, pp. 327-334.
- Polarville J. L. M. 1942 See Magnault.
- Free O., L. N. Katz, L. Kravetz, R. H. Rosenman, A. P. Flehman and W. Hwang 1946 Determination of kinetic energy of the heart in man. *Am. J. Physiol.* 159: 493-497.
- Raketon, H. J., and A. N. Taylor 1945 Streamline flow in the arteries of the dog and cat. *Ibid.* 144: 706-710.
- Rappeport, M. R., E. H. Bloch and J. W. Irwin 1950 A manometer for measuring dynamic pressures in the microvascular system. *J. Appl. Physiol.* 14: 631-635.
- Regnault 1843 Rapport sur la memoire de M. le docteur Polarville ayant pour titre Recherches experimentales sur le mouvement des liquides dans les tubes de tres-petits diameters. *C. R. Acad. Sci., Paris*, 18: 1167-1188.
- Reiner M. 1949 Deformation and flow H. K. Lewis and Co. Ltd., London.
- Reynolds, O. 1883 An experimental investigation of the circumstances which determine whether the motion of water shall be direct or sinuous, and of the law of resistance in parallel channels. *Phil. Trans.* 174: 635-682.
- Taylor M. 1933 The flow of blood in narrow tubes. *Anstr. J. Exp. Biol. Med. Sci.* 5: 1-14.
- Thoma, R. 1927 Die experimentell-mathematische Behandlung des Blutkreislaufes. In *E. Abderhalden's Handbuch der biologischen Arbeitsmethoden*. Abt. V Teil 4/H. 1103-1200. Urban und Schwarzenberg, Berlin.
- Tigstedt, R. 1905 Die Geschwindigkeit des Blutes in den Arterien. *Ergebn. d. Physiol.* 4: 481-516.
- Vejlens, G. 1938 The distribution of leucocytes in the vascular system. *Acta path. et microbiol. Scandinav. suppl.* 33, pp. 1-241.
- Vierordt, K. 1882 Die Erscheinungen und Gesetze des Stromgeschwindigkeit des Blutes Max Försch, Berlin, 212 pp.
- Wachtel, M. N. D. D. Doughy and A. E. Anderson 1938 The transmission of secondary emission image intensifier in image intensifier symposium, October 6-7 U. S. Department of Commerce O.T.S. 151813.
- Warner L., and M. C. Brown 1960 Techniques for studying the microcirculation in the eye *Am. J. Rec.* 138: 399-408.

# PLATE 1

## EXPLANATION OF FIGURES

- 5 The Eastman Kodak High Speed Camera positioned over the microscope to record blood flow in the lung of the rabbit simultaneously with additional time mark pulses (3 on each motion picture frame) from an oscilloscope which is focused on the film by the side lens of the camera. (Enlarged from a 16 mm motion picture frame) For description of the camera stand see Bloch and Nordstrom, 53.
- 6 The Eastman Kodak High Speed Camera. (D) Film supply spool; (A) Argon timing lamp; (S) Shutter Mechanism; (M) dichroic mirror for positioning image from the side lens onto the film; (V) viewing telescope; (T) film take up spool.
- 7 Simplified photograph illustrating the arrangement of the high speed camera (C) with monobjective microscope (M) and the light conduction quartz-rod system (R) when used to record the circulation in vertically mounted tissue. (Enlarged from a 16 mm motion picture frame)
- 8 The modified quartz rod. (R) Delivery tube for the irrigating solution and (T) thermocouple
- 9 Arrangement for transilluminating tissue with monochromatic light. (G) Grating monochromator and light source; (M) monocular monobjective microscope mounted on modified milling machine head; (C) camera (Image Orthicon); (O) optical bench.
- 10 Vertically supported mesentery in position for being transilluminated (T) Irrigating tube which contains a thermocouple (Enlarged from a 16 mm motion picture frame.)

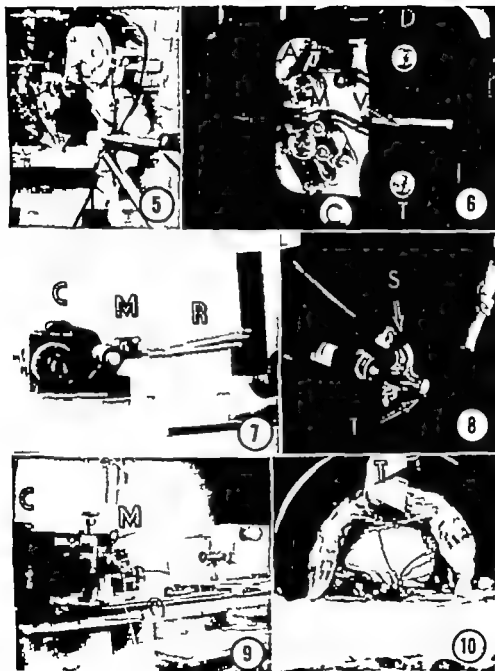


## PLATE 2

### EXPLANATION OF FIGURE 8

- 11 Arterial blood flow (frog) photographed with white light at 24 fps in horizontal mesentery. Note streamlines (S) lack of cellular detail in the axial stream and the apparent absence of a peripheral plasma layer. (Enlarged from 16 mm motion picture frame.)
- 12 Arterial and venous blood (rat) transilluminated with wave length of 510 mμ and photographed at 24 fps in vertical mesentery. (A) Arteriole (B) Venule. Compare with figure 11. Note streamlines lack of cellular detail in blood stream and indistinct peripheral plasma layers. (C) Indicates confluence of peripheral plasma layers in the major stream. Arrows indicate direction of flow. (Enlarged from 16 mm motion picture frame.)
- 13 Blood flow in a terminal arteriole and capillary (frog). Photographed with wave length of 490 mμ at 16 fps in a vertical mesentery. (A) Arteriole (C) Capillary (S) Streamlines. Compare with figures 11 and 12. (Enlarged from 16 mm motion picture frame.)
- 14 Photograph of monitor (Image Orthicon Camera chain) depicting an image of a 30 mesenteric arteriole (frog) which was being transilluminated at wave length of 411 mμ. Contrast has been accentuated to demonstrate the edge of the vessel wall. Absorption of the hemoglobin in the erythrocytes has turned the flowing column of blood black (note that the column of blood extends nearly everywhere to the luminal surface of the arteriole). (Photographed at 1/10 sec.)
- 15 Mesenteric arteriole of the rat transilluminated with white light and photographed at 1/1,000 sec on 35 mm film. Note indistinctness of the peripheral plasma layer. Compare with figure 10.
- 16 The same mesenteric arteriole illustrated in figure 15 re-illuminated with wave length of 414 mμ and photographed 33 secs later.





### PLATE 3

#### EXPLANATION OF FIGURES

- 17 Arterial blood flow photographed in horizontal mesentery (frog) in white light at 24 fps. Note streamlines and lack of cellular detail. This was the control for the circulation illustrated in Figure 18. (Enlarged from 16 mm motion picture frame.)
- 18 The same vessel as in Figure 17 except the circulation was photographed at 2,800 fps. Note the orientation of the cell and the peripheral plasma layer. Elapsed time between the two recordings approximately three minutes. (Enlarged from 16 mm motion picture frame.)
- 19 Arterial and capillary flow in a vertically suspended mesentery (frog) transilluminated with light of 490 mμ. (A) Arteriole (C) Capillary. Note streamline flow, lack of cellular detail, thick wall and indistinct peripheral plasma layer.
- 20 The same blood flow and vessel as in Figure 19 except they were transilluminated with light of wavelength of 414 mμ and recorded at 3,000 fps. In the arteriole note plasma spaces and irregular peripheral plasma layer. Some erythrocytes are oriented parallel to the wall and in the direction of flow, others at various angles. Note the position of the erythrocytes in the capillary. (Enlarged from a 16 mm motion picture frame.)
- 21 Blood flow in an arteriole with capillary branch in vertical mesentery (frog) transilluminated with white light and recorded at 24 fps. Note streamline flow in arteriole and erythrocytes (temporarily) impinged upon the fork of the vessel. Note streamlines in the capillary. (Enlarged from 16 mm motion picture frame.)
- 22 The same vessel as in Figure 21 except that the flow was recorded at 3,700 fps. (Enlarged from 16 mm motion picture frame.)

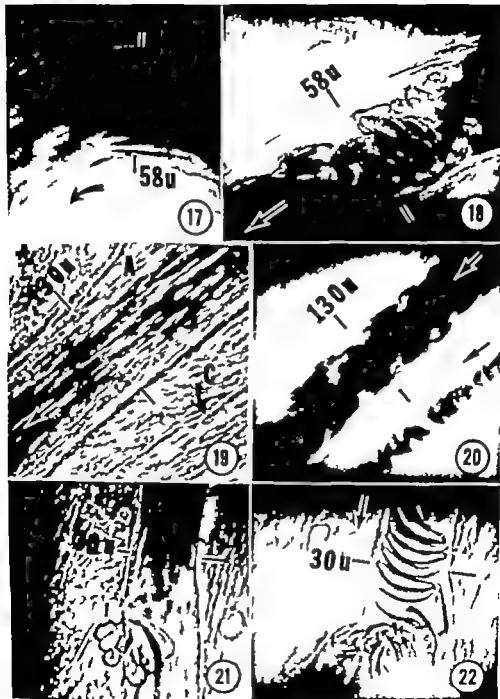


# PLATE 3

## EXPLANATION OF FIGURES

- 17 Arterial blood flow photographed in horizontal mesentery (frog) in white light  $\pm$  24 fps. Note streamlines and lack of cellular detail. This was the control for the circulation illustrated in figure 16 (Enlarged from 16 mm motion picture frame)
- 18 The same case as in figure 17 except the circulation was photographed at 2,600 fps. Note the orientation of the cells and the peripheral plasma layer. Elapsed time between the two recordings approximately three minutes. (Enlarged from 16 mm motion picture frame)
- 19 Arterial and capillary flow in vertically suspended mesentery (frog) transilluminated with light of 490 m $\mu$ . (A) Arteriole (C) Capillary. Note streamline flow, lack of cellular detail, thick wall and indistinct peripheral plasma layer.
- 20 The same blood flow and vessels as in figure 19 except they were transilluminated with light of wave length of 414 m $\mu$  and recorded  $\pm$  3,000 fps. In the arteriole now plasma spaces and irregular peripheral plasma layer. Some erythrocytes are oriented parallel to the wall and in the direction of flow others at various angles. Note the position of the erythrocytes in the capillary (Enlarged from 16 mm motion picture frame)
- 21 Blood flow in an arteriole with capillary branch in vertical mesentery (frog) transilluminated with white light and recorded  $\pm$  34 fps. Note streamline flow in arteriole and erythrocytes (temporarily) impinged upon the fork of the vessel. Not are callous in the capillary (Enlarged from 16 mm motion picture frame.)
- 22 The same vessel as in figure 21 except that the flow was recorded  $\pm$  3,700 fps. (Enlarged from 16 mm motion picture frame.)

# Fat Absorption by Epithelial Cells of the Small Intestine of the Rat<sup>1</sup>

DENNIS LACY AND A. B. TAYLOR

*Department of Zoology and Comparative Anatomy, St. Bartholomew's Hospital Medical College, University of London and the Department of Physiology, University of Illinois, Urbana, Illinois*

As a result of histochemical studies carried out mainly in this century three principal suggestions have been made about the form in which the bulk of the ingested fat enters intestinal epithelial cells. Vezar and McDougall ('36) suggested that the fat is completely hydrolyzed in the intestinal lumen and absorbed as fatty acids and glycerol. Frazer and colleagues ('48, '54, '55 and '58) on the other hand, maintained that lipolysis is only partial. They were of the opinion that the partially hydrolyzed fraction consisting of mono- and diglycerides, assists in rendering the bulk of the fat, still in the unhydrolyzed form into a fine emulsion. They believed that the greater proportion of the fat passes into the epithelial cells in the form of small particles (chylomicrons) which measure less than  $0.5 \mu$  in diameter. In more recent years the work of Borgström and associates has come into prominence. These workers (Bergström and Borgström '55; Bergström et al., '52; Borgström, '52, '52a-e, '53, '54, '55a, '55b, '57; Borgström et al., '57) showed that, while complete hydrolysis of triglyceride molecules is possible, the process is of long duration for the long-chain triglycerides (about 24 hours for corn oil). Borgström and colleagues have also demonstrated that long chain fatty acids released during lipolysis readily form water-soluble molecular aggregates (micellae) with mono- and diglycerides. Thus while lipolysis is probably only partial (as constantly stressed by Frazer) Borgström ('57) maintains that the bulk of the fat is probably absorbed in micellar form.

As early as 1855 Kolliker (1855) stated that fat droplets can be seen, although very rarely in the striated border and just beneath it in the apical cytoplasm. Kol-

liker (1856) was of the opinion that the actual striations of the free border represented fine canals and that the fat, in the form of an emulsion passed through these into the body of the cell. Other workers in the nineteenth century also stated that occasionally they had seen fat droplets in the more apical cytoplasm. However due to the extreme rarity of these observations they were either ignored or regarded with suspicion. On the other hand, there was no doubt that fat could be seen, sometimes in large quantities in the more distal cytoplasm. For many years, therefore it was generally maintained that as far as could be determined by cytological methods fat is probably broken down into fatty acids and glycerol in the intestinal lumen, absorbed in an undetectable form and resynthesized in the cytoplasm. That such a resynthesis could occur was demonstrated by the work of Mink and Rosenstein (1891a, 1891b) and has been confirmed in more recent years (Shorland, '55). It is apparent that the early light microscope work generally supported the views of Vezar and co-workers.

Wotton and Zwemer ('39) showed clearly that after feeding starved animals with fat droplets of fat could be seen within the striations of the epithelial border. They observed no visible difference between the fat droplets within the intestinal lumen and those apparently passing into the cells. Wotton and Zwemer concluded that, any hydrolysis or emulsification that may take place probably serves only to break down connective tissue and free the enclosed fats.

Baker ('43) working at the limits of resolution of the light microscope claimed

This research was made possible by grant from the Wellcome Trust to purchase an electron microscope and auxiliary forms of equipment for use at St. Bartholomew's Hospital Medical College.

that canals are present in the free border but, unlike those described previously by Kolliker and others are located between the striations. Subsequently Baker ('51) by the use of the sensitive lipid coloring agent Sudan black B showed particles of fat apparently passing down the canals. These canals were said to be 0.3  $\mu$  in diameter. This work of Baker was frequently quoted by Frazer (46 '54 '58) in support of his view that fat was entering in the form of chylomicrons.

More recently still, Hewitt ('54 '56) confirmed previous views that particles of fat could be seen in the striated border within the apical cytoplasm and also around the Golgi apparatus and nucleus. Hewitt claimed that some lipid passes between adjacent cells and joins the intracellular lipid at the side of the nucleus. The combined streams of lipid were stated to pass below the nucleus (and within the cell) to be eventually discharged into a lacteal. Histochemical tests suggested that the lipid in its striated border was mainly in the form of fatty acids while that occurring between cells was principally neutral fat.

Several workers have studied fat absorption by electron microscopy. Weiss ('55) did not observe any fat in the striated border or just beneath it. Palay and Harlin ('59b) saw small droplets (850 Å maximum diameter) between the microvilli of which the striated border is composed (Granger and Baker 49 and '50). These droplets were seen at the base of the microvilli within invaginations of the plasma membrane. Palay and Harlin concluded that the purpose of the microvilli is not to facilitate absorption but on the contrary to allow only particles of a certain size to pass between them. They also concluded that lipid is taken into the apical cytoplasm by pinocytosis. Weiss and Palay and Harlin agreed that the fat passes towards the nucleus and is then discharged into the space between adjacent cells. However Weiss was of the opinion that the fat moves through the cytoplasm within discrete Golgi vacuoles. Palay and Harlin believed it travels within a continuous system of membranes. These membranes were frequently studded with

fine granules and were identified as membranes of the endoplasmic reticulum.

The present work was undertaken in an attempt to throw further light on fat absorption and to obtain additional information concerning its route through intestinal epithelial cells.

#### METHOD

Sixteen mature Wistar rats with an average weight of 234 gm, were divided into two equal groups, A and B. The animals of both groups were each placed in a separate cage and starved for 24 hours but allowed water. The cages were designed so that the animals were unable to eat their own feces. Olive oil, colored with Sudan IV was then administered orally to Group A animals in amounts comparable with those found useful by Adamstone ('59) in studies on fat absorption. Two animals each received 0.1 ml, 5 were each given 0.2 ml and one 0.4 ml. The rats which were given 0.1 ml and three which received 0.2 ml were killed 30 minutes after feeding; one which received 0.2 ml was sacrificed 40 minutes after feeding, while the remaining animals were killed after one hour. All the animals were killed by a sharp blow on the head anesthetics being avoided.

Segments of the duodenum and jejunum which contained the most fat as shown by the red color of the Sudan IV were rapidly excised and placed into a 1% solution of osmium tetroxide buffered to pH 7.3 (Palade '52). Within the fixative the intestine was cut into smaller pieces and transferred to fresh fixative for three hours. The tissue was then rinsed in distilled water dehydrated with increasing concentrations of ethanol and embedded in a 1:3 mixture of *n*-methyl and *n*-butyl methacrylate. Rats of Group B of similar age weight and sex as those of Group A were killed along side those of the latter group. Parts of the duodenum and jejunum obtained from rats of Group B were treated in the same way as similar tissue obtained from animals of Group A.

Sections were cut with a glass knife mounted onto copper grids previously covered with a thin carbon film and examined in a Siemens Elmiskop Ia. The instrument was usually operated at 60

K.V. and micrographs obtained at initial magnifications ranging from  $1,000\times$  to  $40,000\times$ . When photographing structures at  $40,000\times$  at least three pictures were taken at slightly different foci.

*Observations on the fine structure of epithelial cells of starved animals*

Our observations were generally similar to those reported by Palay and Karlin ('59a). We did not see any canals of the kind described by Baker ('51). Also we did not see any substance entering the apical regions of the cells, either via the microvilli or between them in pinocytotic vesicles (figs. 1-2). In the supra nuclear region we observed occasional dense bodies. These were generally enclosed by smooth-surfaced membranes (fig. 2). From observations made on fat-fed animals (see below) it seemed likely that these dense bodies represented lipid presumably absorbed during a previous meal or derived more recently from the animal's own body (e.g., sloughed off intestinal epithelia). The endoplasmic reticulum was often in the form of comparatively large interconnected sacs. Cytoplasmic particles were very numerous and occurred both in contact with the membranes of the endoplasmic reticulum and freely in the cytoplasmic matrix. The Golgi apparatus was usually distinctly vacuolar and unified in appearance. Some of the Golgi vacuoles contained a few dense bodies which from work carried out by Weiss ('55) and Palay and Karlin ('59b) and in view of results reported below on fat fed animals, were probably lipoidal. In the Golgi zone of some cells we observed markedly dense spheroidal bodies each about  $0.15\ \mu$  in diameter. These bodies were enclosed by a thin membrane; some (possibly varying with the plane of section) contained two or three pairs of thicker membranes resembling the cristae of mitochondria. The identity of these inclusions is uncertain although they could be lysosomes (Appelmans et al. '59; Novikoff '57).

*Observations on intestinal epithelial cells of animals fed with fat*

The following observations apply to epithelial cells of both the duodenum and

jejunum. They were made on micrographs obtained from all of the animals examined. There was no consistent difference between the appearance of cells taken from animals killed at the specified intervals after feeding. Usually too the appearance of different cells differed in the same section. Hence a definite sequence of events in time insofar as the absorption of fat was concerned was not apparent.

Particularly dense spheroidal bodies each with a maximum diameter of about  $300\ \text{\AA}$ , were seen in the narrow channels separating individual microvilli. This was not a common observation being seen only in a small number of micrographs. Other bodies of similar density were seen in a greater number of micrographs between the two fine membranes (inner and outer limiting membranes) covering the microvilli. These bodies were usually in the form of slivers, a shape which was apparently determined by the parallel arrangement of the two limiting membranes (fig. 4-1). Similar observations were made along part of the lateral surface of the cells. Here the dense slivers were most usually seen between the two limiting membranes on a level with the terminal web zone (fig. 4-1). In a few cells, this dense material was seen between the two surface membranes as far back as about the beginning of the Golgi zone that is, on a level with the most proximally placed double membranes of the Golgi apparatus.

In many micrographs, markedly dense bodies each with a maximum diameter of about  $250\ \text{\AA}$ , were seen within microvilli (figs. 5-6-1). As shown most clearly in microvilli viewed in cross-section, these bodies were located close to the inner limiting membrane. None was observed in the center of a microvillus. The dense bodies were scattered at random along the length of the microvilli. Their numbers increased from the apices to the bases of the microvilli.

Bodies similar to those seen within microvilli were only occasionally observed in the terminal web zone. When present they were very few in number usually only one or two being visible in each cell (as seen in section, fig. 6-1).

Sometimes within but usually lying just beneath the terminal web zone. Inclusions were observed with the following main characteristics: (1) aggregates of moderately dense bodies each about 100 Å in diameter (2) aggregates of moderately dense bodies [similar to those described under (1)] bordered by a membrane and (3) markedly dense bodies each about 1000 Å in diameter and enclosed by a membrane. Inclusions of the last mentioned kind were seen in large numbers in many cells (fig. 3). Due to the presence of various intermediate forms it was concluded that these larger dense bodies were derived from those referred to under (1) and (2) above. For convenience inclusions with an appearance similar to that described under (2) above will be designated *L*, while the larger ones will be termed *I*. In several micrographs some minute particles were seen within the dense bodies comprising inclusions termed *L* (fig. 7 cf. also fig. 8).

In the apical zone were some membranes to which were attached many cytoplasmic particles. These were identified as characteristic components of the endoplasmic reticulum. Also present were membranes to which were attached few such particles and those which lacked such particles. Possibly therefore in the apical zone the endoplasmic reticulum underwent some chemical or physicochemical change resulting in the separation of the particles from the membranes. A few cytoplasmic particles were attached to the membranes bounding a small amount of the material (or inclusions) designated *L*, *I*. Most of these inclusions however were enclosed by non-granular membranes. In accordance with the tentative suggestion made above these non-granular membranes may have been derived from the granular membranes of the endoplasmic reticulum. The non-granular membranes were nearly always approximately circular in outline; there was no evidence to suggest that the dense material they enclosed was passing through a continuous system of membrane-bound spaces. Finally in the apical zone cytoplasmic particles were seen scattered in the matrix.

Inclusions of the kind designated *L*, and *I* were observed as far back as the

Golgi zone. Those termed *I* were more prevalent than those referred to as *L*.

There was a marked difference between the general appearance of the endoplasmic reticulum in the supra-nuclear region of cells containing moderate to large numbers of inclusions of *L* and *I*, and in the cells of starved animals (p. 157). In the former case the membranes of the endoplasmic reticulum delimited relatively few large sacs. These were fairly well distributed throughout the cytoplasm (fig. 10). Between the large sacs were smaller ones. Coincident with the appearance of inclusion *L*, *I*, there appeared to have been a reduction in the volume enclosed by the membranes of the endoplasmic reticulum and a corresponding increase in the proportion of the cell occupied by the matrix. Within the matrix of cells which contained many inclusions of the kind referred to as *L*, *I*, were many freely occurring cytoplasmic particles. There was nearly always an obvious difference in the general appearance of the membranes enclosing inclusion *L*, *I*, and the conspicuously particle-studded membranes of the endoplasmic reticulum (figs. 9, 10).

The appearance of the Golgi zone and of the Golgi apparatus also varied with the number of inclusions designated *L*, *I*. When few or virtually none of these inclusions were visible the Golgi apparatus was a relatively unified or compact structure (cf. p. 157). When many of these inclusions were present the apparatus was comparatively dispersed with paired membranes and adjacent vacuoles scattered about the Golgi zone. So far as could be judged microscopically when even more of the inclusions of the kind termed *I* were present the characteristic arrays of double Golgi membranes (dictyosomes) were scarce while the Golgi vacuoles remained numerous.

In the region of the Golgi apparatus and varying with the number of inclusions of the type termed *I*, *L*, present in the more apical region we observed the following: (1) some inclusions of the former kind and more of the latter (2) many Golgi vacuoles partially or entirely filled with dense bodies each about 100 Å in diameter (fig. 12, 1) (3) a tendency for Golgi vacuoles to lie on the side of the

paired membranes next to the cell surface (fig. 13) (4) invaginations of the cell membrane (sometimes accompanied by the cell membrane of an adjacent cell) and strings of circular and elliptical shaped membranes leading to Golgi vacuoles (fig. 13) and (5) vacuolar-like dilations of the intercellular space within which occurred many bodies similar in size and density to those seen in Golgi vacuoles (fig. 13). These observations suggested that there were canal-like connections between the Golgi vacuoles and the intercellular space; and further that the dense bodies within the Golgi vacuoles were eventually transported via these canals to the vacuolar dilations between adjacent cells.

Finally in a small number of micrographs we observed moderately dense bodies similar to those forming inclusions designated  $L_1$  within Golgi vacuoles (fig. 10). Such vacuoles were clearly seen as dilations of paired Golgi membranes so that their identity was not in doubt.

#### DISCUSSION

Studies on fat absorption by electron microscopy are limited by the lack of specific cytochemical tests for various kinds of lipids. In addition as found in the present investigation it is extremely difficult to establish a definite sequence of events in time. Thus even in the same section and in all the fat fed animals examined we observed cells which had apparently absorbed large quantities of material, those which seemed to be commencing such a process and others which resembled the cells of starved rats. The position of a cell in the villus its contact with lipid being absorbed the quantity of lipid present, the rate of its removal from the cell as well as the motility of the region may all be factors contributing to this variability. Even if corresponding segments of the intestine of different rats are examined it is doubtful whether a time sequence could be established since the results will probably vary from animal to animal. Finally there is the difficulty of interpreting static micrographs in terms of a dynamic process.

It is apparent from the above that any information about fat absorption obtained

from micrographs must depend upon the different appearance of the cells of fat fed animals compared with control (starved) animals and the evidence already available from studies made by light microscopy and by biochemical methods. From the comparison of micrographs obtained from the experimental and control animals we are led to conclude that the dense bodies seen between the microvilli, enclosed by the two limiting membranes of the microvilli, within the microvilli and more rarely in the terminal web zone represented lipid. There also seems little doubt that the larger and similarly dense bodies present in the supra-nuclear regions of many of the cells of the fat fed animals and designated  $L_1$  were also lipoidal. As discussed previously the appearance of this membrane-bound lipid graded morphologically with that termed  $L_1$  and with aggregates of individually smaller less dense bodies not enclosed by a membrane. While such morphological gradations must be regarded with caution it is suggested that these various forms represented morphological variation in the appearance of the lipid. Certainly in some way the lipid seen in the microvilli and terminal web zone must presumably be transposed into the forms termed  $L_1$  and  $L_2$ . The relative abundance of dense bodies in the Golgi vacuoles of the fat fed animals indicates that such bodies were also lipoidal. This also applies to the dense bodies seen between the cells.

Logically it would appear that if lipid were present within the microvilli, in the supra nuclear region of the cells and laterally between the cells that it was being absorbed apically and being discharged laterally. There is also much evidence from light microscopy (see introduction) which is in accord with this view.

Any further suggestions on fat absorption from the observations made during the present study must depend upon the conclusions reached above. The following views therefore are advanced on this basis.

*Material, believed to be lipid was seen between the two membranes bounding the microvilli. From a series of measurements carried out by Zetterqvist (36) it is known that after osmium fixation and*



methacrylate embedding the distance between the afore-mentioned membranes is 25 Å. Bahr Bloom and Friberg ('57) have shown that after osmium fixation and methacrylate embedding various tissues may either swell or shrink, the extremes noted were 9% swelling and 22% shrinkage. It is not known to what extent individual components of cells were affected. However as a rough guide it seems likely that the distance between the two limiting membranes of the microvilli in life is not more than about 30 Å and not less than about 20 Å. Further Sjostrand ('56) in a review of work carried out by high resolution microscopy reported that there was no indication of pores in the surface of the microvilli of a size over 50-100 Å in diameter. We (Lacy and Taylor paper in preparation) have also failed to find any pores and believe that either there are none or that they are very small (less than 25 Å) and difficult to detect. We are led to conclude therefore that the olive oil was absorbed in some extremely minute form. If it entered as neutral fat then the diameter of these droplets was probably not more than about 30 Å. Clearly such particles are much smaller than those postulated by Frazer (see introduction) although it should be emphasized that Frazer's size of particles was determined by light microscopy.

Dense bodies believed to be lipid which were present in the main part of the microvilli, were usually of a greater size than those seen between the two limiting membranes. Apparently some coalescence of lipid occurred within the microvilli. Along the length of the microvilli from their apices to their bases the dense bodies exhibited a numerical gradient. Possibly more lipid was absorbed near the bases of the microvilli than towards their apices. An alternative view is that the gradient reflected a flow of lipid down the microvilli and its accumulation (but only for a short time) in this basal region just above the terminal web. This latter suggestion offers some support for the very tentative idea that the terminal web might participate in a pumping action and be retracted at intervals to allow the free flow of lipid into the apical cytoplasm (Lacy and Taylor paper in preparation).

Dense bodies, of the kind seen within microvilli, were only rarely seen in the terminal web zone and even then were present only in small numbers. As suggested above, this material was presumably converted into the forms designated  $L_1$  and  $L_2$ .

The precise function of the Golgi apparatus in fat absorption is obscure, largely because at present there is no definite evidence as to whether or not this organelle is associated with enzymes which might play some part in fat absorption. What seems reasonably certain is that in the present investigation (in which only small amounts of fat were given to the animals) at least a high proportion of the absorbed lipid passed into Golgi vacuoles before being discharged into the intercellular space.

Dense material, believed to be lipid was seen between the two surface membranes from the bases of the microvilli to about the upper limit of the Golgi zone. Perhaps some lipid was being absorbed laterally from between the cells as suggested by Hewitt ('56). On the other hand, it seems equally possible that some of the lipid, which had penetrated the outer limiting membrane of the microvilli flowed down between the two limiting membranes instead of entering the main body of the processes. In the latter case this lipid would then meet the main stream of lipid leaving the main body of the cell. Whichever view is correct it seems that two pathways existed either for the entry of the lipid [(1) apically via the microvilli and (2) laterally from between adjacent cells] or its discharge [(1) through the main part of the cell into Golgi vacuoles and thence into extracellular channels and (2) peripherally via the surface membranes].

The overall picture which emerges from the present study is that probably most of the olive oil entered the cells apically via the microvilli in some extremely small form of near molecular dimension. This lipid moved down the microvilli and into the terminal web zone where it underwent a morphological transformation. Subsequently it appeared as aggregates of smaller bodies or as individually larger dense bodies enclosed by membranes. These membranes were essentially smooth-

surfaced and were thus different from the characteristically particle-studded membrane of the endoplasmic reticulum seen in the main part of the cell. The lipid was then transported to the Golgi apparatus and appeared in Golgi vacuoles. From there it was discharged along interconnecting canals to vacuolar dilations of the extracellular space. In addition some lipid either entered the cells laterally or was discharged peripherally via the surface membranes.

As noted in the Introduction Borgström has suggested that neutral fat mainly enters the cells in the form of molecular aggregates of micellum. It has also been long maintained that the cells are partially capable of resynthesizing hydrolyzed fat to neutral fat. Recent work by Hewitt, Shorland, Turner et al. ('60) as well as that of Senior and Isselbacher ('61) not only supports the concept of resynthesis of triglycerides by the mucosal cells but suggests that lipids may undergo a variety of chemical changes the nature of which is not completely understood. In the present investigation we have concluded that the olive oil entered the cells in some extremely minute form and underwent a variety of morphological transformations. Such conclusions at least are not contrary to the biochemical evidence referred to above and to some extent support it.

In any one study of moderate length only a very small amount of tissue can be examined by the thin-sectioning technique. Further our observations relate only to the absorption of olive oil as occurs a relatively short time after its ingestion. The possibility cannot be ruled out that some olive oil took additional routes both during the period under examination and afterwards. It is also possible as suggested by the work of Palay and Karlén ('59b) that other long-chain triglycerides may pursue other pathways. The route may also be determined by a variety of experimental factors such as the amount of fat administered whether or not an anesthetic was used and the genus of animal employed.

#### SUMMARY

An attempt has been made to gain further information on the form in which

fat is absorbed and the route it takes during its passage through intestinal epithelial cells. Rats of one group were starved for 24 hours fed with 0.1 ml to 0.4 ml of olive oil and then killed 30 minutes to one hour later. Rats of a second group received similar treatment except that they were not fed with fat. Epithelial cells of the small intestine were examined by electron microscopy.

In the cells of the fat fed animals from the microvilli to approximately the upper level of the Golgi zone small amounts of a dense substance were observed between the two fine membranes covering this region. Dense bodies each about 250 Å maximum diameter were seen within microvilli. Similar bodies were only rarely seen in the terminal web zone and even then in very small numbers. Sometimes within but usually just below the terminal web zone inclusions were observed ranging from aggregates of small, moderately dense bodies to individually larger more dense bodies each enclosed by a membrane. The membranes which enclosed these bodies, both in the terminal web region and below were essentially smooth-surfaced. There was reason to believe however that they might have been derived from the particle-studded membranes characteristic of the endoplasmic reticulum. Dense bodies and rarely smaller less dense bodies were seen within Golgi vacuoles. Bodies of the former appearance were observed in vacuolar-like dilations of the intercellular space between adjacent cells at the level of the Golgi apparatus and below.

It is concluded that the various bodies referred to above and seen in the cells of the fat fed animals represented lipid further that probably most of the lipid entered the cells via the microvilli in some extremely minute form of near molecular dimensions. Thence it passed to the bases of the microvilli where it underwent a morphological transformation. Subsequently it was transported to the Golgi vacuoles where it passed along interconnecting canals or channels to the extracellular space. The dense material seen between the two surface membranes along the upper lateral part of individual cells was probably lipid which was either enter

ing laterally (from between adjacent cells) or being discharged so as to meet the main stream of lipid leaving the cell in the region of the Golgi apparatus. The lipid, therefore pursued two pathways either into or out of the cells.

## LITERATURE CITED

- Adamstone, F. B. 1959 Reaction of the Golgi apparatus of intestinal epithelial cells of the rat to ingestion of a neutral fat or fatty acid. *J. Morph.*, 105: 293-311.
- Appelmann, F., R. W. Haux and C. de Duve. 1955 Three fractionation studies. B. The association of acid phosphatase with special class of cytoplasmic granules in rat liver. *Biochem. J.* 59: 435-445.
- Bahr, G. F., F. G. Bloom and V. Friberg. 1957 Volume changes of tissues in physiological fluid during fixation in osmium tetroxide or formaldehyde and during subsequent treatment. *Exptl. Cell. Res.*, 12: 342-353.
- Baker, J. R. 1942 The free border of the intestinal epithelial cell of vertebrates. *Quart. J. Micro. Sci.*, 84: 73-100.
- . 1951 The absorption of lipid by the intestinal epithelium of the mouse. *Ibid.*, 82: 79-85.
- Bergström, S., and B. Bergström. 1955 The intestinal absorption of fat. In: *Prog. Chem. Fats and Other Lipids*. London, Pergamon Press, 3: 331-393.
- Bergström, S., B. Bergström and M. Rotenberg. 1952 Intestinal absorption and distribution of fatty acids and glycerides in the rat. *Acta Skand. Physiol.*, 25: 180-199.
- Bergström, B. 1952a On the mechanism of the intestinal fat absorption. III. *Ibid.*, 25: 140-149.
- . 1952b On the mechanism of the intestinal fat absorption. IV. *Ibid.*, 25: 291-314.
- . 1952c Incorporation of saturated fatty acids of different chain lengths in small intestinal and lymph phospholipid of the rat during absorption. *Metabolism of lipids*, 7: *Ibid.*, 25: 315-321.
- . 1952d An investigation of the intestinal absorption of ethyl oleate in the rat. *Ibid.* 5: 322-327.
- . 1952e On the action of pancreatic lipase on triglycerides in vivo and in vitro. *Ibid.*, 25: 328-347.
- . 1953 On the mechanism of the hydrolysis of glycerides by pancreatic lipase. *Acta Chem. Scand.* 557-558.
- . 1954 On the mechanism of pancreatic lipolysis of glycerides. *Biochimica et Biophysica Acta*, 13: 491-504.
- . 1955a Randomization of glyceride fatty acid during absorption from the small intestine of the rat. *J. Biol. Chem.* 18: 671-673.
- . 1955b Transport form of <sup>14</sup>C-decanoic acid in portal and inferior vena cava blood during absorption in the rat. *Acta Skand. Physiol.* 34: 71-4.
- . 1957 In *Biochemical Problems I. Lipids*. Poplik and Breton, London, Butterworth, pp. 179-339.
- Borgström, B., A. Dahlquist, G. Lundh and S. Sjövall. 1957 Studies of intestinal digestion and absorption in the human. *J. Clin. Invest.* 36: 1521-1538.
- Fraser, A. C. 1948 The absorption of triglycerides from the intestine. *Physiol. Rev.* 28: 103-119.
- . 1954 Transport of lipid through cell membranes. *Symp. Soc. Exptl. Biol.*, 8: 490-501.
- . 1955 Mechanism of intestinal absorption of fat. *Nature* 173: 491-493.
- . 1958 Fat absorption and its disorders. *Brit. Med. Bull.*, 14: 218-220.
- Granger, R., and R. F. Baker. 1949 Electron microscope investigation of the striated border of intestinal epithelium. *Anat. Rec.*, 103: 459.
- . 1950 Electron microscope investigation of the striated border of intestinal epithelium. *Ibid.*, 107: 423-441.
- Hewitt, W. 1954 A histochemical study of fat absorption in the small intestine of the rat. *Quart. J. Micro. Sci.*, 85: 153-157.
- . 1956 Further observation on the histochemistry of fat absorption in the small intestine of the rat. *Ibid.*, 87: 199-203.
- Kolliker, A. 1853 *Manual of Human Histology* translated by G. Busch and T. Huxley. London, Sydenham Soc., 2: 91.
- . 1856 Nachweis eines besonderen Baues der Cylinderzellen des Darmtraks, der zur Fettresorption in Bezug zu stehen scheint. *Verh. der Phys. Med. Ges. Würzburg*, 11: 253-273.
- Lacy, D., and A. B. Taylor. (In preparation)
- Munk, I., and A. Rowenstein. 1891 Zur Lehre von der Resorption im Darm nach Untersuchungen an einer Lymph (chylus-) fistel beim Menschen. *Virchow Archiv* 123: 230-279.
- . 1891b Zur Lehre von der Resorption im Darm, nach Untersuchungen an einer Lymph (chylus-) fistel beim Menschen. *Ibid.* 123: 481-518.
- Novikoff, A. B. 1957 Biochemical heterogeneity of the cytoplasmic particles of rat liver. *Symp. Soc. Exp. Biol.*, 10: 92-109.
- Palade, G. E. 1952 A study of fixation for electron microscopy. *J. Exptl. Med.* 95: 283-298.
- Palay, S. L., and I. J. Karni. 1959 An electron microscope study of the intestinal villus. I. The fasting animal. *J. Biophys. Biochem. Cytol.* 5: 363-372.
- . 1959b An electron microscope study of the intestinal villus. II. The pathway of fat absorption. *Ibid.* 5: 373-381.
- Senior, J. R., and K. J. Iselbacher. 1961 Fatty acid activation and glyceride synthesis by subcellular particles of rat intestinal mucosa. *Fed. Proc.*, 20: 115.
- Shorland, F. F. 1955 Formation of animal fats. *Prog. Chem. Fats and other Lipids*, London, Pergamon Press, 3: 273-323.
- Sjöstrand, F. S. 1956 The ultra structure of cell revealed by the electron microscope. *Int. Rev. Cytol.*, 5: 453-523.

- Turner D. A., E. V. Cox, J. A. Balint, R. Pirie, R. F. Fletcher, E. Hwang and W. H. Cavallos 1960 Digestion and absorption of fat after a normal meal. *Fed. Proc.*, 19 876-883.
- Vernar F. and E. J. McDougall 1936 Absorption from the Intestine Longmans Green, London.
- Weiss, J. 1955 The role of the Golgi complex in fat absorption as studied with the electron microscope with observations on the cytology of duodenal absorptive cells. *J. Exptl. Med.*, 102: 775-782.
- Wotton, R. M., and R. L. Zwamer 1939 Studies on direct and visible ingestion of fat by differentiated body cells of the cat. *Anat. Rec.*, 71 493-507
- Zetterqvist, H. 1956 The ultrastructural organization of the columnar epithelial cells of the mouse jejunum. *Stockholm. Aktiebolaget* Codon.

All the micrographs are of intestinal epithelial cells of starved or fasted animals. In all cases the tissue was fixed in 1% osmium tetroxide solution buffered in pH 7.3. Cc, Cc adjacent cells; m, cell membranes; p, cytoplasmic particles; ch, extracellular channel; E, extracellular space; E.R., endoplasmic reticulum; f, fibers; Gm., Golgi membrane; G, Golgi vacuole; l-l, material believed to be lipid seen either in various form or locations or both; m, mitochondrion; m.v. microvilli; N, nucleus; p, minute dense particles; pr, sections through channels believed to exist between Golgi vacuoles and extracellular space.

# PLATE I

## EXPLANATION OF FIGURE

1. Micrograph of the upper region of two epithelial cells from rat starved for 24 hours but allowed water. There are no dense bodies within the microvilli (cf. fig. 6) nor inclusions in the proximity of the terminal web (tw) similar to those shown in figure 7 in the malnourished cytoplasm. There are occasional small dense bodies enclosed by membranes. These probably correspond to material identified as lipid in some of the preceding figures of the cell of fasted animals. Accordingly they are marked l. There is marked difference between the amount of apparent lipid in these cells and that shown in the cells of figure 2. E.R., endoplasmic reticulum; m., mitochondrion; m.v., microvilli. 12,500



## PLATE 2

### EXPLANATION OF FIGURE

- 2 Micrograph of epithelial cells from rat starved for 24 hours but allowed water. Many microvilli (m.v.) are shown in cross section. They do not contain dense spheroidal bodies similar to those shown in Figure 0. Similarly there is almost complete absence of material which might be lipid in the region of the terminal web zone (t.w.z.) In the main mass of cytoplasm are occasional dense bodies which probably correspond to material previously interpreted as lipid and marked *l*. These bodies are enclosed by smooth-surfaced membranes. None appear to lie within the conspicuously particle-studded membranes of the endoplasmic reticulum (E.R.) The latter component is most abundant. m., mitochondrion. 15,000 X





### PLATE 3

#### EXPLANATION OF FIGURE

- 3 Lower power micrograph showing several epithelial cells which contain many dense bodies mainly of the kind termed  $l_1$  in the text. Each of these dense bodies is enclosed by membrane. Some dense bodies ( $l_1$ ) also be seen within Golgi vacuoles (G. ). It is believed that these various dense bodies represent lipid m., mitochondrion m., microvilli; c.m., cell membrane; N nucleus. 15,000



## PLATE 4

### EXPLANATION OF FIGURE

- 4 Micrograph showing small amounts of a dense material ( $l_1$ ) lying between the two surface membranes, both where they cover the microvilli (m.) and part of the lateral surface of two adjacent cells ( $Cu_1$ ,  $Ce_1$ ). Dense spheroidal bodies ( $l_2$ ) can be seen within some microvilli. It is believed that the dense inclusions ( $l_1$ ,  $l_2$ ) represent lipid. In some microvilli, the fibers ( $f$ ) although of lower contrast appear to be arranged radially t.w.z., terminal web zone 120,000  $\times$

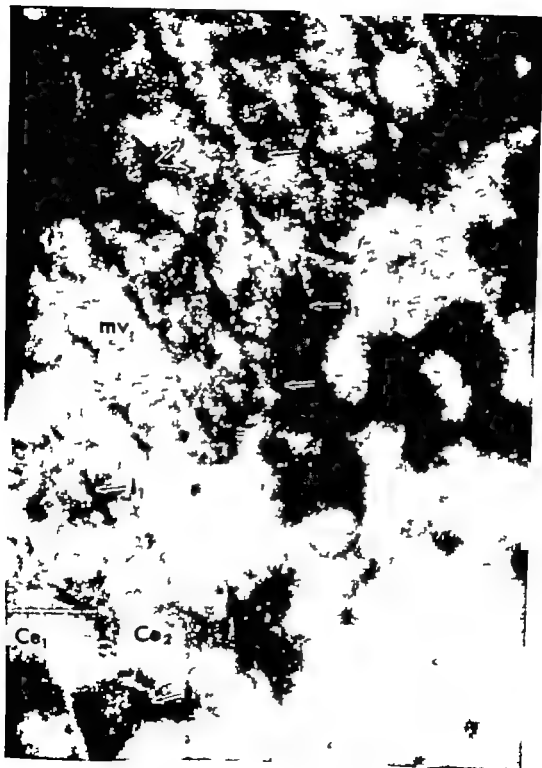


# PLATE 5

## EXPLANATION FIGURE

- 5 Micrograph showing small dense bodies ( $b_1$ ) interpreted as lipid with microvilli ( $m_1$ ). The lipoidal bodies are less numerous towards the poles of the microvilli and most numerous near their bases. (W.S. terminal width zone 100 000  $\gamma$ )



# PLATE 6

## EXPLANATION OF FIGURE

- 6 Micrograph of microvilli (m. ) 1 transverse and longitudinal section to show the location of the dense bodies,  $l_2$  (interpreted as lipid) This lipid clearly lies within the microvilli close to the inner of the two limiting membranes. The arrow points to a single lipoidal body within the terminal web zone (t.w.z.) Both in size and general appearance it is similar to the lipoidal bodies lying within the microvilli. Lipid in this form has been seen only rarely in the terminal web zone (cf fig. 4 5) The reticular pattern of the terminal web is well shown in the upper part of the micrograph 60,000  $\times$

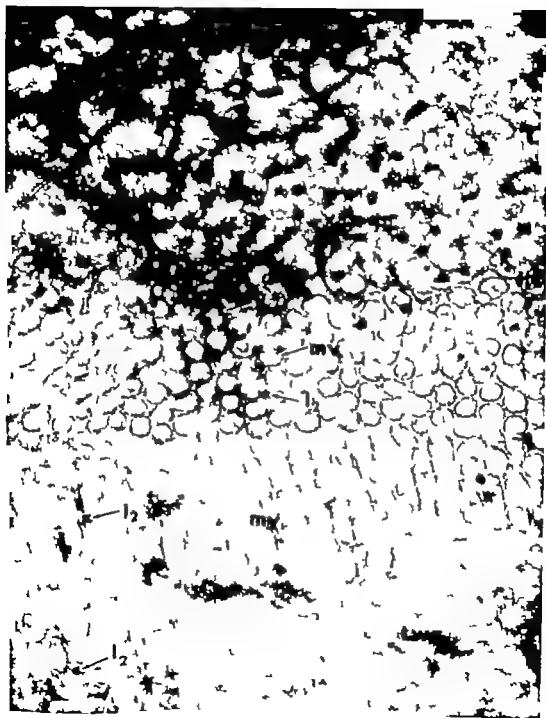




## PLATE 7

### EXPLANATION OF FIGURES

- 7 Micrograph of the regions immediately above and below the terminal web zone (t.w.z.). A small amount of dense material (l<sub>1</sub>) interpreted as lipid lies between the two membranes covering the microvilli (m.). No lipid is discernible in the terminal web zone (t.w.z.). Below the terminal web is an aggregate of many small, moderately dense bodies covered by membranes. These bodies (l<sub>2</sub>) are believed to be lipid. A further aggregate of dense bodies is also present; these bodies (l<sub>3</sub>) are more tightly packed together and more dense than those first described. They are also believed to be lipid. Morphologically they appear to represent a transitional stage between l<sub>2</sub> and l<sub>3</sub> (cf. fig. 8). The membranes enclosing the lipid are not studded with cytoplasmic particles. Associated with the lipid are some rather dense particles (p) m., mitochondrion. 80,000 x
- 8 Micrograph of the region just beneath the terminal web zone. The frequency with which the denser bodies l<sub>3</sub> have been seen in fixed animal seems to leave no doubt that they are lipoidal (cf. fig. 3). Morphologically they appear to be related to the aggregates of individually smaller less dense bodies, l<sub>2</sub> and l<sub>3</sub>. The membranes enclosing the lipid are essentially smooth-surfaced. Some membranes are present to which are attached a small number of cytoplasmic particles (p). They may be a transitional stage between the particle-studded membranes of the endoplasmic reticulum (similar to those seen lower down in the cell, fig. 9) and those which enclose the lipid. A network of fine fibers (f) is present. 80,000 x

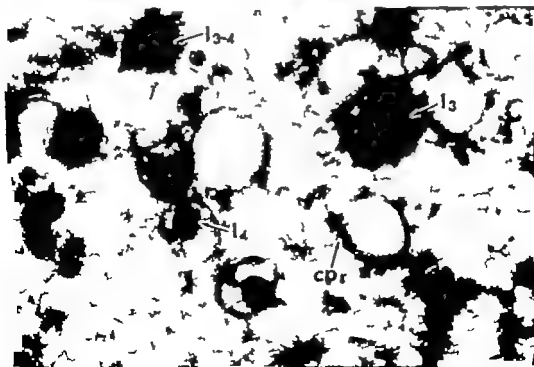
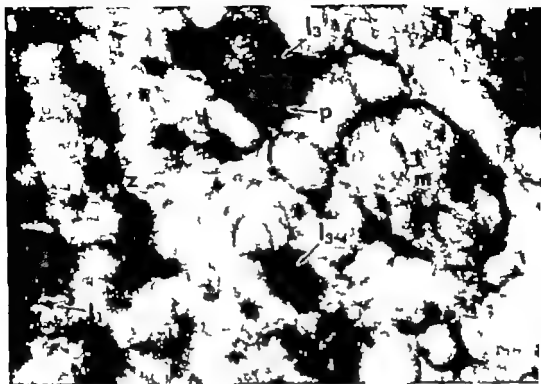


## PLATE 8

### EXPLANATION OF FIGURE

- D Micrograph of region just below that shown in figures 7 & 8. Inclusion interpreted as lipid are again present in the various forms ( $l_1$ ,  $l_2$ ,  $l_3$ ) seen in figures 7 & 8. The membranes enclosing this lipid are not studded with numerous fine particles. Those membranes (E.R.) which are studded with many fine particles do not enclose any lipid. c.p. cytoplasmic particles; m., mitochondrion.  
60,000 X

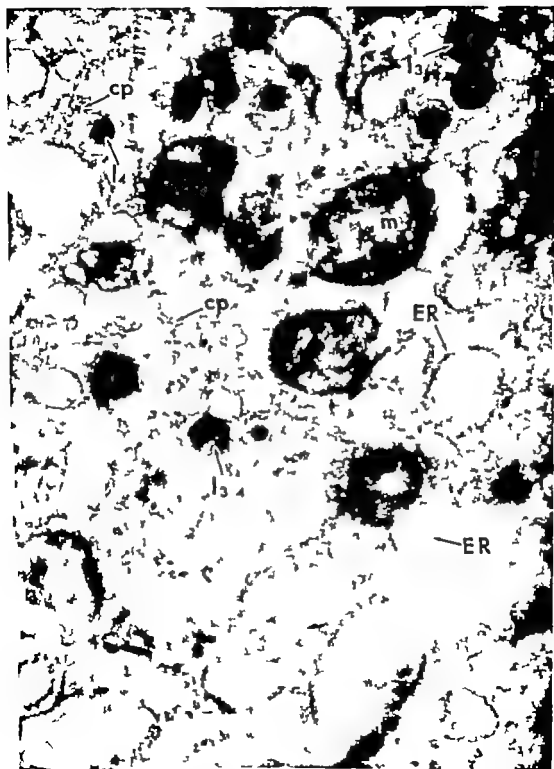


## PLATE 9

### EXPLANATION OF FIGURE

- 10 Micrograph at moderate magnification showing parts of the Golgi apparatus (vacuoles, G.v. and paired membranes, G.m.) and the region above. Inclusions interpreted as representing lipid occur mainly in the form of single dense bodies (l.) As in previous figures, the membranes enclosing this lipid are seen to be essentially smooth-surfaced. Also no lipid lies within the sacs enclosed by the particle-studded membranes of the endoplasmic reticulum (E.R.) A small amount of lipid (l) lies within the Golgi vacuoles. Many cytoplasmic particles (c.p) lie freely in the cytoplasmic matrix. m mitochondrion. 30,000 X



## PLATE 10

### EXPLANATION OF FIGURES

- 11 Micrograph showing material (interpreted as lipid) of the kind designated  $L_2$  (cf. figs. 7-8) within two Golgi vacuoles (Q.v. Q. 4). A indicated by the arrow one of these vacuoles is clearly dilation of a pair of Golgi membranes. Lipid of the kind mentioned above has been only rarely seen within Golgi vacuoles (cf. figs. 12, 13). N = nucleus; p., dense particles. 60,000  $\times$
- 12 Micrograph of part of the Golgi zone showing dense bodies (1) believed to be lipid within Golgi vacuoles (G. ). Some of the single dense bodies probably do not lie within Golgi vacuoles. Accordingly like similar bodies shown in figures 8 and 9 they are termed 1 m., mitochondrion. 40,000  $\times$

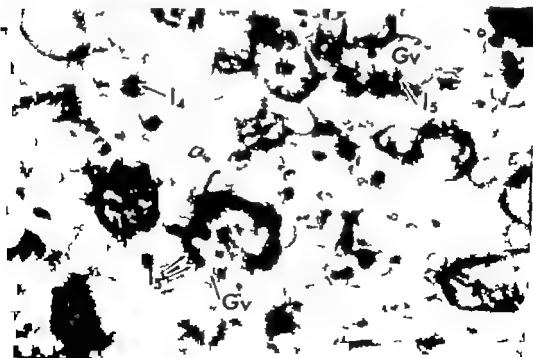
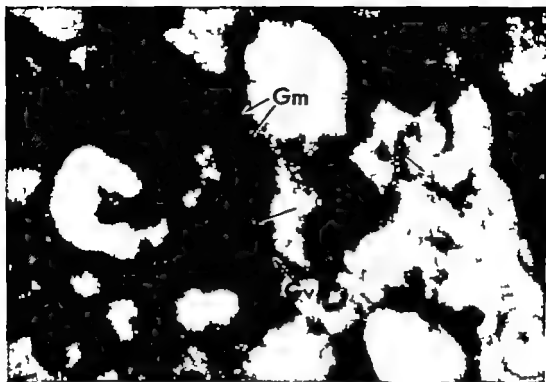




# PLATE 11

## EXPLANATION OF FIGURE

- 13 Micrograph showing some material believed to be lipid ( $l_2$ ) within Golgi vacuoles (Gv) and some ( $l_2$ ) located within vacuolar-like spaces (E) between two adjacent cells (Ce; Ce<sub>2</sub>). The lipid in both of the above mentioned region appears similar in size, shape and density. The Golgi vacuoles are orientated on the side of the paired Golgi membranes (Gm.) nearest to the cell membrane (c.m.) One or both of the two cell membranes pass into the cytoplasm of the upper cell and form narrow extracellular channels (ch.) One of these channels passes close to the Golgi vacuole "G" and, as indicated by the profiles, "pr" probably extends into the cell at least as far as the Golgi vacuole "G". The lipid in the Golgi vacuoles probably passes directly into extracellular channels of the kind described above and accumulates in a more lateral position (as in E.) between the cells.  
60,000 X





# Anatomic and Angiographic Study of the Vertebral Basilar Arterial System in the Dog<sup>1</sup>

ERNESTO DE LA TORRE, OLIVER CHARLES MITCHELL, AND  
MARTIN G. NETSKY

*Department of Neurology and Section on Neurosurgery of the Bowman  
Gray School of Medicine of Wake Forest College Winston-Salem N. C.*

An anatomic study of the intra and extracranial circulations in the dog was presented by de la Torre Netsky and Meschan ('59). The cerebral circulation was shown angiographically with radiopaque material injected into the internal carotid artery. Under normal conditions of cerebral circulation, however, contrast medium thus injected did not pass to the posterior communicating arteries. As a consequence, the vessels of the posterior portion of the circle of Willis were not seen in the living animal (fig. 1).

The territory supplied by the vertebral basilar arterial system, under normal conditions of flow, is different from the territory supplied by the internal carotid complex as was shown first by the distribution of colored dyes after perfusion experiments (Kramer '12; Jewell and Verney '57). Comparable results were obtained by McDonald and Potter ('51) in the rabbit; a similar separation is known to exist in most human brains. This concept of separate flow in two interconnected systems, therefore, has long been known, but angiographic demonstration of these two major territories in the living dog has not been available.

This report deals with a study of the anatomy of the basilar and vertebral arteries, a physiologic method of visualizing these arteries, and an analysis of the results.

## MATERIAL AND METHODS

The cerebral vessels of 5 dogs were injected with methyl methacrylate monomer and then the brain was digested. The casts of the blood vessels were used for comparison with angiograms, and allowed 3-dimensional viewing. Further details of the

method and a study of parts of the circulation not seen angiographically will be reported separately (Netsky and Jackson). The branches of the vertebral artery in the neck were not contained in these plastic models; hence dissection was performed in three other animals to verify interpretation of these angiograms.

Vertebral angiography was done on 9 additional mongrel dogs, ranging in weight from 11.5 to 14 kilograms. Nembutal (R) was given as an intravenous anesthetic (30 mg per kilogram of body weight) and an endotracheal cannula was used to assure a patent airway throughout the experiments. In 5 of the 9 dogs the wing of the atlas was removed to isolate the vertebral artery in the distal part of the neck. We refer to this approach hereafter as "high." Four to 5 cm of the artery was exposed and cannulated with PE-50 polyethylene tubing, attached to a syringe for injection of the radiopaque medium. Ringer's solution was used in a slow continuous drip between injections.

In the other 4 animals the vertebral artery was isolated at the base of the neck, between its origin from the subclavian artery and point of entrance into the vertebral canal. This approach is designated as "low." The contrast medium then was injected either directly with needle and syringe or through a PE-50 polyethylene catheter.

The contrast media used were Diodrast (R) 75% in one animal, Hypaque (R) 50% in one animal, and Renografin 60 (R) in 7 animals. Only 1 ml of radiopaque

<sup>1</sup>This investigation was supported in part by research grants B-282 and B-2117 from the National Institutes of Health, Public Health Service, Special F. How (B7-433) from the National Institutes of Health, Public Health Service.



Fig. 1 Drawing of an angiogram obtained by direct injection of the internal carotid artery in the living dog. The posterior part of the cerebral circulation is not seen despite forceful injection of 1 ml of contrast medium and filling of the extracranial circulation. Compare with figure 2.

material was injected into the vertebral artery in 4 to 5 seconds in the high approach, and 2 ml was used during the same time in the low injections. Single roentgenographic exposures were obtained with standard 54 KV x-ray equipment. Ventrodorsal projections were taken routinely because maximum information was obtained in this position.

### RESULTS

**1 Anatomic aspects** The vertebral artery has multiple branches during its course through the vertebral canal in the neck (fig. 2). These branches are segmental arising in each case at the vertebral interspace then anastomosing freely with branches from the contralateral vertebral artery and with the ventral spinal and cervical arteries. The vertebral artery perforates the transverse foramen in the alar wing of the atlas changing from a dorsal to a ventral position and anastomoses with the inferior branch of the occipital

artery at the level of the upper margin of the wing of the atlas. The combined artery (occipito-vertebral) then courses medially to end in the cerebrospinal circle. The basilar artery originates from the rostral portion of this circle. The caudal end of the circle has ample connections with the ventral spinal artery or arteries.

The basilar artery courses ventrally to the brain stem, usually in a sinuous manner (figs. 2-3). The largest branches of the basilar artery originate in the first 2 cm above the cerebrospinal circle and are cerebellar arteries (fig. 3). Two to 4 branches arise on each side but with many variations. These large vessels supply the anterior and inferior cerebellar surfaces and the medulla. The most rostral of these cerebellar arteries also sends small branches to the caudal portion of the pons. The final division of the basilar artery into the two posterior communicating arteries is at the level of the sulcus between the pons and the midbrain. The superior

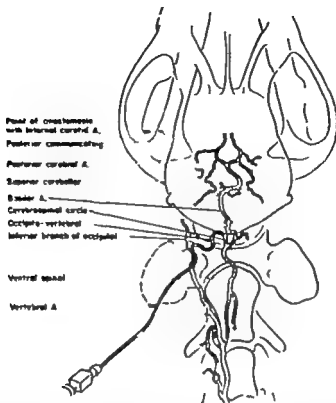


Fig. 3 Composite drawing of results of vertebral angiography. The needle and catheter are inserted as for high injection. Branches of the vertebral artery in the neck and their anastomoses are shown here for completeness, but are visible only with low injections. Compare with figure 1.

cerebellar and posterior cerebral arteries are the two major branches arising from each posterior communicating artery.

Although the blood supply of the pons is provided mainly by numerous minute branches arising directly from the basilar artery the most rostral and ventral portions are nourished by branches coming from the posterior communicating arteries. The ventral surface of the midbrain is supplied by branches arising from the posterior communicating arteries and medial branches from the posterior cerebri.

Both the posterior cerebral and the superior cerebellar arteries course in a parallel direction posteriorly and laterally to surround the cerebral peduncle and then turn medially on the dorsal aspect of the brain stem thereby forming almost a complete circle. The posterior cerebral artery is then slightly cephalad and surrounds

the most caudal portion of the thalamus and lateral geniculate body. It then passes directly back on the undersurface of the occipital lobe near the midline to irrigate the medial aspect and pole of this lobe.

**2. Angiographic aspects.** The details of the experiments are shown in table 1. With injections low in the neck the intracranial portion of the vertebral-basilar arterial complex was not visualized in two of four dogs, even when larger amounts (4 ml) of contrast medium were injected. Anastomoses of the vertebral artery in the neck were seen only in dogs with low injections (fig. 4).

Visualization of the vertebral-basilar distribution was satisfactory in all cases of the high approach (fig. 5). The posterior communicating, posterior cerebral and superior cerebellar arteries were seen bilaterally in each film. Some of the larger

TABLE 1  
Results of injection of vertebral artery

Dog no.	Radiopaque substance	Site of injection	Visualization of other arteries	Outcome after angiogram
233	2 ml Diodrast 75% (R)	High	Middle and anterior cerebral arteries	Died
238	1 ml Hypaque 50% (R)	High	—	Normal
246	1 ml Renographin 60 (R)	High	—	Normal
250	1 ml Renographin 60 (R)	High	Middle and anterior cerebral arteries	Died
253	1 ml Renographin 60 (R)	High	—	Died
255	2 ml Renographin 60 (R)	Low	Ventral spinal and cervical anastomoses	Normal
296	2 to 4 ml Renographin 60 (R)	Low	—	Normal
309	2 to 4 ml Renographin 60 (R)	Low	—	Normal
310	2 ml Renographin 60 (R)	Low	Ventral spinal and cervical anastomoses	Normal

pontile and peduncular branches of the posterior communicating arteries were also visible.

Because the posterior cerebral arteries almost completely surround the brain stem and turn back toward the midline two vessels frequently were seen superimposed on the posterior portion of the circle of Willis. These vessels are the angiographic representation of the posterior cerebral arteries in their dorsal position and should not be confused with arteries arising directly from the circle of Willis (fig. 5).

Contrast medium consistently was seen up to a point in the most anterior portion of the posterior communicating arteries at the site of junction with the internal carotids. The middle and anterior cerebral arteries were seen in only two cases (dogs 233 and 250). These dogs were apneic in shock, and died as a result of the procedure. We consider the filling of the middle and anterior cerebral arteries in these animals to be an abnormal finding because of alterations of flow occurring in shock.

#### DISCUSSION

The vertebral arteries in the dog, with multiple branches at each vertebral inter space are in striking contrast to adult man. The human vertebral artery after

its origin from the subclavian artery has no significant branches until it enters the skull.

The terminal portions of both vertebral arteries in man are the homologue of the rostral half of the cerebrospinal circle. The posterior inferior cerebellar artery arising commonly in man from the vertebral artery comes off the basilar artery in the dog. The basilar artery is then relatively longer in the dog than in man, lying on the ventral surface of both medulla and pons. Furthermore the posterior cerebral and the superior cerebellar arteries are branches of the basilar artery in man, but arise from the posterior communicating arteries in the dog.

Embryologically the posterior communicating vessels are direct continuations of the internal carotid arteries (Padgett, 48). Carotid angiography in man results in filling of the posterior cerebral arteries in about 34% of cases (Neschan, '59) but in the dog only one instance of filling of the posterior communicating arteries has been found by us in more than 100 carotid angiograms obtained in 50 animals. Vertebral angiography causes filling of the posterior communicating arteries consistently in the dog, but seldom in man.

Renographin 60 (R) was used predominantly in this study because Tindall et al. ('58) demonstrated minimal toxicity to the central nervous system caused by methyl glucamine with sodium diatrizoate. Nevertheless three of nine dogs died as a result of the angiography. This lethal effect is in striking contrast to internal carotid angiography with only one death in more than 50 animal studies performed by us. Other substances also may selectively affect different parts of the brain. Kramer ('12) noticed striking changes in respiration and blood pressure caused by small doses of alcohol or ether injected into the vertebral artery of the dog. These effects were negligible with similar doses in the carotid system.

Angiography with 1 ml of contrast medium injected in 4 seconds resulted in satisfactory visualization of the posterior portions of the circulation; other arteries were not clamped. We believe that greater amounts of medium or faster rates of injection are beyond the normal rate of blood flow. The diameter of the basilar artery is radiographically equal to the intracranial portion of the internal carotid and the rate of flow in this last vessel has been calculated to be in the range of 12 to 15 ml per minute (de la Torre, Netsky and Meschan '59). The amount of contrast medium used in our low approach was increased because of the greater dilution and large number of branches to be filled but nevertheless the low approach was less satisfactory for vertebral angiograms.

Cerebral angiograms in the dog obtained by others for the most part have been made under what we consider to be non-physiologic conditions. Halpern and Peyser ('53) and James and Hoerlein ('60) performed angiography by injecting forcefully more than 10 ml of contrast medium into the common carotid artery of dogs. Filling was obtained of the anterior and posterior circulations as well as of the external circulation with this method. Hinwrich et al. ('60) obtained angiograms after surgically produced anastomoses in the carotid and cerebral arterial complexes but they recognize that blood flow was altered by these anastomoses. When alteration of normal flow occurs after ex-

perimental procedures in shock or after death, with increased intracranial pressure or as a result of forceful injections contrast medium injected into one system may pass through the circle of Willis to the other. In the healthy animal, under physiologic conditions each of these two large systems (vertebral-basilar and carotid) is exclusively supplied by its own arteries.

#### SUMMARY

A technique is described for angiographic demonstration of the vertebral basilar circulation in the dog and the anatomy of the vertebral-basilar arterial system is correlated with the angiographic appearance. The vertebral-basilar and carotid systems are physiologically independent. Intermixing occurs only in pathologic conditions. High morbidity and mortality rates occur in vertebral as compared with carotid angiograms.

#### ACKNOWLEDGMENT

Renographin 60 (R) was provided by E. R. Squibb and Sons.

#### LITERATURE CITED

- de la Torre E., M. G. Netsky and I. Mescha 1959 Intracranial and extracranial circulations in the dog: anatomic and angiographic studies. *Am. J. Anat.*, 105: 343-382.
- de la Torre E., and M. G. Netsky 1960 Study of persistent primitive maxillary artery in human fetes: some homologues of cranial arteries in man and dog. *Ibid.*, 106: 185-195.
- Halpern, L., and E. Peyser 1953 The effect of various convulsive procedures on the cranial vessels of the dog angiographically visualized. *J. Neurosurg.*, *Exp. Neurol.* 13: 277-282.
- Hinwrich, W. A., E. Costa, R. C. Canham and S. L. Goldstein 1960 Isolation and injection of selected arterial area in the brain. *J. Appl. Physiol.*, 15: 303-308.
- James, C. W. and S. F. Hoerlein 1960 Cerebral angiography in the dog. *Vet. Med.* 55: 45-56.
- Jewell, P. A. and F. V. Verney 1937 An experimental attempt to determine the site of the neurohypophyseal osmoreceptors in the dog. *Phil. Trans. Roy. Soc. London Ser. E.*, 240: 197-332.
- Kramer S. P. 1912 On the function of the circle of Willis. *Exp. Med.*, 15: 319-364.
- M. Donald, D. A. and J. M. Potter 1951 The distribution of blood to the brain. *J. Physiol.* 114: 356-371.
- Meschan, I. 1960 A. All of Normal Radiographic Anatomy. Saunders Philadelphia.



Netsky M. G., and F. Jackson. Further studies of the canine cerebral circulation. (To be published.)

Padgett, D. H. 1948 The development of the cranial arteries in the embryo. Contrib. Embryol. Carnegie Inst., No. 212, 32, 205-261

Tindall, G. T. P. D. Kenan, R. L. Phillips, G. Margolis and K. S. Grimsen. 1958 Evaluation of roentgen contrast agents used in cerebral arteriography II. Application of a new method. J. Neurosurg. 15: 37-44

# PLATE 1

## EXPLANATION OF FIGURE

- 3 Photograph of ventral surface of brain digested after injecting blood vessels with methyl methacrylate monomer. The upper part of the cerebrospinal circle is seen at the bottom of the photograph. The dye in the sinuous basilar artery is unevenly distributed. All major vessels are filled because the injection was done after death.



## PLATE 2

### EXPLANATION OF FIGURE

- 4 Röntgenogram after injection of contrast medium in living animal. The low approach was used. The segmental arteries in the neck can be seen.



### PLATE 3

#### EXPLANATION OF FIGURE

- 5 Montage of three separate vertebral angiograms using high approach. Filling of the posterior part of the circulation is complete up to the point of anastomosis with the internal carotid artery. Compare with figure 2.



VERTIBRAL-BASILAR ARTERIES IN DOG  
 Fronte de la Terre



# Compensatory Renal Hyperplasia Following Experimental Surgical Deletions of the Kidney Complement<sup>1</sup>

CHARLES E. MCCREIGHT AND NORMAN M. SULKIN  
*Bowman Gray School of Medicine Winston-Salem N C*

Several investigators have shown within recent years that removal of one kidney of young rodents results in significantly increased cellular proliferation in tubular epithelia of the contralateral organ which reaches a peak at two to three days following the operation (Sulkin '49; Rollason, '49; McCreight, '58). McCreight and Sulkin ('59) compared the effects of this procedure in young adult and senile rats. Mitotic figures in proximal convoluted tubules of control kidneys were only one-third as numerous in senile animals as in young adults. However the proliferative response observed in the remaining kidneys of the senile rats following unilateral nephrectomy was of similar degree to that found for young animals.

The history of nephrectomy and partial nephrectomy was reviewed by Hanley ('50). Indications for partial removal of a kidney were enumerated as various traumatic pathologic and congenital disorders. Importance of preservation of as much functional renal tissue as possible was stressed. This investigator discussed compensatory hypertrophy and stated that in removal of up to one-third of one kidney no compensatory growth could be observed in the unoperated kidney. Klotz ('60) in review of the same subject has discussed mortality rates for humans anatomical features which influence feasibility of partial nephrectomy and operative techniques.

The present study was designed to observe proliferative response in varying complements of remaining kidney tissue following partial nephrectomy and to determine whether the amount of kidney epithelium removed could be correlated with the hyperplasia occurring in the remaining tissues.

## MATERIALS AND METHODS

The experimental animals were male albino rats of the C. F. Nelson strain, 4 to 7 months of age. In spite of the vascularity of the kidneys it proved possible to remove portions of these organs with a cutting edge of an electrocautery without severe bleeding. In each case a segment was removed from the lateral, convex side of the kidney leaving the larger vessels and ureter intact to serve the remaining portion of the organ. A loop of surgical thread was sewn into the organ and drawn together to constrict the vessels entering the portion of kidney to be removed and to serve as a guide for cutting.

In one group of animals one-half of each kidney was deleted. In another group a whole kidney and half of the other were removed, and in a third group one kidney and approximately three fourths of the contralateral kidney were removed. Whole kidneys from this procedure were fixed in formalin to serve as control organs. Operations were performed at approximately 1:00 P.M. All animals were sacrificed 50 hours following the surgery or at 3:00 P.M. in consideration of the diurnal pattern of mitotic activity for the rat (Blumenfeld, '39). The remaining kidney fractions were preserved in formalin.

The tissues were embedded in paraffin sectioned at 10  $\mu$ . and stained by the Feulgen method. Eight control kidneys 6 remaining half kidneys from bilateral hemi-nephrectomies 3 single remaining half kidneys, and 4 single remaining quarter kidneys were included in this study. Ob-

<sup>1</sup>Supported in part by Grant from the Floyd Browne's Fund of the Bowman Gray School of Medicine and in part by Grant from the Public Health Service B-345.  
Corworth Farms, New City N. Y.



servations of mitoses were limited to the proximal convoluted tubules where a total of 2,000 epithelial cells from randomly selected fields for each specimen was studied. The numbers of cells in various stages of mitosis for each specimen were tabulated and data was analyzed statistically according to the methods of Hill ('39)

## OBSERVATIONS

The survival rates of rats following the partial nephrectomies were as follows. Three of 4 animals lived following bilateral heminephrectomy until the appointed time of sacrifice. Five out of 7 having one and one-half kidneys removed survived the 50 hours. Of 7 rats having one kidney and three-fourths of the other removed, 4 survived until the time of sacrifice.

Mitotic figures among the cells of the proximal convoluted tubules of control kidneys were infrequent. From one to three mitoses were found in each group of 2,000 cells, with a mean of 2.00. Therefore only 0.10% of these cells were in process of division (table 1).

In remaining half kidneys following bilateral heminephrectomy where approximately one-half of the kidney complement had been removed, the incidence of mitosis among the cells under consideration was 6 to 7 times as great as in control kidneys. From 12 to 14 division figures were observed in each group of 2,000 epithelial cells. The mean number was 13.17. Calculation showed 0.66% of these cells to be in process of dividing (table 1).

Among cells of the proximal convoluted tubules of single remaining half kidneys where approximately three-fourths of the total volume of kidney tissue had been removed, mitotic figures were over 18 times as numerous as in the control tissues. Groups of 2,000 cells observed for each of 5 specimens contained from 32 to 40 dividing cells. The mean number of dividing figures per 2,000 cells was 37.20. The figures proved 1.86% of the cells were in mitosis (table 1).

In the group of animals where the greatest proportion of the kidney tissue approximately seven-eighths was removed the incidence of mitosis in epithelia of the proximal convoluted tubules was over 25

TABLE 1  
Mitotic activity in proximal convoluted tubules of intact kidneys and in remaining portions of the kidneys following partial nephrectomy

	Control			Remaining unilateral kidney halves			Remaining unilateral kidney portions		
	Rat	No. mitoses per 2,000 cells	% cells mitosis	Rat	No. mitoses per 2,000 cells	% cells mitosis	Rat	No. mitoses per 2,000 cells	% cells mitosis
1	1	3	0.10	1	39	1.95	1	53	2.73
2	2	3	0.15	2	31	1.55	2	52	2.60
3	1	1	0.05	3	36	1.80	3	53	2.65
4	3	3	0.15	4	40	2.00	4	47	2.35
5	2	2	0.10	5	39	1.95			
6	1	1	0.05						
7	1	1	0.05						
8	1	1	0.05						
Mean S.E.		2.00 0.33	0.10	Mean S.E.	37.20 3.67	1.86	Mean S.E.	51.75 1.70	2.59

TABLE 2

Comparison of mitotic activity in proximal convoluted tubules of control kidneys and in remaining kidney tissue following partial nephrectomy

Comparison	Mean no. mitoses per 2,000 cells	S.E.	Dist. of mitoses	S.E. of dist. mitoses	Dist./S.E.
Control	2.00	0.33			
Remaining bilateral kidney halves	13.17	0.38	11.17	0.44	25.36
Control	2.00	0.33			
Remaining unilateral kidney halves	37.30	2.67	25.20	2.60	13.09
Control	2.00	0.33			
Remaining unilateral kidney fourths	51.75	1.70	40.78	1.73	28.76
Remaining bilateral kidney halves	13.17	0.38			
Remaining unilateral kidney halves	37.30	2.67	24.03	2.60	9.99
Remaining bilateral kidney halves	13.17	0.38			
Remaining unilateral kidney fourths	51.75	1.70	38.36	1.73	22.10
Remaining unilateral kidney halves	37.30	2.67			
Remaining unilateral kidney fourths	51.75	1.70	18.55	2.17	4.71

The difference of means must be at least twice the standard error of the difference of these means in order to prove that significant difference exists, according to Hilt ('59).

times as great as in control specimens. In groups of 2,000 epithelial cells for each remaining one-fourth kidney from 47 to 55 mitotic figures were observed. The mean number was 51.75. The mitotic count constituted 2.59% of the whole (table 1).

Of the few mitotic figures found in control specimens over half were in prophase stage. The same was found to be true in observations in each of the categories of remaining kidney fractions. Metaphases constituted approximately one-fourth of the mitotic count in each incidence. Three telophases but no anaphases were found in the limited number of mitotic figures seen in the control specimens. In remaining kidney fractions with their greater incidences of mitosis, anaphase and telophase figures constituted each approximately one-tenth of the mitotic count.

When the mean number of mitotic figures per 2,000 cells in the control specimens was compared with that in either the bilaterally remaining half kidneys or the unilaterally remaining half kidneys or the unilaterally remaining fourth kidneys the difference of mean was highly significant. Moreover the mitotic counts in the remaining tissues of the several categories proved significantly different from one another (table 2).

## DISCUSSION

The finding of 0.10% of cells in the proximal convoluted tubules of unilaterally kidneys of young rats in mitosis corresponds with the figure of 0.10% of the same cells for similar animals found by McCright and Sulkin ('59). Comparison of these cells in mitosis in remaining half kidneys 50 hours following bilateral heminephrectomy with the 0.04% of 0.04% for the same cells in control of whole kidneys 72 hours following unilateral nephrectomy (McCright and Sulkin '59) indicates that the amount of kidney tissue removed whether it be a whole or two-thirds kidneys, determines the amount of the proliferative stimulus in the remaining kidney tissue.

Removal of amounts of kidney tissue greater than one-half the whole kidney resulted in a very rapid increase in mitosis in the epithelial cells of the proximal convoluted tubules. While the removal of one-half of the kidneys led to an over 11-fold increase in mitosis over that in control kidneys, the removal of one and one-half kidneys led to an over 16-fold increase in mitosis over that in the control kidneys. The removal of one and three-fourths kidneys led to an over 25-fold increase in mitosis over that in control tissues. Thus the amount of increase in mitosis in the proximal con-

voluted tubules of remaining kidney tissue following partial nephrectomy is proportional to the amount of kidney tissue removed. Although the two factors vary in the same direction, they do not follow the same linear pattern. Within the limits of the experiment the removal of increasing fractions of the kidney complement produced multiple increases in mitotic activity in the remaining tissues.

It is concluded that reduction of the normal quota of kidney tissue provides in some way a stimulus to the cells of the tubular epithelia of the remaining kidney tissue to divide by mitosis. The mechanism responsible for this stimulus whether it be due to increased function of the remaining tissue or to other factors related to presence or absence of kidney tissue, has not as yet been determined.

#### SUMMARY

Mitotic figures in proximal convoluted tubules of kidneys of young adult rats were found to compose 0.10% of the cell population. Removal of half of each kidney produced an over-8-fold increase of mitotic figures among these cells in the remaining kidney tissues after 50 hours. Removal of one and one-half kidneys led to an over 18-fold increase, and removal of one and three-fourths kidneys resulted in an over 25-fold increase of mitotic figures in this epithelium after a similar interval.

The mitotic activity in the control tissues corresponded closely with earlier

findings of the authors. The mitotic increase in two remaining half kidneys was similar to that found in former studies for a single remaining kidney after unilateral nephrectomy. Removal of increasing amounts of kidney tissue led to increased amounts of mitosis in the proximal convoluted tubules of remaining kidney tissue. However the progressive increases of the two factors followed a curvilinear pattern, the increase of mitosis becoming greater in proportion to the increase in amount of the kidney complement removed.

#### LITERATURE CITED

- Blumenfeld, C. M. 1939 Periodic mitotic activity in the epidermis of the albino rat. *Science*, 80: 446-447.
- Hanley H. G. 1950 Discussion on partial nephrectomy. *Proc. Roy. Soc. Med.*, 43: 1027-1042.
- Hill, A. B. 1939 Principles of Medical Statistics 2nd ed., The Lancet Limited, London.
- Klotz, P. G. 1960 Results of partial nephrectomy. *J. Urol.*, 84: 531-535.
- McCreight, C. E. 1958 Mitotic activity in remaining kidney of white mice after unilateral nephrectomy (abstract). *Anat. Rec.*, 130: 338.
- McCreight, C. E., and N. M. Sulkin 1959 Cellular proliferation in the kidneys of young and senile rats following unilateral nephrectomy. *J. Gerontol.*, 14: 440-443.
- Rollason, H. C. 1949 Compensatory hypertrophy of the kidney of the young rat with special emphasis on the role of cellular hyperplasia. *Anat. Rec.*, 104: 283-285.
- Sulkin, N. M. 1949 Cytologic studies of the remaining kidney following unilateral nephrectomy in the rat. *Ibid.*, 105: 95-112.

# The Localization of Nucleic Acids During Oögenesis in the Zebrafish<sup>1</sup>

K. K. HISAOKA AND C. F. FIRLIT

Department of Biological Sciences Loyola University Chicago

It is apparent that several factors influence the development of oöcytes. Serological methods demonstrate that proteins are transferred to the cytoplasm of developing oöcytes from the circulatory system (Nace '53 Telfer '54; Tyler '55) and other studies (Schrader and Leuchtenberger '52) indicate that the follicular cells surrounding the oöcytes play some role in the formation of yolk. Other investigations (Brachet, 42 Wittek, '52; and Vincent, '57) have led to the conclusion that the nucleic acid content of the nucleus plays a major role in the synthesis of cytoplasmic components of the oöcytes.

In investigations concerning the role of nucleic acids in the development of oöcytes the amphibian oöcyte has been a popular selection (Brachet, 40 '50 '60a, '60b; Wischnitzer '57 '58; Bieker et al., '59). Since the precise role of nucleic acids in the development of the oöcyte is not yet completely understood, further studies on the oöcytes of different species should be carried out. Relatively little attention has been given to the teleost ovary in this regard (Marza et al. '37; Yamamoto '56).

Although the embryology of the zebrafish has been presented (Hisaoka and Battle '58 Hisaoka and Firlit '60) no studies have been directed to the ovaries of the zebrafish, *Brachydanio rerio*. Mature female zebrafish when maintained at 26 C, ovulate and reproduce at intervals of 5 days with precise regularity (Hisaoka and Firlit unpublished results). The ovaries of the zebrafish are particularly well suited for histochemical studies because their oöcytes are completely free of pigmentation. The zebrafish oöcyte is characterized by the presence of relatively large and numerous nucleoli which are rich in

ribonucleic acid (RNA). This investigation was initiated with the aim of contributing further to the understanding of the growth and development of the oöcyte.

## MATERIALS AND METHODS

The ovaries of the zebrafish were dissected from selected immature and mature females which were reared in our laboratory. The ovaries were fixed in cold Carnoy's solution and following transfers to three changes of cold absolute alcohol were embedded in Tissuemat (M.P. 56-58.5 C). For histochemical studies the ovaries were sectioned at 8  $\mu$ . The methyl green-pyronin method (Brachet, 41 '42) as modified by Long and Taylor ('56) was used routinely to demonstrate the presence of deoxyribonucleic acid (DNA) and ribonucleic acid. However in order to obtain optimal staining for the zebrafish oöcyte purified methyl green was used in an acetate buffer of pH 5. Feulgen's technique was also used to demonstrate the presence of DNA. As a control, unhydrolyzed sections were placed in distilled water at 60 C for 8 minutes before staining with Schiff's reagent. Feulgen's technique confirmed the localization of DNA as indicated by methyl green (National Aniline).

As a control for the demonstration of RNA by pyronin Y (National Aniline) 1 mg/ml of purified protease-free ribonuclease (Worthington Biochemical Corporation Freehold, N. J.) was routinely used for the digestion of control sections. Digestion in ribonuclease was carried out at 37 C for two hours. Also a solvent control (distilled water) of sections was run at 37 C for two hours.

<sup>1</sup>This investigation was aided by an Institutional Grant from the American Cancer Society.

Further checks were made to test the specificity and reliability of pyronin Y for demonstration of RNA. Further in order to check Carnoy's fixative as a preservative for RNA ovaries were also fixed in cold 10% formalin and in cold Bouin's fluid. Each of the tissues fixed in formalin, Carnoy's or Bouin's fluid was processed and stained with toluidine blue and also the methyl green-pyronin technique control sections were digested with ribonuclease. The localization of RNA by toluidine blue was found to be identical to that brought about by pyronin Y. Formalin and Bouin's fluid fixed RNA in the same manner as Carnoy's. However, Bouin's fixative was undesirable because it caused excessive shrinkage and distortion of the nucleus. Sections of ovaries were also stained with Harris hematoxylin and eosin and with iron hematoxylin.

In taking the photomicrographs, panchromatic film (Adox KB-14) was employed. A green filter Kodak Wratten no. 58 was utilized. Since the cell membrane of the early oocyte was such that it could not be clearly reproduced in a photomicrograph when the light microscope was used, the phase contrast microscope was used to show more detail.

## OBSERVATIONS

### Growth of oocytes

**General changes** The ovaries of the zebrafish are lobulated and contain very little stroma (fig. 1). The oocytes arise from the germinal epithelium as a cluster of cells (figs. 2 and 3). The larger centrally located cells are destined to become oocytes and the smaller peripheral cells to become follicular cells. Numerous cords of oögonia are present in the ovaries of females which have just reached sexual maturity. The diameter of the oögonia ranges from 6 to 11  $\mu$  and of the nuclei from 4.5 to 7.5  $\mu$ . Each nucleus contains a single nucleolus which measures 1 to 1.5  $\mu$  in diameter. The chromosomes of the oögonia stain with methyl green and are Feulgen positive. The cytoplasm stains slightly with pyronin.

An oocyte is formed from an oögonium which has undergone growth and then becomes detached from an oögonial cluster. Such an oocyte has been designated to be

in stage 1 (fig. 3). Five distinct stages of oocyte formation can be recognized in the ovary of a mature zebrafish. Only the early stages of oocytes are present in the ovary of an immature female. For example in an immature female measuring 32 mm only oögonia and oocytes in stages 1 and 2 are present.

Throughout oögenesis the oocytes are surrounded by a single layer of follicular cells. The nucleus of each follicular cell possesses chromosomes which stain intensely with methyl green and are also Feulgen positive. The cytoplasm stains with pyronin and therefore contains RNA. The zona radiata (vitelline membrane) surrounding the oocyte first becomes visible during stage 2 (figs. 2, 3) following the initiation of vitellogenesis. The zona radiata is located between the cell membrane and the follicular cells (fig. 8). Under phase contrast microscopy the striations of the zona radiata (fig. 14) can be clearly seen. The zona radiata will later become the chorion (Hisaoka, '58) of the fertilized egg.

During stages 1 and 2, the oocytes possess a nuclear membrane which is characterized by its smooth oval outline. However when vitellogenesis begins the nuclear membrane becomes irregular in outline. Outpocketings of the nuclear membrane taper into the cytoplasm of oocytes during stage 3 and persist throughout the stages which follow. Many nucleoli make contact with the nuclear membrane.

**Stages** The diameter of a stage 1 oocyte is relatively small (9-20  $\mu$ ) (table 1). The thin cytoplasmic mass possessed by this oocyte contains relatively little RNA (figs. 3, 5). The diameter of stage 2 oocytes ranges from 17-69  $\mu$ . The oocytes in stage 2 are characterized by a definite increase in cytoplasmic volume and also an increase in pyroninophilic material (fig. 4). A few small vacuoles, each containing a small yolk inclusion, form during this stage. In stage 3 (figs. 6, 7) numerous yolk vesicles are distinctly visible in the cytoplasm. The diameter of stage 3 oocytes ranges from 97-273  $\mu$ . Each vesicle contains a yolk inclusion which does not stain with pyronin. The cytoplasm which is located between the

TABLE 1  
Summarized data for 5 stages of oöcytes of *Brachydanio rerio*

Stage no.	Diameter of oöcytes in $\mu$	Diameter of nucleus in $\mu$	Diameter of nucleolus in $\mu$	Average no. of nucleoli in median section through nucleolus	Approx. no. of nucleoli per nucleus
1	9-20	7-15	1-1.5	1-2	4
2	17-60	11-63	4.5-6.0	5-25	25
3	97-273	42-70	1.5-2.5	150-300	1000
4	270-378	51-68	0.1-3.0	160-250	1500
5	370-560	93-113	0.1-3.0	10-30	250

yolk vesicles contains RNA. The oöcyte in stage 4 is considerably larger (270-378  $\mu$  in diameter) than that of earlier stages. This stage is characterized by the presence of a thick, perinuclear band of cytoplasm which stains intensely with pyronin (figs. 8-9). Thin cytoplasmic strands are present between the enlarged yolk-containing vesicles which are located in the more peripheral areas of the oöcyte. There is also a RNA positive ring of cytoplasm which borders the cell membrane. The oöcyte undergoes further growth and at stage 5 the perinuclear band of cytoplasm is no longer evident. The diameter of the oöcytes in stage 5 ranges from 370-560  $\mu$ . The narrow strands of cytoplasm which are confined between the enlarged yolk platelets are still pyroninophilic.

The order in which the greatest amount of RNA appears in the cytoplasm of oöcytes is as follows: stage 2 > stage 3 > stage 4 > stage 5 > stage 1. The cytoplasm of all oöcytes is basophilic and stains with hematoxylin.

#### Nuclear changes

**Chromosomes.** The chromosomes of the oögonia and stage 1-oöcytes (figs. 2, 3) stain intensely with methyl green and are also Feulgen positive. The chromosomes of stage 2-oöcytes are Feulgen negative stain with pyronin and do not stain with methyl green (fig. 4). The chromosomes of oöcyte stages 3 to 5 are Feulgen negative and do not stain with methyl green nor with pyronin and therefore are not visible in figures 10 to 11. On the other hand, the chromosomes of all stages of oöcytes stain with hematoxylin. For example an oöcyte in stage 5 is Feulgen negative but can be shown to possess chro-

mosomes in the diplotene stage (fig. 13) if stained with hematoxylin. Diakinesis stages can also be found in stage 5-oöcytes but it is apparent that subsequent stages of meiosis are attained after fertilization.

RNA is intimately associated with the chromosomes only during stage 2. The affinity of the Feulgen-negative chromosomes of stage 2-oöcytes to pyronin (fig. 4) is confirmed by the fact that after digestion in purified protease-free ribonuclease, the chromosomes do not stain with pyronin. The chromosomes lose their affinity for pyronin at stage 3.

**Nucleoli.** Two to four nucleoli are present in stage 1-oöcytes (table 1). The nucleoli attain their greatest size during stage 2 and range from 4.5 to 6  $\mu$  in diameter. During stage 2, the large nucleoli characteristically possess a large clear central vacuole. Some nucleoli possess two nucleolar vacuoles whereas others possess as many as 6 small vacuoles. The majority of the nucleoli are attached to the chromosomes during stage 2 (fig. 4).

The nucleoli increase in number during stage 3 but individually they are smaller (1.5-2.5  $\mu$  in diameter) than those present in stage 2. In a median section, 150-300 nucleoli are more or less evenly distributed throughout the nucleoplasm. Nucleolar vacuoles are present in some of the stage 3-oöcytes but they are rarely seen in the later stages. The distribution of the nucleoli in a stage 3-oöcyte can be seen in figures 6 and 7.

During stage 4 the nucleoli which are located in the central area of the nucleoplasm (100-150 in a median section) become smaller (0.1-0.7  $\mu$ ) whereas the nucleoli which are against the nuclear membrane (60-250 in a median section) re-

main approximately the same size as the nucleoli in stage 3 (table 1). Stage 4 oöcytes possess the largest number of nucleoli and total approximately 1,500 to 2,000 per nucleus.

When the oöcytes develop into stage 5 fewer nucleoli are present (figs. 10-11). In a median section 10 to 50 nucleoli ranging from 2.5 to 3.0  $\mu$  are located close to the nuclear membrane and only 1 to 5 nucleoli (0.1-0.7  $\mu$  in diameter) are located in the central region of the nucleoplasm. The nucleoli in the central region of the nucleus subsequently disappear.

During stage 2, the chromosomes are in intimate contact with several small nucleoli. This is evident in sections stained with pyronin (fig. 4) and can also be demonstrated in stage 2-oöcytes stained with iron hematoxylin. The larger nucleoli in stage 2 are not in contact with the chromosomes and are located close to the nuclear membrane. The oöcyte represented in figure 5 is actually a stage 1 oöcyte which is developing into a stage 2-oöcyte. Reference to figure 5 will demonstrate that many small nucleoli are in intimate contact with the chromosomes.

**Yolk formation.** Yolk formation appears to be initiated during stage 2. It seems that two different types of yolk are formed in the zebrafish oöcyte. The first type of yolk is intravascular. Vesicles which contain a small yolk inclusion are formed during stage 2. The yolk inclusion or platelet is an alcohol and xylol insoluble portion of the yolk. As the oöcyte grows the vesicles enlarge. The yolk inclusion does not completely fill a yolk vesicle until the oöcyte attains stage 5. During the early stages the intravascular yolk platelets stain slightly with hematoxylin. At stage 4 the intravascular yolk platelets which are near the nuclear membrane become acidophilic and stain lightly with eosin. At stage 5 all of the intravascular yolk becomes eosinophilic.

The second type of yolk is extravascular. Small yolk platelets form in the cytoplasm between the yolk vesicles during stages 2 and 3. At stage 4 the groups of extravascular yolk which are near the nuclear membrane stain with eosin. Gradually the more peripheral extravascular yolk becomes deeply stained with eosin.

At stage 5 the extravascular yolk is more eosinophilic than the intravascular yolk.

Extravascular yolk particles never attain the size of the intravascular yolk platelets. At stage 5 the extravascular yolk bodies range in size from 13 to 33  $\mu$  in diameter and the intravascular yolk platelets measure 66 to 119  $\mu$  in diameter (fig. 12). Throughout oögenesis the intravascular yolk does not contain RNA. However RNA is present in the extravascular yolk in all stages except stage 5.

#### DISCUSSION

The chromosomes of fish oöcytes vary in their receptivity to Schiff's reagent. In *Fundulus* the chromosomes are reported to be Feulgen negative until the period of diakinesis (Marza et al. '37) and in the flounder the chromosomes are Feulgen positive during pre-synaptic and synaptic stages. In the zebrafish, the chromosomes of oögonia and the yolk-free oöcytes (stage 1) stain intensely with methyl green and are Feulgen positive. Nuclear DNA cannot be demonstrated in oöcytes stages 2 to 5 by these histochemical stains although the chromosomes stain with hematoxylin. Since methyl green is highly specific for polymerized DNA (Pollister and Leuchtenberger '49) it might be concluded that DNA does not exist in the polymerized state during stages 2 to 5. However Brachet's demonstration of Feulgen-positive material in the nucleus of amphibian oöcytes only after centrifugation (Brachet, '60b) seems to offer another explanation namely that DNA in oöcytes may be too dilute in the nucleoplasm to show a visible coloration with Schiff's reagent.

The fact that RNA is associated with the chromosomes of the zebrafish oöcyte during stage 2 seems to be significant. During stage 2, numerous small nucleoli which are demonstrable with pyronin and iron hematoxylin are in intimate contact with the chromosomes. This suggests the possibility that the synthesis of these nucleoli is directly influenced by the chromosomal DNA. In stage 2-oöcytes there are many large nucleoli which are not in contact with the chromosomes. These nucleoli may have been detached from the chromosomes although a possibility of a *de novo* synthesis exists.

In stage 2-oocytes, the nucleoli which are not in contact with the chromosomes attain the maximal size of  $6 \mu$  in diameter. During stage 3 the nucleoli decrease markedly in size ( $1.5$ – $2.5 \mu$  in diameter) but increase in number. The number of nucleoli increases to a maximum (1,500 per nucleus) during stages 3 and 4 and at this time yolk formation is very active. The nucleoli which are present in the central zone of the nucleoplasm diminish in size during stage 4 and disappear during stage 5. The significance of this change is not known at this time but it is a fact that the completion of yolk formation and oocyte growth during stage 5 is correlated with the diminution and disappearance of nucleoli.

The nuclear membrane of the early yolk free oocyte is smooth and oval in outline but after yolk formation is initiated during stage II the nuclear membrane of the successive stages forms undulations which taper into the cytoplasm. Outpocketings of the nuclear envelope have been described for the amphibian oocyte also (Wischnitzer '58). Several investigators describe the extrusion of whole nucleoli into the cytoplasm of oocytes of various species (Duryee, '30; Dodson '53; Wischnitzer '58; Yamamoto '56). In reviewing experimental data on the function of nuclear components, Sirin ('60) concludes that nucleolar RNA is contributed to the cytoplasm of oocytes. It is likely that nucleolar RNA is also distributed to the cytoplasm of the zebrafish oocyte.

During stage 2, several significant changes occur in the zebrafish oocyte. At this time the nucleoli attain maximal size and many of them contain vacuoles. Although the significance of the RNA free vacuoles is not known at this time they are only visible during stage 2. It is at this time that the cytoplasm possesses the heaviest concentration of RNA. Shortly after stage 2, the nuclear membrane becomes undulated and yolk formation proceeds intensively in a cytoplasm which undergoes increased growth.

Cytoplasmic RNA is apparently involved in yolk formation especially in the protein component. Separate studies (Malone and Hirooka unpublished results) on the

zebrafish oocyte using bromophenol blue according to the method of Mazia et al. ('53) show that protein is synthesized in both the intravesicular and extravesicular yolk. High concentrations of cytoplasmic RNA are correlated with the synthesis of cytoplasmic and yolk proteins. As the RNA level decreases at stage 5 the protein component of yolk is fully formed.

The results of this investigation favor the hypothesis advocated by Caspersen ('50) and Brachet ('60a, '60b) namely that high concentrations of RNA in cells are concerned with protein synthesis. This study suggests an intimate relationship between the chromosomes, nucleoli and cytoplasmic RNA in the zebrafish oocyte.

#### SUMMARY

Growing oocytes of the zebrafish *Brachydanio rerio* were studied by using various histochemical methods including toluidine blue, methyl green-pyronin and Feulgen's reaction. Iron hematoxylin, Harris hematoxylin and eosin were also used. The oocytes were classified into 5 distinct stages on the basis of morphology and histochemistry.

The chromosomes of the oögonia and stage 1-oocytes stain with methyl green and are Feulgen positive. The chromosomes of oocytes during stages 2 to 5 do not stain with methyl green and are Feulgen negative. The chromosomes of oocytes in stage 2 stain with pyronin and are in intimate association with the nucleoli. The levels of both nucleolar and cytoplasmic RNA are high during yolk formation but decrease markedly when the synthesis of yolk is completed at stage 5.

All nucleoli contain RNA. During stage 1 the oocytes contain approximately 4 nucleoli. During stage 2, the nucleoli attain a maximal size ( $4.0$ – $6.0 \mu$  in diameter) and possess vacuoles. During stage 3 the nucleoli increase in number but become markedly reduced in size. During stage 4 the nucleoli increase to a maximal number (1,500–2,000 per nucleus). The nucleoli which are located in the central zone of the nucleoplasm diminish in size during stage 4 and disappear during stage 5.

Two types of yolk platelets are formed. The first type is intravesicular (66–119  $\mu$



in diameter) and the second type is extravascular (13-33  $\mu$  in diameter) yolk. As the yolk is completely formed at stage 5 it becomes eosinophilic. An increased synthesis of nuclear and cytoplasmic RNA parallels an increase in the synthesis of yolk proteins. This study suggests an intimate relationship between the chromosomes, nucleoli and cytoplasmic RNA.

#### ACKNOWLEDGMENT

The photomicrographs were prepared by Mr R. J. Thomas.

#### LITERATURE CITED

- Bleher S., J. A. Spence and G. H. Hitchings 1959 Nucleic acids and their derivatives and the development of *Rana pipiens*. I. Oögenesis. *Exp. Cell Res.* 16 209-314.
- Brachet J. 1940 Étude histochimique des protéines au cours du développement embryonnaire des poissons, des amphibiens et des oiseaux. *Arch. de Biol.* 51 167-207.
- 1941 La détection histochimique et le microdosage des acides pentose-nucléiques. *Enzymologia*, 10 87-96.
- 1943 La localisation des acides pentose-nucléiques dans les tissus animaux et les œufs d'amphibiens en voie de développement. *Arch. Biol.* 53 207-253.
- 1950 Chemical embryology Interscience Publishers, New York.
- 1960a Ribonucleic acid and the synthesis of cellular proteins. *Nature*, 196 194-196.
- 1960b The Biochemistry of Development. Pergamon Press, N. Y. New York.
- Casperson, T. 1950 Cell Growth and Cell Function. Norton, New York.
- Dodson, E. O. 1953 Nucleoli and the formation of yolk in the eggs of vertebrates. *J. Roy. Micro. Soc.* 72: 177-178.
- Duryee W. B. 1950 Chromosomal physiology in relation to nuclear structure. *Ann. N. Y. Acad. Sci.* 50: 920-933.
- Hisaoka, K. K. 1958 Microscopic studies of the earliest chorion. *Trans. Am. Micro. Soc.* 77 240-243.
- Hisaoka, K. K., and H. L. Battle 1958 The normal developmental stages of the zebrafish, *Brachydanio rerio* (Hamilton-Buchanan) *J. Morph.*, 102: 311-337.
- Hisaoka, K. K., and C. F. Fridt 1960 Further studies of the embryonic development of the zebrafish, *Brachydanio rerio* (Hamilton-Buchanan) *J. Morph.*, 107 205-233.
- Long, M. E., and H. C. Taylor 1956 Nucleolar variability in human neoplastic cells. *Ann. N. Y. Acad. Sci.*, 63 1093-1108.
- Maria, V. D. E. Maria and M. J. Guthrie 1937 Histochemistry of the ovary of *Fundulus heteroclitus* with special reference to the differentiating oocytes. *Biol. Bull.*, 53: 67-92.
- Mazia, D., P. A. Brewer and M. Alfert 1953 The cytochemical staining and measurement of protein with mercuric bromophenol blue. *Biol. Bull.*, 104 57-67.
- Nace G. W. 1953 Serological studies of the blood of the developing chick embryo. *J. Exp. Zool.*, 122: 433-439.
- Pollister A. W., and L. Leuchtenberger 1949 The nature of the specificity of methyl green for chromatin. *Proc. N. A. Acad. Sci.*, 35 111-116.
- Shrim, J. L. 1960 Facts and speculation on the function of nuclear components. *The Cell Nucleus*. Academic Press, N. Y., pp. 35-48.
- Schrader, F. and C. Leuchtenberger 1953 The origin of certain nutritive substances in the eggs of Hemiptera. *Exp. Cell Res.* 3 138-146.
- Telfer W. H. 1954 Immunological studies of insect metamorphosis. II. The role of serulimited blood protein in egg formation by the *Cecropia* silkworm. *J. Gen. Physiol.* 37 539-558.
- Tyler A. 1953 Ontogeny of immunological properties. *Analysis of Development*. W. B. Saunders Co., Philadelphia, pp. 556-573.
- Vincent, W. S. 1957 Some studies on differentiation and development of the oocyte. *The Beginnings of Embryonic Development*. AAAS Washington, pp. 1-22.
- Wischmayer S. 1957 The ultrastructure of yolk platelets of amphibian oocytes. *J. Biophys. and Biochem. Cytol.* 3 1040-1042.
- 1958 An electron microscope study of the nuclear envelope of amphibian oocytes. *J. Ultrastr. Res.* 1 201-223.
- Whitt, M. 1952 La vitellogenèse chez les amphibiens. *Arch. Biol.*, 63 133-197.
- Yamamoto, K. 1956 Studies on the formation of fish eggs. II. Changes of the oocyte of *Lymnaea obscura* with special reference to the activity of the nucleolus. *J. Fac. Sci. Hokkaido Univer Ser VI*, 12: 375-390.

## PLATES

## PLATE I

### EXPLANATION OF FIGURES

All sections were cut at 8  $\mu$  and stained with methyl green-pyronin.

- 1 Section through mature ovary. A typical area of the ovary shows the relative size of the oocytes (stages 2, 3, 4 and 5) and the relative intensities of pyronin taken up by the cytoplasm of different stages.  $\times 350$ .
- 2 A nest of oögonia (O). Each oögonium possesses a small amount of cytoplasm which stains slightly with pyronin. The section is through the ovary of mature, virgin female.  $\times 600$ .
- 3 Area of an ovary to show differences in the size of an oögonial cluster (O) with that of stage 1 and stage 3-oocytes. The photomicrograph was taken with the phase contrast microscope to show cellular detail to best advantage.  $\times 600$ .
- 4 Stage 2-oocytes (with phase contrast microscopy). The nucleoli and the chromosomes are in contact and both stain with pyronin.  $\times 650$ .
- 5 Stage 1-oocyte (with phase contrast microscopy). Note pyronin-positive nucleoli which are in contact with the chromosomes. Actually the nuclear events in this oocyte are more typical of stage 3-oocyte.  $\times 1,000$ .

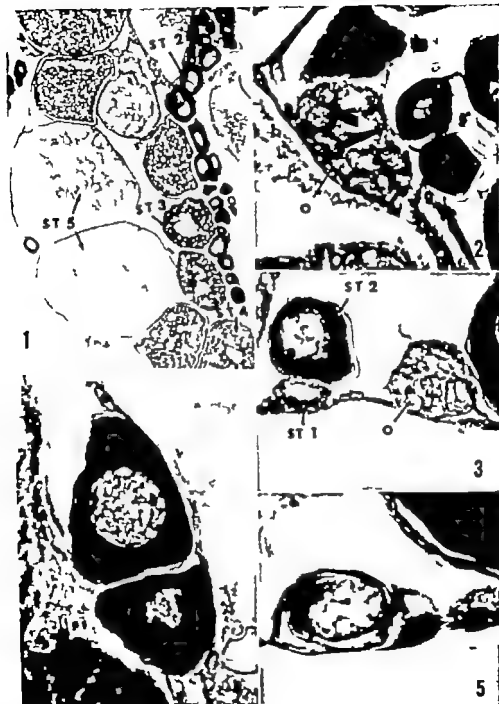


### PLATE 3

#### EXPLANATION OF FIGURES

All sections were cut at 8  $\mu$ .

- 10 Oocyte in stage 5. Methyl green-pyronin stain.  $\times 150$ .
- 11 Nucleus of a stage 5-oocyte. Only a few nucleoli remain in the central zone of the nucleus. Methyl green pyronin stain.  $\times 650$ .
- 12 Cytoplasm of stage 4-oocyte under high magnification. Note the larger intravascular yolk (IY) and the smaller extravascular yolk (EY)  $\times 800$ .
- 13 Stage 5-oocyte stained with hematoxylin and eosin. The chromosomes are in the diplotene stage. Note the large nucleoli which are close to the nuclear membrane.  $\times 960$ .
- 14 Photomicrographs taken with the aid of the phase contrast microscope to show the striated appearance of the zona radiata (ZR) of stage 5-oocyte. The zona radiata will later become the chorion of the fertilized egg. Methyl green-pyronin stain.  $\times 1,000$ .





# The Reticulum of Lymph Nodes in Mice Studied with the Electron Microscope<sup>1</sup>

SAM L. CLARK, JR.

Department of Anatomy Washington University School of Medicine  
St. Louis, Missouri

The internal framework of lymph nodes is a spare and delicate reticulum of argyrophilic fibers intimately associated with spindle cells (see the reviews by Maximow '32 and Bloom, '38). These reticular cells are described as forming a syncytium which encloses the fibers within its cytoplasm; presumably it manufactures the fibers as well. In addition, the cellular reticulum is phagocytic, capable of mitosis, and can differentiate into other types of cells. The limits of its capacity for differentiation are unknown, but many investigators believe it to be a rest of embryonic mesenchyme with all the potentialities for development which that tissue possesses.

Reticular fibers surround and traverse the sinuses in lymph nodes, but here too they are covered by cells which line the sinuses and extend as thin sheaths over the traversing fibers. These cells are phagocytic, potentially mobile and perhaps multipotent. They are said to form a lacy perforated wall for the sinus and to extend in continuity with the adjacent syncytial reticulum. In the embryo according to Downey ('22) sinuses begin as clefts between mesenchymal cells and only later do they establish connections with lymphatics lined by endothelium. Thus the cells lining sinuses resemble reticular cells, may be continuous with them and perhaps share the same embryonic origin. The two may even be interconvertible as suggested by Gillman and his colleagues ('32) who examined mesenteric lymph nodes of rats describing great variation in the relative abundance of sinuses, cortical nodules and medullary cords and concluding that sinuses are not permanent structures but develop and disappear from time to time according to need. Nevertheless sinuses do possess a

degree of integrity. Regardless of the abundance or dearth of sinuses within a node there is a subcapsular sinus which receives afferent lymph. Furthermore India ink entering a node through afferent lymphatics stays within the sinuses, and penetrates dense lymphoid tissue only in the region of the inner wall of the subcapsular sinus, as if sinuses elsewhere possessed complete unperforated walls. (Drinker, Wislocki and Field '33)

To determine more precisely the relationships between reticular fibers and cells between dense lymphoid tissue and sinuses requires greater resolution than the light microscope provides. Although the electron microscope has been used in a number of studies of lymphoid tissue only two have dealt significantly with these problems. Fresen and Wellensiek ('39) examined the mesenteric nodes of rats and monkeys. They identified reticular cells, and described the lining of sinuses as a single layer of interlocking cells which did not appear syncytial, possessed no basement membranes and resembled reticular cells. Both reticular cells and cells lining sinuses formed sheaths for bundles of fibrils imbedded in an amorphous ground substance. The fibrils were identified as collagen by their characteristic dimensions and cross-banding, and they were described as lying in an intercellular space surrounded by the processes of one or more cells. Sorenson ('60) studying popliteal lymph nodes in rabbits made similar observations except that he found a delicate and inconsistent basement membrane beneath the

<sup>1</sup>This work was supported in part by grants HG-3-71 and PG-7174(C1) from the National Institutes of Health, United States Public Health Service.

<sup>2</sup>This work was performed during the tenure of a 1 year leave of absence from the National Institutes of Health, United States Public Health Service.



cells lining sinuses. Thus the electron microscope has been used to observe details of the reticulum not visible in the light microscope but most of these data need to be amplified before being interpreted. The chief conclusion which can be drawn is that reticular fibers consist of bundles of collagenous fibrils which although closely invested by cells are extracellular. The present report is a consideration of the architecture of the reticulum and of the relationships between reticular cells and cells lining sinuses. In addition specialized venules with cuboidal endothelium, characteristic of lymphoid tissue (see Smith and Henon, '59) are described as they appear in the electron microscope.

#### MATERIALS AND METHODS

Mesenteric and occasionally other lymph nodes were obtained from 11 mice of various strains fixed one or two hours at room temperature in 1% osmium tetroxide rinsed in water dehydrated by serial dilutions in ethanol and imbedded in a mixture of methyl and *N* butyl methacrylate, polymerized with heat and benzoyl peroxide. For fixation the osmium tetroxide was dissolved in three different buffers: the veronal-acetate mixture of Palade ('52) to which 3.5% sucrose had been added Dalton's potassium dichromate solution ('55) and a balanced salt solution designed for tissue culture by White ('54) but adapted as a diluent for osmium tetroxide by Dr. Walter C. Bauer (personal communication '60). The solution contained all of the constituents specified by White except ferric nitrate and its pH was 7.4. In some instances methyl cellulose was added to a concentration of 0.5% and sometimes the fixative was cooled to 0°C.

Thin sections were cut with glass knives in a Porter Blum microtome (Serrall) and examined in an RCA EMU 2E electron microscope. In order to enhance the contrast of connective tissue fibers some sections were stained on the supporting grid by floating for one to three hours on a saturated solution of uranyl acetate and rinsing in distilled water. The destructive effects of the electron beam were mitigated in some instances by covering stained sections with a film of collodion (Watson '57).

Sections 2 to 4  $\mu$  thick were examined by phase contrast microscopy or after staining with Glomans stain. The argyrophilic reticulum was demonstrated with the silver staining method of Siders, Fraser and Lendrum ('58) applied to thick sections soaked for an hour in dichloroethane to remove the methacrylate and hydrated through acetone.

#### RESULTS

All three fixatives afforded the same picture of interrelationships between cells and fibers but the one containing White's ('54) balanced salt solution seemed the best preserver of structure. It fixed large blocks of tissue more uniformly with a less coarsely granular precipitation of nuclear material than did either of the other two fixatives. There was less leaching of the tissue than Palade's fixative produces on the other hand the tissue was not so dense as that fixed in Dalton's mixture thus being easier to section and having greater contrast when viewed in the electron microscope. There were fewer interruptions in cell membranes and pseudopods of macrophages were found in a state of expansion not seen with the other fixatives but resembling pseudopods observed *in vitro* (figs 18-19-20). Experiments have not been extensive enough to establish the value of cold fixation, but methyl cellulose, added because of its usefulness in preserving the viability of isolated cells suspended in salt solution (Phillips and Andrews '59) reduced the swelling and fragmentation which afflict cells near the surfaces of blocks of tissue fixed at room temperature.

As observed by light microscopy lymph nodes lacked trabeculae and were not easily divisible into cortex and medulla; instead, nodular accumulations of lymphocytes alternated in varying proportions with loose heterogeneous groups of cells in a spongy framework of sinuses but the whole was enclosed in a regular fashion by an extensive subcapsular sinus and a well-defined hilum. Silver impregnation stained a uniformly delicate reticulum which permeated the entire node but was concentrated in the walls of blood vessels and sinuses.

Both loose and dense lymphoid tissue examined in the electron microscope after

staining with uranyl acetate contained small bundles of fibrils banded like collagen (fig. 4) and disposed in a network comparable in delicacy and arrangement to the argyrophilic reticulum seen in the light microscope. Accompanying the collagenous fibrils in some places were thicker less dense fibers resembling those identified as elastin by Rhodin and Dalhamn ('55) (figs. 3 4 14 16). A third very finely fibrillar component without apparent cross-striation was found either closely associated with elastic fibers, as described by Rhodin and Dalhamn ('55) (figs. 3 14) or lying among collagenous fibrils (fig. 12). The fibrous reticulum was enclosed in all its extent by a system of cells which separated it from the spaces occupied by lymphocytes and other free cells.

In dense lymphoid tissue it was the reticular cells which sheathed the fibers. Their nuclei were large and pale and their cytoplasm, tenuous in shape contained ergastoplasm similar to that seen in fibroblasts (Porter and Pappas '59) as well as some phagocytic inclusions (figs. 2 3 4). Cytoplasmic processes of the same or adjacent cells abutted forming junctions resembling mesaxons and enclosing the fibers in an extracellular space analogous to that occupied by neurites in Schwann cells (Gasser '55). The discontinuity of cytoplasm observed at the junctions is the basis for a tentative conclusion implicit in this description that reticular cells do not form a syncytium. In places the approximation of cytoplasmic processes was not exact, but it is not obvious whether the resultant gaps in the reticular sheath were present in life or developed by shrinkage during preparation of the tissue (fig. 3). Nothing resembling a basement membrane was found in relation to reticular cells.

Blood vessels had sheaths also. A single layer of flattened reticular cells, similar in structure to those just described separated the collagenous adventitia of arterioles (fig. 5) the scanty accumulation of collagen around capillaries (figs. 11 7) and a similar accumulation around the so-called high endothelial postcapillary venules (see Smith and Henon '59) (figs. 11 10) from the surrounding lymphoid

tissue. Here too there were some short gaps between adjacent reticular cells, but again one may ask whether they represent artifact or nature (fig. 6). Although the endothelium of each of these types of vessel possessed a basement membrane none was found in relation to their ensheathing reticular cells.

Sinus were lined by more than littoral cells their walls were three layers thick, consisting of two cellular layers separated by a layer of reticular fibers. Except in the subcapsular sinus these components formed an apparently uninterrupted barrier between the lumen of the sinus and the surrounding lymphoid tissue; there were no signs of diapedesis. The cells next to the lumen—littoral cells—had cytoplasm which was either flattened and vesicular (figs. 10–13) or thicker and to judge by the inclusions phagocytic (fig. 14). The middle layer contained the same three fibrous components found in the reticulum elsewhere in the node and the outer layer which separated the fibers from the surrounding lymphoid tissue, consisted of flattened cells resembling the reticular cells already described. In some locations they differed from the cells lining the sinus in the possession of well-developed ergastoplasm (figs. 13 14) but elsewhere the cytoplasm in the two layers was indistinguishable (fig. 12). In fact, except for the relative concentration of free cells, it sometimes was difficult to decide when looking at a micrograph of a restricted field which side of the barrier was the lumen of the sinus. Both of the cytoplasmic layers in the wall of the sinus appeared to be cellular rather than syncytial, in that both contained numerous junctions where cytoplasmic processes abutted but did not fuse. In neither layer were these junctions marked by terminal bars and no basement membranes were seen. The layer of littoral cells extended to sheathe strands of fibrous reticulum traversing the lumens of sinuses (figs. 15 16) and such extensions when cut longitudinally looked like sections of the wall of the sinus except that both cellular layers bordered a lumen (fig. 12). The outer layer of the wall of the sinus was continuous with the cellular reticulum in the

methods more comprehensive than the isolated observation of killed tissues.

The cellular reticulum may be viewed as a continuous sheet of cells which permeates both loose and dense lymphoid tissue forms the walls of sinuses and in all these places separates a tenuous space containing reticular fibers from a much larger space containing free cells. This separation may or may not be absolute depending upon whether the small gaps observed between reticular cells in places are natural or artificial, but in either case the domain of connective tissue fibers is distinct from that of the free cells. Visualizing the continuity of the cellular reticulum is a problem in topology. The sinuses of the node are all interconnected, so their lining cells form a continuous sheet. In a more complicated way the reticular fibers which traverse dense lymphoid tissue and surround sinuses and blood vessels form a presumably continuous network; thus the reticular cells sheathing them also form a very complex, but probably unbroken sheet. These two sheets connect at the edges of the pores in the inner wall of the subcapsular sinus to constitute a continuous simple epithelium with reticular fibers against one surface and free cells next to the other. Instead of speaking of the reticular fibers as enclosed one may reverse the point of view and consider the free cells as lying in something like a vascular space enclosed and separated from connective tissue by a sort of endothelium.

According to this interpretation, lymphoid follicles are analogous to sinuses, in that their free cells lie in a space walled off by fixed cells and indeed, some areas of lymphoid tissue look like sinuses filled unusually full of cells. Furthermore the space in dense lymphoid tissue occupied by free cells connects with the lumens of the sinuses through perforations in the inner wall of the subcapsular sinus so that the entire node seems to be one continuous vascular space with regions where cells flow rapidly—the sinuses—and other places where stasis is the rule. Perhaps this continuity is the structural basis for the interconversion of sinuses and dense lymphoid tissue proposed by Gillman and his colleagues ('32) but there is, as

yet, no direct evidence that it occurs. Sinuses do not look ephemeral when observed in fixed tissues except for the subcapsular sinus their walls appear continuous and diapedesis is not seen. Furthermore, Drinker, Wislocki and Field ('33) did not find any seepage of India ink from sinuses into adjacent lymphoid tissue except along the inner wall of the subcapsular sinus where perforations are visible in the electron microscope. Therefore sinuses have at least a temporary integrity.

There was no visible difference between the inner wall of the subcapsular sinus and the walls of other sinuses to explain why only the former should be perforated. Perhaps the migratory cells which filled the pores made them in the first place by pushing through what was only a potential avenue between adjacent cells. The direction of migration cannot be established from fixed sections, although by their pseudopods many cells seemed to be going toward the subcapsular sinus but even if this were known, it would not be clear why it happens only in this location.

By describing the lymph node as a labyrinthine vascular space in which free lymphoid cells lie crowded together but separated from connective tissue one speaks in terms of the cellular environment. In this sense each cell functions in an environment consisting of neighboring cells and their products of the permeating medium—be it plasma lymph or connective tissue ground substance, and of any mechanical substrate which may be present such as a basement membrane fibers or a matrix. If cellular differentiation is partly the response of a cell to its environment, within the limits of its genetic endowment then cellular ecology—knowledge of the neighborhood in which a cell grows up—becomes critically important in the approach to questions of the origin and fate of cells. Following Burnet's ('38) lead one would study lymphoid tissue as a community in which clones of cells reproduce wax, wane and die in competition with one another in which each cell both influences and is influenced by its neighbors. Then these questions arise: do the environments of connective

tissue and of lymph nodes differ in ways that affect the differentiation of lymphoid cells what are the temporal and spatial relationships of mitosis and differentiation of cellular birth and death what cells surround dividing cells macrophages, plasma cells? To answer these the electron microscope is indispensable as the best available tool for determining the structure of cells and thus of judging their morphological differentiation but alone it is not enough because, limited as it is to the examination of dead cells it cannot indicate the direction in which differentiation is moving. Ancillary measures such as autoradiography to label cells in particular functional states or stages of reproduction and histochemical staining to identify cellular constituents or products will be useful, as well as comparative studies of lymphoid tissue at different stages of embryological development or during the course of a response to antigenic or other stimuli.

The peculiar venules with high endothelium may play a role in molding the environment of lymphoid tissue as avenues of migration for small lymphocytes. In which direction do the lymphocytes go? Are they in the process of leaving lymphoid tissue for the blood stream as suggested by most previous investigators (see Smith and Ilenson, '39) or do they perhaps go in the opposite direction completing the circuit of lymphocyte recirculation from thoracic duct to blood to thoracic duct proposed by Gowans ('39)?

#### SUMMARY

The argyrophilic reticulum of lymph nodes in mice viewed in the electron microscope consists of collagenous fibrils a few elastic fibers and a fine fibrillar material all enclosed in a sheath of cells. These reticular and littoral cells cover fibers traversing both dense lymphoid tissue and sinuses they line sinuses and they sheathe the outsides of sinuses and blood vessels so that they separate the fibrous reticulum from the spaces occupied by free cells. The walls of sinuses consist of three layers a layer of littoral cells a layer of reticular fibers and a layer of reticular cells separating the fibers from the adjacent dense lymphoid tissue. There

are no visible interruptions in the walls of the sinuses except for the inner wall of the subcapsular sinus, where there are numerous pores filled with macrophages apparently in the act of migrating between the dense lymphoid tissue and the lumen of the sinus. At the edges of the pores the sheet of littoral cells lining the sinus is continuous with the sheet of reticular cells separating the reticular fibers in the wall of the sinus from the adjacent dense lymphoid tissue. These observations are interpreted to indicate that the lymph node is one continuous vascular space separated everywhere from connective tissue fibers by a continuous sheet of reticular and littoral cells. In parts of this space — the sinuses — cells flow rapidly and in other regions — the follicles — stands is the rule. Thus the free cells lie in a peculiar environment which may influence their reproduction, growth and differentiation. In addition, venules with cuboidal endothelium, characteristic of lymphoid tissue are described as they appear in the electron microscope.

*Note added in proof* Since the submission of this paper S S Hsu has published a description of "The Ultrastructure of the Mesenteric Lymph Node of the Rat" (*Am. J. Anat.*, 109 183-225 '61) in which he reinforces previous reports that the reticular fibers everywhere are enclosed in reticular cells which do not seem to be syncytial. His observations are consonant therefore with the thesis proposed here.

#### LITERATURE CITED

- Bloom, W. 1938 Lymphatic tissue lymphatic organs. 1 Handbook of Hematology Ed. by H Downey Paul B Hoeber Inc New York, 1938, Vol., 2 142-1467  
Burnet M. 1958 The clonal selection theory of acquired immunity Vanderbilt University Press, Nashville 1959.  
Dalton, A. J. 1935 A chronic-selenium sensitive for electron microscopy *Anat. Rec.*, 121 281  
Downey H. 1928 The structure and origin of the lymph sinuses of mammalian lymph nodes and their relations to endothelium and reticulum. *Haematologica* 3 431-468  
Drinkwater K. G. B., Whitlock and M. E. Field 1933 The structure of the sinuses in the lymph nodes *Anat. Rec.* 68 261-274

- Fressen, O., and H. J. Wellensiek 1959 Zur elektronoptische struktur des lymphknotens. *Verh. Deutsch. Ges. für Path.*, 42: 353-363.
- Gasser H. S. 1953 Properties of dorsal root unmyelinated fibers on the two sides of the ganglion. *J. Gen. Physiol.*, 38: 709-728.
- Gillman J. T. Gillman, C. Gilbert and I. Spence 1952 The pathogenesis of experimentally produced lymphoma in rats (including Hodgkin-like sarcoma). *Cancer* 5: 792-846.
- Gowans, J. L. 1959 The recirculation of lymphocytes from blood to lymph in the rat. *J. Physiol.*, 140: 54-66.
- Karrer H. E. 1958 The fine structure of connective tissue in the tunica propria of bronchioles. *J. Ultrastruct. Res.*, 2: 96-121.
- 1960 Electron microscope study of developing chick embryo aorta. *J. Ultrastruct. Res.*, 4: 420-454.
- Maximow A. A. 1933 The macrophages or histiocytes. In *Special Cytology* Ed. by E. V. Cowdry Paul B. Hoeber Inc., New York, 1933. 709-770.
- Marchesi, V. T. and H. W. Flory 1960 Electron micrographic observations on the emigration of leucocytes. *Quart. J. Exp. Physiol.*, 45: 343-348.
- Palade G. E. 1963 A study of fixation for electron microscopy. *J. Exp. Med.*, 93: 285-299.
- Phillips, H. J. and R. V. Andrews 1959 Some protective solutions for tissue cultured cells. *Exp. Cell Res.*, 16: 678-682.
- Porter K. R. and G. H. Pappas 1959 Collagen formation by fibroblasts of the chick embryo dermis. *J. Biophys. and Biochem. Cytol.*, 5: 153-166.
- Rhodin, J., and T. Dalhamn 1955 Electron microscopy of collagen and elastin in lamina propria of the tracheal mucosa of rat. *Exper. Cell Res.*, 9: 371-378.
- Sidders W. S., D. S. Fraser and A. C. Lendrum 1954 Silver impregnation of reticulin. *J. Path. and Bact.*, 75: 478-481.
- Smith, C., and B. K. Hanson 1959 Histological and histochemical study of high endothelium of post-capillary veins of the lymph node. *Anat. Rec.*, 135: 807-814.
- Sorenson C. D. 1960 An electron microscopic study of popliteal lymph nodes from rabbit. *Am. J. Anat.*, 107: 73-93.
- W. Ison M. L. 1967 Reduction of beating artifacts in thin sections examined in the electron microscope. *J. Biophys. and Biochem. Cytol.*, 5: 1017-1022.
- White P. R. 1954 The cultivation of animal and plant cells. The Ronald Press Co. New York 1954. 90.

All figures represent electron micrographs of mesenteric lymph nodes from mice imbedded in methacrylate. All tissues except that shown in figure 7 were fixed at 0°C in a buffered balanced salt solution containing 1% osmium tetroxide (Bauer '60 personal communication) and that in figure 7 was fixed at room temperature in Palade fixative ('62) containing 3.5% sucrose. All sections except those shown in figures 7, 13, 18 and 19 were stained with uranyl acetate and covered with a second film of collodion.

## PLATE 1

### EXPLANATION OF FIGURE

- 1 In this low-power view of part of a dense lymphoid nodule most of the cells are lymphocytes of various sizes. The elongated pale nucleus, (R) probably belongs to a reticular cell. The small bundles of collagen (c) the arrows which are enclosed in thin cellular sheaths, together with the collagen in the walls of the blood capillaries (Cap) correspond in size and disposition with the argyrophilous reticulum observed in the light microscope.  $\times 4,800$ .



- Freese, O., and H. J. Wallensiek 1956 Zur elektronoptische struktur des lymphknotens. *Verh. Deutsch. Ges. für Path.*, 42: 353-363.
- Gasser H. B. 1955 Properties of dorsal root unmyelinated fibers on the two sides of the ganglion. *J. Gen. Physiol.*, 38 709-728.
- Gillman, J. T. Gillman, C. Gilbert and L. Spence 1957 The pathogenesis of experimentally produced lymphomata in rats (including Hodgkins-like sarcoma). *Cancer* 5 792-846.
- Gowans, J. L. 1959 The recirculation of lymphocytes from blood to lymph in the rat. *J. Physiol.*, 146 54-69.
- Karrer H. E. 1958 The fine structure of connective tissue in the tunica propria of bronchioles. *J. Ultrastruct. Res.*, 2 96-121.
- 1960 Electron microscope study of developing chick embryo aorta. *J. Ultrastruct. Res.*, 4 420-454.
- Maximow A. A. 1933 The macrophages or histiocytes. In *Special Cytology* Ed. by E. V. Cowdry Paul B. Hoeber Inc., New York, 1933. 709-770.
- Marchesi, V. T. and H. W. Florey 1960 Electron micrographic observations on the emigration of leucocytes. *Quart. J. Exp. Physiol.* 45: 343-348.
- Palade E. E. 1952 A study of fixation for electron microscopy. *J. Exp. Med.*, 95 285-299.
- Phillips, H. J. and R. V. Andrews 1956 protective solutions for tissue culture. *Exp. Cell Res.*, 16 678-682.
- Porter K. R., and E. D. P. 1959 formation by fibroblasts of the chondrodermal. *J. Biophys. and Biochem* 153-166.
- Rhodin, J., and T. Dalhamn 1955 I. microscopy of collagen and elastin propriis of the tracheal mucosa. *J. Cell Res.*, 9 371-375.
- Slidders, W. B., D. S. Fraser and A. C. 1956 Silver impregnation of Path. and Bact., 75 478-481.
- Smith, C., and B. K. Hénon 1950 and histochemical study of high of post-capillary veins of the. *J. Anat. Rec.*, 125 207-214.
- Sorenson G. D. 1960 An electron study of popliteal lymph nodes. *J. Am. J. Anat.*, 107 73-82.
- Watson, M. L. 1957 Reduction of facts in thin sections examined microscope. *J. Biophys. and B* 3 1017-1022.
- White, P. R. 1954 The culture of plant cells. The Ronald P. York, 1954 80.

All figures represent electron micrographs of mesenteric lymph nodes from mice in methacrylate. All tissues except that shown in figure 7 were fixed at 0°C in balanced salt solution containing 1% osmium tetroxide (Bauer '60 personal communication, and that in figure 7 was fixed at room temperature in Palade fixative ('32) mg 35" sucrose. All sections except those shown in figures 7 12 16 and 19 were with uranyl acetate and covered with a second film of collodion.

## PLATE 1

### EXPLANATION OF FIGURE

- 1 In this low-power view of part of a dense lymphoid node, most of the cells are lymphocytes of various sizes. The elongated pale nucleus, (N) probably belongs to a reticulated cell. The small bundles of collagen at the arrows, which are enclosed in thin sheaths together with the collagen in the walls of the blood capillaries (Cap) respond in size and disposition with the argyrophilic reticulum observed in the macrophage.  $\times 4,800$ .

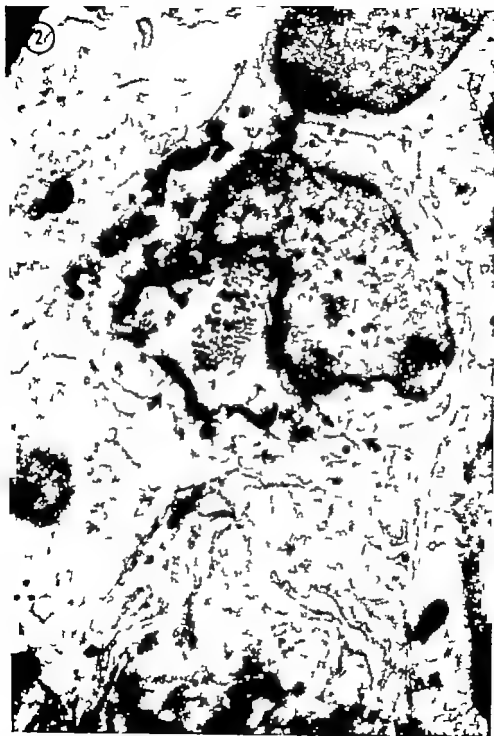




### PLATE 3

#### EXPLANATION OF FIGURE

- 3 These intersecting bundles of collagenous fibrils (C) traverse dense lymphoid tissue accompanied by larger less dense homogeneous fibers, presumably elastic (E) and an associated very finely fibrillar material. They are separated from the surrounding lymphocytes by the thin processes of reticular cells (R) very attenuated in places and even interrupted for short distances (arrows) but forming a distinct partition  $\times 20,000$ .



# PLATE 4

## EXPLANATION      FIGURE

- 4 This thin bundle of collagenous (O) and elastic (E) fibers traversing dense lymphoid tissue is enclosed on one side by the flattened process of reticular cell (R) and on the other by cell containing large dense phagocytic inclusions, a vacuole with variety of particulate materials in it (V) and numerous ribonucleoprotein particles (P). The collagenous fibrils are striated with major period that measures approximately 45 mμ. × 36,000.



## PLATE 5

### EXPLANATION OF FIGURE

- 5 The lumen of this small artery in dense lymphoid tissue contains an erythrocyte, the endothelium (End) is thrown into thick ridges, and the media consists of a single layer of smooth muscle cells (SM). In the adventitia are bundles of collagenous fibrils (C) and reticular cells (R) beset the whole vessel.  $\times 18,000$



## PLATE 5

### EXPLANATION OF FIGURE

- 5 The lumen of this small artery in dense lymphoid tissue contains an erythrocyte, the endothelium (End) is thrown into thick ridges, and the media consists of a single layer of smooth muscle cells (SM). In the adventitia are bundles of collagenous fibril (C) and reticular cells (R) sheathe the whole vessel.  $\times 18,000$ .





# PLATE 9

## EXPLANATION OF FIGURES

- 10 This is part of post-capillary venule in dense lymphoid tissue. The lumen  $\downarrow$  in the upper right corner of the picture. The endothelial cells (End) contain numerous small vacuoles near their luminal surfaces and abundant ergastoplasm. Terminal bars (T) mark the junctions between endothelial cells, but the lymphocyte (L) lying between endothelial cells is not connected to them by terminal bars. Outside the endothelium is basement membrane surrounded by thin connective tissue space containing collagenous fibrils (C). Next to that, instead of the usual layer of reticular cell, a littoral cell with many vesicles in its cytoplasm (S) separating the connective tissue space from the lumen of sinus. There is no smooth muscle in the wall of the venule. 13,000



## PLATE 10

### EXPLANATION OF FIGURES

- 11 This sinus lies in the depths of node. The lumen above, below and to the left is separated from the dense lymphoid tissue to the right by continuous boundary three layers thick, consisting of layer of cells lining the sinus (S) layer of reticular cells (R) bordering the dense lymphoid tissue, and layer of collagenous fibril (C) between. The blood capillary (Cap) shares a reticular cell with the adjacent sinus. Small bundles of collagen (arrows) traverse the dense lymphoid tissue, wrapped in reticular cells. The free cells in both the sinus and the surrounding tissue are mostly lymphocytes. / 4,600.

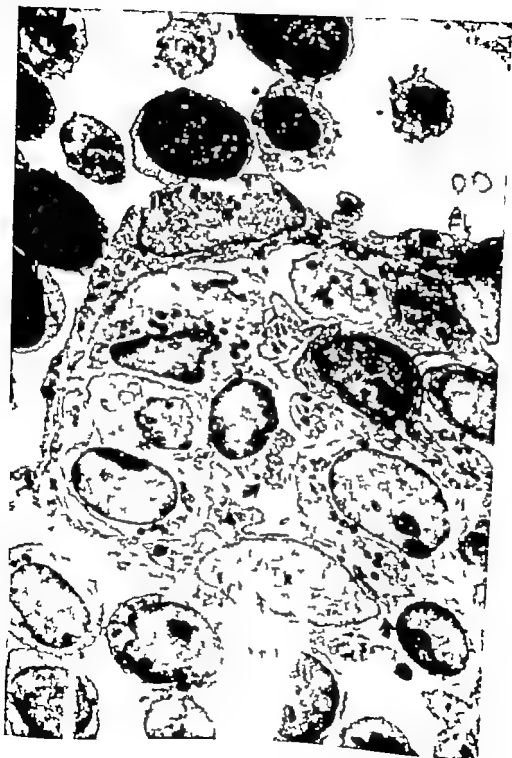


## PLATE 11

### EXPLANATION OF FIGURE

- 12 This is an enlargement of the previous picture taken from an area on the left border and rotated 90° clockwise. The lumen of the sinus (above) is subdivided by what is probably a bundle of connective tissue fibers traversing the lumen and it is separated from the dense lymphoid tissue (below) by a layer of littoral cells (S). A space containing collagenous fibrils (C) and some very fine fibrillar material, and a layer of reticular cells (R). The barrier subdividing the lumen of the sinus is similar except that both cellular layers line a sinus. No basement membranes can be seen.  $\times 20,000$

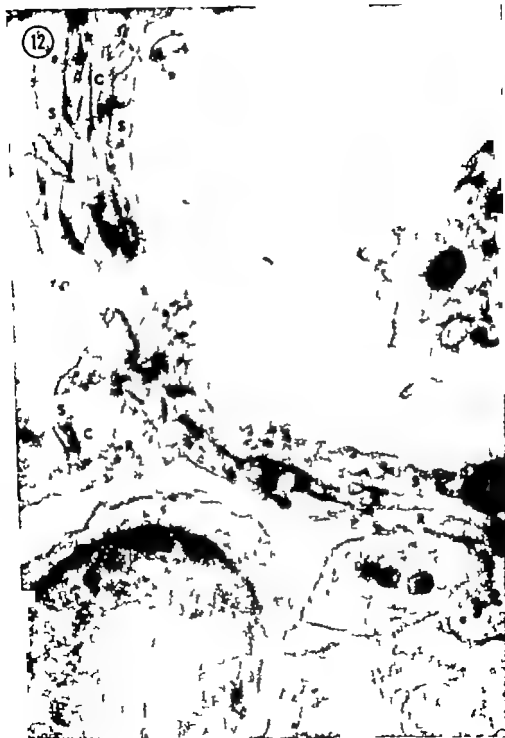


## PLATE 12

### EXPLANATION OF FIGURE

- 13 At this border between a sinus deep within node and the neighboring dense lymphoid tissue the littoral (L) lining the sinus differs from the reticular cell (R) bordering the dense lymphoid tissue in possessing large vacuoles but scant ergastoplasm. Between the two cellular layers is thin connective tissue space (C) but there are no basement membranes. The free cell in the lower right displays an elaborate pseudopod characteristic of those found on cells fixed in balanced salt solution. This section was not stained or covered with collodion.  $\times 21,000$





## PLATE 13

### EXPLANATION OF FIGURE

- 14 The lumen of this sinus, deep within node, is lined by cell (S) containing many large vacuolar inclusions, presumably phagocytic. Beneath it is connective tissue space containing collagenous fibrils (C) larger fibers which are probably elastic (E) and some very fine fibrillar material, but no basement membranes. A reticular cell (R) with well developed ergastoplasm separates this space from the dense lymphoid tissue to the lower right. The lymphocyte in the lumen of the sinus has extended small pseudopod to touch the cell lining the sinus.  $\times 21,000$



# PLATE 15

## EXPLANATION OF FIGURE

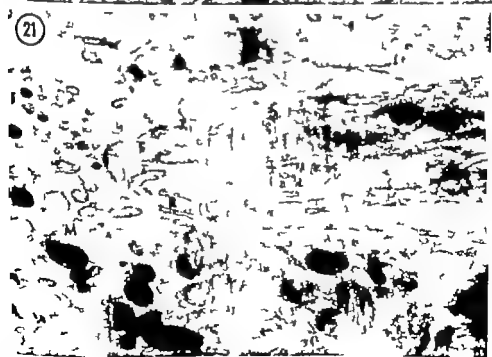
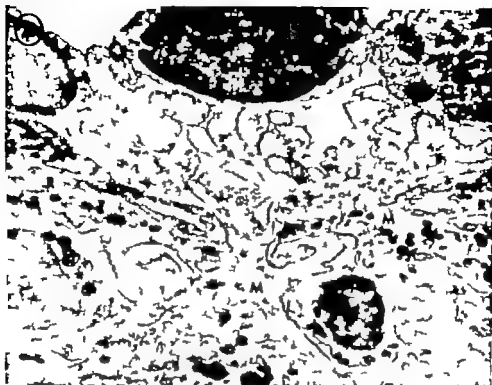
- 15 This subcapular sinus contains several free cells with expanded pseudopods. The capsule of the node is in the upper left corner and the inner wall of the sinus extends an irregular line of cells (S,S,S,S) along the right side. A macrophage (M) containing numerous inclusions fills an interruption in the inner wall, extending into the sinus on one side and into dense lymphoid tissue on the other. In the lower part of the picture the wall of the sinus can be seen to be two cells thick; reticular cell (R) opposes the cell lining the sinus (S) and the two layers enclose thin connective tissue space. This section was not stained or covered with collodion.  $\times 8,500$ .



## PLATE 17

### EXPLANATION OF FIGURES

- 20 Two lymphocytes and a mast cell lie in the lumen of this subcapsular sinus (above). The inner wall of the sinus consists of two cellular layers: one lining the sinus (S,S) and the other (R,R) bordering the dense lymphoid tissue. There is an interruption in the wall, filled by the processes of two macrophages (M,M) which lie in the dense lymphoid tissue with pseudopods extended into the sinus.  $\times 8,000$
- 21 This is an enlarged view of the right hand edge of the interruption in the inner wall of the subcapsular sinus shown in figure 20. The interruption is filled by a macrophage (M) which lies in the dense lymphoid tissue (below) with pseudopod extended into the sinus (above). The cell lining the sinus (S) and the reticular cell apposing it (R) abut at the edge of the interruption in the wall, separating the connective tissue spaces enclosed between them (C) from both the sinus and the dense lymphoid tissue, which at this point are continuous.  $\times 29,000$





# Morphogenetic Studies of the Rabbit

## XXXI. WEIGHTS AND LINEAR MEASUREMENTS OF SOME OF THE BONES OF 35 RACE III RABBITS

HOMER B. LATIMER AND PAUL B. SAWIN

*Department of Anatomy University of Kansas Lawrence and  
Roscoe B. Jackson Memorial Laboratory Bar Harbor Maine*

The skeleton has been the subject of many quantitative studies and individual bones, especially of the human skeleton, have received even more attention. Many of the reports on the human skeleton have been reviewed in a recent report on some Asiatic skeletons (Latimer and Lowrance '60). Growth of the skeleton has received some attention (Latimer '27 '44 and Hammar '32) and the adult skeletons of various animals have been weighed and measured (Schultz, '37 Latimer '37 '38). These papers give additional references to further data on adult skeletal material.

The ossification of the bones of the rabbit skeleton has been reported by Sawin and Cray ('56) Cray and Sawin ('57) Sawin, Cray and Webster ('59) and these papers list previous publications on the early ossification of the rabbit skeleton. Hammar ('32) gives measurements of many bones of the small Swedish rabbit in its postnatal development. Haardick ('56) has studied the postnatal growth of the various parts of the skeleton in several races of rabbits. The postnatal increase in length of the tibia and calcaneus of the rabbit has been studied by Lowrance ('33) and the closure of the cranial sutures, by Selman and Sarnat ('55). Linear measurements of the skull, the long bones and the vertebrae in 16 adult skeletons normal, homozygous and heterozygous for the Dachs (Dz) gene of the New Zealand White race have been reported by Sawin and Cray ('57).

The weights and the methods of preparation of the entire moist skeletons of these 63 race III rabbits have been published (Latimer and Sawin, '55a '57). The frequent use of the rabbit in laboratory and experimental work seems to justify the

publication of a detailed study of the bones of the normal adult rabbit. Furthermore this study adds one more system to the series of reports which have been published on race III rabbits (Latimer and Sawin, '57 '58 '59b and '60). This report will present the room dry weight of the entire skeleton together with weights and linear measurements of the bones and also a few linear measurements of the skull of race III rabbits.

### MATERIALS AND METHODS

The skeletons are from 35 male and 30 female adult rabbits of race III of New Zealand White origin which have been inbred for 25 years as closely as possible without losing their reproductive capacity. Further details of these rabbits and the methods of dissection and study together with the weights of the entire "ligamentous skeleton and the moist cartilaginous skeleton are listed in the earlier report (Latimer and Sawin, '57).

The bones of each skeleton were air dried and then stored in an air conditioned room for at least 5 years, or until this study was begun. The room dried bones of each skeleton were all weighed together to obtain the dry skeletal weight or the skeletal weight of table 1.

In removing the brain and spinal cord for an earlier report (Latimer and Sawin, '55b) the calvarium of the skull and the laminae of all vertebrae were removed and hence no linear measurements of these parts could be made. The spinal cord did not extend into the sacrum; consequently this bone was not disturbed. All of the bony

This investigation was supported (in part) by P.H.S. research grant C56 C from the National Cancer Institute, Public Health Service, and aided by grant from the American Cancer Society.



parts were carefully saved and weighed with the entire skeleton. The skeletal weight includes all of these parts as well as all of the bones. There is a possibility that these weights of the entire skeleton may not be as large as they should be due to the loss of some of the very small pieces of bone but at least all of the skeletons were uniformly prepared and all of these small pieces were saved so far as possible.

The entire skeleton was weighed on a laboratory balance sensitive to 0.1 gm and the individual bones on an analytical balance sensitive to 0.1 mg but the weights of the individual bones were recorded only to the nearest milligram. The weights of all paired bones are the sums of the weights of the right and left bones of the pair and the linear measurements are the averages of the measurements of the two bones of each pair. These averages should be more reliable than the measurements of only one bone of the pair.

All of the measurements except the lengths of the femur and tibia were made with a sliding straight armed calipers read to 0.1 mm. The bones too long to be measured with the calipers were measured on a small osteometric board made especially for these rabbit bones. The maximum lengths were used for all of the long bones (Stewart '52) including the tibia. The rabbit tibia does not have pronounced intercondylar eminences and hence the total length of the tibia was measured. The length of the os coxae is the maximum length measured with the back of the calipers parallel to the long axis of the bone. The lengths of the three parts of the os coxae were measured from the center of the acetabulum to the most distal end of the respective part. The transverse diameters of the long bones were all taken at the proximal ends and are the maximum diameters. The width of the femur was measured distal to the neck or between the lesser and the third trochanters. This is slightly less than that between the head and the greater trochanter. These dimensions seemed more reliable than measurements at the middle of the shafts of the bones and they also afforded comparisons with the existing data on rabbit bones (Sawin and Cray '57).

A few modifications of the methods of Stewart ('52) were necessary for some of the irregular bones and they are as follows. The length of the mandible was measured from the tip of the incisor tooth to the posterior angle. The length of the scapula is the distance from the dorsal lip of the glenoid cavity to the vertebral border at tip of spine and the width is the distance between the superior and inferior angles with the back of the calipers parallel to the vertebral border. The superior angle is not distinct in these rabbit scapulae and hence the arm of the calipers extended out to the most superior part of the superior border some distance from the vertebral border. The length of the atlas is the maximum distance between the edges of the superior and inferior articular surfaces measured on the right side and the length of the axis was measured from the tip of the dens to the inferior articular surface. The width of both atlas and axis is the maximum overall width.

The superior parts of the skull and the laminae of the vertebrae had been removed for the study of the brain and spinal cord and hence most of the measurements of the skull were made on its base. The nasal bones were removed intact and their lengths are the maximum lengths. Figure 1 will adequately show how these linear measurements were made on the skull. It was thought that the distance between the free edges of the auditory meati (AM fig 1) would vary more than the distance measured from the rounded auditory bullae (AB) and the coefficients of variation in panel A of table 4 show that the measurements between the bullae are about half as variable as between the edges of the ossified external acoustic meati.

#### Weights (in grams)

The weights of the skeleton and of some of the bones together with their standard deviations for males and for females are shown in panel A, table 1. The coefficients of variation are listed in columns two and four and the last column has the  $t$  values of the differences with the heavier sex indicated.

The femur is the heaviest bone in both sexes with the ankylosed tibia and fibula a close second. The clavicles are the light

TABLE 1

Weights and percentage weights of some of the bones of the rabbit skeleton. Weights are the sums of the weights of all paired bones

	Males		Females		T
	Average and stand. dev	Coef. of variation	Average and stand. dev	Coef. of variation	
Panel A Weights in grams					
Skeleton	147.428 ± 13.936	9.45	154.117 ± 12.013	7.79	92.03
Mandible	8.975 ± 0.886	9.87	9.187 ± 0.878	9.02	90.98
Clavicle	0.101 ± 0.018	12.15	0.102 ± 0.014	14.16	90.42
Scapula	4.506 ± 0.672	14.91	4.690 ± 0.562	11.54	92.43
Humerus	8.958 ± 0.954	10.65	9.216 ± 0.783	8.49	91.16
Radius and ulna	6.483 ± 0.693	10.73	6.627 ± 0.611	9.23	90.87
Sacrum	2.748 ± 0.302	10.99	3.028 ± 0.423	13.96	93.07
Ox coxae	11.312 ± 1.396	12.26	11.903 ± 1.118	9.34	90.56
Femur	18.391 ± 1.838	9.99	18.383 ± 1.348	7.32	91.02
Tibia and fibula	18.596 ± 1.496	8.02	18.947 ± 1.316	7.64	91.06
Calcaneus	2.493 ± 0.221	8.87	2.514 ± 0.306	8.19	90.29
Panel B Percentages of skeletal weight					
Mandible	6.09 ± 0.29	4.80	5.96 ± 0.34	5.79	91.58
Clavicle	0.068 ± 0.0068	9.84	0.066 ± 0.0068	10.28	91.18
Scapula	3.01 ± 0.29	7.48	3.14 ± 0.17	5.43	92.68
Humerus	6.07 ± 0.30	3.36	5.96 ± 0.20	3.43	91.80
Radius and ulna	4.40 ± 0.25	5.73	4.30 ± 0.18	4.27	91.77
Sacrum	1.81 ± 0.12	6.63	1.97 ± 0.25	12.85	93.28
Ox coxae	7.66 ± 0.28	4.02	7.79 ± 0.26	4.58	91.11
Femur	12.48 ± 0.59	4.61	11.94 ± 0.48	4.04	91.89
Tibia and fibula	10.57 ± 0.46	4.36	10.36 ± 0.48	4.42	91.81
Calcaneus	1.69 ± 0.07	4.01	1.63 ± 0.08	5.18	92.12

T values of 2.04 and above are significant at 5% and T values of 2.78 and above are significant at 1%

est and also the most variable in weight in the females while the scapula is the most variable in the males. The thin plates of bone in the supra and infraspinous fossae of the scapula were lost in cleaning many of these scapulae and this may account for their high variability. The femur is the least variable bone in the females and the calcanei in the males. The 4 bones least variable in weight in both sexes but not in the same order are femur tibia and fibula, calcaneus and mandible. The coefficients of variation average 10.86% in the males and 9.70% in the females.

The larger female rabbits have heavier bones with only one exception namely the femur; but only three bones (scapula, sacrum and ox coxae) are significantly heavier in the females. The weight of the femur is very nearly the same in both sexes. The two pelvic bones sacrum and ox coxae, are the only bones significantly different at the 1% level. These pelvic bones might be expected to be larger in the females to provide a larger parturient canal.

#### Weights as percentages of total skeletal weight

Panel B table 1 shows the weights of these bones as percentages of the entire skeleton. Seven of these percentages are larger in the males and three bones scapula, sacrum and ox coxae are heavier as percentages of total skeletal weight in the females but only the first two are significantly heavier. Thus the scapula and sacrum are significantly heavier in grams and as percentages of total skeletal weight in the females. The heavier female sacrum is expected but the heavier scapula is not so easily accounted for. In 4 footed animals, the weight of the head is carried on the fore limb but the head is absolutely and relatively heavier in these male rabbits (Latimer and Sawin '57) and so this will not explain the heavier female scapulae.

These relative weights unlike the weights in grams, are more variable in the females than in the males. The averages of these coefficients of variation are 6.02% for the females and 5.54% for the males. In both

sexes the weight of the humerus has the lowest coefficient of variation, or the weight of the humerus follows the weight of the entire skeleton more closely than that of any of the other bones. The weight of the femur in the females is second while in the males it is fourth from the least variable. The percentage weights of the clavicle have the highest coefficients of variation in the males and next to the highest in the females. Although the male bones vary more in actual weight (panel A) their relative weights are more constant than those of the females.

The three bones of the fore limb of the males form 10.5% of the weight of the entire skeleton and 10.3% in the females. Similar percentages for the three bones of the hind limb are respectively 23.0% and 22.3% or in both sexes the relative weights of the three bones of the hind limb are 2.2 times as heavy as those of the fore limb. A similar ratio for the bones of the human skeleton is 2.7 times (Latimer and Lowrance, 60). Thus the weights of the bones in the two extremities are more alike in

the rabbit than in man, although in both cases the upper extremities are lighter in weight than the bones of the lower extremities.

### Linear measurements

Table 2 shows all of the linear measurements except those of the skull which will be presented in table 4. The arrangement of the data and the  $t$  values of the sex differences are the same as in table 1.

The bones of the hind limb are all longer than the corresponding bones of the fore limb. All of the bones of the appendicular skeleton are longer in the males except the clavicle, humerus and os coxae but only the clavicle and os coxae are significantly longer in the females. The tibia and ulna are the longest bones in their respective extremities in the rabbit while the femur and humerus are the longest in the human skeleton.

Eleven of the 26 measurements of these bones are longer in the males and 15 in the females. None of the measurements of the males are significantly longer while

TABLE 2

Linear measurements in millimeters. The lengths are the averages of the paired bones. The  $t$  values are the same as in table 1.

	Males		Females		$t$
	Average and stand. dev.	Coef. of variation	Average and stand. dev.	Coef. of variation	
Atlas length	31.83 $\pm$ 0.68	5.76	31.49 $\pm$ 0.68	5.87	0.196
Atlas width	33.33 $\pm$ 1.25	3.76	33.68 $\pm$ 1.34	3.99	0.110
Axis length	19.81 $\pm$ 0.79	3.98	19.71 $\pm$ 0.75	3.78	0.105
Axis width	17.35 $\pm$ 0.84	4.87	17.41 $\pm$ 1.46	8.36	0.020
Sacrum length	44.84 $\pm$ 1.80	4.01	46.84 $\pm$ 2.34	5.00	0.385
Sacrum width	29.57 $\pm$ 2.23	7.60	31.22 $\pm$ 1.66	6.02	0.218
Manubrium length	19.84 $\pm$ 2.09	10.53	11.70 $\pm$ 1.86	8.56	0.031
Clavicle length	23.58 $\pm$ 1.46	6.17	24.41 $\pm$ 1.60	6.53	0.067
Scapula length	64.16 $\pm$ 2.98	4.65	63.70 $\pm$ 3.36	5.71	0.025
Scapula width	39.57 $\pm$ 2.96	7.92	40.83 $\pm$ 2.41	5.90	0.178
Humerus length	76.72 $\pm$ 2.49	3.24	76.83 $\pm$ 1.95	3.54	0.019
Humerus width	16.28 $\pm$ 0.55	3.38	16.23 $\pm$ 0.42	3.59	0.015
Radius length	70.21 $\pm$ 3.02	2.67	69.63 $\pm$ 1.95	3.60	0.112
Radius width	8.27 $\pm$ 0.33	3.89	8.17 $\pm$ 0.31	3.73	0.136
Ulna length	83.55 $\pm$ 2.44	2.91	83.22 $\pm$ 2.36	2.83	0.104
Ulna width	7.84 $\pm$ 0.28	3.52	7.81 $\pm$ 0.31	4.00	0.040
Os coxae length	63.91 $\pm$ 2.41	3.63	67.65 $\pm$ 2.19	3.24	0.203
Ilium length	53.02 $\pm$ 2.28	4.36	54.16 $\pm$ 2.01	3.70	0.297
Ischium length	43.09 $\pm$ 1.95	4.53	44.76 $\pm$ 1.28	2.87	0.350
Pubis length	19.93 $\pm$ 1.95	10.31	22.81 $\pm$ 1.71	7.48	0.023
Femur length	102.34 $\pm$ 3.60	3.54	102.16 $\pm$ 3.26	2.22	0.029
Femur width	21.77 $\pm$ 0.93	4.29	22.03 $\pm$ 0.86	3.89	0.114
Tibia length	112.60 $\pm$ 2.99	2.63	111.64 $\pm$ 2.73	2.45	0.171
Tibia width	18.34 $\pm$ 0.48	2.60	18.38 $\pm$ 0.53	2.89	0.022
Fibula length	41.75 $\pm$ 1.91	4.58	41.56 $\pm$ 1.60	4.24	0.040
Calcaneus length	29.68 $\pm$ 0.94	3.17	29.26 $\pm$ 0.77	2.63	0.137

8 of the measurements in the females are significantly longer. The length of the os coxae and of its three segments, and the length and width of the sacrum are all significantly longer in the females. The greatest sex difference is in the length of the pubic bones and second in the length of the entire os coxae.

The average of the coefficients of variation for the two sexes are 4.67% for the males and 4.27% for the females. Thus the males vary more in the linear measurements as well as in the weights of the bones (table 1).

In general, the dimensions of the bones of the appendages are somewhat greater in the males and also more variable. The 4 measurements of the os coxae are greater in the females but more variable in the males.

#### Linear measurements as percentages of body length

The linear measurements as percentages of body or nose-ear length are shown in table 3 with the arrangement of

the data and the *t* values of the sex differences the same as in table 1.

Eighteen of the 26 dimensions are longer in the males and all except one of these (scapula width) are significantly longer. There are 8 dimensions with larger percentages of body length in the females but only two of these are significantly longer in the females. The larger number of significantly longer percentage measurements in the males in table 3 compared with the linear measurements in table 2 may be explained at least in part, as due to the longer bodies of the female rabbits (Latimer and Sawin, '59). The index of body build (Latimer and Sawin '57) also indicates a longer body relative to body weight in the females.

The coefficients of variation of these percentage lengths average 4.38% for the males and 4.14% for the females or a reduction of about 6% for the males and 3% for the females from the respective averages of the coefficients of variation of the dimensions of the bones in table 2. The diameters of the long bones in the

TABLE 3  
Linear measurements as percentages of body length. The significance of the *t* values is the same as in table 1.

	Males		Females		<i>t</i>
	Average and stand. dev.	Coeff. of variation	Average and stand. dev.	Coeff. of variation	
Adas, length	2.12 ± 0.14	6.49	1.96 ± 0.11	6.36	0.447
Adas, width	5.55 ± 0.34	4.01	5.81 ± 0.20	3.49	0.248
Azla, length	3.49 ± 0.12	3.45	2.40 ± 0.12	3.48	0.300
Azla, width	2.10 ± 0.10	5.30	3.00 ± 0.23	7.52	0.206
Sacrum, length	8.01 ± 0.32	4.07	8.09 ± 0.41	5.09	0.085
Sacrum, width	5.25 ± 0.46	8.80	5.39 ± 0.32	5.89	0.107
Manubrium, length	2.54 ± 0.32	9.02	3.74 ± 0.30	7.90	0.253
Clavicle, length	4.18 ± 0.22	5.52	4.31 ± 0.24	5.08	0.082
Scapula, length	11.45 ± 0.35	3.26	10.99 ± 0.36	3.22	0.485
Scapula, width	7.05 ± 0.43	6.04	7.61 ± 0.38	5.26	0.010
Humerus, length	13.70 ± 0.34	2.47	13.26 ± 0.28	2.25	0.487
Humerus, width	8.21 ± 0.08	2.89	8.60 ± 0.07	3.52	0.558
Radius, length	12.54 ± 0.27	2.94	12.03 ± 0.40	3.37	0.582
Radius, width	1.48 ± 0.06	3.78	1.41 ± 0.04	2.81	0.558
Ulna, length	14.08 ± 0.41	2.72	14.37 ± 0.45	3.17	0.582
Ulna, width	1.40 ± 0.06	4.26	1.35 ± 0.06	4.28	0.323
Os coxae, length	16.78 ± 0.36	2.14	16.85 ± 0.30	1.79	0.094
Ilium, length	9.29 ± 0.20	3.12	9.35 ± 0.24	2.54	0.085
Isthmus, length	7.66 ± 0.24	3.14	7.73 ± 0.28	3.22	0.083
Pubis, length	3.37 ± 0.28	8.23	3.94 ± 0.28	7.02	0.797
Femur, length	18.29 ± 0.32	2.82	17.64 ± 0.51	2.92	0.499
Femur, width	3.89 ± 0.15	3.06	3.80 ± 0.15	3.99	0.233
Tibia, length	20.16 ± 0.53	2.73	19.28 ± 0.58	3.08	0.609
Tibia, width	3.28 ± 0.12	3.84	3.17 ± 0.09	2.81	0.377
Fibula, length	7.46 ± 0.36	4.80	7.18 ± 0.35	4.92	0.311
Calcaneus, length	5.27 ± 0.21	4.05	5.07 ± 0.15	3.04	0.419

males but not in the females are more variable than their lengths. The greatest sex difference in the percentage lengths, as in the linear measurements in millimeters, is in the length of the pubic bone.

#### *Dimensions of the skull*

Since the removal of the brain destroyed the calvaria of the skulls the number of possible measurements was reduced, and the measurements are chiefly on the base of the skull. The locations of these are illustrated in figure 1. These measurements are arranged in table 4 panel A, as in the preceding tables and the "t" values of the sex differences are likewise the same. Several of the temporal bones

became separated from the rest of the skull in the process of cleaning the skulls and therefore the measurements of the diameters at the ends of the osseous acoustic meati and of the bullae were obtained in only 14 male and 13 female skulls. The other measurements were made upon all 65 skulls.

The length of the palatine bridge and also the diastema are so frequently used in taxonomic studies that they are included. The diastema (D) measured on the left maxilla only is fairly constant, but the length of the palatine bridge (PB) is the most variable dimension in the females and exceeded only by the length of the nasal bones in the male rabbits. The

TABLE 4

*Measurements of the skull in millimeters and as percentages of body length. The significance of the "t" values is the same as in table 1*

	Males		Females		"t"
	Average and stand. dev.	Coef. of variation	Average and stand. dev.	Coef. of variation	
Panel A Measurements in millimeters					
Basion-alveolar pt.	79.68 ± 2.71	3.40	80.98 ± 2.68	3.31	91.90
Basion-post. nasal sp.	30.23 ± 2.56	8.53	30.09 ± 2.28	5.86	93.91
Post. n. spine-alv. pt.	43.06 ± 1.61	3.70	44.94 ± 1.54	3.43	93.30
Palatine bridge	13.99 ± 1.94	8.89	14.59 ± 1.02	6.88	92.11
Diastema	18.46 ± 1.30	4.80	20.80 ± 1.50	5.03	93.79
Barygonatic diam.	45.57 ± 1.28	2.81	45.15 ± 1.38	2.83	91.30
Bitemporal, and. tube	38.56 ± 3.24	8.66	37.53 ± 1.77	4.71	90.97
Bitemporal, bullae	33.87 ± 1.04	2.11	32.53 ± 0.95	2.89	91.15
Bicondylar diam.	17.76 ± 0.93	5.26	17.88 ± 0.71	3.98	90.47
Alveolar process	28.87 ± 0.72	2.48	29.40 ± 1.84	5.24	91.45
Basioccipital length	13.50 ± 0.43	3.94	13.34 ± 0.48	3.62	91.23
Basioccipital width	12.73 ± 0.68	5.25	13.00 ± 0.53	4.06	91.70
Basisphenoid length	12.62 ± 0.61	4.85	13.12 ± 0.54	4.10	93.42
Basisphenoid width	9.23 ± 0.41	4.44	9.37 ± 0.45	4.86	91.58
Nasal bone length	40.67 ± 4.37	10.46	42.01 ± 2.90	6.74	92.11
Mandible length	72.00 ± 2.36	3.28	73.23 ± 2.07	2.81	93.42
Mandible ramus	46.49 ± 1.78	3.83	46.60 ± 1.64	3.52	90.28
Panel B Percentages of body length					
Basion-alveolar pt.	14.33 ± 0.30	2.73	13.96 ± 0.50	3.60	93.39
Basion-post. nasal sp.	7.01 ± 0.52	7.43	6.74 ± 0.43	6.42	92.19
Post. n. spine-alv. pt.	7.80 ± 0.37	3.47	7.77 ± 0.28	3.33	90.45
Palatine bridge	2.50 ± 0.23	8.86	2.52 ± 0.17	6.82	90.40
Diastema	3.06 ± 0.24	4.73	3.14 ± 0.23	4.54	91.00
Barygonatic diam.	8.14 ± 0.30	3.62	7.80 ± 0.30	2.53	90.38
Bitemporal, and. tube	6.79 ± 0.69	8.91	6.49 ± 0.33	4.89	91.51
Bitemporal, bullae	5.85 ± 0.34	4.10	5.68 ± 0.22	3.84	91.89
Bicondylar	3.14 ± 0.22	6.94	3.08 ± 0.20	6.54	91.35
Alveolar process	5.18 ± 0.20	3.84	5.08 ± 0.25	5.01	91.73
Basioccipital length	2.36 ± 0.08	3.48	2.30 ± 0.08	2.76	92.74
Basioccipital width	2.27 ± 0.10	4.53	2.23 ± 0.15	6.91	91.31
Basisphenoid length	2.25 ± 0.10	4.60	2.27 ± 0.09	4.03	90.81
Basisphenoid width	1.64 ± 0.08	3.97	1.62 ± 0.08	5.25	91.00
Nasal bone length	7.25 ± 0.71	9.73	6.82 ± 0.43	6.38	92.09
Mandible length	12.44 ± 0.36	2.82	12.77 ± 0.42	3.28	90.93
Mandible ramus	8.30 ± 0.28	3.33	8.04 ± 0.25	3.15	90.87

maximum width of the alveolar processes (AP) is apparently a rather constant dimension. The length of the nasal bones (average of the two bones) is the maximum length. The bones themselves are longer than their internasal suture, which was measured in the preceding report (Sawin and Cray '57) and they are highly variable in both sexes.

Only 4 of the measurements of the skull are greater in the males and none of these is significantly longer. Of the 13 dimensions of the skull which are longer in the females, 8 are significantly longer and all of these are measurements made parallel to the long axis of the skull. Thus, since none of the transverse dimensions are significantly different in the two sexes, it seems that the skull of these rabbits tends to be longer in the females while there is no apparent sex difference in its width, at least as far as these measurements indicate.

The average of the coefficients of variation for the males in panel A, table 4 is 4.99% and for the females, 4.35% both of these are slightly greater than the averages of the coefficients for the linear dimensions of the bones in table 2. As in

the preceding tables the measurements of the males are more variable than those of the females.

*Measurements of the skull as percentages of body length*

Panel II table 4 shows the linear measurements of the skull expressed as percentages of body length (nose-anus). Only three of these percentages are greater in the females compared to 13 in panel A, and none of these is significantly greater. There are 14 linear measurements which as percentages of body length are longer in the males and 6 of these are significantly longer. This is due probably to the greater body length in the female rabbits as was suggested in connection with table 3.

Changing the linear measurements to percentages of body length (table 3) reduces the average of the coefficients of variation 8% in the males and 3% in the females, and this is generally expected. However in these measurements of the skull and mandible the average of the coefficients of variation of 4.99 in the males is increased to an average of 5.13 for the percentages. Similar values for the females are 4.35 to 4.72. Thus these percentage lengths are more variable than the lengths in millimeters. This suggests that the dimensions of the skull are not closely related to the body length. In an earlier study of the rabbit (Latimer and Sawin, '60) it was shown that the length of the head is not significantly correlated with either body length or body weight, although the head width is significantly correlated with both of these dimensions of the body. A study of the rabbit brain (Latimer and Sawin, '55b) shows that the weight of the brain in the rabbit, as in many other animals seems to be rather independent of body size and these percentage measurements of the skull would indicate that the skull as well as its contained brain develops more or less independently of the size of the body.

Four of the more variable measurements in both sexes of these rabbits are lengths of nasal bone palatine bridge basion-posterior nasal spine and the bi-condylar diameter. The length of the mandible and of the ramus of the mandi-

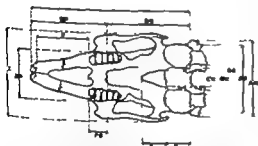


Fig. 1 Drawing of ventral surface of skull to show methods of making the measurements.

- AB Maximum width, auditory bullae
- AM Maximum width, osseous external acoustic meati
- AP Maximum width, alveolar processes
- BC Biccondylar width
- BP Basion-prealveolar point
- BS Basion-posterior nasal spine
- BZ Bitygonatic
- D Diastema
- OL Length basioccipital
- OW Width basioccipital
- PL Length palatine bridge
- SL Length basisphenoid
- SP Posterior nasal spine-prealveolar point
- SW Width basisphenoid

bile are among the most constant percentage measurements in both sexes.

To summarize these measurements in millimeters of the skull seem to indicate that the dimensions of the skull are generally more variable than the measurements of some of the other bones of the skeleton. Unlike the dimensions of the bones of the extremities and of the body these percentage measurements are more variable than the measurements in millimeters. In all of these measurements the females are generally larger and less variable than the males while as percentages of body length more of the male dimensions are larger due to the greater body length of the females.

#### DISCUSSION

Sawin and Crary ('37) have reported linear measurements comparable to those of race III for homozygous (Dachs) heterozygous and normal rabbits derived from the New Zealand Whites. Most of their measurements of the normal rabbits are longer than in this present series. All of the skull measurements of their normal rabbits are greater than in the present series except the width of the basioccipital and the axis and the length of the nasal bones. The greatest difference is in the length of the nasal bones. They measured the length of these along the internasal suture and the present measurements are the maximum lengths which are greater than the length of the internasal suture.

The lengths of the long bones in race III rabbits are all shorter than in these controls. There is less difference in the widths than in the lengths of the long bones in the two groups which suggests that race III long bones are somewhat shorter but stouter than in the control rabbits. All of the measurements of the skull of the control rabbits fall within the range of one standard deviation of the averages of the present series except the nasal bones and the two dimensions of the mandible in race III. The lengths of the long bones however differ more than one standard deviation from the controls although their diameters fall within these limits.

The coefficients of variation of the two series show that the 65 rabbits of race

III are more variable than those used by Sawin and Crary ('37). In both series, the widths of the long bones are more variable than their lengths. Four of the comparable dimensions of the skull are less variable in the present series and 11 are more variable.

Lowrance ('53) reports the length of the calcaneus of the adult rabbit as 27.6 mm and the tibia, 109.3 mm. Both of these measurements are slightly less than the similar measurements in table 2 but the body weights of his rabbits were also less than in race III. His coefficients of variation of 8.85% for the calcaneus and 5.43% for the tibia are somewhat greater than for this series of rabbits. His rabbits were obtained from a dealer and probably not as closely bred as in race III. He reports a coefficient of variation for body weight of 20.1% and this is nearly twice the similar coefficients for these rabbits or 11.3% for the males and 9.9% for the females (Latimer and Sawin '37). In his rabbits as well as in race III, the length of the tibia is less variable than the length of the calcaneus.

Bader ('56) in a study of 17 measurements on the skulls of wild and inbred specimens of three species of rodents found the variability of the inbred races lower in 16 of the 26 comparisons made.

Hammar ('32) lists weights of the entire skeleton and of several of the individual bones from the native Swedish rabbit. His rabbits average only 2-42 gm in body weight or only 82% of the average weight of this series and as expected all of the individual bones are lighter in weight. However if his bone weights are reduced to percentages of body weight the resulting percentages are very similar to those in table 1 panel B. The greatest differences are in the relatively heavier humerus and femur in race III.

MacDowell ('14) has published 17 linear measurements of the skull and of 4 of the long bones in several races of rabbits. He reports sex differences and the coefficients of variation for these measurements and also for each litter of several families of rabbits. Castle ('22) lists three skull measurements and the lengths of the three longest bones of the extremities for several races of rabbits. Most of these

data are not comparable with the present measurements. The measurements of many of these races are less than in race III rabbits.

The weights of human bones, of course are heavier than those of the rabbit, but the weights of the scapula, humerus, radius, ulna and os coxae, expressed as percentages of total skeletal weight, are not appreciably different in the rabbit and in man (Lowrance and Latimer '57). The relative weights of femur and tibia plus fibula are heavier in man, while the rabbit mandible is about 2.5 times the relative weight of the human mandible. The length of the rabbit femur is 1.3 times the length of the humerus and the tibia is also 1.3 times the length of the ulna. The ratios for the similar bones in the human skeleton are both 1.4 times. Thus the lengths of the two bones in the two segments of the extremities are more alike in the rabbit than in man, and in both man and the rabbit the ratios are almost identical for the comparable segments of the two extremities. The human bones are more variable in weight than the rabbit bones. The average of these coefficients is 67% greater in man than for the similar coefficients in the rabbit. Likewise the average of the coefficients of variation of the linear measurements in the human bones is 28% greater than in the rabbit bones. The linear measurements of the human skulls are not yet available for comparison and most of the above comparisons are for the bones of the appendicular skeleton.

This series of rabbit bones are somewhat variable in weight and in their linear measurements when compared with other data on rabbit bones. They are less variable however than the human bones, but it must be remembered that the human bones represent a random selection, while these rabbits have been closely bred for many generations and therefore are likely to be more uniform.

#### SUMMARY

The weight of the dry skeleton and of 10 of its parts together with 17 linear measurements of the skull, and 26 additional measurements on the remainder of the skeleton are presented. These mea-

surements were made on the skeletons of 35 male and 30 female rabbits of race III, derived from the New Zealand White race.

All but one of the weights in grams are greater in the larger females but as percentages of body weight, 7 are greater in the males and three in the females. The weights in grams are more variable in the males and the percentage weights in the females.

Likewise the linear measurements are, in general, longer in the females but as percentages of body length they are generally longer in the males due probably to the longer body length in the females. All of the linear measurements and also these measurements as percentages of body length are more variable in the males.

Thirteen of the 17 linear measurements of the skull, chiefly on the base of the skull, are longer in the females and only 4 longer in the males. The majority of the longitudinal dimensions of the skull are greater in the females and none of the transverse dimensions are significantly greater in either sex, hence we may conclude that the female skull is longer and about the same width as that of the male. Fourteen of the linear dimensions of the skull as percentages of body length are greater in the males and only three in the females. Six of the 14 male percentages are significantly greater and none of the female percentages. The male head is relatively larger. Again these skull measurements are more variable in the males and, unlike the other measurements the averages are larger when expressed as percentages of body length.

#### LITERATURE CITED

- Bader R. S. 1936 Variability in wild and in-bred mammalian populations. *Quart. J. Florida Acad. Sci.* 19 14-34.  
 Castle, W. E. 1922 Genetic studies of rabbits and rats. *Carnegie Inst. of Wash.*, publication no. 320.  
 Cray D. D. and P. B. Sawin 1957 Morphogenetic studies of the rabbit. XVIII. Growth of ossification centers of the vertebral centra during the twenty-first day. *Anat. Rec.*, 127 131-150.  
 Haarduck, H. 1936 Die Gestaltung der Körperproportionen durch Begrenztes Wachstum der Skelettelemente. *Acta. Anat.*, Suppl. 25, 27 1-99.  
 Hammar J. A. 1932 Über Wachstum und Rückgang, der Standardisierung, Individualisierung und bauliche Indivdualtypen in Laufe



- des normalen Postfötallebens. Konstitution-  
san tunische Studien an Kaninchen. Ztschr  
f. Mik-Anat. Fors., 29: 1-340.
- Latimer, H. B. 1927 Postnatal growth of the  
chicken skeleton. *Am. J. Anat.*, 40: 1-57
- 1937 Weights and linear measurements  
of the skull and of some of the long bones of  
the kunk (*Mephitis mephitis avia*) *J*  
*Morph.*, 60: 379-391.
- 1938 Weights and linear dimensions  
of the skull and of some of the long bones of  
the red-tailed hawk (*Buteo borealis borealis*)  
*Univ. of Kans. Sci. Bull.*, 23: 199-212.
- 1944 The prenatal growth of the cat.  
XIV The weight of the skeleton in fetal and  
in the adult cat. *Growth*, 8: 149-158.
- Latimer, H. B., and E. W. Lowrance 1960 Rel-  
ative weights and lengths of the bones from  
106 human skeletons from Asia. *Anat. Rec.*,  
137: 119-125.
- Latimer H. B., and P. B. Sawin 1953a Morpho-  
genetic studies of the rabbit. XII. Organ size  
in relation to body weight in adults of small  
and large race X. *Ibid.*, 123: 81-108.
- 1953b The weight of the brain, of its  
parts and the weight and length of the spinal  
cord in the rabbit. *J. Comp. Neur.*, 103: 513-  
539
- 1957 Morphogenetic studies of the rab-  
bit. XIX. Organ size in relation to body size  
in large race III and in small race X. *Anat.*  
*Rec.*, 129: 457-473.
- 1958 Morphogenetic studies of the rab-  
bit. XX. A comparison of the weights of the  
brain and of its parts in large and in small  
race of rabbits. *Ibid.*, 132: 619-631
- 1959a Morphogenetic studies of the  
rabbit. XXII. Linear measurements of large  
race III and small race X. *Ibid.*, 134: 69-86.
- 1959b Morphogenetic studies of the  
rabbit. XXIV The weight and thickness of the  
ventricular walls in the rabbit heart. *Ibid.*, 134:  
141-147
- 1960 Morphogenetic studies of the rab-  
bit. XXVI. Correlation coefficients of external  
measurements of two inbred races of rabbits.  
*Ibid.*, 136: 417-425.
- Lowrance, E. W. 1953 Roentgenographic rec-  
ord of skeletal growth in relation to age and  
body weight of the rabbit; calcaneus and tibia.  
*Growth*, 17: 183-189.
- Lowrance, E. W., and H. B. Latimer 1957  
Weights and linear measurements of 106 hu-  
man skeletons from Asia. *Am. J. Anat.*, 101:  
443-450
- MacDowell, E. C. 1914 Size inheritance in rab-  
bits. *Carnegie Inst. Wash.*, publication no. 196.
- Sawin, P. B., and D. D. Crary 1958 Morpho-  
genetic studies of the rabbit. XVI. Quantitative  
racial differences in ossification pattern of the  
vertebrae of embryos as an approach to basic  
principles of mammalian growth. *Am. J. Phys.*  
*Anthrop.*, 14: 635-648
- 1957 Morphogenetic studies of the rab-  
bit. XVII. Disproportionate adult size induced  
by the DA gene. *Genetics*, 42: 78-91.
- Sawin, P. B. D. D. Crary and J. Webster 1959  
Morphogenetic studies of the rabbit. XXIII.  
The effects of the dachs gene da (chondro-  
dystrophy) upon linear and lateral growth of  
the skeleton as influenced in time. *Genetics*,  
44: 609-624.
- Schultz, A. H. 1937 Proportions, variability  
and asymmetries of the long bones of the  
limbs and the clavicles in man and apes. *He-  
man Biol.*, 9: 281-328.
- Seiman, A. J. and B. G. Sernat 1953 Setural  
bone growth of the rabbit snout. *Am. J. Anat.*,  
67: 396-408.
- Stewart, T. D. 1932 Hrdlicka's Practical An-  
thropometry Philadelphia, Wistar Press, 941  
pp.

# Functions of the Haversian System

DONALD H. ENLOW

*Department of Anatomy The University of Michigan,  
Ann Arbor Michigan*

The Haversian system or osteone has been traditionally adopted as a universal unit of structure in compact bone. The basic functions and the structural significance of primary and secondary Haversian tissue, however, are poorly understood. Two explanations on the functional meaning of the secondary Haversian system have been proposed. These are (a) the interpretation of the osteone as an exclusive response to stress and (b) the interpretation of the secondary osteone as an exclusive structural result of mineral mobilization and redistribution. However the characteristic absence of the Haversian system in the compact bone of many vertebrate species, including widely used experimental forms such as the white rat, and the characteristic patterns of distribution of Haversian systems in the bone of those species which do possess these structural systems, cannot be entirely explained on the basis of these existing functional concepts. This report will propose that the Haversian system has several basic, previously unrecognized functions.

The bone tissues from a large number of individuals and from a variety of species were studied in an attempt to establish the developmental, functional, and structural relationships which are associated with the process of secondary Haversian reconstruction. It was found that localized or widespread areas of non-pathological osteocyte necrosis can be present as a natural condition in specific types of bony tissue, and that resorptive and reconstructive activity may be associated with such regions. It is suggested that the secondary osteone can function as a replacement mechanism in the internal reconstruction and reorganization of primary bone in cortical areas involving necrosis.

A variety of the secondary osteone independent of necrosis, is characteristically

associated with areas of re-location in muscle attachment on a growing bone and in remodeling processes involving resorption of periosteal bone surfaces during metaphysical reduction in diameter and regional changes in shape. The hypothesis is advanced that this type of Haversian system functions as an anchoring mechanism which can maintain muscle continuity and attachment with bone during such remodeling changes. All secondary osteones regardless of particular function, are structurally comparable and represent a product of internal reconstruction within compact bone.

*History* Leeuwenhoek (1678) was the first to notice the microscopic canal system in bone, and he reported his observations to members of the Royal Society in a series of personal communications which were later published. Soon after Clopton Havers presented several lectures before the Royal Society in which he described in greater detail the microscopic structure of bone and joints. Havers, a versatile English physician, later compiled his extensive observations and published the first monograph, "Osteologia Nova, dealing with the structure and function of bone as a tissue (1691). Havers did not recognize or first identify the Haversian system but he did describe in some detail the "longitudinal and transverse pores in compact bone. These were becoming generally known, by the middle of the eighteenth century as the canals of Havers (Albinus, 1757). Havers suggested that canals in compact bone function to transport medullary oils in order to "moilify" the substance of the bone, and he believed that the canals located near the ends of the bone carry lubricating oils to nearby joints. These logical notions were popularly accepted and persisted for another half a century (Mouso 1763). It is in-

interesting to remember that one entire school of thought, led by prominent anatomists and physiologists as late as the nineteenth century denied the existence of any canal system in bone (Bostock, 1825). Several early writers observed blood vessels in the larger spaces of bone but Albinus (1757) confirmed the presence of vessels in small cortical canals by the use of vascular injection methods. The Haversian system of concentric lamellae with its central canal was described defined and named by Todd and Bowman (1845). The Haversian space (resorption canal) was identified by Tomes and DeMorgan (1853) and these workers were the first to recognize that the Haversian system represents a substitution mechanism. The term osteone was introduced by Biedermann ('14) and the hypothesis that the osteone develops as a mechanical response to tension was formulated largely by Gebhardt ('05). Biochemical considerations relative to the interpretation of secondary bone reconstruction have been investigated and discussed by Amprino (48 '51 '52) and by Ruth ('53). The presence of secondary osteons near a periosteal surface particularly in bony tuberosities was noticed by Petersen ('30) and he termed these Haversian systems "marginal osteons" (Randosteonen).

It is well known that necrotic bone tissue can be associated with a variety of pathological processes particularly those involving vascular interruption. Empty lacunae in areas of dead bone were observed by Barth (1895). Necrotic bone unrelated to pathological processes and located specifically in interstitial areas (between Haversian systems) was noticed by Mueller ('26). Jaffe and Pomeranz ('34) by Sherman and Selakovich ('57) and by Frost ('60). These workers did not suggest that the Haversian system functions as a specific replacement mechanism in response to the presence of necrosis. By counting proportions of empty lacunae in random microscopic fields Frost confirmed the proposition that necrotic bone in the human is more frequent in older individuals and that it is more widespread in extra-Haversian bone. The results of the present study are consistent with these

findings. It will be demonstrated that areas of bone necrosis appear in definite patterns of distribution and with predictable structural relationships.

#### MATERIALS AND METHODS

**Forms studied.** Bone tissues from 89 Rhesus monkeys from 29 dogs, and from survey samples of other representative vertebrate groups were examined for (a) the distribution and structural relationships of primary and secondary Haversian tissues, and (b) the presence and distribution of non-pathological necrosis in compact bone. In order to determine the sequence of Haversian changes and age relationships, observational data of monkey bone tissues were organized according to primary mixed or permanent dentition. Bone from the femur tibia, humerus radius and mandible was studied in most of the monkeys. Multiple entire transverse sections were made through many of the bones from their proximal to distal ends.

**Experimental necrosis.** To test the response of secondary Haversian reconstruction to the presence of necrotic bone localized areas of diaphyseal bone in the femora of white rats were experimentally necrotized. The bone was exposed by surgical entrance through the lateral intermuscular septum. The periosteum was reflected, and an area measuring about 2 mm was necrotized by thermal cautery. The animals were sacrificed at intervals through a period of 6 months. The cauterized areas were then examined histologically and compared with normal bone in the opposite femur and with bone from control animals.

**Methods of tissue preparation.** Ground thin-sections were made using a power driven polishing lap wheel. To demonstrate canalicular calcification in necrotic bone (a process to be considered later), the thin-sections were coated with an impervious seal of parlodion (Enlow '54) or were impregnated with fuchsin or silver nitrate (Frost, '60). Using these techniques areas in which canaliculi have been filled with mineral (micropetrosis) appear transparent and are easily recognized. The transparent nature of this bone is due to the absence of trapped air normally

present in canaliculi as viewed in ground sections. Ordinary mounting of ground thin-sections in balsam or other standard media without such treatment will give uncertain results since seepage of the media into unprotected canaliculi may displace the air and thereby prevent differentiation between areas of micropetrosis and areas in which the canaliculi are not filled with mineral. Micropetrosis cannot be recognized in decalcified preparations. Microradiographs were compared with ground sections in order to determine possible differences in radio-density between vital bone and necrotic areas containing canalicular calcification.

Decalcified and stained sections were prepared by standard methods using a microtome. Preparations were also made by a special technique in which ground thin-sections were decalcified and stained (Enlow '61a). This method gave assurance that necrotic areas were not regions of artifact resulting from poor fixation. Early in the study sections were prepared from tissue blocks 2-5 mm thick, but there was still concern that empty lacunae (an indicator of necrosis) might be a result of incomplete fixation. To exclude this possibility blocks of bone were removed from animals immediately following sacrifice and polished thin-sections approximately 80-110  $\mu$  were prepared and decalcified at once in Decal solution. They were washed and then placed in 10% formalin. A paper-thin, completely decalcified section of bone therefore was exposed to the fixative in not more than 30 minutes following death. Sections in this range of thickness contain 4 or 5 layers of osteocytes, thereby insuring complete enclosure and protection of cells. Microtome preparations were sectioned at about 50  $\mu$ , since very thin sections will not demonstrate all nuclei present.

**Cellular necrosis in bone** Areas of bone which involve osteocyte necrosis may be identified, in decalcified and stained sections by the absence of nuclei within lacunae. Using routine methods of preparation intercellular tissues appear otherwise unchanged. In any local or extensive region of necrosis most or all of the lacunae within that region are totally devoid of cells.

The presence, distribution, and extent of normal osteocyte necrosis appears to be directly related to the particular arrangement of tissue components involved in the structure of that bone. Areas of bone which are composed predominantly of primary osteones or of a closely-meshed, symmetrical network of primary canals ("Plexiform bone" fig. 11 Enlow and Brown, '58) seem to be relatively resistant to the appearance of necrosis, since regions of empty lacunae are infrequently observed. The distribution of canals in these tissues is typically dense. Ordinary circumferential lamellar bone which contains a crowded concentration of primary vascular (non-Haversian) canals also appears resistant to necrosis (fig. 3). The degeneration and subsequent disappearance of osteocytes seems to occur initially at selective focal points which are farthest removed from adjacent vascular canals (fig. 1). In a microscopic section of any bone, the pattern of necrosis depends largely on the amount and pattern of any sparsely vascularized, circumferential lamellar bone which is present in that section. Necrotic bone may appear thus, as isolated patches (figs. 1-10) or in a widespread circumferential zone (fig. 2). As an area of necrosis becomes enlarged in extent, cells in those regions immediately surrounding canals may also die (fig. 6). In extreme or advanced necrosis, primary osteones and plexiform bone can become involved, although this situation has not often been observed.

Examination of a variety of skeletal elements from the same individual, and of multiple sections made at different levels from the same bone indicates that the distribution of cellular necrosis is determined by the particular combinations of tissue types present, as described above. In view of the consistent and predictable frequency in the occurrence of necrotic tissue the presence of limited osteocyte necrosis is considered a normal or natural situation (table 1).

Based on these observations it may be stated that, in general a greater density in the number of vascular canals in any region of compact bone favors a greater resistance in that particular bone locality

to the death of its osteocytes. Conversely a sparse distribution or total regional absence of vascular canals is conducive to local cellular degeneration and necrosis. Death in any population of osteocytes is a regional situation which is governed by the pattern and arrangement of component tissue types.

**Resorption spaces.** Bone tissues in which canals are partially or completely surrounded by a community of living osteocytes but which contain scattered isolated patches of necrotic bone in interstitial areas between canals, have been observed to demonstrate infrequent scattered resorption spaces. However bone tissues containing areas of extensive necrosis in which canals are located directly within

necrotic bone and with all surrounding lacunae lacking cells, demonstrate an increased number and distribution of resorption spaces and formative secondary osteones (table 2, figs. 4 5 6, 7). It is significant to note that such secondary Haversian formation can be located in regional zones of compact bone which in individuals of the same species possessing only living bone characteristically lack secondary osteones. The resorption spaces represent enlarged cavities derived from canals located immediately within the region of necrosis. The fact that necrotic areas can occur prior to resorptive activity (fig. 1) suggests that Haversian replacement is not necessarily an immediate process and that a period of time is in-

TABLE 1

		Rhesus monkeys				Data not known
		Primary description	Mixed description	Permanent description	Unknown description	
Micropetroses <sup>1</sup>	Absent	17	11	13	15	23
	Scattered patches (as in fig. 15)	4 <sup>2</sup>	2	2	4	2
	Extensive (as in fig. 16)	0	4	7	0	2
Necrosis	Absent	5	2	0	7	5
	Scattered patches (as in fig. 10)	0	3	16	9	20
	Extensive (as in fig. 2)	1	0	3	1	4

<sup>1</sup>Specimens examined for micropetroses were not necessarily checked for osteocyte necrosis, since some bone samples were available only in dried condition. The total number of specimens for which micropetroses is reported, therefore, is larger than the number examined for cellular necrosis.

<sup>2</sup>Dried specimens. Extent of osteocyte death not known.

TABLE 2

Necrosis	Rhesus monkeys number of individuals examined	Dogs number of individuals examined	Resorption spaces in necrotic bone <sup>1</sup>		Resorption spaces in living bone <sup>1,2</sup>	
			monkeys	dogs	monkeys	dogs
Absent	15	3	11	0	11	26
Scattered patches (fig. 10)	27	20	22	24	20	114
Extensive (fig. 2)	4	4	23	215	5	20

<sup>1</sup>Total number of resorption spaces and partially-formed secondary osteones from transverse and diaphyseal sections of the femur in all specimens. Haversian spaces and formative osteones in areas of bony thickening and in are produced during endosteal growth are not included regardless of necrosis present, since such secondary reconstruction may result from other growth circumstances.

<sup>2</sup>Characteristically located in peripheral bone on or near junction between endosteal and periosteal bones of the cortex.

involved. This is supported by the experimental findings to be described in a later section and by the data presented in table 2. Whether or not "buds" from nearby canals in living bone can penetrate and replace adjacent necrotic bone has not been determined. Observations of blind canals (Dempster and Enlow '59) suggest this possibility but it may also be true that such canals represent plugged osteons (Cohen and Harris, '38). Closed canals have been observed in microscopic sections, particularly in areas of extensive necrosis. Lacunae surrounding such canals are typically empty.

**Age relationships.** The conspicuous absence of major necrotic areas in younger individuals (table 1) can be attributed to the almost exclusive presence of richly vascularized bone. Compact bone in such forms is composed of either closely packed primary osteons, plexiform bone or of lamellated bone tissue containing a dense concentration of simple, primary vascular canals. As described earlier these bone types are less sensitive to necrosis than thick expanses of lamellar bone containing only scattered vascular canals. With increased age and as local growth rates and remodeling alterations result in progressively changing tissue combinations, increased deposits of sparsely vascularized, circumferential lamellar bone accumulate. This latter variety of bone found in quantity only in individuals beyond very young age is the tissue type most commonly associated with necrosis. During periods of active skeletal growth new cell populations are constantly being added and older cell communities are being removed as bones change in size and regional shape. When adult proportions are reached, this process becomes slowed so that subsequent changes within compact bone proceed largely by internal Haversian replacement.

**Placement of secondary osteons.** Conforming with the distributional pattern observed in the arrangement of resorption canals secondary Haversian systems are selectively positioned in either regional or extensive areas of necrotic bone (figs. 4, 5, 6, 7). Deposition of concentric lamellae within resorption canals will convert these spaces directly into secondary oste-

ones. The secondary osteone thus, appears to be a structural product following the superimposition of a newly formed population of living bone cells within older regions of localized dead bone. Remnants of former necrotic bone which are not completely replaced now persist as dead interstitial bone tissue between Haversian systems (figs. 6, 7).

Currey ('60) in comparing the blood supply of Haversian and plexiform bone comments that Haversian bone is less efficient than the latter. This conclusion is consistent with the observations reported in the present study. Currey speculates that the presence of previously established Haversian systems may cause the eventual death of surrounding interstitial cells and that this would be followed by an increase in the number of secondary osteons produced during progressive replacement. It has been assumed by earlier workers that the relative immunity of the Haversian system to necrosis, compared with interstitial bone, is attributable to the isolation of interstitial tissue from its vascular supply (Mueller '26, Jaffe and Pomeranz, '34, Frost, '60). That the proximity of the vascular supply is a significant factor in the presence of necrosis has been discussed and this situation is true also for the Haversian system. However the characteristic, selective localization of resorption canals and secondary osteons within necrotic bone which was previously primary in nature strongly supports the replacement interpretation of this secondary tissue.

With the continued reappearance of necrosis, secondary osteons themselves may succumb to osteocyte death. These are then partially replaced by newer systems (fig. 17) and second and third generations of superimposed Haversian systems are thereby produced.

**Species correlation.** Growth rate in conjunction with animal size and longevity determines the particular combinations of basic bone tissue types found in the skeleton of any vertebrate species. Examination of bone tissues from a variety of representative vertebrates indicates that species having bone tissues composed largely of tissue types which are more resistant to necrosis as described above,

do not possess significant amounts of true secondary Haversian tissue in periosteal layers of the cortex. Examples would include most amphibians some reptiles and a great many smaller mammals such as the white rat. Conversely species which characteristically have more massive deposits of circumferential lamellar bone containing a relative deficiency of vascular canals as in portions of the human skeleton, commonly possess more or less extensive areas of secondary Haversian bone. Even in older human bone how ever much primary although densely vascular bone can be found. Secondary Haversian tissue in any species typically exhibiting this particular bone type can be arranged in isolated clusters or as extended zones depending on the pattern and extent of necrosis.

**Experimental evidence** To test experimentally the response of secondary Haversian reconstruction to the presence of aseptic necrosis in a species which does not normally have either widespread bone necrosis or secondary Haversian systems small areas of cortical bone in the white rat were necrotized by thermal cautery. An encrusting callus developed around the periphery of the necrotic area and eventually covered it. The initial stage of the callus involved the formation of fine cancellous non-lamellar bone with subsequent lamellar compaction. Immediate extensive resorption and replacement of necrotic bone did not take place. Within the six-month period, typical scattered resorption canals had appeared within areas of necrosis and concentric lamellar deposition within these spaces was observed (fig. 28). This is the same formative sequence involved in secondary Haversian formation.

The results of this experiment must be interpreted in perspective. The experiment performed by Ruth ('53) demonstrated that secondary osteones can develop in the rat by artificially induced, severe calcium deprivation (causing resorption) followed by a period of dietary calcium excess (available calcium for regenerative redeposition). This work demonstrates how secondary osteones can develop under controlled conditions. It does not, however define natural circumstances

which determine why they do or do not develop since the rat normally does not possess secondary Haversian systems whereas certain other species do. To say that the functional significance of the Haversian system is a singular result of calcium need and mobilization followed by redeposition would be overextending the conclusions of Ruth's study which the author did not intend since his purpose was to demonstrate the osteone as a mechanism of replacement. Similarly the parallel response to cautery-induced necrosis demonstrates a laboratory circumstance which can produce secondary reconstruction. In itself this does not confirm that the Haversian system is a unique result of regeneration following necrosis. It does, however indicate that the observations described in this study can be reproduced experimentally.

**Canalicular calcification.** In association with natural necrosis a normal condition can be present which involves the deposition of mineral within canaliculi.

Soon after the surprisingly recent discovery of lacunae by Deutsch and Purkinje in 1834 (Leeuwenhoek may have seen them in the late 1600's but his descriptions are vague) there was much speculation concerning their contents. It was suggested by Muller (1834) and Miescher (1836) that the lacunae with their canaliculi are filled with chalk (sacculi and canaliculi chalicophori) Bruns (1841) and Gerlach (1848) using injection techniques demonstrated that they are hollow in ground sections and suggested that they contained plasma in living bone. Lessing (1846) showed that lacunae and canaliculi appear dark in dried thin-sections due to the presence of air and he argued that they represent an air-filled lacunar system in life. But during the same period, the cell doctrine was becoming established. The presence of nuclei and cytoplasm in the lacunae of cartilage was identified by Schwann (1837) and cells located in the lacunae of bone were reported by Mayer (1841) and by Donders (1848). Tomes (1843) confirmed the cellular nature of bone tissue but he also recognized and reported that many canaliculi can be filled with mineral. This observation was recently rediscovered by Frost ('60) who

correctly related canalicular calcification with osteocyte death. He has termed this process micropetrosis. Calcified canaliculi appear to be comparable with sclerotic or transparent dentin (Orban '57) in which dentinal tubules within dead tracts are plugged with mineral deposits.

Patterns of distribution and structural relationships. Areas of micropetrosis can appear (a) in interstitial bone (figs. 17, 24) (b) as isolated patches (fig. 15) or (c) as extensive circumferential zones or layers (figs. 16, 18). Micropetrosis when present, may often be recognized macroscopically on cut surfaces of bone by its transparent appearance. The initial onset of micropetrosis appears in restricted spots located within thick lamellar bone containing relatively few vascular canals. Calcification near canals seems to be avoided until the extent of the micropetrosis becomes more widespread (fig. 16). Microradiographs of micropetrotic bone (figs. 20, 21) show that the overall density of the matrix, when compared with adjacent areas of vital bone, is not noticeably affected in the bones of the young, growing individuals examined.

Both resorption spaces and secondary osteons are frequently and characteristically located in areas of micropetrosis (figs. 15, 18, 19, 24). Interstitial micropetrotic bone between secondary osteons represents the remnants of older necrotic tissue (fig. 17).

It is apparent that the distribution of canalicular calcification coincides both in pattern and structural relationships with necrosis. Necrosis, sometimes even rather widespread in extent, can be present in a bone, yet that same bone may or may not show micropetrosis. Apparently calcification of canaliculi is a sequel to necrosis.

Relationship of secondary reconstruction with gross remodeling. The progressive remodeling of a bone during its prenatal growth involves considerable reorganization and alteration in the minute structure of the bone tissue itself (Enlow '61b). Detailed analysis of this remodeling process makes possible a developmental interpretation of the complex architectural patterns and structural combinations observed (a) in different areas of the same bone (b) in different bones of the same

individual, (c) in different ages of the same species, and (d) between different species. The formation of the true secondary osteone which is concerned with the internal reconstruction of compact bone can also be involved in general remodeling processes concerned with the gross shaping of bone during growth. The development of this particular variety of the Haversian system may be quite independent of necrosis.

Secondary Haversian formation regularly occurs in defined areas so that distinct "Haversian zones" can be identified. The shifting of zones following gross remodeling changes will often result in the relocation of such Haversian zones into new positions within the cortex. Haversian bone associated with muscle reattachment, for example and with endosteal growth or with cancellous compaction, can come to lie deep within the cortex in a new relationship at some distance from its former location.

Bone structure in areas of muscle attachment. The composition and arrangement of bone tissue within prominent processes, depressions, or unmodified bone surfaces to which muscles or tendons attach can be distinctive. Within such regions concentrations of secondary osteons are observed as a characteristic and localized component (figs. 8, 23). The initial formation of these secondary systems is not a response to necrosis although this process can also be involved as independent complication (fig. 12).

During longitudinal growth of a bone muscle attachment necessarily becomes shifted as a muscle is relocated in its migration up or down the elongating shaft. Also the sectional shape of a bone undergoes considerable change during metaphyseal-diaphyseal transition. If tubercles are involved, a continual drift in the relative location of the tubercle takes place during remodeling. Continuous release of muscle insertion is required in this process and progressive muscle reattachment must be maintained during such growth changes. There is no problem if the shift in location involves simply periosteal deposition of new bone enclosing new Sharpey's fibers. But if muscle attachment is to be preserved on a sur-



face undergoing active resorption rather than deposition, the continued insertion of that muscle must survive even though the bone into which the muscle is attached is being removed. If rate of growth is relatively slow this is apparently accomplished by waves of localized resorption and surface apposition so that at least parts of a muscle are anchored at any one time. The process involved has been discussed by Peterwen ('30). In species which show periods of rapid skeletal growth however the structural arrangement illustrated in figure 13 is common. The tubercle is drifting across the surface of the bone. One side of this bony process has received lamellar apposition whereas the opposite side is a resorptive surface. Muscle attachment must be maintained on a resorptive as well as on the depositional surface. While periosteal attachment is not necessarily completely severed during periods of periosteal resorption, the muscle nevertheless must be relocated and reattached on this resorptive surface. The resorptive enlargement of canals in the underlying compacta and subsequent deposition of new bone within these canals can serve to reestablish intimate periosteal bond with the substance of the bone even though the surface of that same area is being progressively destroyed. The whole substance of the osteone is in direct contact with the periosteum since the fibrous matrix of the entire Haversian cylinder is continuous with the fibrous component of the periosteum. In figure 13 the secondary osteons follow in the direction of the drift but are in advance of the resorptive surface. In this situation the secondary Haversian system appears to represent a pinning or pegging mechanism which can serve to anchor the muscle to that area of bone which is itself undergoing removal or within which the attachment of a muscle is shifting in location. A comparable process will be discussed below in connection with endosteal bone growth during metaphyseal remodeling.

**Compaction of coarse cancellous bone**  
Reduction in diameter of the bone during metaphyseal and diaphyseal remodeling involves the lamellar compaction of coarse cancellous bone. This is a process of

endosteal growth in combination with corresponding periosteal resorption. Spongy bone in the medulla of the metaphysis is converted into compact, cortical bone as the metaphysis is relocated in position to become the diaphysis. Considerable remodeling and internal reconstruction can be involved. The original trabeculae of fine-cancellous endochondral bone are partially removed and replaced by lamellar trabeculae of coarse-cancellous bone. This coarse-cancellous bone itself is subject to extensive removal replacement, and structural readjustment. Reversals in direction as the bone grows outward, inward and then outward together with the formation and reformulation of trabeculae and the closure reopening, and reclosure of cancellous spaces during these growth reversals produce complex patterns of microscopic architecture. When individual trabeculae are incorporated into the cortex by compaction during inward growth the resulting compact bone often has a brecciated structure with unorganized abrupt angles of lamellar orientation. Incomplete segments or vestiges of lamellae are embedded within the former trabeculae and spaces of widely varying sizes showing progressive stages of compaction are present (figs 14-25). Structural results produced by this process of cancellous compaction are associated only with endosteal growth as coarse-cancellous bone is not involved in periosteal apposition. The structure is a mosaic of osteones demonstrating a variety of irregular shapes, proportions and sizes. This characteristic type of bone can usually be recognized by these features in addition to the convoluted whorled configuration always present in the interstitial bone (fig 14). The canal system, following compaction, may be classed as Haversian since each canal is surrounded by a concentric often irregular lamellar sheath. Since reconstruction is involved to a greater or lesser degree in the formation of this bone type it is to be considered as secondary in nature. Regeneration of necrotic bone is not involved in its original formation but like other bone tissues it is also subject to this process. Endosteal Haversian bone resulting from coarse cancellous compaction is frequently found in routine section

preparations. It is typically a significant structural component in the compact bone of larger species having a thick cortex. When persisting in the middle third of a long bone it occurs in well marked zones which are usually enclosed on one or both sides by more recently formed periosteal and endosteal layers.

*The problem of muscle attachment during metaphyseal remodeling* It is apparent that the resorption of an external surface complicates the process of re-attachment during endosteal growth periods involving muscle relocation. This situation is similar to that previously discussed relative to shifts in location of muscle attachment and to tubercle drift in the elongating shaft. In figure 27 metaphyseal diameter is being reduced by external resorption in combination with endosteal apposition. Resorption spaces have formed in front of the inwardly advancing external surface and lamellar deposition within these spaces has proceeded progressively in an endosteal direction. Note also that the secondary canals become abruptly "primary" toward the inner part of the cortex. This process appears to be a mechanism providing progressive periosteal anchorage or continuity within the substance of the compact bone. The entire cylinder wall of each Haversian system is directly continuous with the fibrous matrix of the periosteum. The interstitial bone, thus is endosteal, but the network of osteones embedded in this endosteal bone is periosteal in nature. Progressive lamellar deposition in each osteone, and the subsequent formation and reformation of new osteones serves to provide continual periosteal attachment as the periosteal surface itself is being removed. Following reversal in direction of growth, this accumulation of osteones will remain in the cortex as defined zones enclosed by other layers composed of different tissue types. The bone illustrated in figure 28 is entirely endosteal. Note the inner circumferential lamellae the inward-advancing secondary periosteal osteones and the external resorptive surface. The section illustrated in figure 29 demonstrates the relationships of such bone following outward reversal in direction of growth. Outer circumferential lamellae now enclose a distinct

"zone of older endosteal bone containing secondary osteones. Remnants of such zones following extended increase in diameter are seen in figures 15 and 16 on the inner margin of the cortex. Secondary osteones are commonly observed to overlap reversal lines separating broad zones produced by inward and outward growth. Haversian systems located within both periosteal and endosteal bone near such a junction are continuous, thereby providing continuity between these two zones (table 2)

Reduction in metaphyseal diameter involving compaction of coarse-cancellous bone will produce interstitial bone which is characteristically whorled and convoluted, as previously described. Even when this bone becomes relocated from its original position to become a zone embedded in the cortex which is located farther down the shaft, it can be identified and its developmental relationships can be recognized. If inward growth takes place in areas of the metaphysis located near the diaphysis, however cancellous compaction may not be involved. In this situation, endosteal apposition is in the form of extended sheets of inner circumferential lamellae and following Haversian reconstruction during inward growth, these more regularly arranged lamellae become interstitial in position. The "whorled" appearance therefore, is not characteristic, and recognition of this bone as endosteal in nature is somewhat more difficult than in other locations which involved cancellous compaction. That it is endosteal, however can be confirmed by tracing serial sections which demonstrate the direct continuity between these two varieties of secondary Haversian bone tissue produced as a result of inward growth.

The classical pattern of bone structure involving outer and inner circumferential lamellar layers enclosing a middle Haversian zone can be one result of this remodeling sequence. In figure 22 the inner layer of circumferential lamellae and the middle zone of secondary Haversian bone were both produced during inward growth. Following reversal, the outer layer of circumferential lamellae was added. It is to be emphasized that the occurrence of

periosteal resorption in combination with endosteal deposition is widespread during the remodeling of the proximal and distal thirds of the bone. The resulting arrangement of structure may persist in the cortex as these areas later become relocated into the middle regions of the shaft, as in figure 22 following increase in the overall length of the bone. The consistent and predictable relationship of the secondary osteone with this particular remodeling process as well as with its specific presence in areas of muscle relocation, supports the interpretation of the secondary Haversian system as a functional mechanism providing progressive muscle anchorage during remodeling changes.

#### DISCUSSION

*The primary osteone* This variety of the Haversian system (fig. 9) is formed by the deposition of concentric lamellae within tubular anastomosing spaces located in surface deposits of fine-cancellous, non-lamellar bone. Secondary resorption and reconstruction of pre-existing bone is not involved. Although similar in structural appearance primary and secondary osteones represent different functional systems within compact bone. The primary osteone appears to be associated with either regional or widespread areas involved in the relatively rapid accumulation of bone. The extent of its presence seems to be determined by the body size of the individual and rate of skeletal growth. The primary osteone is quite common, for example in the skeleton of the young growing dog and monkey but is though present it is relatively limited in the white rat. Primary osteones are arranged into distinct zones which have become enclosed by additional zones of different bone tissue types. Clusters of these structures may be observed within tubercles, crests, and other bony processes. Their presence in such locations appears to be a response to growth circumstances rather than a direct adaptation to tension forces in the traditional sense that "Haversian systems develop and become oriented in patterns determined by lines of stress."

Plexiform bone a basic variation in the primary pattern of bone structure is rather common in many species in-

cluding the dog (fig. 11). It is comparable with the primary osteone in that it develops by lamellar filling in fine cancellous spaces which were formed within variable amounts of non-lamellar bone. Rather than forming anastomosing, elongated osteones however the canals are arranged as a closely meshed symmetrical plexus. Like the primary osteone it is observed to develop in areas of rapidly forming bone and when present, it is usually distributed in widespread areas of the cortex. Plexiform bone is commonly associated with periosteal apposition but this type of bone has also been observed within deposits produced during endosteal growth.

*The secondary osteone* Unlike most tissues bone contains cells which are entombed in isolated lacunae within a calcified matrix. Adjacent lacunae are interconnected only by canaliculi, and vascular supply can be far removed from cells. It has long been known that osteocytes do not undergo mitotic cell division (v Ebner 1875 Broesike 1882). The repopulation of any local area in bone with a new generation of osteocytes as in the regeneration of necrotic bone tissue cannot stem from the mitotic division of adjacent cells already present. Rather regeneration can only proceed by (1) removal of bone through the formation of resorption canals, and (2) reformation of young bone by lamellar deposition within these erosion canals. The structural result is a secondary osteone composed of concentric Haversian lamellae enclosing a central Haversian canal.

The true secondary osteone has a restricted but predictable distribution in (a) the variety of vertebrate species which have this special type of bone and (b) the extent in compact bone of those species which do possess secondary osteones (Foote '18 Amprino and Godina '47; Enlow and Brown '56 '57 '58). A great many species lack both the primary and the secondary osteone and their bone tissues contain primary vascular (non Haversian) canals only. In certain groups bone may even be virtually non-vascular. Many species possess bone tissues which are composed of mixed bone containing both primary osteones and primary vascular

omish. Only a relatively few vertebrate forms have true secondary osteones as a component structure in their bone tissues, and even then, their skeleton may contain regionally massive amounts of primary bone at all age levels. When secondary Haversian systems do occur they are always found in predictable locations and patterns of distribution.

The nature of this distribution makes it difficult to explain the function and significance of the secondary osteone. Any inclusive explanation must satisfy the distribution outlined in the previous paragraph.

Several conclusions become evident. First, the designation of the Haversian system as a universal unit of structure is unwarranted, even if both primary and secondary osteones are considered. Second, one may question the broad generalization that the presence and the orientation of the Haversian system represent a direct adaptation to patterns of physical stress. Many vertebrate species do not possess these structures yet they are subject to the same mechanical forces in their skeleton as forms which do have secondary osteones. Similarly mineral redistribution can only represent a partial explanation of the osteone relative to secondary reconstruction within compact bone. The observations reported by Amparo (52) suggest that secondary reconstruction can be involved in calcium mobilization, particularly in older individuals. However the total absence of secondary osteones in numerous species, including many having a long life span, together with the characteristic distribution of secondary osteones in particular and predictable relationships and locations when present in the cortex, indicates that secondary reconstruction is not restricted to this biochemical function.

*Variation in the types of Haversian system.* It is apparent that the formation of the Haversian system does not represent a single developmental or functional circumstance. The situation is complex in that several varieties of the osteone as previously described, exist in compact bone. The structure of each, however is essentially comparable since the osteone itself regardless of developmental factors

involved, is a structural system involving the deposition of bone within a confined space.

The distribution of most Haversian bone tissues observed in this investigation may be accounted for by combinations of (1) the primary osteone (2) the secondary osteone associated with replacement of necrotic bone, (3) the secondary osteone produced by the compaction of coarse-cancellous bone during endosteal growth, (4) the secondary osteone concerned with muscle relocation, and (5) the secondary osteone produced during inward growth involving periosteal resorption and metaphysical remodeling. That the utility of the osteone extends beyond the developmental and functional circumstances recognized in this study is suspected because of the inherent versatility of the Haversian system itself. Studies are now needed on (1) specific correlation between aging in bone tissue and corresponding mineral availability and release mechanisms (2) biochemical relationships of calcium mobilization in the different varieties of bone tissue and (3) diffusion or permeability rates in the calcified bone matrix.

*The non-Haversian canal system in bone.* One of the most widely distributed types of vascular canals in compact bone is the simple non-Haversian canal (figs. 1-3). It is not surrounded by an individual sheath of concentric lamellae either primary or secondary. This canal type appears in all but a very few vertebrate groups and at all age levels. It is the typical canal present, for example, in the cortex of the white rat and other laboratory rodents. The non-Haversian canal is found in widespread areas of monkey compact bone and in significant numbers within human cortical bone even in the aged skeleton. This canal type strangely has remained virtually unknown to the general histologist. The non-Haversian canal is termed simply a "primary vascular canal" in this report to distinguish it from both primary and secondary osteones.

In view of its extensive distribution in the bone of most vertebrates, and because of its presence in significant quantities in the bone of many common experimental animals an increased recognition of the primary vascular (non-Haversian) canal

as a major structural component of bone is urged.

**Osseous necrosis** The present report is primarily concerned with the functional significance of the Haversian system and not with a detailed cytological study of necrosis in bone. Interest in the process of necrosis itself however has led to a preliminary examination of necrotic bone at the cellular level. The results of this work are being continued and expanded as a separate cytochemical study.

Bone sections containing areas of necrosis were stained with oil red O in order to determine the extent of neutral fat accumulation within osteocytes. Scattered throughout compact bone many individual bone cells were found to contain fatty inclusions which largely obscured or displaced other cytological components. Patterns of distribution and tissue relationships, however were not recognizable with certainty from the preparations at hand. Bone sections containing necrosis were also stained with PAS. Differences in the intercellular organic matrix between contiguous living and necrotic zones were not evident using this procedure. The bone samples examined however were from Rhesus monkeys having mixed dentition so that any necrosis present must represent a relatively recent development. Possible matrix changes in necrotic bone of long standing are not known.

A great deal of information is needed on the metabolic circumstances involved in osteocyte death and the resulting influence on surrounding intercellular matrix. It is possible that the disappearance of a community of bone cells does not necessarily result in an immediate total necrosis of the remaining interstitial tissue in this area, since some interchange between ground substance and collagen with circulating canaliculi and lacunar tissue fluids might survive. This situation may parallel the normal decrease in fibroblast population within aging connective tissues. A limited distribution of cellular necrosis in bone may be physiologically compatible with surrounding areas possessing vital cells but calcareous deposits within communicating canaliculi would subsequently produce a metabolic isolation of acellular regions. With continued plug-

ging of canaliculi, the spread of necrosis to adjacent regions of living tissue would be encouraged by the blocking of supply channels. The result would be a progressive enlargement of necrotic zones.

It is evident that necrosis and canicular calcification are intimately related, but a full understanding of the relationship as well as the fundamental nature of osseous necrosis itself is lacking.

#### ACKNOWLEDGMENTS

This work was supported by the United States Public Health Service, Grant D-1123 and by the Upjohn Company. A large number of bone specimens from normal, untreated Rhesus monkeys were provided by Dr. Paul Ayres Parke Davis and Company, Rochester, Michigan. Bone specimens from monkeys of known age were supplied by Dr. James A. Gavan, Anatomy Department, Medical College of South Carolina, and by Dr. G. van Wagonen, Department of Obstetrics and Gynecology, Yale University. Bone samples from a variety of vertebrate forms were provided by Dr. E. T. Hooper and Dr. N. E. Hartweg of the University of Michigan Museum of Zoology.

#### SUMMARY AND CONCLUSIONS

1. The secondary osteone is regarded as a structural adaptation to a variety of functional and developmental circumstances. Secondary Haversian reconstruction is a mechanism which provides interstitial tissue replacement within compact bone yet which does not disturb the gross form of the bone.

2. The secondary Haversian system appears to be concerned with a process of replacement or regeneration in areas involving extensive natural, non-pathological osteocyte necrosis.

3. Normal osteocyte necrosis is characteristically associated with particular types of bone tissue structure. Bone varieties possessing a sparse distribution of vascular canals are most sensitive to the appearance and spread of necrosis. Bone tissues containing a dense concentration of canals are more resistant to the onset of necrosis.

4. A bone is usually composed of several basic varieties of tissue. The distribution of cellular necrosis in any part of a

bone, or at any age level, can be either widespread or restricted to scattered patches depending on the distribution and extent of component tissue types which are more susceptible to necrosis.

5. Bone from very young individuals of certain species and from all age levels of many other species, are composed of densely vascular bone tissues. These forms do not have widespread cellular necrosis, nor do they possess a widespread distribution of secondary Haversian systems in periosteal bone deposits.

6. An increased distribution of resorption canals and secondary osteones were observed in areas of extensive necrosis. Secondary reconstruction in periosteal bone is not marked when necrosis is confined to scattered, interstitial regions.

7. A noticeable degree of canalicular calcification has been observed in a significant number of bone samples which display necrosis. The presence of both extensive and restricted necrosis in many bones which have not experienced canalicular calcification, however suggests that this process follows rather than triggers the first appearance of osteocyte death. Detailed relationships between the process of mineral deposition in canaliculi and with necrosis have not been established.

8. A distinctive type of secondary osteone is involved in the compaction of coarse-cancellous bone during growth reversals in metaphyseal-diaphyseal remodeling. This variety of the Haversian system is distinguished by the convoluted contours and brecciated construction of interstitial bone located between Haversian systems of irregular shape and size. Reconstruction of necrotic bone is not necessarily involved in the original formation of this type of secondary osteone.

9. The hypothesis is advanced that the secondary osteone functions as a muscle anchoring structure during shifts in the location of muscle attachment produced by growth changes and in tubercle drift.

10. The secondary osteone appears to function as a periosteal and muscle securing mechanism during the active resorption of external bone surfaces. Widespread periosteal resorption is involved in

the reduction of metaphyseal diameter during gross remodeling.

11. It is emphasized that bone is composed of a wide variety of basic bone tissue types and that each type represents a structural response to a particular regional situation. This important generalization must be considered in all experimental and descriptive studies dealing with bone as a tissue.

#### LITERATURE CITED

- Althaus, H. S. 1757 *Academicarum annotationum*, 3 23-84.
- Amprino, R. 1948 A contribution to the functional meaning of the substitution of primary by secondary bone tissue. *Acta Anatomica*, 5, part, 3 291-300.
- 1951 Relations entre la structure et la physiologie de l'os. *Ann. Soc. Royale Sc. Med. et Natur. de Bruxelles*, 4 part, 8 209-225.
- 1953 Rapporti fra processi di ricostruzione distribuzione dei minerali nell'osso. I. Ricerche eseguite col metodo di studio dell'assorbimento dei raggi roentgen. *Zeitschrift für Zellforschung*, 37 144-183.
- Barth, A. 1895 Histologische Untersuchungen über Knochentransplantationen. *Beitr. Path. Anat.*, 17 65-142.
- Biedermann, W. 1914 *Handbuch der Vergleichenden Physiologie*. By H. Winterstein.
- Bostock, J. 1835 An elementary system of physiology. Wells and Lilly Boston, 1.
- Broadbent, G. 1882 Über die feinere Struktur des normalen Knochengewebes. *Arch. Mikrosk. Anat.*, 21 665-705.
- Bruns, V. 1941 *Lehrbuch der Allgemeinen Anatomie des Menschen*.
- Cohen, J. and W. H. Harris 1953 The three-dimensional anatomy of Haversian systems. *J. Bone and Joint Surg.*, 40-A, No. 2: 419-434.
- Currey, J. D. 1939 Differences in the tensile strength of bone of different histological types. *J. Anat.*, 93, part, 1 87-95.
- 1960 Differences in the blood supply of bone of different histological types. *Quart. Jour. Micro. Sci.*, 101 3, 351-372.
- Dempster, W. T. and D. H. Enlow 1959 Patterns of vascular channels in the cortex of the human mandible. *Anat. Record*, 123, No. 3 189-206.
- Deutlich, C., and Parkinjs 1834 De periodici osteum structura observationes.
- Donders, F. C. 1848 *Hollandische Beitr. Anat. u. Physiol. Wiss.*, 1.
- Elmer, V. V. 1878 Über den feineren Bau des Knochenstanzes. *Bd. der Sitzber. Akad. Wiss.*, III, 73: 49-138.
- Enlow, D. H. 1954 A plastic seal method for mounting sections of ground bone. *Stain Tech.*, 29 1 21-22.
- 1961a Decalcification and staining of ground thin-sections of bone. *Stain Tech.*, 36, 4 250-251.

- 1961b A study of the post-natal growth and remodelling of bone. *Am. J. Anat.*, in press.
- Enlow D. H. and S. H. Brown 1956 A comparative histological study of fossil and recent bone tissues. Part I. *Tex. J. Sci.*, 8, No. 4, 405-443.
- 1957 A comparative histological study of fossil and recent bone tissues. Part II. *Tex. J. Sci.*, 9, No. 2, 185-214.
- 1958 A comparative histological study of fossil and recent bone tissues. Part III. *Tex. J. Sci.*, 10, No. 2, 187-330.
- Frost, H. M. 1960 *In vivo* osteocyte death. *J. Bone and Joint Surg.*, 42-A, No. 1, 138-143.
- 1960 Microosteoids. *J. Bone and Joint Surg.* 42-A, No. 1, 144-150.
- Havers C. 1891 *Osteologia nova*. London.
- Jaffe, H. L., and M. M. Pomerans 1934 Changes in the bones of extremities amputated because of arteriovascular disease. *Arch. Surg.*, 80, 535-538.
- Lacaze de Beaulieu, A. 1878 Microscopical observations of the structure of teeth and other bones. *Phil. Trans. Roy. Soc., London* 12, 1003-1003.
- 1883 Observations on the texture of the bones of animals compared with that of wood. *Phil. Trans. Roy. Soc., London*, 17, 838-843.
- Leesing, S. 1846 *Über ein plasmatisches Gefäßsystem in allen Geweben insbesondere in Knochen und Zähnen*. Hamburg.
- Mayer G. W. 1841 *Über die Bedeutung der Knochenkörperchen*. *Müllers Arch.*, 210-215.
- Miescher F. 1836 *De inflammatione ossium*. Berlin.
- Moore, A. 1783 *The anatomy of the human bones*. Edinburgh.
- Müller J. 1834 *Osteologie und Myologie*. Abh. Berl. Akad. Wiss.
- Müller W. 1928 *Über das Verhalten des Knochengewebes bei besterger Zirkulation und das Bild von Nekrose der Zwischenlamellen*. *Beit. z. Klin. Chir.* 138, 614-624.
- Murray P. D. F. 1936 *Bones*. Cambridge University Press.
- Orban, B. J. 1957 *Oral histology and embryology*. C. V. Mosby Co., St. Louis, 4th ed.
- Petersen, H. 1930 *Die Organe des Skeletsystems. Handbuch der Mikroskopischen Anatomie des Menschen*, herausgegeben von V. Mollendorff. Berlin. Zweiter Teil, 604-618.
- Ruth, E. B. 1933 Bone studies. II. An experimental study of the Haversian-type vascular channels. *Am. J. Anat.*, 23, 429-458.
- Schwann, T. 1937 *Microscopical researches*. Sydenham Society London.
- Sherman, M. S., and W. G. Selikowitz 1937 Bone changes in chronic circulatory insufficiency. *J. Bone and Joint Surg.*, 39-A, 893-901.
- Smith, J. W. 1960 Collagen fiber patterns in mammalian bone. *J. Anat.*, 94, Part, 2, 339-344.
- 1960 The arrangement of collagen fibers in human secondary osteones. *J. Bone and Joint Surg.*, 42-B, No. 3, 583-605.
- Todd, R. B., and W. Bowman 1843 *The physiological anatomy and physiology of man*. Blanchard and Lee, Philadelphia.
- Tomes, J. and C. De Morgan 1853 Observations on the structure and development of bone. *Phil. Trans. Roy. Soc., London*, 143, part, 1, 109-130.
- Vigilanti, F. 1953 *Accrescimento e rinnovamento strutturale della ossoepita in sua rapporto alle sollecitazioni meccaniche*. *Zell schrift für Zellforschung*, 43, 17-47.
- Whitlow J. B. 1734 *Exposition of the structure of the human body*. Translated by G. Douglas, M. D. London.

## PLATE 1

## EXPLANATION OF FIGURE

- 1 Osteocyte necrosis ( ) in regions between primary vascular (non-Haversian) canals. Lacunae in necrotic areas lack cells. Shadows appear in some of the empty lacunae and do not represent nuclei. Living cells may be identified by the presence of a distinct darkly staining nucleus. Cells located in close proximity to canals have survived. Femur Rhesus monkey 112.5 X Decalcified and stained ground-section.





## PLATE 2

### EXPLANATION OF FIGURES

- 2 Necrosis (x) in a sparsely vascularized zone in circumferential lamellae. Living osteocytes are present in these lacunae close to the primary vascular canals. Rhesus monkey 62 X Decalcified and stained ground-section.
- 3 Primary non-vascular canal in compact bone. Cellular necrosis is absent. This variety of bone tissue is widely distributed in most vertebrate species. It is produced by sub-periosteal apposition of lamellae which enclose primary canals. The individual canals are not surrounded by a broad, tubular sheath of concentric lamellae. Not that these canals are present in varying proportions in many other sections illustrated in this study. Femur Rhesus monkey 62 X Decalcified and stained ground-section.



### PLATE 3

#### EXPLANATION OF FIGURES

- 4 Secondary osteones (A) and resorption canal (B) in an extensive zone of osteocyte necrosis (X). The interstitial lacunae in this zone are all without osteocytes. Dark shadows appear in some of the lacunae due to the thickness of the section and do not represent nuclei. The lacunae of the secondary osteones do contain cells. Osteocytes in the richly vascular zone (D) have not experienced necrosis. Femur Rhesus monkey 68.9 / Stained and decalcified preparation.
- 5 Enlarged view of the area of secondary reconstruction seen in figure (4) above. The resorption canal (B) has formed within the area of osteocyte necrosis (X). Deposition of concentric Haversian lamellae within such spaces has resulted in the formation of secondary osteones (A) which are now superimposed over the older bone. Note that the lacunae surrounding primary canals (C) in this region are entirely empty of cells. Femur Rhesus monkey 106 X Decalcified and stained preparation.

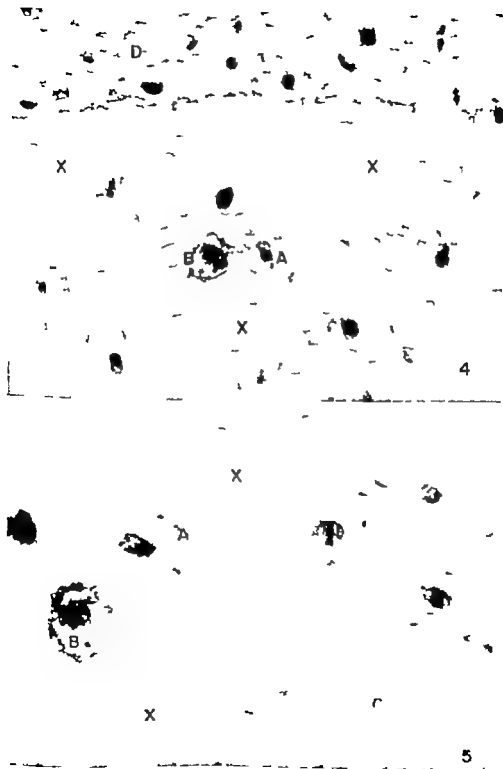


## PLATE 8

### EXPLANATION OF FIGURES

- 9 An external layer of small, primary osteones in the formative stage. With subsequent deposition of outer circumferential lamellae this layer will form a thin "zone" when it later becomes embedded in the cortex. Femur Rhesus monkey 62 x Decalcified and stained ground-section.
- 10 Necrosis (x) in a circumferential layer of compact bone. Note that the empty lacunae are located in areas which are distant from vascular supply. Femur dog 62 x Decalcified and stained ground-section.



## PLATE 6

### EXPLANATION OF FIGURES

- 11 Plexiform bone frequent variety of primary bone tissue found in certain vertebrate groups, including some carnivores and most arilloclactyla. Mid-diaphyseal section of the femur transverse section dog. 56x Decalcified and stained ground-section.
- 12 Secondary osteones in an area of muscle attachment. Note the resorption pit (A) in an adjacent zone of necrosis ( ) The secondary osteones in the tubercle itself (B) did not form as a response to metastasis. Femur Rheumatoid monkey 56x Decalcified and stained ground-section.

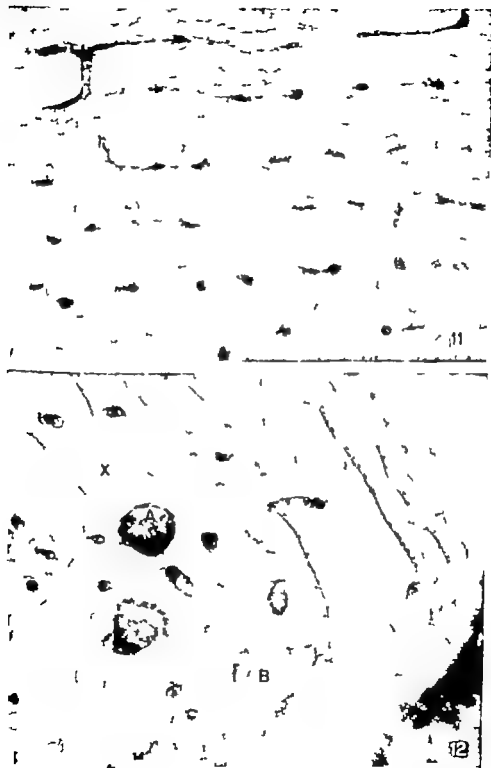




## PLATE 7

### EXPLANATION OF FIGURES

- 13 Secondary osteones in an area of muscle attachment. Note that the tubercle is drifting from side (B) to side (A) and that the secondary osteones (D) and resorption spaces (C) have developed from primary non-Haversian canals (E) in the direction of the drift. Humerus, *Cercopithecus* 57 X Decalcified and stained ground section.
- 14 Secondary osteones associated with endosteal growth. The compaction of reverse-cancellous bone and periosteal anchorage are both involved. Note the irregular contours of the interstitial bone. Following reversal in direction of growth, outer circumferential lamellae (arrows) form a broad zone which now encloses the older endosteal zone. Femur Rhesus monkey 57 X Decalcified and stained ground section.

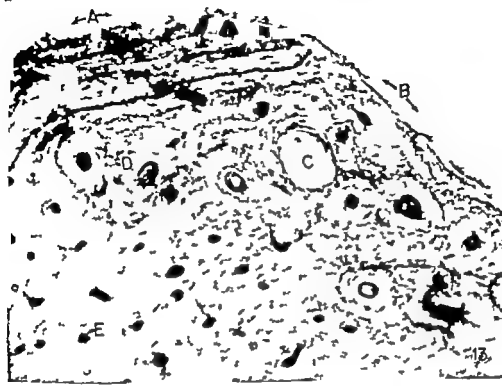
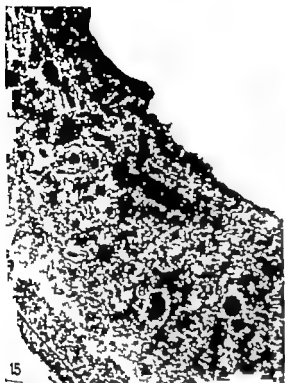


## PLATE 8

### EXPLANATION OF FIGURES

- 15 Irregular patches of canalicular calcification containing superimposed resorption spaces (B) and secondary osteones (A) Femur Rhesus monkey 12.3 x Ground section.
- 16 Necrotic areas involving canalicular calcification (micropetrous) can be identified by their lighter transparent appearance (A) Femur Rhesus monkey 12.3 x Ground-section.
- 17 Extensive interstitial micropetrous between first and second generations of secondary osteones. Tibia human. 12.3 x Ground-section.
- 18 || tubes of micropetrous showing partial replacement by secondary osteones (B) Note the peripheral zone of circumferential micropetrous (A) and the sparse distribution of canals. Tibia, Rhesus monkey 12.3. Ground-section.



EXPLANATION OF FIGURES

- 19 Secondary osteones in patches of micropetrotic bone in species from vertebrate group rarely possessing dense secondary H versian tissues. Femur Gopher Tortoise (*Gopherus*) 22.8 X Ground-section.
- 20 Microradiograph of the same area as (11) below. Note that micropetrotic does not effect the overall density of the interstitial matrix between osteones. 22.8 X
- 21 Secondary osteones located within an area of micropetrotic bone. Femur Rhesus monkey 22.8 X Ground-section.
- 22 This is the classic arrangement of bone tissue structure. A zone of periosteal circumferential lamellae (A) encloses two zones of endosteal bone (B) and (C). Zone (B) is the result of secondary H versian reconstruction which was involved with inward growth during decrease in the diameter of the shaft. Note the irregular & convoluted contours of the interstitial bone in this area. Zone (C) is composed of inner circumferential lamellae. It is the structural result of endosteal deposition which did not involve cancellous compaction, since coarse-cancellous trabeculae are reduced in number or absent in the middle third of the diaphysis. Although this particular arrangement of zones has been traditionally adopted as a standard, representative pattern of bone structure it is important to realize that many other common patterns of arrangement may be found in compact bone tissue. Femur Rhesus monkey mid-diaphyseal transverse section. 57 X Ground preparation.

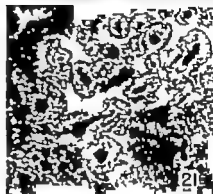
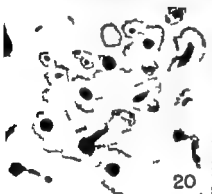
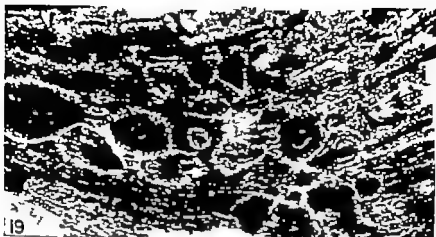


## PLATE 10

### EXPLANATION OF FIGURES

- 23 Area of muscle attachment in the femur of the Rhesus monkey. Note the concentration of secondary osteones (A) in this specific region. Canal lateral to the tubercle on both sides are primary non-Haversian canals (B). Bundles of Sharpey fibers can be seen in the interstitial areas. 208  $\times$  Ground-section.
- 24 Secondary osteones located within patches of micropetrotic bone. Femur Rhesus monkey. 728  $\times$  Ground-section.





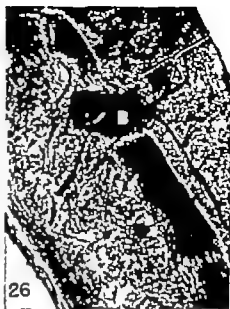
## PLATE II

### EXPLANATION OF FIGURES

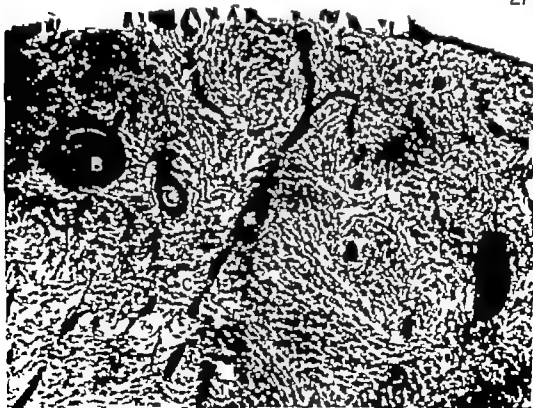
- 25 Compression of coarse cancellous bone during endosteal growth in the metaphysis. Secondary osteones have formed as a result of progressive periosteal invasion of the inwardly shifting cortex. Humerus Rhesus monkey 26.1  $\times$  Ground-section.
- 26 Resorption canal in experimentally induced necrotic bone (B) Note the deposition of some concentric lamellae within the canal. The external layers of the cortex (A) represent a callus which has enclosed the area of centerized bone. Femur white rat 49.5  $\times$  Ground-section.
- 27 Progressive formation of secondary osteones during decrease in metaphyseal diameter. Note that the external surface is undergoing resorption, and that the endosteal surface (lower part of the figure) is receiving lamellar deposits. Development of the Haversian systems (A) and resorption spaces (B) has proceeded in an inward direction. The same canals become primary (C) toward the inner third of the cortex. Radius Rhesus monkey 69.6  $\times$  Ground-section.



25



26

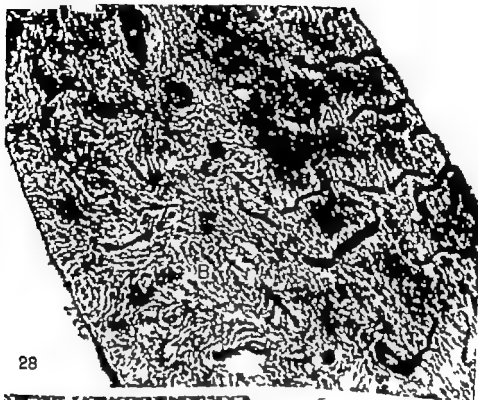


27

## PLATE 19

### EXPLANATION OF FIGURES

- 28 This pattern is produced by inward growth during reduction in metaphyseal diameter. Compaction of cancellous bone is not involved, and endosteal deposits are in the form of circumferential lamellar sheets (A). A broad zone of secondary osteones (B) has developed within the outer part of this endosteal bone. Humerus Rhesus monkey 53 x Ground-section.
- 29 Following periosteal reversal in direction of growth, the arrangement seen in the previous figure (18) will now have the pattern seen in this section. The zone of secondary Haversian tissue (B) formerly located on the outside of the cortex forms an inner zone following periosteal deposition of outer circumferential lamellae (A). This arrangement is commonly observed in the middle third of the bone. Femur Rhesus monkey 53 x Ground-section.



28



29



# Lesions of the Medial Longitudinal Fasciculus in the Cat<sup>1</sup>

MALCOLM B. CARPENTER and GEORGE B. HANNA

*Department of Anatomy College of Physicians and Surgeons  
Columbia University New York*

Although the medial longitudinal fasciculus represents one of the oldest fiber systems of the brain stem and maintains a fairly constant position, the size, shape and fiber composition of this complex bundle undergo appreciable changes at different levels. In spite of numerous studies of this composite fasciculus in man and animals, existing discrepancies indicate that the origins, terminations and courses of fibers entering and leaving the medial longitudinal fasciculus are not fully understood.

The largest constituents of the medial longitudinal fasciculus (abbreviated as MLF) are probably secondary vestibular fibers that enter this bundle mostly in the region of the abducens nucleus. Recent studies by Brodal and Pompeiano ('57b) indicate that ascending vestibular projections in the MLF are diffusely organized and derived from all 4 vestibular nuclei, the interstitial nucleus of the 8th nerve (Cajal, '09-'11) and cell group X (Brodal and Pompeiano '57a). Most authors (Leider '16; Gray '26 P van Gehuchten, '28 Rasmussen, '32 and Buchanan, '37) report that the superior vestibular nucleus projects only uncrossed ascending fibers in the MLF while others (Langworthy '28 van Beusekom, '55) suggests that ascending fibers from the nucleus are both crossed and uncrossed. The view of Muskens (14) that the superior vestibular nucleus contributes descending fibers to the ipsilateral MLF is not supported by other investigations and is open to several objections. Recent evidence (Pompeiano and Brodal, '57) clearly indicates that the superior vestibular nucleus does not project fibers to spinal levels. While the lateral vestibular nucleus gives rise to both ascending and descending fibers, only ascending fibers from this nucleus pass in

the MLF (Carpenter '60); most of these fibers appear to be crossed. Descending fibers from Deiters nucleus are ipsilateral, somatotopically organized and constitute the vestibulospinal tract (Pompeiano and Brodal, '57 Carpenter '60). The medial vestibular nucleus appears to contribute both ascending and descending fibers to the MLF (Muskens, 14 P van Gehuchten, '28 Rasmussen, '32 Buchanan, '37 Ferraro, Pacella and Barrera, 40) but opinions concerning whether these fibers are all crossed vary. It seems likely that the medial vestibular nucleus may be the only nucleus of this complex projecting descending fibers in the MLF since lesions of the descending vestibular nucleus (Carpenter, Alling and Bard, '60 Carpenter '60) produce no detectable spinal degeneration.

The other described constituents of MLF in the brain stem are non-vestibular and descending. These include (1) fibers from the interstitial nucleus of Cajal (Lewandowsky '04 Cajal, '09-'11 Riley 43; Bucher and Bürgi '52 Savas '54; Hassler and Hess, '54; Sie '56 Pompeiano and Walberg, '57 Busch '61) (2) tectobulbar and tectospinal fibers (predorsal bundle Pavlov '00 Collier and Buzzard, '01 Bechterew 1897 Rasmussen '22; Papez and Freeman, '30 Marburg and Warner 47 Bürgi, '57 Altman and Carpenter '61) (3) reticulospinal fibers from pontine and medullary levels (Bechterew 1885 Cajal, '09-'11 van der Schueren, '12 Gray '26 Papez, '26; van Beusekom, '55 Sie '56 Busch '61) and (4) fibers descending to particular parts

This investigation was supported by grant E-1534(C3) from the Institute of Neurological Diseases and Blindness of the National Institutes of Health, Bethesda 14, Maryland.  
Friedrich G. Wilson is neuroanatomy supported by grant E8-3247C, from the Institute of Neurological Diseases and Blindness.

of the inferior olivary nucleus (Massopust, '58) referred to as the medial tegmental tract by Busch ('61). In addition there are presumed to be some fibers in the MLF concerned with the mediation of conjugate horizontal eye movements which interconnect the abducens and oculomotor nuclei (Spiegel and Sommer '44; Grinker and Bucy '49; Crosby '50-'53). Whether these fibers arise from the vestibular nuclei or other sources (e.g. parabrachial nucleus Truex, '59) is unknown, as is the termination of these fibers.

Clinically lesions involving the MLF rostral to the abducens nuclei are described as producing disturbances of conjugate eye movements known as internuclear ophthalmoplegia (Spiller '24; Spiegel and Sommer '44; Cogan, Kubik and Smith, '50; Christoff, Anderson, Nathanson and Bender '60). In most of the clinical material examined pathologically brain stem lesions have been so extensive as to preclude reliable anatomical correlations. Experimental studies in the monkey (Bender and Weinstein, '44-'50; Shatzner, Wagman and Bender '59) indicate that unilateral lesions of the MLF in the pons produce paresis of adduction in the ipsilateral eye and monocular nystagmus in the contralateral abducted eye. While these excellent physiological observations establish the importance of the MLF in this interesting syndrome the neural mechanism responsible for it is not understood.

The object of the current research was to study the physiological effects and anatomical degeneration resulting from discrete lesions in the medial longitudinal fasciculus in the cat. Attempts were made to determine the course, distribution and probable terminations of fibers in the medial longitudinal fasciculus in the hope that such information might contribute to the understanding of this complex neural pathway and the structures it relates.

#### MATERIAL AND METHODS

Twenty-eight adult cats were used in this study. In these animals attempts were made to produce unilateral and bilateral lesions in the medial longitudinal fasciculus at various locations by stereotaxic methods. Coordinates were determined

from dissections of formalin fixed heads with brains *in situ* (Carpenter and Whittier '52). Animals were anesthetized with Nembutal injected intravenously and surgery was performed under aseptic conditions. Following a suboccipital craniotomy an electrode was introduced at a slight angle to the axis of the brain stem. Electrodes usually traversed portions of the cerebellar vermis and entered the brain stem from the ependymal surface of the fourth ventricle. After initial placement of the electrode stimulating square wave currents of small voltages were applied to attempt confirmation of the position of the electrode tip. Physiological effects produced by these stimulations were recorded. At what appeared to be optimal locations lesions were produced by a direct current of 2 or 3 ma and 400 volts applied for intervals of 10 seconds.

Physiological observations and neurological examinations of these animals were made periodically. In selected animals attempts were made to stimulate the labyrinth calorically. Animals were permitted to survive for variable periods of time ranging from 8 to 18 days.

At the conclusion of the observation period animals were anesthetized and perfused with 500 ml of 10% neutral formalin via the left ventricle of the heart. Brains and spinal cords were removed *in toto* in each animal and further fixed in 10% neutral formalin. After adequate fixation, different brains were sectioned: (1) perpendicularly to the axis of the brain stem, (2) horizontally in the axis of the brain stem, and (3) in sagittal planes. Blocks of spinal cord were cut transversely. The brains and selected segments of the spinal cords in animals with appropriate lesions were cut serially at 25  $\mu$ ; all sections were preserved in small plastic containers. Multiple sections through the area of the lesions in each animal were stained with cresyl violet, or by the Weil technique to facilitate determination of the location, disposition, and extent of the lesions. Representative sections from all levels of the brain stem and selected spinal segments were stained according to the Laidlaw modification of the Nauta and Gyax ('54) technique.

## OBSERVATIONS

*Anatomical findings*

In 15 of the 28 cats lesions destroyed portions of the medial longitudinal fasciculus on one or both sides. Unilateral lesions were made on the right side. Lesions involving these fiber bundles were in the vicinity of the abducens nuclei in 14 cats. Because the composition of the medial longitudinal fasciculus undergoes considerable alteration in this region by the addition of both ascending and descending fibers from different sources (Busch '61) the rostro-caudal extent of lesions in this area seemed particularly important. Fiber degeneration resulting from these lesions was studied in 12 animals.

*Unilateral lesions of the MLF.* Lesions in 8 animals (C-514 C-537 C-569 C-571 C-572 and C-574) destroyed significant portions of the right medial longitudinal fasciculus with little or no involvement of this bundle on the left side. These lesions extended longitudinally in the MLF from levels immediately caudal to the abducens nuclei to levels slightly rostral to the sixth nerve nuclei. Because of the slight angle at which electrodes were introduced most of the lesions were located in the dorsal part of the MLF caudal to the abducens nuclei, in the central part of the MLF medial to the abducens nuclei, and in the more ventral parts of this bundle at higher levels. In two animals (C-514 C-571) portions of the right abducens nuclei were concomitantly injured, while in 3 cats (C-569 C-571 and C-572) some fibers in the facial nerve were destroyed. Preterminal degeneration resulting from unilateral lesions in the MLF was studied in 5 animals. Sections of brains of these animals were cut transversely (C-514) horizontally (C-569 and C-571) and sagittally (C-537 and C-572). Although fiber degeneration observed as a consequence of these lesions was fairly consistent in distribution, precise comparisons of particular findings in individual brains sectioned differently was sometimes difficult. In spite of these problems an attempt was made to present a synthetic description of the resulting degeneration.

At the level of the lesion numerous degenerated fibers were seen among the cells

of the ipsilateral abducens nucleus. These fibers passed between the cells, but did not form arborizing networks about individual cells. Degenerated fibers on the side of the lesion projected ventrally into the paramedian reticular formation and laterally into the vestibular nuclei. In the nucleus reticularis pontis caudalis preterminal degeneration was found bilaterally in areas immediately lateral and ventral to the MLF. Some of these fibers were noted to closely surround large reticular neurons. In sagittal sections the large number of fibers passing ventrally from the MLF into the reticular formation at various locations was impressive.

Fibers passing lateral from the MLF to the vestibular nuclei on both sides appeared to originate from levels both rostral and caudal to the abducens nuclei. For the most part these fibers entered the vestibular nuclear complex ventrally and were dispersed to all components. Scanty degeneration in the superior vestibular nucleus usually was present caudally and laterally. In the medial vestibular nucleus degeneration was modest or minimal except in the most rostral parts. While preterminal degeneration in Deiters' nucleus was greater than that seen in either the superior or medial vestibular nuclei, fibers did not closely surround the large cells which characterize this nucleus. The largest number of fibers entered the descending vestibular nucleus, probably via the lateral vestibular nucleus. Degenerated fibers in the descending vestibular nucleus were arranged in small fascicles and passed caudally to all parts of the structure.

From the area of the lesion a large number of degenerated fibers crossed the median raphe. Although many of these fibers entered the contralateral medial longitudinal fasciculus in this region, other fibers were distributed to the contralateral (1) abducens nucleus, (2) lower pontine and upper medullary reticular formation, and (3) vestibular nuclear complex. Fiber degeneration in the contralateral abducens nucleus was similar to that present on the side of the lesion. The distribution of preterminal degeneration in the reticular formation and the vestibular nuclear complex was the same as described



above on the side of the lesion, though quantitatively less. In two animals of this group preterminal degeneration was seen in the uncinate fasciculus of Russell though no direct involvement of the fastigial nuclei was evident. Fastigial efferent fibers were apparently interrupted in their intracerebellar course during placement of the stereotaxic lesions. While the number of degenerated fastigial efferent fibers was not great degeneration in the vestibular nuclei unquestionably was increased by fibers from this source.

Above the level of the lesion ascending fiber degeneration was present bilaterally in the MLF but was always greatest on the right side. Ascending fibers entering the contralateral MLF crossed almost exclusively in the vicinity of the abducens nuclei for practically no degenerated fibers were seen crossing the median raphe at higher levels. In the ipsilateral MLF degenerated fibers were seen in all parts of the fasciculus, including the lateral wing-like extension which characterizes this structure at caudal midbrain levels. Degenerated fibers within the contralateral MLF tended to occupy the lateral portions of the bundle in the upper pons. Sections cut horizontally revealed that most of the fibers adjacent to the raphe were normal or only partially degenerated. At caudal midbrain levels where the configuration of the MLF changes, very few degenerated fibers were found in the lateral wing-like process on the side opposite the lesion.

Ascending preterminal degeneration entered the trochlear nucleus on each side from the respective MLF. Fibers were distributed to cells in all parts of the nucleus. Quantitative differences in the amount of degeneration within the right and left trochlear nuclei were not discernible.

At higher levels degenerated fibers entered the oculomotor nuclear complex from its lateral borders. Degenerated fibers were distributed throughout the large-celled, lateral somatic cell columns. In most cases differences in the amount of degeneration on the right and left sides were very small. The midline visceral nuclei of the oculomotor complex contained little or no preterminal degeneration. Although degenerated fibers closely surrounded somatic cells of the oculomotor nuclei extensive

arborizing fiber networks about cells were not common. On both sides degenerated fibers were seen passing into the interstitial nucleus of Cajal. In this location degeneration seemed appreciably greater on the right side. Some degenerated fibers on both sides entered the periaqueductal gray dorsomedial to the interstitial nuclei. It was presumed that, at least, a few of these fibers probably passed to the nuclei of Darkschewitch but precise identification of the cells composing this entity could not be made in these Nauta stained preparations. The locations of these fibers corresponded to the descriptions and diagrams given by Pompeiano and Walberg ('67). A few degenerated fibers on both sides were noted to pass dorsally about the borders of the periaqueductal gray to the nuclei of the posterior commissure. Fibers passed to these nuclei bilaterally but were more numerous on the right side. None of these fibers were observed to cross in the posterior commissure.

Degeneration traced rostral to the oculomotor nuclear complex occupied positions in advance of the interstitial nucleus of Cajal. From this location fibers curved ventrally and rostrally to enter the dorsal part of the pre-rubral field. In this location fibers were situated along both the medial and lateral borders of the fasciculus retroflexus though most fibers were lateral to this bundle. From this locus degenerated fibers passed laterally along the ventral surface of the centromedian nucleus to enter portions of the posterovenral medial nucleus of the thalamus. In these cases degeneration within the arcuate nucleus was present bilaterally and seemed to be present about clusters of large and medium sized cells in the ventrolateral part of the nucleus. Preterminal degeneration was observed also in the caudal and dorsal portions of the centromedian nuclei. Fibers projecting to these thalamic nuclei were not numerous and would appear to constitute a relatively small proportion of the ascending degeneration. The bulk of the ascending fibers of the MLF appeared to project to the trochlear and oculomotor nuclei.

In addition to the ascending degeneration described distinct groups of degenerated fibers in the reticular formation

passed rostrally in the location of the central tegmental fasciculus. Degeneration in this region was bilateral, though always greatest ipsilateral to the lesion. Quantitatively the largest number of degenerated ascending fibers in the reticular formation were seen in cats C-514 and C-571 but some degeneration in this region was present in all 5 animals. The number of degenerated fibers in the area of the central tegmental fasciculus diminished conspicuously at mesencephalic levels. A considerable part of these fibers projected laterally into the magnocellular portion of the medial geniculate body. Preterminal degeneration among cells of the latter group was especially prominent in cats C-514 and C-571. At diencephalic levels the projections of these fibers could not be distinguished from those ascending in the MLF.

Ascending degeneration was present also in the lateral lemniscus in most of these animals as a consequence of concomitant interruption of fibers in the dorsal acoustic stria. The number of degenerated fibers in the lateral lemniscus was very small and largely limited to the side opposite the lesion. Only in cat C-514 with a lesion extending into the most ventral part of the MLF were large numbers of auditory fibers degenerated bilaterally. Degeneration in the lateral lemniscus could be followed into the nuclei of the lateral lemniscus and the lower portions of the inferior colliculus, but no degeneration was seen in the inferior quadrigeminal brachium or in the parvocellular part of the medial geniculate body.

In brains sectioned sagittally (C-537 and C-572) one additional observation concerning ascending degeneration was made. Immediately rostral to the lesion of the MLF a small number of degenerated fibers near the midline ascended dorsal to the MLF in the subependymal gray. This small bundle of fibers could be traced rostrally in the periaqueductal gray dorsal to the trochlear and oculomotor nuclei and into the posterior hypothalamic area above the mammillary bodies. None of these fibers appeared to reach the mammillary bodies. Although attempts were made to identify these fibers in brains sectioned in other planes such efforts were not successful.

Caudal to the lesion descending fiber degeneration was present in all parts of the ipsilateral MLF. In the contralateral MLF degeneration was minimal immediately caudal to the lesion, but at lower levels degenerated fibers in the bundle gradually increased as fibers crossed the median raphe. Degeneration on this side appeared to be situated largely in the most medial part of the MLF. At medullary levels rostral to the hypoglossal nuclei degenerated fibers from the MLF projected profusely into the nucleus prepositus while a few passed ventral to the oral part of the hypoglossal nucleus to arborize about cells of the nucleus of Roller. Some preterminal degeneration was occasionally seen in the rostral portions of the nucleus intercalatus and in the hypoglossal nuclei. In all of these cases degeneration in the perihypoglossal nuclei was greatest on the side of the lesion.

Intense preterminal degeneration arborized about cells of the paramedian reticular nuclei in the medulla (Brodal, '53) on the side of the lesion. Such degeneration was usually greatest about cells of the dorsal and dorsal accessory nuclear groups which lie along the lateral borders of the MLF. Degeneration seen about cells in the ventral nuclear group was not as profuse. Contralaterally degeneration about cells of the paramedian reticular nuclei was relatively modest. On both sides preterminal degeneration was observed in the more medial and dorsal regions of the medullary reticular formation. Degeneration was greatest ipsilateral to the lesion and did not appear to extend laterally beyond the limits of the nucleus reticularis gigantocellularis.

The raphe nuclei (Taber Brodal and Walberg, '60) contained numerous degenerated fibers oriented vertically. Particularly abundant preterminal degeneration was seen in the dorsal part of the nucleus raphe magnus and in portions of the nuclei raphe obscurus and pallidus.

In the medulla a distinct group of fibers issuing from the MLF coursed ventrolaterally to enter specific portions of the inferior olivary nuclear complex. Abundant degeneration passing into the rostral and medial parts of medial accessory olive and the ventrolateral outgrowth (Brodal, '40)

was seen in two animals (C-514 and C-571). This degeneration was ipsilateral to the lesions, but a small amount of degeneration in corresponding locations was seen contralaterally in cat C-514. In a third animal (C-537) profuse preterminal degeneration was present in the ventrolateral outgrowth while only scattered degeneration was found in various parts of the medial accessory olive. In the latter animal degeneration in the inferior olivary nuclear complex was ipsilateral. Significant localized preterminal degeneration could not be demonstrated in the inferior olivary nuclei in other animals of this group despite many attempts using variations of the staining technique. In the lower medulla fibers of the MLF shifted ventrolaterally to enter the ventral white column lateral to the pyramidal decussation. Caudal to the decussation fibers entered the sulcomarginal area of the cervical spinal cord. Although degeneration in the MLF was bilateral, the number of degenerated fibers on the right side appeared several times greater than on the left. At various spinal levels degenerated fibers from the sulcomarginal area were observed to project laterally or dorsolaterally into the anterior horn. In upper cervical spinal segments preterminal degeneration was present throughout most parts of the anterior horn, though it was most abundant in the medial areas nearest the ventromedial sulcus. While degenerated fibers passed near both large and small cells, networks of fibers did not enmesh the large cells. At mid-cervical spinal levels a conspicuous diminution in the number of degenerated fibers in the MLF was evident. In the anterior horn preterminal degeneration was localized to a relatively small medial area adjacent to the ventral funiculus. This same pattern of fiber distribution was seen in lower cervical segments.

In upper thoracic spinal segments practically no degeneration could be detected in the sulcomarginal area on either side and only a few degenerated fibers were seen among anterior horn cells. Essentially the same observations were made in sections of the lower thoracic spinal cord. In sections through the lumbar enlargement good quality preterminal degeneration was again seen among cells of the

medial cell column in the anterior horn. Other areas of the central gray contained no degenerated fibers. Throughout all spinal levels, except possibly the upper cervical segments, preterminal degeneration was greatest on the right side. At lumbar spinal levels degeneration was scanty on the left side.

*Unilateral destruction of the abducens nucleus* In one cat (C-570) the lesion destroyed the entire right abducens nucleus part of the fibers of the right facial nerve, and small number of fibers in the lateral part of the right MLF. This lesion extended slightly beyond the rostral and caudal poles of abducens nucleus. Preterminal degeneration resulting from the lesion was similar in distribution to that associated with unilateral lesions of the MLF at this level, but certain quantitative differences were evident. Extensive degeneration was present in the fibers of the sixth and seventh nerves ipsilaterally; degeneration also projected into the contralateral abducens nucleus. From the lesion degenerated fibers projected bilaterally to the vestibular nuclear complex with the greatest amount of degeneration on the right side. Almost no degeneration was seen in the medial vestibular nuclei and very little was evident in the superior vestibular nuclei. The lateral and descending vestibular nuclei contained moderate amounts of diffuse preterminal degeneration. Degeneration within the reticular formation at the level of the lesion was similar to that described previously in association with lesions of the MLF.

Ascending degeneration present bilaterally in the MLF was the largest on the left side. Although ascending degenerated fibers in the MLF projected bilaterally to the trochlear and oculomotor nuclei, preterminal degeneration was more abundant on the left side. Degeneration in the oculomotor nuclear complex was confined to the lateral somatic cell columns. Practically no degeneration was seen in the midline visceral nuclei of the third nerve. A few degenerated fibers on each side entered the interstitial nuclei and the nuclei of Darkschewitch. Rostral to the oculomotor nuclei few degenerated fibers were seen these projected rostrally near the

*fasciculus retroflexus* and appeared to terminate about cell groups in the arcuate nuclei. In the pontine and caudal mesencephalic tegmentum a few degenerated ascending fibers were seen lateral to the MLF. These fibers could not be clearly followed to diencephalic levels. Minimal degeneration, noted in the basal portions of the left inferior colliculus suggested that some fibers of the dorsal acoustic stria were interrupted by the lesion.

Descending degeneration in the MLF was much greater on the side of the lesion, though present bilaterally. Fibers could be followed into the nucleus prepositus bilaterally but degeneration was profuse only on the right side. Almost no degeneration was seen in other peritrigeminal nuclei. The paramedian reticular nuclei on the side of the lesion were enmeshed by degenerated fibers while those contralaterally contained few degenerated fibers. Degeneration passing to the ipsilateral inferior olivary nucleus projected largely to the ventrolateral outgrowth, though a few degenerated fibers were seen in the medial accessory olive. Bilateral degeneration was seen in the external cuneate nuclei with the greatest amount ipsilateral to the lesion.

Spinal degeneration was essentially the same as described in association with unilateral lesions of the MLF. It could be followed to lumbar levels where it was distributed to the more medial cell columns of the gray in the anterior horn. Degeneration in the anterior horn in thoracic segments was slightly greater than that usually seen with lesions limited to the medial longitudinal fasciculus.

Bilateral lesions of the MLF rostral to the abducens nuclei. In two animals (C-519 and C-535) stereotaxic lesions destroyed small dorsal portions of the MLF bilaterally rostral to the abducens nuclei. Fibers of the olivo-cochlear bundle (Rasmussen, 46) crossing in this area were interrupted but no destruction was evident in the abducens nucleus or the facial nerve on either side. Preterminal degeneration resulting from these lesions was studied in sections cut transversely.

In these animals preterminal degeneration found bilaterally in the abducens nuclei was modest in amount and evenly

distributed. Bilateral degeneration in the crossed fibers of the olivo-cochlear bundle could be traced laterally under and through the facial nerve to the point where they entered the medial part of the vestibular nerve root. Rostral to the genu of the facial nerve degenerated fibers from the MLF passed laterally and slightly caudally to enter the vestibular nuclear complex. Degeneration within the vestibular nuclei was bilateral, nearly symmetrical and had essentially the same pattern of distribution as that described for unilateral lesions of the MLF.

In the pontine reticular formation fiber degeneration was found bilaterally only in areas immediately adjacent to the MLF. It was not profuse and no significant degeneration was evident in the central tegmental fasciculus on either side.

Ascending degeneration was seen only in the dorsal part of the MLF on each side. At caudal midbrain levels no degenerated fibers were present in the lateral wing like process of the MLF in cat C-510 though a few fibers were seen in this area in cat C-535. In one animal (C-535) preterminal degeneration was seen in the caudal part of the superior central nucleus; fibers appeared to be oriented vertically and none arborized about cells. Degeneration in the trochlear and oculomotor nuclei was bilateral and similar to that described in association with unilateral lesions of the MLF but not as profuse. In only one (C-535) of these animals could preterminal degeneration be traced into the interstitial nuclei of Cajal and the nuclei of the posterior commissure.

Degenerated fibers projecting to diencephalic levels were seen only in cat C-535. A small number of degenerated fibers was found bilaterally in the magnocellular part of the medial geniculate body and in the posteroventral medial nuclei of the thalamus. Fibers reaching these areas constituted a very small fraction of the degenerated ascending bundle.

Descending degeneration within the MLF was located dorsally immediately rostral to the lesion but at more caudal levels these fibers shifted ventrally. At medullary levels fibers of the MLF projected bilaterally to: (1) components of the peritrigeminal nuclear group, (2) the para-

profuse than that found in animals with lesions in the MLF at more rostral levels. These data suggest that a larger proportion of the descending degeneration in this case consisted of reticulospinal fibers.

#### *Physiological findings*

*Disturbances of conjugate eye movements.* Three animals in this series exhibited paralysis of lateral gaze to the right. Lesions in these animals destroyed significant portion of the right MLF and directly involved the abducens nucleus. Right lateral gaze paralysis was transient in one animal (C-514) but enduring in the other two cats (C-570 and C-571). In the latter animals the eyes were never seen to be directed to the side of the lesion. However there was no forced direction of the eyes to the opposite side. On attempted left gaze the left eye abducted fully in a normal fashion but the right eye remained in a neutral straight ahead position, indicating a paresis of adduction ipsilateral to the lesion. This pattern of eye movement persisted without change in animals. Observations concerning

convergence were not unequivocal, but it was our impression that convergence was preserved. Further observations of the lateral gaze paralysis in one animal (C-570) suggested that the paresis of adduction in the left eye might be greater than the paresis of abduction in the right eye. In both of these animals caloric stimulation of the labyrinths tended to exaggerate ocular disturbances. Ice water injected into the right auditory meatus produced apparently normal physiological horizontal nystagmus with the rapid phase to the left. Attempts to stimulate the left labyrinth in both animals required repeated trials (i.e., 5 times) before any response could be elicited. The initial response noted in both animals was a forceful abduction of the left eye while the right eye remained in a straight ahead position. As horizontal nystagmus developed with the rapid phase to the right (1) neither eye seemed to move past the midline in its excursion to the right, and (2) the amplitude of the nystagmus appeared greater in the left eye.

Two other animals (C-569 and C-572) were noted to have weakness of ocular ad-

duction. Impairment of adduction of the right eye was the only disturbance of ocular movement in cat C-569. In the other animal (C-572) bilateral impairment of ocular adduction was observed. On attempts to direct the eyes into the left field of gaze the left eye abducted, but no adduction of the right eye occurred. Attempts to look to the right produced abduction of the right eye and no adduction of the left eye. Caloric stimulation of the labyrinth produced normal physiological nystagmus in cat C-569. In the other animal (C-572) stimulation of the labyrinth produced nystagmus with the rapid phase to the opposite side but movements of the eyes usually were not conjugate.

*Other ocular findings.* Two animals (C-521 and C-535) exhibited a detectable rotation of the right eye which appeared to be an intortio. The slit pupil was oriented diagonally with the dorsal border nearest the midline. In both animals this intortio was transient and associated with bilateral lesions destroying fibers in the dorsal part of the MLF. No satisfactory explanation of this finding is possible since three other animals (C-513, C-519 and C-522) with nearly comparable lesions did not have this ocular intortio.

Only three animals in this series were found to have nystagmus and it was never as prominent or as enduring as that associated with lesions of the labyrinth (Carpenter, Fabrega and Glimsman, '39) or the vestibular nuclei (Carpenter, Alling and Bard, '60). In two animals (C-513 and C-537) minimal bilateral horizontal nystagmus was observed on lateral gaze to both the right and left. This was seen only for a few days after stereotaxic surgery. In the third animal (C-521) combined horizontal and vertical nystagmus independent of the position of the eyes was seen for a few days.

In 5 animals with unilateral lesions of the right MLF it was noted that it was more difficult to successfully stimulate the left labyrinth calorically and that the reactions to stimulation were diminished when compared with those obtained on the right side. The most important qualitative features of labyrinthine stimulation were described in relation with the disturbances of conjugate eye movements.

Only one animal (C-569) with a unilateral lesion of the MLF had bilaterally symmetrical and apparently normal ocular responses upon caloric stimulation. Divergence in the responses to caloric stimulations on the right side were seen in two animals (C-522 and C-537) with lesions of the MLF even though these lesions involved primarily or only the bundle on the right side.

Pupillary inequality was a common finding in animals in this series, occurring in all but two cats. In animals with lesions in the more dorsal fibers of the MLF anisocoria tended to be transient. With larger lesions the pupillary inequality was more enduring, but the larger or smaller pupil was not always on the same side. It would appear that the pupillary inequality was due to interruption of descending autonomic fibers in either the dorsal longitudinal fasciculus of Schütz or in the reticular formation near the MLF. Complete or partial interruption of descending sympathetic fibers was probably responsible for the protrusion of the nictitating membrane seen in some of these animals. It was notable that in one animal (C-571) with a large lesion destroying virtually all of the right MLF no anisocoria or protrusion of the nictitating membrane was seen.

*Coordination and equilibrium.* None of these animals developed notable disturbances of equilibrium or postural abnormalities. A rather mild unsteadiness of gait, particularly involving the hindquarters was seen frequently immediately after surgery but tended to diminish rapidly. These disturbances may have been due in part, to edema associated with penetration of the cerebellar vermis by the electrodes; no lesions were found in the cerebellum. Disturbances characteristic of lesions in the fastigial nucleus (Carpenter, Britten and Pines '58) were never seen. No significant disturbances of placing reactions or tendon reflex were noted.

#### DISCUSSION

One significant observation made in this study is that unilateral lesions of the MLF in the region of the abducens nucleus provoke bilateral ascending and descending degeneration in this bundle.

While the amount of degeneration in the contralateral MLF is always less, it is appreciable. Ascending degeneration in the MLF is usually greater than descending degeneration, as reported by A. van Gehuchten ('04). Immediately rostral to the lesion numerous degenerated fibers crossed to the opposite side, but at higher brain stem levels no degenerated fibers were seen to decussate or enter the median raphe. The nuclei of the raphe (Taber, Brodal and Walberg '60) above the lesion appeared free of preterminal degeneration, except for a few fibers in the caudal part of the superior central nucleus in animals with bilateral lesions.

Fiber degeneration in the contralateral MLF produced by a unilateral lesion in this bundle would appear to be a consequence of interrupting fibers originating from the medial (Muskens '14; Gray '26; P. van Gehuchten, '28; Rasmussen, '32; Buchanan, '37; Ferraro, Bacella and Barrera, '40) and lateral (Mott 1895; Russell, 1897; Probst, '00; Fraser '01; Leidler '16; Sachs and Alvis '21; Tsai, '25; Hashimoto '28; Satoh, '29; Buchanan, '37; Gerebtzoff '40; Carpenter '60) vestibular nuclei prior to their decussation. Some of the crossed degenerated fibers may originate from the oral part of the descending vestibular nucleus (van Gehuchten, '04; van der Schueren, '12; Leidler '16; P. van Gehuchten, '28; Rasmussen, '32). If ascending fibers from these vestibular nuclei undergo a symmetrical decussation, fibers from these same vestibular nuclei would be interrupted in the ipsilateral MLF by a unilateral lesion in the vicinity of the abducens nucleus. Thus degeneration in these crossed ascending fiber components of the MLF is bilateral, though probably not symmetrical, following a unilateral lesion in the above described location. Additional degeneration in the ipsilateral MLF would appear to be uncrossed fibers from the superior (Muskens '14; Leidler '16; Gray '26; P. van Gehuchten '28; Rasmussen, '32; Buchanan, '37; Busch, '61) and lateral (Russell 1897; Probst, '00; Fraser '01; Leidler '16; Sachs and Alvis, '21; Tsai, '25; Buchanan '37; Gerebtzoff '40; van Beusekom '55; Carpenter '60) vestibular nuclei. Since uncrossed ascending fibers originating from the superior vesti-

bular nucleus are described (Busch '61) as entering the MLF rostral to the facial genu, some fibers from this source may have been preserved.

Although the MLF is adjacent to the ventral tegmental nucleus of Gudden, no degeneration was seen in this nucleus. The bulk of the ascending degeneration in the MLF on both sides appears to terminate in the trochlear and oculomotor nuclei as found by almost all authors. It is notable that significant differences in the amount and distribution of preterminal degeneration within these nuclei could not be detected in Nauta stained preparations. Relatively few degenerated fibers in the MLF were observed to enter the visceral nuclear component of the oculomotor complex. In all animals with unilateral lesions of the MLF in the region of the abducens nucleus preterminal degeneration could be followed into the interstitial nucleus of Cajal, the nuclei of the posterior commissure, and the region of the periaqueductal gray containing the nucleus of Darkschewitz (Pompeliano and Walberg, '57). Degeneration in these locations was bilateral, but somewhat greater on the side of the lesion. The interstitial nucleus of Cajal appeared to be the principal nucleus in which these fibers terminated. No fibers were observed to cross in the posterior commissure. Recent investigations by Brodal and Pompeliano ('57b) using the modified Gudden method indicated that a considerable number of fibers from all vestibular nuclei ascend beyond the oculomotor nuclei. Their investigation suggested that fibers to the trochlear and oculomotor nuclei were derived primarily from the medial and superior vestibular nuclei even though all vestibular nuclei appear to project fibers to the nuclei of the extraocular muscles.

A relatively small number of degenerated fibers passed rostral to the interstitial nucleus of Cajal. These fibers project largely to portions of the posteroventral medial nucleus of the thalamus though a few enter the centromedian nucleus. Degeneration in these locations is bilateral but greatest on the side of the lesion. These data suggest that a few crossed and uncrossed fibers in the MLF reach thalamic levels. The crossed fibers would appear to

originate from the medial and lateral vestibular nuclei, while uncrossed fibers probably are derived from the lateral and superior vestibular nuclei.

Although a few investigators have reported that ascending vestibular fibers reach the inferior colliculus (Sachs and Alvis, '21; Gerebtzoff '40) and the superior colliculus (Russell 1897) evidence from this study indicates that degeneration in the inferior colliculus was due to concomitant damage to the dorsal acoustic stria. Using the modified Gudden technique Brodal and Pompeliano ('57) found that lesions in the superior and inferior colliculus failed to provoke retrograde cell changes in the vestibular nuclei.

Several authors have indicated that ascending fibers in the MLF project to the thalamus but precise information concerning the area of distribution is poor (Gee and Tooth 1898; Fraser '01; A. van Gehuchten, '04; van der Schueren, '12). Cajal ('09-'11) simply states that the arcuate nucleus receives a certain number of fibers from the medial longitudinal fasciculus. In Golgi material Lorente de N6 ('33b) illustrates an ascending vestibular fiber in the MLF which passes into the reticular nucleus of the thalamus. According to Spitzer (1899) fibers of the medial longitudinal fasciculus pass to the centromedian, arcuate and ventral nuclei of the thalamus; in this case multiple ascending fiber systems were involved by the lesion. Whitaker and Alexander ('32) described multiple sites of thalamic termination including the parafascicular and arcuate nuclei; Gerebtzoff ('04) reported that ascending fibers from the superior and medial vestibular nuclei projected in the homolateral MLF to the parafascicular nucleus of the thalamus. In an electrophysiological study Mickle and Ades ('52) recorded evoked potentials from a small area between the medial geniculate body and the posterolateral ventral nucleus of the thalamus by stimulating the vestibular nerve. The precise cell groups activated could not be identified in thionin stained sections.

The most extensive studies of the termination of secondary vestibular fibers in the thalamus are those reported by Haasler ('48-'55-'56) based largely upon Marchi

preparations. According to this author ascending secondary vestibular fibers originating from the ipsilateral triangular part of Deiters' nucleus (i.e. medial vestibular nucleus), the principal lateral part of Deiters' nucleus and to a lesser extent from the superior vestibular nucleus as well as a few fibers from the contralateral inferior vestibular nucleus, reach the thalamus. Fibers from these sources were described as ascending in the dorsolateral tegmentum, joining Forel's Habenularfaserkel, and entering the thalamus by penetrating the arcuate nucleus and the ventral part of the centromedian nucleus. These fibers were considered to terminate in the intermediate ventral nucleus of the thalamus. While the course taken by these fibers is obviously different than that described in the present study the areas of apparent termination in the thalamus are very close. In a few animals (C-514 C-535 and C-571) ascending degeneration lateral to the MLF could be followed into the magnocellular part of the medial geniculate body bilaterally. While it is possible that some of these fibers might represent uncrossed vestibulo-mesencephalic fibers considered to originate from the superior vestibular nucleus, it is unlikely that these fibers would degenerate bilaterally as a consequence of a unilateral lesion in the MLF. It is possible that these fibers may represent an ascending component of the central tegmental fasciculus. Busch ('81) described similar degeneration in association with lesions of the superior vestibular nucleus but noted that most of the fibers disappeared in the rostral mesencephalic reticular formation.

Lesions of the MLF in the vicinity of the abducens nucleus also produced ascending degeneration in the region of the dorsal longitudinal fasciculus of Schütz which could be followed rostrally into the dorsal and posterior hypothalamic region. The precise site of termination of these ascending fibers could not be determined from this material. These fibers pursued a distinct and separate course and did not appear to constitute a component of the MLF. Since most of the fibers in this bundle are usually described as descending Thompson ('42) it seems likely that descending de-

generation in this fiber system was also present, but it was not conspicuous.

Descending degeneration in the MLF was bilateral following unilateral lesions in this structure near the abducens nucleus. Degeneration was always greatest on the side of the lesion. Immediately caudal to the lesion relatively few degenerated fibers crossed to the contralateral MLF but at lower levels numerous crossing fibers were seen. Since the literature indicates that the medial vestibular nucleus is probably the only vestibular nucleus projecting descending fibers to the MLF (Pompeiano and Brodal, '57) it is apparent that a good part of the descending degeneration seen in association with these lesions must be derived from non-vestibular sources. It is notable that most investigators who have placed lesions in the medial vestibular nucleus (Muskens '14; P. van Gehuchten, '28 Rasmussen, '32 Ferraro Pacella and Barrera, '40 Busch, '81) described bilateral descending degeneration in the MLF. Because most of these authors used the Marchi technique these studies provided information concerning primarily the course of these fibers. While it is impossible in a study like the current one to determine the origins of all the descending degenerated fibers in the MLF resulting from lesions in this bundle, it seems likely that the largest non-vestibular component probably arises from the reticular formation. Numerous authors (Bechterew 1885 Spitzer 1899 Cajal, '09; van der Schueren, '12; Gray '28 Papez, '36 Mettler '44 van Busekom, '53; Sie '56; Busch '81) indicate that a considerable number of reticulospinal fibers enter the MLF in the pons and medulla.

Descending fibers in the medial longitudinal fasciculus project to three specific nuclear groups in the medulla: (1) the perihypoglossal nuclei (2) the paramedian reticular nuclei of the medulla and (3) parts of the inferior olivary nuclear complex. These descending fibers appear to be located in the dorsal part of the MLF at pontine levels, since lesions confined to this part of the MLF alone caused degeneration in these sites. In most animals with lesions of the MLF profuse preterminal degeneration arborized about cells of the nucleus prepositus and the nucleus



of Roller: only occasional degenerated fibers were seen in the nucleus intercalatus except in a few instances (C-513 C-535). With unilateral lesions most of the degeneration is ipsilateral. Recent studies (Brodal '52 Torvik and Brodal, '54 Carpenter Fabrega and Glinsman '59) have shown that the perihypoglossal nuclei project to specific parts of the cerebellar cortex and the fastigial nuclei. Although the sources of afferent fibers to these nuclei are largely undefined, Brodal ('52) noted that lesions of the brain stem at pontine levels produced abundant terminal degeneration in these nuclei while spinal lesions provoked only modest degeneration. Recently Walberg ('61) has demonstrated that lesions of the fastigial nuclei produce both crossed and uncrossed degeneration in these nuclei. The current study indicates that descending afferent fibers to portions of the perihypoglossal nuclei pass in the MLF. These descending fibers appear to be mostly uncrossed.

Lesions of the MLF provoke intense preterminal degeneration in the paramedian reticular nuclei (Brodal '53) which is greatest in more dorsal cell groups. Unilateral lesions indicate that most of these fibers are uncrossed. The paramedian reticular nuclei like the perihypoglossal nuclei project fibers to the cerebellum (Brodal '53) including the fastigial nuclei (Carpenter Bard and Alling '59). Sources of afferent fibers to these nuclei are multiple (Brodal and Gogstad '57) and include (1) cerebral cortex, (2) vestibular nuclei (3) cerebellum (4) ponto-mesencephalic reticular formation and (5) ascending fibers from spinal levels. It appears likely that fibers passing in the MLF to these nuclei probably arise largely in the vestibular nuclei or the reticular formation.

Descending fibers contained within the MLF also project to specific portions of the inferior olivary nuclear complex. These fibers appear to terminate primarily in the ventrolateral outgrowth (Brodal, '40) and are probably uncrossed. With larger lesions of the MLF degeneration was seen also in the most rostral part of the medial accessory olive. Although Walberg ('56 '60) in his extensive studies of descending olivary afferent fibers states

that the MLF does not contain olivopetal fibers, Massopust ('58) and Busch ('61) describe descending fibers in the MLF projecting to the inferior olive as a consequence of lesions in this structure at various levels. Observed degeneration was reported to project to parts of the principal olive and the medial accessory olive. Massopust ('58) considered these fibers to originate from the region of the interstitial nucleus of Cajal, the nucleus of the posterior commissure and/or the neighboring central gray. It is of particular interest that lesions of the vestibular nuclei (Walberg '56) produce no apparent degeneration in the inferior olivary nuclei. In view of these consistent findings it seems likely that some descending fibers of the MLF project to the inferior olivary nuclei, even though agreement as regards localization within these nuclei is lacking. According to Brodal ('40) the ventrolateral outgrowth projects fibers to the contralateral dentate nucleus.

In addition to the above degeneration a considerable number of fibers from the MLF appeared to be distributed to the caudal pontine and medullary reticular formation. Most of these fibers occupied areas adjacent to the MLF. These fibers would appear to be either reticulo-reticular or vestibulo-reticular fibers, but this cannot be established from available data. Little if any preterminal degeneration was present in the lateral third of the medullary reticular formation.

Spinal degeneration as a consequence of these lesions in the MLF was bilateral, confined to the sulcomarginal area, and detectable in the anterior horns as far caudally as lumbosacral segments. Prior studies (Carpenter '60) have shown discrete lesions of the descending and lateral vestibular nuclei in the cat do not produce descending fiber degeneration in the MLF or in the sulcomarginal area of the spinal cord. Lesions of the medial vestibular nucleus (Rasmussen, '32 Buchanan, '37; Ferraro Pacella and Barrera, '40) in studies done with the Marchi technique have been reported to cause spinal degeneration in the ventral funiculus as far caudally as thoracic segments. From information presented above it is apparent that lesions in the MLF interrupt significant numbers of

reticulospinal fibers coursing in this structure. Although reticulospinal fibers have not been demonstrated (Bodian 46 van Bensekom, '55; Torvik and Brodal, '57) to pass caudal to thoracic spinal segments, it seems likely that some of the fibers extending into lumbosacral segments may be reticulospinal. Busch ('81) mentions an unpublished study (Staal) done at Leiden which has shown fibers of the medial reticulospinal tract to be degenerated in the lumbosacral spinal cord. Similar unpublished studies in this laboratory (Petras) seem to confirm this preliminary finding in Nauta stained material. Comparisons indicate that degeneration resulting from lesions of the MLF and lesions in the medullary reticular formation are distributed similarly in the spinal cord. Maximal degeneration is present in cervical spinal segments, while degeneration in thoracic segments is sparse. In the lumbosacral region more degeneration is seen, particularly in the lumbar enlargement. Most of these fibers are distributed to the more medial portions of the anterior horn. From this material it is obviously impossible to determine the caudal extent of descending vestibular fibers.

Other significant degeneration observed as a consequence of lesions in the MLF in the caudal pons was found in the abducens and vestibular nuclei. In animals with unilateral and bilateral lesions of the MLF both rostral and caudal to the abducens nuclei, preterminal degeneration was found bilaterally in the abducens nuclei. While some of these fibers probably traversed the abducens nuclei, others appeared to terminate there. This finding is in agreement with observations of practically all observers that ascending vestibular fibers project to, or give off collaterals to, the abducens, trochlear and oculomotor nuclei. It is of interest that lesions in the MLF in the medulla do not produce ascending degeneration in the MLF or in any of the nuclei of the extraocular muscles, as reported by Fraser ('01) and A. van Gehuchten ('04).

Preterminal degeneration in the vestibular nuclei following lesions of the MLF revealed a fairly consistent differential distribution. Maximal degeneration was usually seen in the descending vestibular nu-

cleus, though appreciable degeneration was regularly present in Deiters nucleus. In the descending vestibular nucleus preterminal degeneration, distributed to all parts of the nucleus was arranged in small fascicles. Fibers entering the vestibular nuclei appeared to come primarily from the MLF near the rostral border of the facial genu. Such fibers enter the nuclei from the reticular formation. A review of the literature (Pompelano and Walberg '57) concerning afferent reticular fibers projecting to the vestibular nuclei indicated that while many authors have described fibers from the reticular formation entering the MLF and it seems highly probable that some of these project to the vestibular nuclei, specific information regarding these connections is meager. The Golgi studies of Cajal ('09-'11) and Lorente de N6 ('33a) provide evidence that axons and collaterals of cells in the reticular formation reach the vestibular nuclei not only from the MLF but also from the reticulospinal tracts. Electrophysiological investigation (Feldman, Wagman and Bender '61) has shown that stimulation of the midbrain reticular formation, MLF and areas adjacent to the oculomotor nucleus evokes bilateral responses in the vestibular nuclei. While the authors state that there is some uncertainty as to whether all potentials obtained were orthodromic or antidromic, their experiments suggest that fibers from the midbrain reticular formation may project directly to the vestibular nuclei either in a paramedian zone or in the MLF.

Part of the degeneration in the vestibular nuclei might be explained by the interruption of commissural fibers which connect the vestibular nuclei of each side. These commissural fibers have been mentioned in the investigations of Gray ('26) Kaida ('29) Rasmussen ('32) and Ferraro Pacella and Barrera ('40). In a study of the descending and lateral vestibular nuclei (Carpenter '60) some commissural fibers were noted to traverse the MLF. Fiber degeneration in the medial vestibular nuclei, while not abundant in these animals, might be accounted for by interruption of descending fibers in the dorsomedial part of the MLF originating

from the interstitial nucleus of Cajal (Pompeiano and Walberg, '57)

Lastly it is inevitable that some cerebellar efferent fibers were interrupted by electrodes traversing the cerebellar vermis. While none of these animals was found to have lesions in the fastigial nuclei, degenerated fibers in the uncinate fasciculus were seen definitely in two animals. Of special interest in this regard is the finding of Walberg and Jansen ('61) that lesions in various parts of the vermal cortex produced degeneration particularly in the lateral and descending vestibular nuclei. However the dorsal half of Delors' nucleus received the majority of fibers following these lesions, thus indicating a minor but perhaps significant, difference with respect to our data.

With respect to physiological observations it should be mentioned that disturbances of conjugate eye movements are more difficult to detect and appraise in the cat than in the monkey. Subsequent studies in the monkey indicate that even minute lesions in the MLF produce disturbances that can be readily recognized. The observations reported here nevertheless, appear consistent with those described by Shanzler, Wagman and Bender ('59) in the monkey and Klossowsky and Levikowa ('31) in the cat. While unilateral lesions of the MLF at the level of the abducens nuclei may produce paresis of adduction in the ipsilateral eye, other lesions in this area may provoke bilateral paresis of ocular adduction. Whether the paresis of ocular adduction is ipsilateral or bilateral would appear to depend upon number of crossing fibers interrupted by the lesion. If the lesion is confined to the MLF on one side and interrupts relatively few fibers directed towards the opposite MLF the paresis of ocular adduction is likely to be ipsilateral. However a unilateral MLF lesion situated so as to interrupt a large number of ascending fibers destined for the contralateral MLF will probably result in a bilateral paresis of ocular adduction. This thesis is suggested by the findings in two animals (C-569 and C-572) but more conclusive evidence would be required to establish this point. The fact that relatively few if any fibers of the MLF decussate at levels some distance rostral to the

facial genu strengthens this hypothesis. Since bilateral paresis of ocular adduction can occur as a consequence of a unilateral lesion in the MLF near the abducens nucleus it would appear that interruption of crossed ascending fibers considered to originate largely in the medial and lateral vestibular nuclei might be responsible for this disturbance of conjugate eye movements. Because lesions involving the lateral and descending vestibular nuclei in the cat (Carpenter '60) do not provoke such ocular phenomena, it seems likely that interruption of fibers originating from the medial vestibular nucleus may be of particular importance in this syndrome. It should be noted that two animals (C-539 and C-574) with excellent unilateral lesions of the MLF did not have detectable disturbances of conjugate eye movements.

Paralysis of lateral gaze ipsilateral to the lesion was seen in two animals (C-570 and C-571) with lesions involving the MLF and the abducens nucleus unilaterally. This syndrome would appear to consist of two principal elements: (1) a paresis of contralateral ocular adduction and (2) paralysis of ipsilateral ocular abduction. Paralysis of the lateral rectus muscle on the side of the lesion accounts for part of the syndrome, while interruption of fibers destined for the contralateral MLF prior to decussation, would seem to explain the paresis of contralateral ocular adduction. Anatomical data in one of these animals (C-570) appear particularly pertinent to this argument and the preceding one. Although ascending degeneration in the MLF was bilateral, it was most abundant contralateral to the lesion. Preservation of ocular convergence in the presence of lateral gaze paralysis is difficult to explain and suggests that the neural mechanism for convergence functions independently. It is of interest that caloric stimulation of the labyrinth ipsilateral to a unilateral lesion of the MLF tends to exaggerate disturbances of conjugate eye movements. Conversely it is generally more difficult to obtain ocular re-

Although disturbances of conjugate horizontal eye movements were not detected in cats with lesions in the lateral vestibular nucleus, subsequent studies in the monkey (Carpenter, McMonery and Hanna, '62, *Anat. Rec.*, 142: 521) have shown that lesions involving portions of Delors' nucleus produce unilateral paresis of contralateral ocular adduction.

spores in these animals by stimulation of the contralateral labyrinth. The exaggeration of disturbances of conjugate eye movements by caloric stimulation confirms earlier observations made by Bender and Weinstein ('50) and suggests that these disturbances may be essentially an expression of interruption of secondary ascending vestibular pathways.

#### SUMMARY AND CONCLUSIONS

Attempts were made to produce localized lesions in the medial longitudinal fasciculus (MLF) in a series of 28 adult cats by stereotaxic methods in order to study resulting physiological disturbances and fiber degeneration. In 15 of these animals lesions destroyed portions of the medial longitudinal fasciculus on one or both sides. Unilateral lesions in the MLF near the abducens nucleus were produced in 8 animals while lesions in this structure both rostral and caudal to the abducens nuclei, were bilateral in 7 other animals. Lesion in other animals destroyed: (1) the abducens nucleus and small portions of the MLF and (2) portions of the MLF in the medulla. Fiber degeneration resulting from these lesions was studied by the Nauta-Gygax technique ('54) in 12 animals.

The following conclusions were drawn from this study.

1. Unilateral lesions in the MLF in the vicinity of the abducens nucleus in the cat produce bilateral ascending and descending degeneration in the MLF which is most numerous ipsilaterally. Ascending degeneration in the MLF is more abundant than descending degeneration.

2. Ascending degeneration in the MLF as a consequence of unilateral lesions in this bundle near the abducens nucleus projects bilaterally to: (a) the abducens, trochlear and oculomotor nuclei, and (b) the interstitial nucleus of Cajal, the nuclei of the posterior commissure and to the vicinity of the nucleus of Darkschewitch.

3. A small number of ascending fibers in the MLF pass rostrally beyond the interstitial nucleus of Cajal and appear to project to portions of the posteroverventral medial nucleus of the thalamus.

4. Few if any ascending fibers in the MLF appear to cross the midline in the upper pons and mesencephalon.

5. Descending degeneration in the MLF as a consequence of lesions in this bundle near the abducens nucleus projects to: (a) the perihypoglossal nuclei, particularly the nucleus prepositus and the nucleus of Roller (b) the paramedian reticular nuclei of the medulla, and (c) the ventrolateral outgrowth of the inferior olivary nuclear complex. These descending fiber components of the MLF appear to be largely uncrossed.

6. Lesions of the MLF near the abducens nuclei produce bilateral preterminal degeneration in the adjacent pontine and medullary reticular formation and in the vestibular nuclei, particularly the lateral and descending.

7. Spinal degeneration resulting from lesions in the MLF at pontine and medullary levels is bilateral, confined to the sulcomarginal area of the ventral funiculus, and appears to terminate mainly among the more medial cell groups of the anterior horn as far caudally as lumbosacral segments. A significant proportion of the descending spinal fibers with this course and distribution are probably reticulospinal.

8. Unilateral lesions of the MLF near the abducens nucleus in the cat may produce paresis of ocular adduction ipsilaterally or bilaterally depending upon the localization of the lesion and the fibers interrupted by it.

9. In animals with unilateral lesions of the MLF near the abducens nucleus caloric stimulation of the labyrinth: (a) ipsilaterally to the lesion, tends to exaggerate disturbances of conjugate eye movements; while (b) stimulation contralateral to the lesion produces diminished responses.

The hypothesis is presented that disturbances of conjugate horizontal eye movements in the cat associated with lesions of the medial longitudinal fasciculus are primarily the physiological expression of vestibular imbalance due to interruption of ascending secondary vestibular pathways.

#### LITERATURE CITED

- Altman, J. and M. R. Carpenter 1961. Fiber projections of the superior colliculus in the cat. *J. Comp. Neur.* 118: 157-178.  
Bechterew W. von 1883. *Über die Leitungstränge der Formatio reticulari medullae ob-*

- longatus et pontis. *Neur. Centralbl.*, 15: 337-347.
- 1897 Über centrifugale aus der Seh- und Vierzehngegend ausgehende Rückenmarksbahnen. *Neur. Centralbl.*, 16: 1074-1077.
- Bender M. B. and E. A. Weinstein 1944 Effects of stimulation and lesion of the median longitudinal fasciculus in the monkey. *Arch. Neur. Psychiat.*, 52: 106-112.
- 1950 The syndrome of the median longitudinal fasciculus. *Proc. Assoc. Res. Nerv. Ment. Dis.*, 28: 414-420.
- Beurckens, G. T. van 1933 *Fibre analysis of the anterior and lateral funiculi of the cord in the cat.* Thesis. Edward 11de M. V., Leiden, 143 pp.
- Bodian, D. 1948 Spinal projections of the brain-stem in rhesus monkey deduced from retrograde chromotolysis. *Anat. Rec.*, 94: 512-513.
- Brodal, A. 1940 Experimentelle Untersuchungen über die olivocerebelläre Lokalisation. *Zschr. f. d. ges. Neur. und Psychiat.*, 169: 1-133.
- 1953 Experimental demonstration of cerebellar connections from the peri-hypoglossal nuclei (nucleus intercalatus, nucleus prepositus and nucleus of Roller) in the cat. *J. Anat.*, 88: 110-129.
- 1953 Reticulo-cerebellar connections in the cat. An experimental study. *J. Comp. Neur.* 93: 113-153.
- Al, A. and A. C. Gogstad 1957 Afferent connections of the paramedian reticular nucleus of the medulla oblongata in the cat. *Acta Anat.*, 30: 133-151.
- Brodal, A. and O. Pompeiano 1957a The vestibular nuclei in the cat. *J. Anat.*, 91: 435-454.
- 1957b The origin of ascending fibers of the medial longitudinal fasciculus from the vestibular nuclei. *Acta Morphologica Neerlandico-Scandinavica*, 1: 305-328.
- Buchanan, A. R. 1937 The course of the secondary vestibular fibers in the cat. *J. Comp. Neur.* 67: 183-204.
- Bueker V. M., and S. M. Bürgi 1953 Some observations on the fiber connections of the olivocerebellum in the cat. II. Fiber connections of the pretectal region and the posterior commissure. *J. Comp. Neur.* 90: 139-178.
- Bürgi, S. M. 1957 Das Tectum Opticum. Seine Verbindungen mit der Kerne und seine Bedeutung beim Menschen. *Dtsch. Zschr. f. Nervenheilk.* 178: 701-729.
- Busch, H. F. M. 1961 An anatomical analysis of the white matter in the brain stem of the cat. Thesis. Te Assen Bij van Gorcum N. V. Leiden, pp. 116.
- Cajal, R. R. 1902-1911 *Histologie du Système Nerveux de l'Homme et des Vertébrés.* Maloine Paris, I et II.
- Carpenter M. B. 1960 Fiber projections from the descending and lateral vestibular nuclei in the cat. *Am. J. Anat.*, 107: 1-22.
- Carpenter M. B., Y. A. Alling and H. B. Bard 1960 Lesions of the descending vestibular nuclei in the cat. *J. Comp. Neur.* 114: 39-50.
- Carpenter M. B., D. S. Bard and F. A. Alling 1959 Anatomical connections between the fastigial nuclei, the labyrinth and the vestibular nuclei in the cat. *J. Comp. Neur.* 111: 1-26.
- Carpenter M. B., G. M. Brittin and J. Pines 1958 Isolated lesions of the fastigial nuclei in the cat. *J. Comp. Neur.*, 109: 63-90.
- Carpenter M. B., H. Fabrega and W. Glimman 1959 Physiological deficits occurring with lesions of labyrinth and fastigial nuclei. *J. Neurophysiol.*, 22: 222-234.
- Carpenter M. B. and J. R. Whitner 1959 Study of methods for producing experimental lesions of the central nervous system with special reference to stereotaxic technique. *J. Comp. Neur.* 67: 73-122.
- Christoff, N., P. J. Anderson, M. Nathanson and M. B. Bender 1960 Problems in anatomic analysis of lesions of the median longitudinal fasciculus. *A.M.A. Arch. Neur.* 2: 293-304.
- Cogan, D. G., C. E. Kubik and W. L. Smith 1950 Unilateral internuclear ophthalmoplegia. Report of 8 clinical cases with one postmortem study. *Arch. Ophthalmol.*, 44: 783-796.
- Coiler J. and P. Buzzard 1961 Descending mesencephalic tracts in cat, monkey and man. "Blockow" bundles, the dorsal longitudinal bundle; the ventral longitudinal bundle; the ponto-spinal tracts, lateral and ventral; the vestibulo-spinal tract; the central tegmental tract (centrale f. überbahn); descending fibers of the fillet. *Brain*, 84: 177-221.
- Crooby E. C. 1950 The application of neuro-anatomical data to the diagnosis of selected neurological and neurosurgical cases. *J. Neurosurg.*, 7: 566-583.
- 1953 Relations of brain centers to normal and abnormal eye movements in a horizontal plane. *J. Comp. Neur.* 89: 437-460.
- Feldman, R., L. H. Wagnan and M. B. Bender 1961 Anterior brain stem and sciatic nerve connection to vestibular nuclei in cat. *J. Neurophysiol.*, 24: 350-363.
- Ferraro, A., B. L. Pacella and S. E. Barrera 1940 Effects of lesions of the medial vestibular nucleus. — An anatomical and physiological study in macacus rhesus monkeys. *J. Comp. Neur.* 73: 7-36.
- Fraser E. H. 1901 An experimental research into the relations of the posterior longitudinal bundle and Deltoid nucleus. *J. Physiol.* 27: 373-397.
- Gee E., and H. H. Tooth 1896 *Hypomastix into the pons, secondary lesions of the hemispheres, posterior longitudinal f. and cerebellum.* *Brain*, 21: 1-20.
- Gebuchten, A. van 1904 *Conexions centrales du noyau de Deltoid et les masses grises voisines (Faisces v. vestibulo-spinal, faisces longitudinal posterieur etries medullaires).* *Névrose*, 8: 19-73.
- Gebuchten, P. van 1928 *Les voies nerveuses d. syst. sens.* *Rev. Neurol.*, 2: 649-679.
- Gerebtoff M. A. 1930 Recherches sur la projection corticale du labyrinthique. II. Etude anatomico-experimentale de la voie vestibulo-cerebrale. *J. Belge Neur. et Psychiat.*, 45: 417-432.

- Goy L. F. 1935 Some experimental evidence on the connections of the vestibular mechanism in the cat. *J. Comp. Neurol.* 41: 319-364.
- Gsch, E. L., and P. C. Bucy 1949 *Neurology* Springfield, Ill. C. C. Thomas, Chapt. IX. p. 108.
- Kellmott, I. 1928 Experimentelle Untersuchungen über die spinale Bahn des N. vestibularis, mit besonderer Berücksichtigung auf dem Gabel der Dorsum descendens et ascendens Willers. *Folia Anat. Japon.* 8: 537-596.
- Keller, R. 1948 Forth. Ha. bentafisch als vestibuläre Eingangsbahn mit Bemerkungen über einige andere sekundäre Bahnen des Vestibularis und Trigemina. *Arch. f. Psychiat. u. Zentr. f. Neurol.* 180: 33-63.
- 1953 Functional anatomy of the thalamus. *Comp. Lathamer Neurosci.* VI, Montevideo, Uruguay 754-786.
- 1956 Die zentralen Apparate der Wahrnehmungen. II. Die neuronalen Apparate der vestibulären Korrekturwendungen und der Abwehrbewegungen. *Arch. f. Psychiat. u. Zentr. f. Neurol.* 194: 481-516.
- Keller, R., and W. E. Hess 1954 Experimentelle und anatomische Befunde über die Dorsalbewegungen und ihre nervösen Apparate. *Arch. f. Psychiat. u. Zentr. f. Neurol.* 192: 488-508.
- Kikyo, Y. 1939 Ueber den zentralen Verlauf des N. vestibularis und der Fasern aus dem Dorsalen Kern. *Fukuroku-Ikudaisigyo-Zasshi*, 22: 3-4.
- Kisimovsky, B., and A. M. Levikova 1931 Der Mechanismus der vestibulären Nystagmus (Ueber die homonyme kreuzweise cruciate Inversion der Maculae recti lateralis von dem Oculomotorischen beim Nystagmus. *Arch. f. d. ges. Physiol.* 258: 198-212.
- Langworthy, O. R. 1928 The behavior of post-yeung of opposites correlated with the myelination of tracts in the nervous system. *J. Comp. Neurol.* 49: 201-247.
- Leider, R. 1916 Experimentelle Untersuchungen über das Endigungsgebiet des Nervus vestibularis. 2. Mitteilung. *Arch. Neurol. Inst. Univ. Wien*, 21: 181-215.
- Levinsowsky, M. 1904 Untersuchungen über die Leitungsbahnen des Truncus cerebri und ihren Zusammenhang mit denen der Medulla oblongata und des Cortex cerebri. G. Fischer, Jena.
- Lewine, D. M., R. 1933a Vestibulo-ocular reflex arc. *Arch. Neurol. and Psychol.* 30: 245-251.
- 1933b Anatomy of the eighth nerve. The central projection of the nerve endings of the internal ear. *Laryngoscope*, 43: 1-38.
- Marburg, O., and F. J. Warner 1947 The pathways of the tectum (anterior colliculus) of the midbrain in cats. *J. Nerv. and Ment. Dis.* 104: 415-448.
- Marsland, L. C., Jr. 1956 Terminal degeneration study of the spinal component of the medial longitudinal fasciculus. *Anat. Rec.* 127: 370.
- Merrill, F. A. 1944 Physiologic consequences and anatomic degenerations following lesion of the primate brain stem plantar and palatal reflexes. *J. Comp. Neurol.* 80: 69-148.
- Mickle, W. A. and H. W. Ades 1953 Rostral projection pathway of the vestibular system. *Am. J. Physiol.* 176: 843-846.
- Mott, F. W. 1903 Experimental enquiry upon the afferent tracts of the central nervous system of the monkey. *Brain*, 18: 1-20.
- Mushens, L. J. J. 1914 An anatomico-physiological study of the posterior longitudinal bundle in its relation to forced movements. *Brain*, 36: 352-426.
- N. uta, W. J. H., and P. A. Gyax 1954 Silver impregnation of degenerated axons in the central nervous system. A modified technique. *Stain Tech.* 29: 91-93.
- Papez, J. W. 1926 Reticulo-spinal tracts in cat; Marchi method. *J. Comp. Neurol.* 41: 365-399.
- Papez, J. W. and G. L. Freeman 1930 Superior colliculi and their fiber connections in the rat. *J. Comp. Neurol.* 33: 409-439.
- Pavlov, M. 1900 Les voies descendantes des tubercules quadrifunctorum superiores. I-II. *Nervosa*, 1: 67-78, 129-136.
- Pompeiano, O. and A. Brodal 1937 The origin of vestibulospinal fibers in the cat. An experimental-anatomical study with comments on the descending medial longitudinal fasciculus. *Arch. Ital. Biol.* 35: 166-185.
- Pompeiano, O., and F. Walberg 1937 Descending connections to the vestibular nuclei. An experimental study in the cat. *J. Comp. Neurol.* 108: 466-603.
- Probst, M. 1900 Experimentelle Untersuchungen über die Schleifenbahnung, die Flaubenbahnen, das dorsale Längsbündel und die hintere Commissur. *Arch. Psychiat. Nervenheilk.* 33: 1-87.
- Rasmussen, A. T. 1923 Experimental demonstration of the entire course of a descending tract by single alcoholic injection in the mid-brain of the cat. *Proc. Soc. Exp. Biol. Med.* 20: 104-107.
- 1932 Secondary vestibular tracts in the cat. *J. Comp. Neurol.* 54: 143-159.
- Rasmussen, G. L. 1946 The olivary peduncle and other fiber projections of the superior olivary complex. *J. Comp. Neurol.* 84: 114-220.
- Riley, H. A. 1943 An Atlas of the Basal Ganglia, Brain Stem, and Spinal Cord Based on Myelin-stained Material. Williams and Wilkins, Baltimore. p. 633.
- Rosell, J. E. R. 1897 The origin and destination of certain efferent and afferent tracts in the medulla oblongata. *Brain*, 20: 409-440.
- Sachs, E., and E. Y. Alvis 1921 Anatomic and physiologic studies of the eighth nerve. *Arch. Neurol. and Psychiat.* 6: 119-143.
- Saitoh, K. 1919 Experimentelle Untersuchungen über die Beziehungen zwischen dem Vestibularis Dorsum und dem Kerngebiete des dorsalen Längsbündels nach Edinger. *Folia Anat. Japon.* 7: 45-61.
- Saves, A. 1954 Faseranalyse des Fasciculus longitudinalis medialis. *Act. Anat.* 21: 808-822.

- Schueren, A. van der 1912 Etude anatomique du faisceau longitudinal postérieur Névrose 13 183-309
- Schanzer S., I. H. W. Gman and M. B. Bender 1959 Further observations on the medial longitudinal fasciculus. Trans. Am. Neur. Assoc., 14-17
- Sle P. C. 1956 Localization of Fibre Systems within the White Matter of the Medulla Oblongata and the Cervical Cord in Man. Eduard Ijdo N. V. Leiden, 218 pp
- Spiegel, E. A., and I. Sommer 1944 Neurology of the Ear Nose and Throat. Grune and Stratton, New York. Chapt. VI pp. 344-414.
- Spiller W. G. 1924 Ophthalmoplegia internucleari anterior; a case with necropsy Brain, 47 345-357
- Spitzer A. 1899 Ein Fall von Tumor am Boden der Rautengrube. Beitrag zur Kenntnis des hinteren Längsbündels. Arb. Neur. Inst. Univ. Wien, 6 1-53.
- Taber E., A. Brodal and F. Walberg 1960 The raphe nuclei of the brain stem in the cat. I. Normal topography and cytoarchitecture and general discussion. J. Comp. Neur. 114 161-187
- Thompson, E. L. 1942 The dorsal longitudinal fasciculus in Didelphis Virginiana. J. Comp. Neur. 76: 238-281
- Torvik, A., and A. Brodal 1934 The cerebellar projection of the perihypoglossal nuclei (nucleus intercalatus, nucleus prepositus and nucleus of Roller) in the cat. J. Neuropath. and Exper. Neur. 13 515-527
- 1957 The origin of reticulospinal fibers in the cat. An experimental study Anat. Rec., 126 113-137
- Truex, R. C. 1956 Strong and Elwyn's, Human Neuroanatomy Williams and Wilkins, Baltimore 4th Ed., Chapt. XVI p. 309
- Tsai, C. 1925 The descending tracts of the thalamus and mid-brain of the opossum, Didelphi Virginiana. J. Comp. Neur. 39 217-248.
- Walberg F. 1956 Descending connections to the inferior olive. An experimental study in the cat. J. Comp. Neur. 104 77 173.
- 1960 Further studies on the descending connections to the inferior olive. Reticulolary fibers an experimental study in the cat. J. Comp. Neur. 114 79-87
- 1961 Vestibulofugal fibers to the perihypoglossal nuclei in the cat. Exper. Neur. 5 525-541
- Walberg, F. and J. Jansen 1961 Cerebellar corticovestibular fibers in the cat. Exper. Neur. 5 23-32.
- Whitaker J. G. and L. Alexander 1932 Die Verbindungen der Vestibulariskerne mit dem Mittel- und Zwischenhirn. J. f. Psychol. u. Neur. 44 253-370.

## PLATE 1

## EXPLANATION OF FIGURES

- 1 2 Cats C-514 and C-574 Photomicrographs of unilateral lesions in the right MLF. Weil.  $\times 7.5$ ,  $\times 8$ .
- 3 Cat C-570. Photomicrograph of horizontal frozen section showing lesion destroying the right abducens nucleus and part of the MLF. Nissl.  $\times 7.5$ .
- 4 Cat C-571. Photomicrograph of horizontal frozen section showing unilateral lesion in the right MLF. Portion of the abducens nucleus and facial nerve were destroyed by this lesion. Nissl.  $\times 7.5$ .
- 5 Cat C-513. Photomicrograph of small lesion involving fibers of the MLF bilaterally caudal to abducens nuclei. Weil.  $\times 7$
- 6 Cat C-537. Photomicrograph of sagittal section showing small lesion in the right MLF. Nissl-Gyax.  $\times 7$

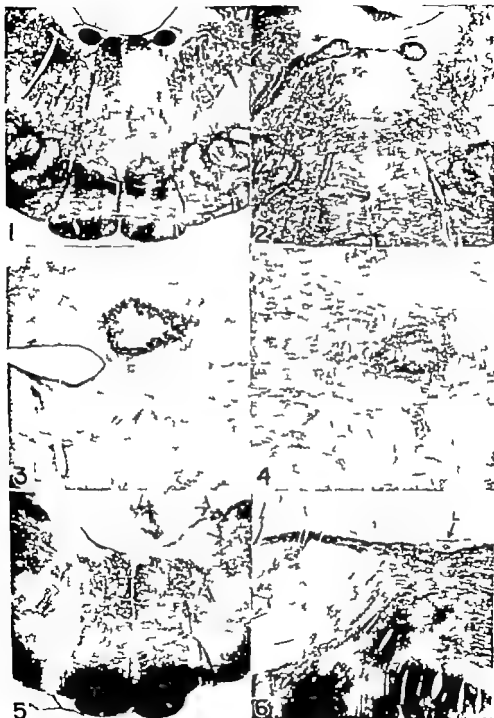




## PLATE 2

### EXPLANATION OF FIGURES

- 7 Cat C-537. Photomicrograph showing preterminal degeneration in the trochlear nuclei in sagittal section. Nauta-Gygax.  $\times 63$ .
- 8-9 Cat C-537. Photomicrographs of preterminal degeneration in the oculomotor nuclei, as seen in sagittal sections. Nauta-Gygax.  $\times 63$ ,  $\times 110$ .
- 10 Cat C-535. Preterminal degeneration in the interstitial nucleus of Cajal. Nauta-Gygax.  $\times 160$ .
- 11 Cat C-535. Photomicrograph showing small area of preterminal degeneration in the arcuate nucleus of the thalamus. Nauta-Gygax.  $\times 470$ .
- 12 Cat C-571. Photomicrograph of horizontal section demonstrating preterminal degeneration in the nucleus prepositus. Nauta-Gygax.  $\times 160$ .



### PLATE 3

#### EXPLANATION OF FIGURES

- 13 Cat C-537 Preterminal degeneration about cells of the nucleus of Roller Nauta-Gygax.  $\times 430$ .
- 14 Cat C-537 Preterminal degeneration arborizing about cells of the paramedian reticular nuclei. Nauta-Gygax.  $\times 430$ .
- 15 Cat C-533. Photomicrograph demonstrating degenerated fibers passing to the rostro-lateral outgrowth of the inferior olivary complex. Nauta-Gygax.  $\times 470$ .
- 16 Cat C-514 Photomicrograph of the rostral part of the medial accessory olive showing preterminal degeneration. The lesion in the animal (Fig 1) extended laterally beyond the MLF. Nauta-Gygax.  $\times 470$ .
- 17 Cat C-537 Photomicrograph of part of anterior horn on the right of the fifth cervical spinal segment showing distribution of preterminal degeneration. Nauta-Gygax.  $\times 350$ .
- 18 Cat C-53 Photomicrograph of degeneration in anterior horn at fourth lumbar spinal segment. Nauta-Gygax.  $\times 470$ .





# Index

## A

AMANN, RUPERT P. Reproductive capacity of dairy bulls.

III. The effect of ejaculation frequency unilateral vasectomy and age on spermatogenesis 40

IV. Spermatogenesis and testicular germ cell degeneration 60

Anatomic and angiographic study of the vertebral-basilar arterial system in the dog 187

ANDREW WARREN. An electron microscope study of age changes in the liver of the mouse 1

Angiographic study of the vertebral-basilar arterial system in the dog, anatomic and 187

Antioxidants, fetal resorption in the rat as influenced by certain 20

## B

BLOCH, EDWARD H. A quantitative study of the hemodynamics in the living microvascular system 125

Bone, a study of the post-natal growth and remodeling of 70

Bones of 60 race III rabbits. Morphogenetic studies of the rabbit. XXXI. Weights and linear measurements of some of the 250

## C

CARPENTER, MALCOLM B. AND GEORGE R. HANA. Lesions of the medial longitudinal fasciculus in the cat 307

Cat, A. Cross structures in the adult, spinal cord segments 37

Cat, lesions of the medial longitudinal fasciculus 307

CLARK, SAM L., JR. The reticulum of lymph nodes in mice. Studied with the electron microscope 217

COMES E. MURPHY. See Thomas, Carolyn Eyster 37

Compensatory renal hyperplasia following experimental surgical deletions of the kidney complement 180

CONKLIN, JAMES L., MAYNARD M. DEWEY AND RAYMOND H. KARN. Cytochemical localization of certain oxidative enzymes. Cytochemical localization of certain oxidative enzymes 19

## D

Degeneration, IV. Spermatogenesis and testicular germ cell. Reproductive capacity of dairy bull 60

DE LA TORRE, ERNESTO, OLIVER CHARLES MITCHELL AND MARTIN G. NEMEKY. Anatomic and angiographic study of the vertebral-basilar arterial system in the dog 187

DEWEY, MAYNARD M. See Conklin, James L. 19

Dog, anatomic and angiographic study of the vertebral-basilar arterial system in the 187

## E

Ejaculation frequency unilateral vasectomy and age on spermatogenesis, III. The effect of reproductive capacity of dairy bulls 40

Electron microscope study of age changes in the liver of the mouse, an 1

Electron microscope, the reticulum of lymph nodes in mice studied with 217

ESLOW, DONALD H. A study of the postnatal growth and remodeling of bone 70

ESLOW, DONALD H. Functions of the Haversian system 200

Epithelial cells of the small intestine of the rat, fat absorption by 155

## F

Fasciculus in the cat, lesions of the medial longitudinal 307

Fat absorption by epithelial cells of the small intestine of the rat 155

Fetal resorption in the rat as influenced by certain antioxidants 20

Fibers of the rat, histochemical classification of individual muscle 103

FINLEY, C. F. See K. K. Hiseaka 203

F functions of the Haversian system 200

## G

Growth and remodeling of bone, study of the post-natal 70

## H

HANA, GEORGE R. See Carpenter Malcolm B. 307

Haversian system, functions of the 200

Hemodynamics in the living microvascular system, quantitative study of the 125

Histochemical classification of individual skeletal muscle fibers of the rat 103

Hyperplasia following experimental surgical deletions of kidney complement, compensatory renal 180

HISAOKA, K. K., AND C. F. F. LIT The localization of nucleic acid during oögenesis in the Zebrafish

## I

Intestine of the rat, f t absorption by epithelial cells of the small

## K

KAHN, RAYMOND H. See Conklin, J. and L. Kidney complement, compensatory renal hyperplasia following experimental surgical deletion of the

## L

LACY DENNIS, MD A. B. TAYLOR F t absorption by epithelial cells of the small intestine of the rat

LATIMER, H. MERB AND P. ULB. SAWIN Morphogenetic studies of the rabbit. XXXI. Weights and linear measurements of some of the bones of 65 race III rabbits Lesions of the medial longitudinal fasciculus in the cat

LIMFORD, RAY H. See Telford, Ira R. Liver of the mouse, an electron microscope study f t changes in the

Localization of certain oxidative enzymes, cytochemical

Localization of nucleic acids during oögenesis in the Zebrafish the

## M

MC CREIGHT, CHARLES E. AND NORMAN M. S. LEVIN Compensatory renal hyperplasia following experimental surgical deletions f t kidney complement

Mice studied with electron microscope the reticulum of lymph nodes, the

Microscope study of age changes in the liver of the mouse, an electron

Microscope, the reticulum of lymph nodes f mice f t died with the electron

Microvascular system, quantitative study of the hemodynamics in the living

MITCHELL, OLIVER CHARLES. See de la Torre Ernesto

Morphogenetic studies of the rabbit XXXI. Weight and linear measurements f some of the bones of 65 race III rabbits Mouse, an electron microscope study of the changes in the liver of the

## N

NET, Y. MARTIN G. See de la Torre Ernesto

Nodes in mice studied with the electron microscope the reticulum of the lymph

## O

Oögenesis in the Zebrafish the localization f nucleic acid during  
Oxidative enzymes, cytochemical localization of certain

## P

PADYKULA, HELEN A. See John M. Stein Post-natal growth and remodeling of bone study of the

## Q

Quantitative study of the hemodynamics in the living microvascular system

## R

Rabbit. XXXI. Weights and linear measurements of some of the bones of 65 race III rabbits, morphogenetic studies of the

Rabbits, morphogenetic studies of the rabbit XXXI. Weights and linear measurements of some of the bones f 65 race III

Rat as influenced by certain nitrofurantoin, fetal resorption in the

Rat, f t absorption by epithelial cells of the small intestine of the

Rat, histochemical classification of individual skeletal muscle fibers of the

Reticulum of lymph nodes in mice studied with the electron microscope the

Reproductive capacity of dairy bulls. III. The effect of jacobson frequency unilateral vasectomy and age on spermatogenesis

IV. Spermatogenesis and testicular germ cell degeneration

## S

Skeletal muscle fibers of the rat histochemical classification of individual

Spermatogenesis and testicular germ cell degeneration. IV. Reproductive capacity of dairy bull

Spermatogenesis III. The effect of jacobson frequency unilateral vasectomy and age on Reproductive capacity of dairy bull

Spinal cord segments. A. Gross structure in the adult cat

STEIN, JOHN M., AND HELEN A. PADYKULA. Histochemical classification of individual skeletal muscle fibers of the rat

Structure in the adult cat. A. Gross, spinal cord segment

Study of the post-natal growth and remodeling of bone

SULKIN, NORMAN M. See McCreight, Charles E.

## T

- TAYLOR, A. B. See Lacy Dennis
- TELFORD, IRA R., CAROLINE S. WOODRUFF  
AND RAY H. LINFORD. Fetal resorption in  
the rat as influenced by certain antioxi-  
dants 29
- Testicular germ cell degeneration. IV Sper-  
matogenesis and, reproductive capacity of  
dairy bulls 69
- THOMAS, CAROLYN EVERTS AND C. MURPHY  
COMBS. Spinal cord segments. A. Gross  
structure in the adult cat 37

## V

- Vasectomy and age on spermatogenesis.  
III. The effect of ejaculation frequency  
unilateral. Reproductive capacity of dairy  
bulls 49

## W

- WOODRUFF CAROLINE S. See Telford, Ira R. 29

## Z

- Zebrafish the localization of nucleic acids  
during oögenesis in the 203





